Plant developmental plasticity and mechanical forces : the role of FERONIA

Alice Malivert

Numéro National de Thèse : 2022ENSL0001

THESE

en vue de l'obtention du grade de Docteur, délivré par

l'ECOLE NORMALE SUPERIEURE DE LYON

Ecole Doctorale N° 340
Biologie Moléculaire, Intégrative et Cellulaire (BMIC)

Discipline : Sciences de la vie et de la santé

Soutenue publiquement le 02/09/2022, par :

Alice MALIVERT

Plant developmental plasticity and mechanical forces: the role of FERONIA

Plasticité du développement végétal et forces mécaniques : le rôle de FERONIA

Devant le jury composé de :

DUMAIS, Jacques, Professeur, Universidad Adolfo Ibáñez (Chili), Rapporteur
GASPERINI, Debora, Professeure, Leibniz Institute of Plant Biochemistry (Allemagne), Rapporteure
SÁNCHEZ-RODRíGUEZ, Clara, Professeure, ETH Zurich (Suisse), Examinatrice
LAPLAZE, Laurent, Directeur de Recherche, DIADE, IRD Montpellier, Examinateur
INGRAM, Gwyneth, Directrice de Recherche, RDP, ENS de Lyon, Examinatrice
HAMANT, Olivier, Directeur de Recherche, RDP, ENS de Lyon, Directeur de thèse

Acknowledgments

Puisque la recherche est avant tout un travail d'équipe, vous êtes nombreux à mériter ma reconnaissance.

Tout d'abord, bien sûr, Olivier Hamant. Dès notre rencontre, tu as initié un véritable dialogue scientifique. J'ai eu la chance de pouvoir orienter mon projet dans la direction qui me plaisait, tout en sachant que tu saurais me guider si je faisais fausse route. Merci pour ta confiance et ta bienveillance. Le rôle scientifique du directeur de thèse n'est pas tout, et si je réalise la chance que j'aie eu de ce côté-là, ton côté humain a tout autant compté pour faire de moi la scientifique que je suis aujourd'hui.

Sur chacun de mes stages, j'ai bénéficié d'un encadrement formidable : merci à Bernard Reynaud, Henrik Jönsson, Benoit Landrein, Staffan Persson, Stéphane Verger et encore Olivier Hamant. Vous avez été pour moi fondateurs. En particulier merci à toi Benoit. Ton accueil à Cambridge a été formidable, et n'oublions pas que tu es celui qui m'a présenté Olivier. Je suis très heureuse de t'avoir retrouvé au RDP et d'avoir pu t'impliquer dans mon projet avec le CST.

Pour la relecture du manuscrit, j'ai deux Olivier à remercier. Comme toujours Olivier Hamant tu as été impressionnant sur ton rythme de relecture, et tes conseils m'ont aidé à mettre en œuvre mes idées. Merci à toi Olivier Ali pour ta relecture des parties de physique de ma thèse, tu m'as beaucoup rassurée (et désolée j'ai préféré éviter de parler d'urine).

Merci aussi aux chercheurs qui ont accepté d'être membres de mon jury de thèse : les rapporteurs Debora Gasperini et Jacques Dumais, et les examinateurs Gwyneth Ingram, Clara Sánchez-Rodríguez et Laurent Laplaze. C'est une joie pour moi de vous présenter mon travail.

Je voudrais remercier toutes les personnes qui ont participé à cette thèse. Özer Erguvan, Antoine Chevallier, Antoine Dehem, Rodrigue Friaud, Mengying Liu, Marjolaine Martin, Théophile Peyraud, Olivier Hamant et Stéphane Verger ont travaillé sur le premier projet. Corentin Mollier, Mylan Ansel, Amaya Richer, Dorota Borowska-Wykręt, Alexis Bédiée, Bertrand Muller, Myriam Dauzat, les équipes de Yuchen Long et Grégory Mouille et son équipe ont travaillé sur le deuxième projet. Merci aux trois stagiaires que j'ai encadrés, Théophile,

Mylan et Amaya. J'ai aussi discuté de mon sujet avec beaucoup de gens qui m'ont aidé à mieux le comprendre : merci à Long, Arezki Boudaoud et Ibrahim Cheddadi pour les explications de physique, elles ont été essentielles à l'avancée de mon projet de thèse et je vous suis très reconnaissante pour ces cours accélérés. Merci aux membres de mon CST, Naomi Nakayama et Benoit Landrein pour leur enthousiasme et leurs commentaires utiles qui m'ont évitée de trop me disperser.

Vous êtes très nombreux à remercier au RDP, pour les discussions scientifiques et l'accompagnement à la recherche. Merci aux équipes culture, gestion, logistique et imagerie pour leur aide tellement précieuse au quotidien. Et merci à toutes les personnes qui assurent des responsabilités supplémentaires pour que l'ensemble du laboratoire fonctionne. Je voudrais aussi remercier l'ensemble du RDP pour un an de stage et trois ans de thèse sous le signe de la convivialité. Les PhD meetings, skiminars, nombreux pots, les discussions de salle des cribles, les cafés du GN1 et les foyers, en font un laboratoire unique où j'ai eu beaucoup de chance de travailler. Le GN1 en particulier a été un espace de partage formidable, qui a beaucoup évolué mais a gardé une ambiance bien particulière. Merci d'avoir répondu aussi nombreux à l'appel à la glace après ma rédaction de manuscrit. Et je garde un souvenir ému de la team GN1 quand on a démarré. Merci aux membres passés, présents et futurs de l'équipe MechanoDevo, et à tous mes cobureaux, Corentin, Leïa, Antoine et Zoé, pour votre soutien.

Merci aussi au département de biologie de l'ENS pour la formation pré-thèse mais surtout pour l'opportunité d'enseigner en thèse. J'ai énormément apprécié cette expérience, et je tiens ici à remercier mes collègues d'enseignement. Avant tout merci à Aurélie Vialette, tu m'as beaucoup appris en pédagogie et ton enthousiasme m'a aidé au quotidien. Merci à Christophe Trehin, Christine Miège, Cendrine Moskalenko, Pradeep Das, Nathalie Depège-Fargeix, Nathalie Alazard, Gilles Christoph et Sabine Remanofsky, Laurence Belgarbi-Dutron, Florence Lormières et François Roudier. Je me souviens de votre encadrement quand j'étais élève, surtout les « planteux » du lot que j'ai vu plus souvent que la moyenne, et vous découvrir « de l'autre côté » a été un grand plaisir pour moi.

Un grand merci à ma famille, qui m'a toujours encouragée à aller plus loin, et sans qui je ne serais pas là aujourd'hui. Merci à mes parents d'être toujours présents, dans les bons moments comme dans les moments de stress qui peuvent arriver en thèse. Merci à mes

grands-parents d'aussi bien comprendre mes manques de temps et états d'âme. Merci à mes sœurs qui me font passer par toutes les émotions mais le plus souvent me font rire et dans tous les cas me changent les idées. Merci à Benoit mon parrain, et à Kalie, vous êtes un support sur lequel je peux compter. Merci à ma future belle famille pour leur accueil chaleureux. Je suis fière de vous présenter à tous mon travail, et j'espère que je serai assez claire pour que vous le compreniez.

Je voudrais aussi remercier mes amis du labo et d'en-dehors. Les gens de la danse, des brookies, le nouveau gang, Lokifer, la coloc géante, et tous les autres, vous avez été un soutien constant. Nous avons partagé des moments forts ces dernières années, et j'espère que les changements à venir vont encore nous rapprocher.

Enfin merci à toi Emile. Pendant ces trois ans, tu m'as vu passer par tous les états et tu as été là dans tous les cas. Tu m'écoutes et me consoles, tu me fais rire et tu me calmes. Tu m'apprends à accepter de ne pas toujours dépasser mes limites, merci de jouer au petit diable sur mon épaule.

RDPiade 2019

Résumé

Si les multiples réponses des plantes à la sécheresse sont bien documentées, comment une plante intègre l'ensemble de ces informations reste mal connu. Durant ma thèse, j'ai testé la contribution des signaux mécaniques. Les cellules végétales sont gonflées par une pression osmotique importante à laquelle elles résistent grâce à une paroi rigide. J'ai montré que, parmi un ensemble de récepteurs moléculaires, le récepteur FERONIA est nécessaire à l'intégrité mécanique des cellules, et donc à la réponse des cellules à leur propre pression osmotique. Chez le mutant *feronia*, les cellules de l'épiderme explosent suite à une tension trop importante de leur paroi. Alors que le renforcement de la paroi en réponse aux contraintes mécaniques pourrait passer par la réorientation des microtubules et le guidage du dépôt des microfibrilles de cellulose, j'ai montré que FERONIA n'est au contraire pas nécessaire à la réponse des microtubules aux contraintes mécaniques. Il existe donc deux voies distinctes maintenant l'intégrité mécanique des cellules végétales, une passant par FERONIA, et une autre passant par les microtubules. J'ai ensuite cherché à disséquer les processus associés à la réponse de FERONIA, notamment en caractérisant les propriétés mécaniques, hydrauliques et biochimiques de la paroi chez le mutant. Ces études ouvrent un nouveau champ de recherche, le mechano-eco-sensing, c'est-à-dire la perception de l'environnement par une voie intégratrice, la mécanotransduction, et ses implications pour adapter la croissance en conséquence.

Abstract

While the many responses of plants to drought are well documented, how plants integrate them remains poorly understood. During my PhD, I tested the contribution of mechanical signals in this process. Plant cells are inflated by water, creating a high turgor pressure to which they resist thanks to their stiff cell wall. I showed that, among a set of molecular receptors, the FERONIA receptor is necessary to maintain the mechanical integrity of plant cells, and therefore for the response of cells to the mechanical stress caused by their own turgor pressure. In the *feronia* mutant, epidermal cells burst due to excessive tension in their cell wall. While the reinforcement of the wall in response to mechanical stress usually happens through microtubule reorientation and guidance of the deposition of cellulose microfibrils, I showed that FERONIA is not necessary for the microtubule response to mechanical stress. There are therefore two distinct pathways maintaining the mechanical integrity of plant cells, one involving FERONIA, and another one involving microtubules. I then tried to understand the processes associated with the FERONIA response, in particular by characterizing the hydraulic properties of the mutant, as well as the mechanical and biochemical properties of the wall in the mutant. These studies open a new field of research: mechano-eco-sensing, i.e. the perception of the environment through an integrative pathway, mechanotransduction, and its implications for adapting growth accordingly.

Table of contents

Table of contents

Introduction

As Lewis Wolpert puts it, “it is not birth, marriage, or death, but gastrulation which is truly the most important time in your life” (1986). Beyond humans, development involves many regulated processes from the fertilized egg to the mature adult to generate all living shape and function. In parallel to these intrinsic controls, environmental conditions contribute as instructive cues through developmental plasticity: variations in phenotypes (shape, size, behaviour, etc.) at different scales, adapting growth to local environmental cues. The nematode *Pristionchus pacificus* for example can present two different mouth forms allowing either strict bacterial feeding or predation on other nematods (Figure 1A). The future adult mouth form is selected during the early development of the nematode, in a process depending on the culture conditions (Sieriebriennikov and Sommer, 2018). Indeed, the variation in the mouth shape is tightly regulated by environmental signals, including the diet composition and pheromone profile. In plants, developmental plasticity is particularly spectacular as most of plant development is post-embryonic. As such, developmental plasticity occurs all along the plant life, which allows for adaptation to an ever-changing environment. An example of that can be found in phototropism: plants usually grow towards a light source even after perturbations and sometimes in a gravity-defying manner (Liscum et al., 2014) (Figure 1B). This example also highlights the importance of developmental plasticity for fixed life. In particular, plants being sessile organisms (i.e. lacking mobility), in essence they have to face environmental conditions that can be transiently or more permanently far their optimum (Žádníková et al., 2015).

Developmental plasticity requires a way to detect different environmental factors and to integrate them into their own molecular networks. Plants are able to sense a wide range of biotic and abiotic environmental factors that impact their traits: light, pathogen attacks, temperature, drought, etc. For example, they are able to sense nitrate availability: nitrate can stimulate the expression of auxin receptor AUXIN SIGNALING F-BOX 3 (AFB3) to promote lateral root growth and inhibit primary root growth (Vidal et al., 2010), and nitrate transporters like NITRATE TRANSPORTER 1.1 (NRT1.1) can also transport auxin (Krouk et al., 2010). This also translates into shape changes in the shoot. In particular, the size of the pool of stem cells they can use to create new organs, in particular the size of their shoot apical

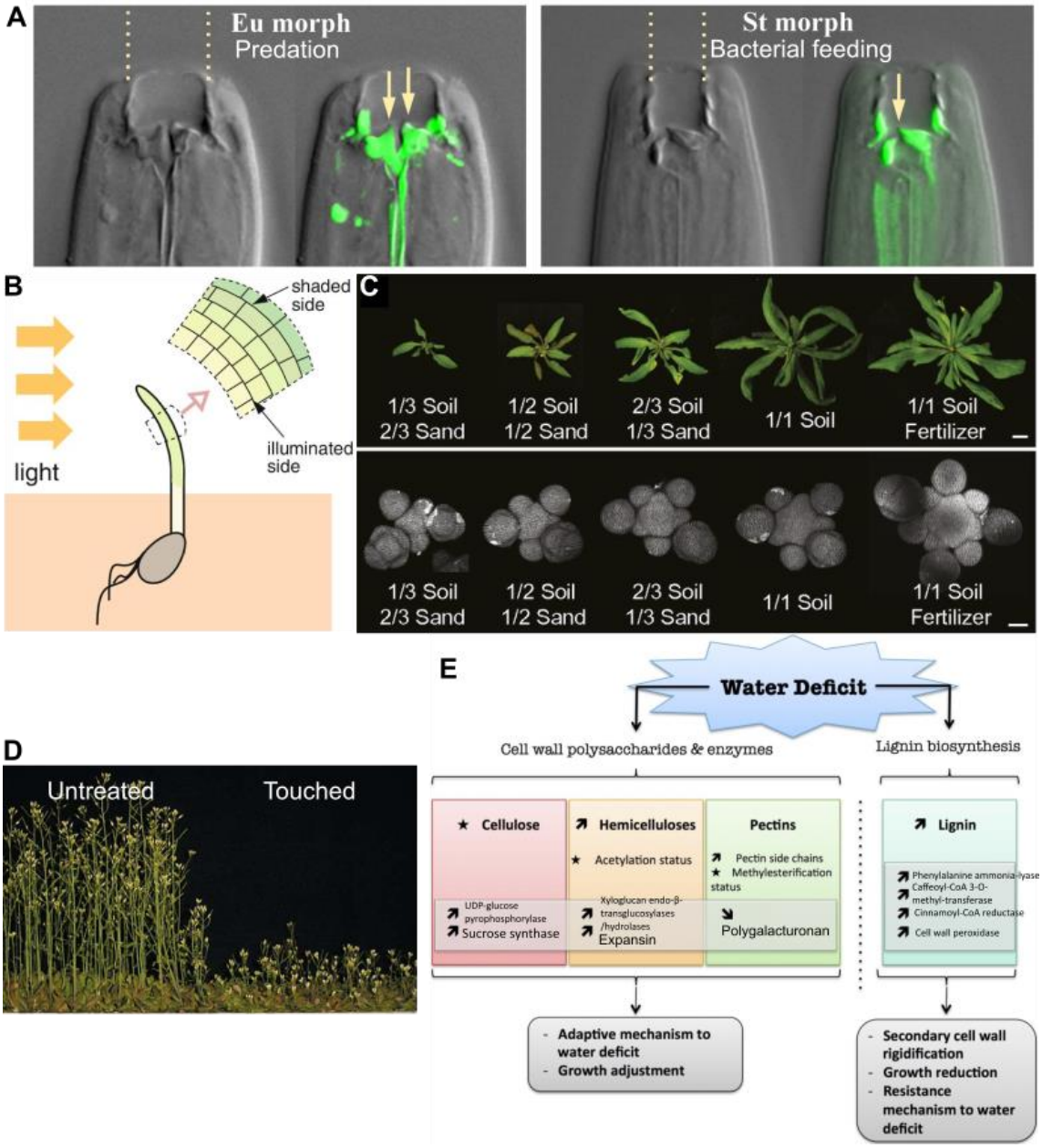

Figure 1: Several environmental signals are integrated for developmental plasticity. **(A)** *Adapted from (Sieriebriennikov and Sommer, 2018)*. Nematode mouth forms (fluorescence includes teeth, arrows point at the tip of teeth) depends on their environment and condition their alimentation mode (predation or bacterial feeding). **(B)** *Adapted from (Pietruszka and Lewicka, 2007)*. Plants can grow towards sources of light in a process called phototropism (involving auxin transport). **(C)** *Adapted from (Landrein et al., 2018)*. Nutrient availability conditions the size of the shoot apical meristem (down) and consequently of the rosette (up). **(D)** *Adapted from (Braam, 2005)*. Touching plants (here twice a day, right) leads to shorter and thicker stems compared to untreated plants (left). **(E)** *Adapted from (Le Gall et al., 2015)*. Arrows mean increased/decreased abundance and stars mean unclear evolution.

meristem (SAM), increases with the concentration of nitrates in the soil (Landrein et al., 2015) (Figure 1C). This modulates the weight of aerial organs produced, and in the long term adjusts the number and size of aerial organs to the available nutrient pool. Interestingly, this phenomenon is subject to fast changes and can mediate the size of the SAM through cytokinin signaling within one day.

As D'Arcy Thompson noticed, to study development is to study the evolution of shape in time (Thompson, 1942). D'Arcy Thompson inspired the revolution that has been quantitative biology with morphometry (Gregor, 2017): biological processes can be studied as dynamic geometry with precise measurement (of area, length, curvature, etc.). But geometry alone lacks active forces to explain morphometry, and molecular biology cannot answer certain questions at the organ scale. Integrating them with physics is then a more complete way to understand the creation of shape. Biological systems can be studied as subjects of mechanical forces, with mechanical characteristics and reactions to forces. As molecular principles explaining plant development have been and still are studied in great details, I chose to focus on the domain of biomechanics, even when dealing with complex signaling pathways (and even more so in an attempt to deal with complex signaling pathways).

The response to mechanical forces is a central part of developmental plasticity in plants. If some plants display a fast and dramatic response to mechanical stimuli, such as the closing trap of the Venus flytrap (*Dionaea muscipula*) (Forterre et al., 2016) or the folding leaves of the sensitive plant (*Mimosa pudica*) (Toriyama and Jaffe, 1972), plants constantly integrate external mechanical factors without displaying such remarkable responses. For example, roots are thought to sense drought in the soil before water runs out, i.e. through the progressive stiffening of the soil (Whitmore and Whalley, 2009). Beyond their response to soil stiffness, most plants display a gradual morphogenetic response to touch, stimulated by wind, rain, or rubbing: their shoot gets shorter and thicker (Braam and Davis, 1990; Jaffe, 1973) (Figure 1D). This response is called thigmomorphogenesis and is accompanied by the activation of touch response *TOUCH (TCH)* genes*,* transient calcium waves and pH decrease, and leads to phenotypic adaptations, either through tissue stiffening or instead increased flexibility (Braam, 2005).

Plants can also integrate internal mechanical forces. For example, trees adapt their radial growth to their own weight (Alonso-Serra et al., 2020), and create a stiffer kind of wood

called tension wood on bending stems (Donaldson and Singh, 2016; Sawada et al., 2018). Note that in this case, gravity plays a major role, and thus this form of proprioception (perception of one's own shape) integrates an environmental cue. More strikingly, plant cells generate their own internal pressure caused by water intake, and they constantly resist it since the cell wall is continuously synthesized and remodelled to avoid mechanical failure (Malivert et al., 2021). Note again that this form of mechanosensing involves external variables (water availabibility, osmotic conditions, etc.).

Although development of living organisms is usually seen as controlled by genes, morphogens or hormones in biology textbooks, it appears that such so-called developmental "programs" have to cope with many environmental factors. This apparent discrepancy is most obvious in plants, when compared to mammals: the final architecture of an oak tree will highly depend on its local environment, while the shape of its flower will not. How can plants sense environmental cues? Where does the robustness of intrinsic molecular networks come from, e.g. to reach similar shapes no matter how the environment changes? Could mechanical forces play an integrating role in morphogenesis? Because it is the cause of mechanical stress in young, developing, plant tissues, in the following parts, I will focus on turgor pressure and its role in plant development, using angiosperms (i.e. plants bearing flowers and producing seeds) as model systems. I will study these questions at different scales: the scale of the cell, of the tissue and of the organ.

I◦ The central cause of mechanical stress: turgor pressure

The evolutive strategy adopted by many organisms – amongst which the ancestors of plants – to regulate water intake, was to create a cell wall surrounding the inflated protoplast (inner part of the cell surrounded by the plasma membrane) and preventing explosion. Multicellularity generated other challenges and protection in water management, notably by allowing the formation of osmotic gradients within tissues. Water uptake and water transport reached another milestone during evolution in vascular plants colonizing emerged land, as a mean of photosynthesis, support and growth (Wolf, 2022). Today, in an anthropocentric view, the regulation of water is particularly important in agriculture, where most crops are vascular plants, most of them also being annuals, i.e. very sensitive to water fluctuations (Figure 1E). In particular, water stress (caused by drought, salinity, wind and extreme temperatures) is one

of the principal causes of crop loss worldwide (Wang et al., 2003b). As water stress is a growing danger with climate change, understanding the control of water uptake by plants is an ever more so relevant issue (Ndoye et al., 2022).

I.1◦ Osmotic pressure, cell wall mechanical properties and turgor pressure

The absorption of water by plant cells is determined by the osmotic pressure Π, which is proportional to the concentration of solutes. Osmotic pressure is often represented using the case of a container divided by a semi-permeable membrane in two parts with different solute concentrations. The semi-permeable membrane is, by definition, permeable to water but not to the solutes present in the two compartments. In this experiment, water moves to the compartment with the highest concentration of solute (Figure 2A). The difference of osmotic pressure between the two compartments corresponds to the hydrostatic pressure needed to stop the flow of water. More precisely:

$$\Pi = R * T * c_M * i \qquad \text{(equation 1)}$$

with R the molar gas constant at 8.32 $J{\cdot}K^{-1}{\cdot}mol^{-1}$, T the temperature (in K), c_M the molar concentration of solute (in $mol.L^{-1}$), and i the Van't Hoff index, which takes into account the actual number of particles when a substance is dissolved (e.g. 1 for sucrose, 2 for NaCl). Equation 1 shows that, in the case of two neighbouring compartments, osmotic pressure only depends on one variable, the product $c_M * i$, also called osmolarity.

The same phenomenon happens in living cells, for which water is driven to the compartment with the highest osmotic pressure (and thus highest osmolarity), whether it be a cell or the medium (Figure 2A). When placed in a medium where water leaves the cells, the medium is considered hypertonic and hyper-osmotic. Note that the use of the terms hypertonic and hyper-osmotic relate to different objects while reflecting comparable situations: hypertonic describes water behaviour (and so water potential, described later) whereas hyper-osmotic relates to osmolarity. They can differ slightly due to membrane permeability, depending on the solute (Caon, 2014). While other definitions invert those two meanings, I will keep the first one for this part. In the following paragraph, I will discuss idealized cells with solutes passing freely through the membrane, in which tonic behaviour is equal to the osmotic behaviour. In this case, a hypertonic medium exhibits a higher osmolarity than that of the cells. This leads to cell plasmolysis: the protoplast shrinks and detaches from

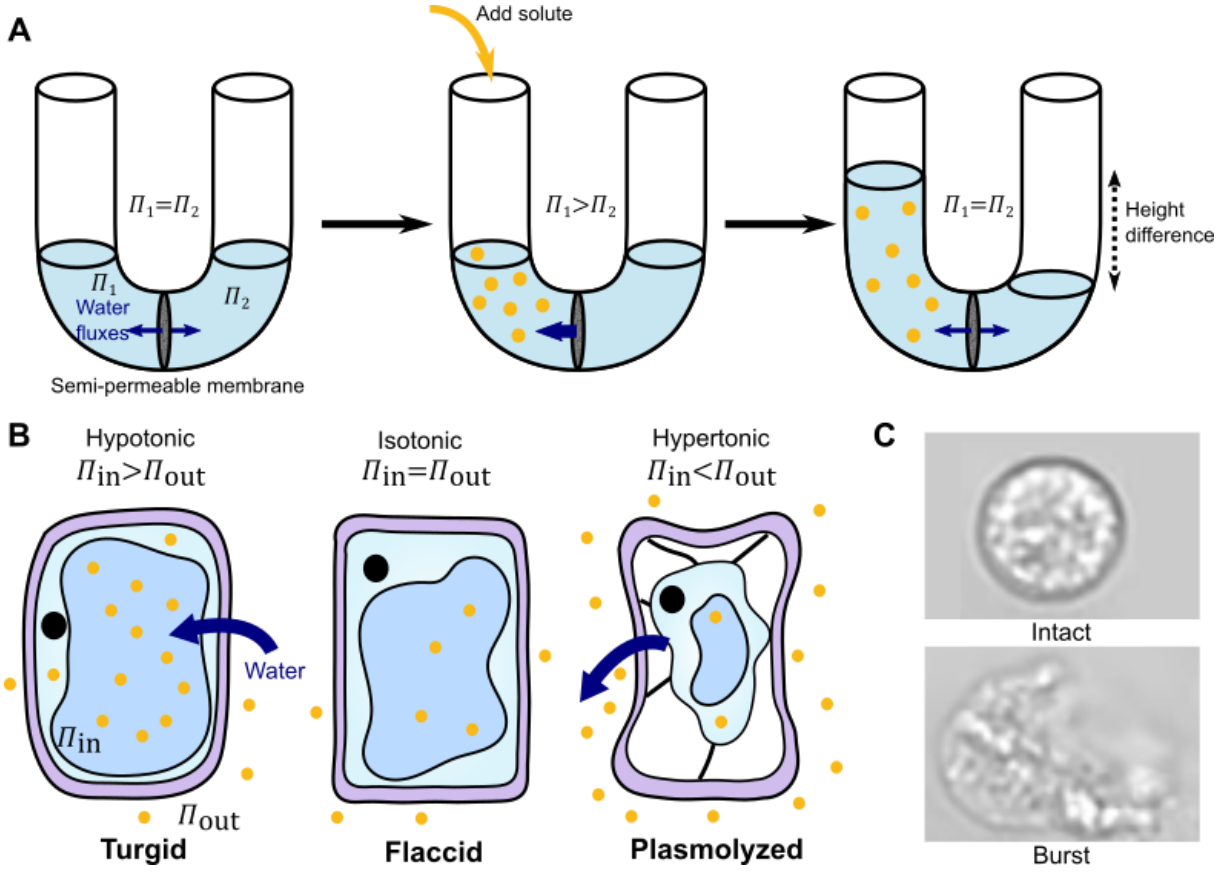

Figure 2: Water is attracted to the compartment with the highest osmotic pressure. **(A)** In a tube separated into two compartments by a semi-permeable membrane, water will flow to the compartment with the highest osmotic pressure, i.e. the one with the most solutes. The solution height difference between the two compartments can be used to calculate the difference between their osmotic pressures. **(B)** When the osmotic pressure of a plant cell is higher than the one of its medium (hypotonic medium), the cell attracts water and swell: it is turgid. The cell is flaccid when there is no exchange of water, i.e. isotonic medium. In a hypertonic medium with a higher osmotic pressure than in the cell, water flows out and the protoplast shrinks and detach from the cell wall: the cell is plasmolyzed. **(C)** *Adapted from the youtube video* (Osmotic burst of blood cells, 2012). In a hypotonic medium (e.g. pure water), a red blood cell attracts water and swell to the point of bursting.

the cell wall (Figure 2B). Decreasing the concentration of solutes in the medium can bring it to the same osmolarity as the one in the cells. No movement of water is generated by differences in osmotic pressures and cells are then considered to be in an isotonic environment (Figure 2B). In growing tissues, plant cells have a high concentration of solutes and thus a high osmolarity compared to their environment. They absorb water and become turgid (inflated) thanks to a hypotonic environment and the ability of the wall to resist such pressure (Figure 2B). The same behaviour (water uptake and turgescence) is observed in all kingdoms in hypotonic environments. However, in absence of cell walls (e.g. in red blood cells), cells ultimately burst because of the lack of a peripheral mechanical protection (Figure 2C).

In contrast, plant cells do not generally burst, even when placed in a highly hypotonic medium e.g. pure water. This is due to the presence of a stiff cell wall, a composite extracellular compartment made of polysaccharides (cellulose, hemicellulose, pectins) associated with some proteins and solutes (Cosgrove, 2005). Even if the osmotic pressure of plant cells is similar to animal cells (~150-500 mOsm) (Batchelder et al., 2011; Durand-Smet et al., 2014), plant cells are generally surrounded by a hypo-osmotic environment, their cell wall: the difference in osmotic pressure between the protoplast and the apoplast in plant cells is in the range of 0.6–1.0 MPa (Schopfer, 2006).

Due to their relative hyperosmolarity and the resulting swelling, protoplasts exert pressure forces onto the cell walls. At mechanical equilibrium, these forces are balanced by the rheological (or visco-elastic) response of the walls. The force exerted on the cell wall results in a pressure, called the turgor pressure (noted *P*). Under normal conditions, plant cells are generally turgid, with a high turgor pressure. As such we can model a plant cell as an inflated balloon – with air for a balloon and with water for a plant cell – with the envelope of the balloon representing the plant cell wall. The same occurs at larger scale: since the epidermis in most aerial tissues is under tension (Kutschera and Niklas, 2007). Therefore, in a very simple model, the balloon analogy can be applied at the scale of an organ and organism. It follows that turgor pressure plays the role of a hydroskeleton: a turgid plant stays upright, by opposition to wilted plants in water stress.

At equilibrium, turgor pressure is numerically is equal to the difference in osmostic pressure between the cell and the environment, assuming that the environment is at atmospheric pressure (so in the order of 1 MPa). However, during growth, we can most often

consider that it is not the case. It is thus more pertinent to relate osmotic pressure and turgor pressure through water fluxes, using a descriptor for water behaviour called the water potential (noted Ψ):

$$\Psi = P - \Pi \qquad \text{(equation 2)}$$

In a medium with non-dissolved aggregates (like colloids in soil), a component called the matric potential, due to the adhesion of water to those aggregates, must be added to the water potential. It is generally ignored in the case of plant cells, but may play a role in the cell wall. Similarly, in plants with tall aerial structures, a gravimetric component can be added. In herbaceous plants, the pressure due to aerial tissues is not significant (contrarily to tall plants) especially at the tissue scale. Thus, it is usually ignored. A hygrometry potential can also be added, but it should not change between two neighbouring compartments, so it can also be omitted.

More precisely, Fick's law of diffusion describes water fluxes between two compartments separated by a membrane using the water potential:

$$J_{1\to2} = -D * S * \frac{\Delta\Psi_{1\to2}}{\delta} \qquad \text{(equation 3)}$$

with $J_{1\to2}$ ($m^3.s^{-1}$) corresponding to the flux of water from the compartment 1 to the compartment 2, *D* the diffusion coefficient ($m^2.s^{-1}$), *S* the surface of diffusion, δ the membrane thickness and $\Delta\Psi_{1\to2}$ the difference of water potentials between the two compartments. At equilibrium, when there is no flux of water, $\Delta\Psi_{1\to2} = 0$ (Figure 3A). Water flows from the compartment 1 to the compartment 2 for positive values of $J_{1\to2}$ and thus for negative values of $\Delta\Psi_{1\to2}$ i.e. for $\Psi_2 < \Psi_1$ (Figure 3B). By integration into equation 2, this corresponds to low turgor pressure (e.g. low stiffness of the cell wall) or a high osmotic pressure (e.g. high concentration of solutes inside the cell) in the compartment 2 compared to the compartment 1 (Figure 3C). To rephrase it, osmotic pressure drives water intake in a cell while turgor pressure opposes it, with the difference between the two (evaluated by the water potential Ψ) expressing where the tipping point is. Turgor pressure exerted on the cell wall engenders a tension in the cell wall (around 10-50 MPa (Cosgrove, 1993)), that the cell has to resist to keep its mechanical integrity: for example, by reinforcing the cell wall or by decreasing the turgor pressure.

Open questions:

- How to visualise water fluxes in vivo?
- What is the water content in the cell wall?
- What role does the composition of the cell wall play on water behaviour?

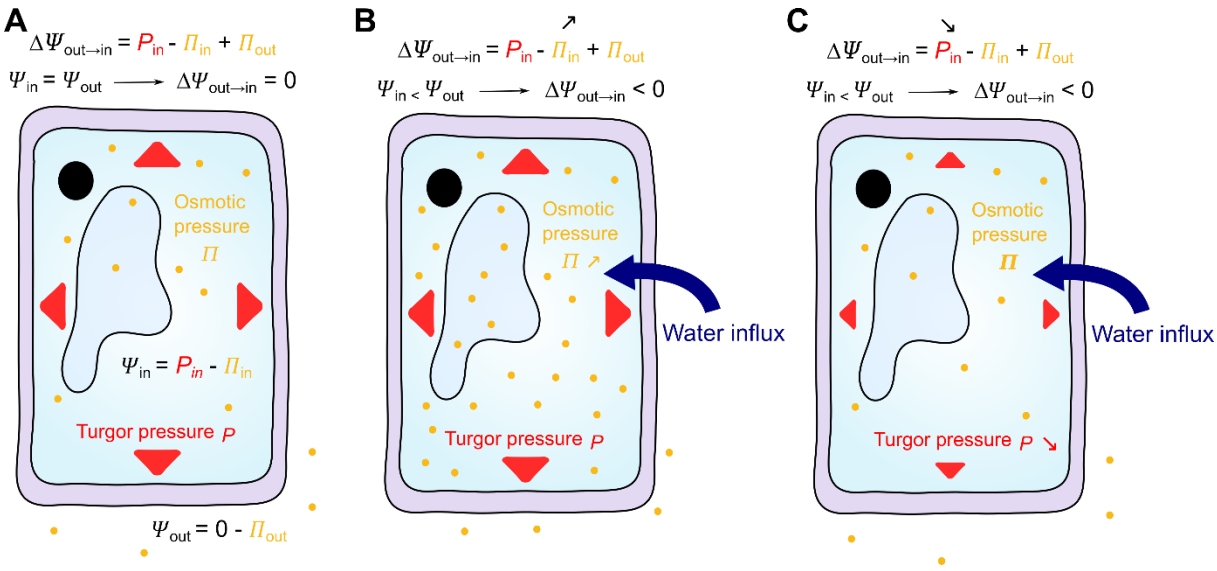

Figure 3: Water is attracted to the compartment with the lowest water potential Ψ. **(A)** If the cell is at equilibrium with the medium, $\Delta\Psi_{out\rightarrow in} = 0$ and there is no water flux. **(B, C)** When the difference of water potential between the cell and the medium is negative, i.e. when $\Delta\Psi_{out\rightarrow in} < 0$, water enters the cell. This can be caused by (B) a higher difference of osmotic pressure (higher *Π* in the cell) or (C) a lower turgor pressure *P* in the cell.

I.2◦ Measuring cell mechanical properties

The cell wall being a composite material with various components, the biochemical composition of the cell wall largely determines its ability to respond (deform or resist) to changes in cell volume due to water fluxes. Thus, knowing the biochemical composition and the physical organization of the components of the cell wall *in situ* can help estimate the mechanical properties of the cell wall. To do so, a wide array of tools can be used: optical microscopy after staining with generic dyes (Bidhendi et al., 2020) or more specific cell wall probes (Rydahl et al., 2018), immunostaining of specific cell wall components (Haas et al., 2020), Mass Spectrometry (Bauer, 2012), Nuclear Magnetic Resonance (NMR) spectroscopy (Yeats et al., 2016), Raman spectroscopy (Mateu et al., 2020). However, these analyses are usually more relevant to address the molecular mechanisms by which the cell is reinforcing its cell wall, but do not provide mechanical measurements. In fact, several reports revealed counterintuitive results. For instance, the *xyloglucan xylosyltransferase 1/2* (*xxt1xxt2)* double mutant which does not produce xyloglucans, as shown by immunostaining, exhibits a WT-like phenotype, despite the supposed role of xyloglucans in tethering cellulose microfibrils (Cavalier et al., 2008).

The mechanical properties of the cell wall can be measured more or less directly and at different scales (Geitmann, 2006; Vogler et al., 2015). Extensometer assays on *in vitro* (Doineau et al., 2021) and *in vivo* (Wei et al., 2006) material relate a force *F* and a deformation *d*, which through Hooke's law (*F = kd*), can lead to the stiffness *k* (Figure 4A). Depending on the set-up and applied force, other mechanical parameters can be determined, like the strength (the point of rupture), the shear modulus (a measure of the resistance of the material to shear deformation) and the dynamic viscosity of the material. Such methods provide global average of a tissue, with a bias induced by cell geometry and tension (Majda et al., 2022).

Recently, a label-free spectrometry method to measure a material mechanical properties has been developed, first for animal cells (Scarcelli et al., 2015) and then for plant cells (Elsayad et al., 2016). Its principle is based on Brillouin light scattering: the encountering of an acoustic wave by a light wave (a laser beam) alters the frequency and energy of the light wave (Antonacci et al., 2020) (Figure 4B). The emitted Brillouin spectrum depends on the viscoelastic properties of the material and can be interpreted to obtain the viscoelastic

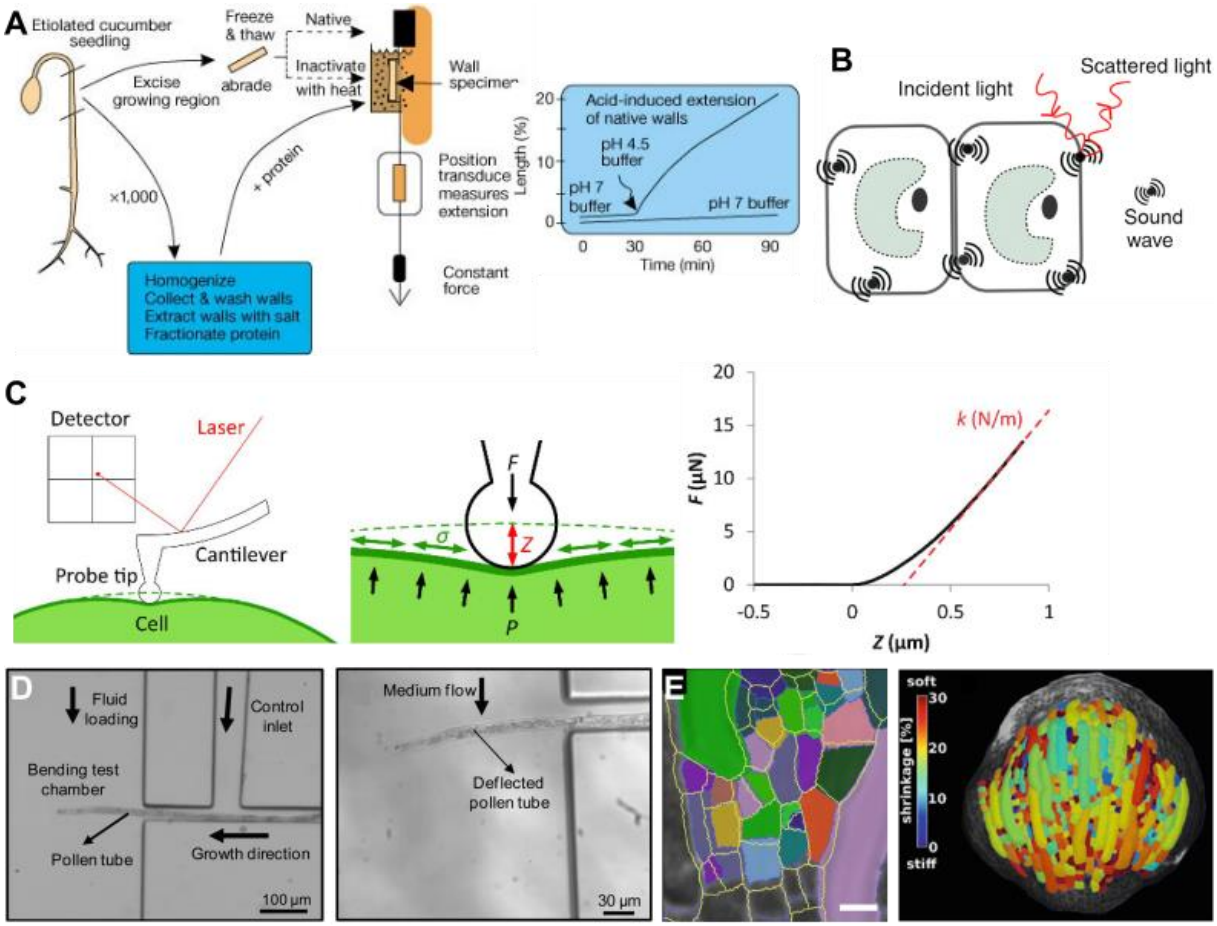

Figure 4: Methods to measure cell wall mechanical properties. **(A)** *Adapted from (Cosgrove, 2000)*. Here an extensometer assay is used with a fragment of cell wall to determine the effect of pH on mechanical properties. **(B)** *Adapted from (Trinh et al., 2021)*. In Brillouin microscopy, the scattering of light by sound waves is used to determine the viscoelastic properties of the cell. **(C)** *Adapted from (Verger et al., 2018)*. With local indentations, the deformation caused by the pressure of a probe tip can reveal the cell wall mechanical properties as well as turgor pressure. **(D)** *Adapted from (Nezhad et al., 2013)*. With this device, pollen tubes grow into a flow that can deform them, depending on its resistance. **(E)** *Adapted from (Sapala and Smith, 2020)*. The reduction in size that comes with plasmolysis (left) reveals a shrinkage (right) depending on the cell wall mechanical properties.

signature of the cell wall, the cellular hydrostatic pressure and the cytoplasm viscoelasticity (Elsayad et al., 2016). This quantitative technique has been able to establish the molecular receptor THESEUS1 (THE1) as a regulator of cell wall mechanical properties (Bacete et al., 2022), despite the difficulties inherent to the interpretation of heterogeneous materials.

To acquire information at a finer scale, local indentation techniques can be used (Figure 4C). When using nanoindentation (Verger et al., 2018) and microindentation (Peaucelle et al., 2011) techniques, the sample is in contact with a tip (indenter) which applies a force amenable to indent the cell in the nm to the µm range. The force *F* necessary to create a deformation *d* can yield the apparent cell wall elastic modulus *E* (related to Young's modulus in material science, a measure of the resistance of a material to tension/compression with $E = \frac{\sigma}{\varepsilon}$, see Box 1) and of the apparent stiffness of the material *k* (with $k = \frac{F}{d}$) (Beauzamy et al., 2015b; Bovio et al., 2019). Note that *E* relates to deformations along an axis, with the actual measurement happening on a single point in 1D. It follows that for a heterogeneous material, an average elastic modulus *E* can be deduced only when measuring at multiple positions. Note that indentation methods measure the mechanical properties in the orthogonal direction to their relevance to the cell, and as such should be considered carefully.

Wall properties can also be extracted by measuring the wall deformation in response to changes in cell volume. For instance, cell wall mechanical properties have been inferred by observing the deformation of the pollen tube in microfluidic devices where the osmolarity of the medium can be controlled (Nezhad et al., 2013) (Figure 4D). Another method consists in bathing a protoplast, a tissue or an organ into solutions with increasing concentrations of a solute (successive plasmolysis), which leads to its deformation due to water fluxes. This deformation has been modelled, and can be interpreted to get an estimate of the osmotic pressure, of cell wall mechanical properties, and of the turgor pressure (Sapala and Smith, 2020) (Figure 4E).

Conversely, measuring wall properties through osmotic changes requires a precise assessment of the osmolarity of the medium. This can be done with various kinds of osmometers: (i) in membrane osmometers, the osmolarity can be deduced from the difference of water height between two compartments separated by a semi-permeable

Box 1:

Water intake in a cell with a stiff cell wall generates turgor pressure, which in turn puts the cell wall under tension (*F*). Because the same tension will have less impact on wall deformation if the wall is thicker, mechanical stress, σ is introduced to normalize the force by the surface area (*A*, here the section of the wall) on which it is applied:

$$\sigma = \frac{F}{A} \qquad \text{(equation Box 1.1)}$$

with *F* the force applied stretching the cell wall and *A* the area of a section of the cell wall on which the stress is applied to (*adapted from (Mirabet et al., 2011)*).

To grasp what tensile stress really represents, it can be described as the force per unit surface needed to bring together the two edges of a cut on the cell wall in a model where the inner pressure would stay the same (Boudaoud, 2010). Tensile stress can be related to the strain ε, i.e. the deformation ($(l-l_0)/l_0$ with l_0 the length before deformation and *l* the length after deformation) and therefore can be calculated:

$$\sigma = E * \varepsilon \qquad \text{(equation Box 1.2)}$$

with *E* elastic modulus (see Introduction ◦ I.2). This way, the tensile stress applied to the cell wall by the turgor pressure can be measured in real life experiments using a measure of the deformation.

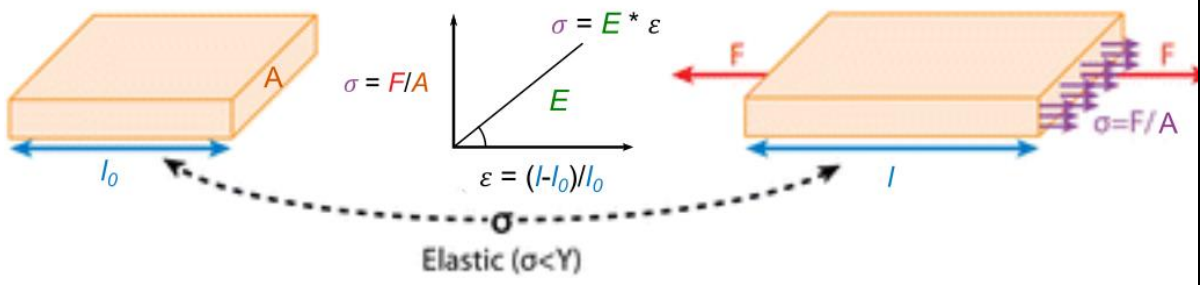

Adapted from (Mirabet et al., 2011).

membrane (Figure 2A), (ii) in cryo-osmometers, the freezing point of a solution (decreasing when the concentration of solutes increases) is measured to deduce its osmolarity and (iii) in vapour osmometers, the gas pressure of the liquid solution is in equilibrium with its own vapor, providing its osmolarity and which, compared to a cryo-osmometer, avoids artefacts due to viscosity.

However, none of those methods can measure the osmotic pressure inside a living cell and indirect methods have to be used for estimation. As discussed above, successive plasmolysis can give an estimate of the osmotic pressure in a cell or an organ. Another method to evaluate the osmotic pressure is to extract cell contents and use one of the different kinds of osmometers previously described. Finally, after extracting cell contents, it is possible to measure the osmolarity of the sample by using a psychrometer i.e. a small chamber where the sample and the atmosphere reach saturation vapour pressure (Figure 5A). It is associated with a thermocouple on which a droplet of a known water potential is placed, and which creates an electrical current whenever experiencing temperature changes due to condensation/evaporation. This is a way to measure the water potential of the chamber, equal to the osmotic pressure of the sample extracted from cells. This last technique can also help to get a measure of the water potential of a tissue by putting it entirely into the psychrometer (Martinez et al., 2011). By adding the osmotic pressure to the water potential, both calculated with the same method, one can also deduce the global turgor pressure in the tissue.

The only direct technique to measure turgor pressure is to use pressure probes (Colombani and Forterre, 2011; Green, 1968), a challenging procedure because a microcapillary filled with oil has to be introduced into a cell (Figure 5B). The turgor pressure will move the oil inside the capillary, filling it with cell contents instead, and the pressure necessary to bring the oil meniscus back to the cell surface will correspond to the turgor pressure in the cell.

In addition to the indirect techniques for the measurement of turgor pressure seen above (indentation and successive plasmolysis), the use of a pressure chamber can be noted (Beauzamy et al., 2014) (Figure 5C). The device, also called Scholander bomb is composed of a chamber, in which an organ or the whole plant can be placed, with the cut shoot basis emerging from the chamber. When increasing the pressure inside the chamber, some sap starts to exude at the cut extremity, and the pressure reached at this moment is equal to the water potential. After measurement of the sap osmolarity and of the cell osmotic pressures

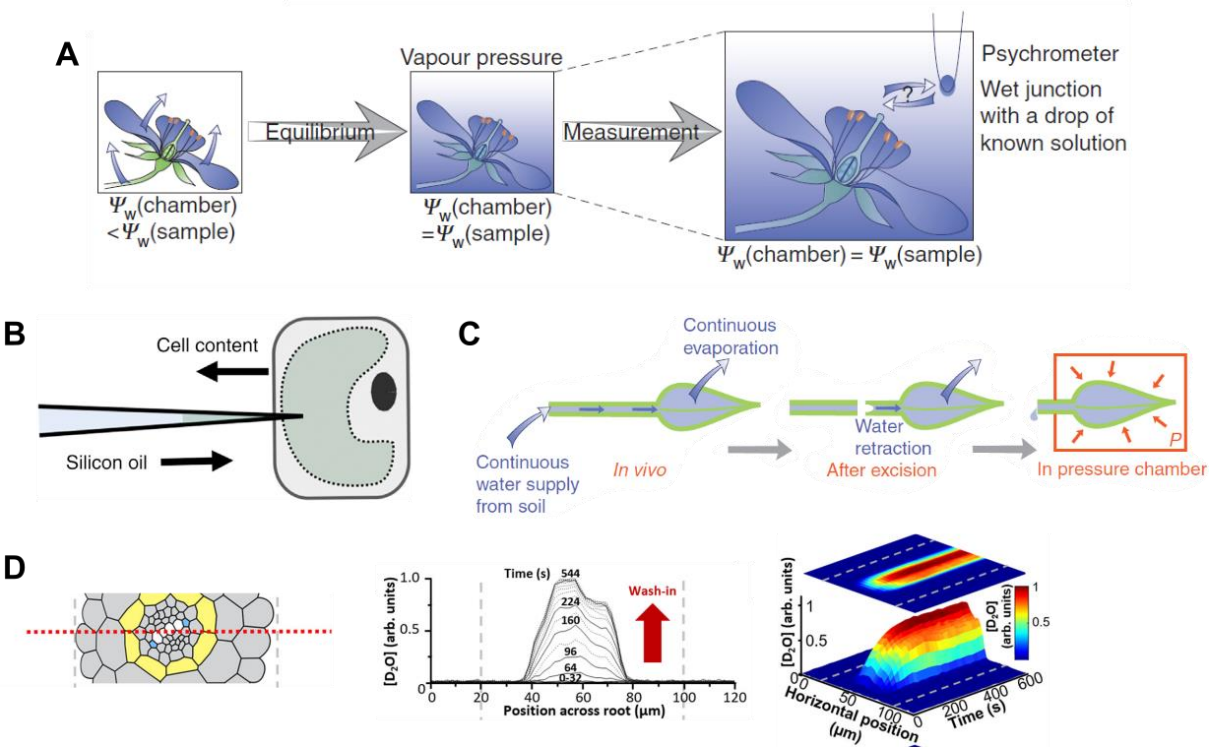

Figure 5: Methods to measure cell hydraulic properties. **(A)** *Adapted from (Beauzamy et al., 2014)*. Psychrometers give a measure of the water potential in a sample and as such can be used to determine its osmolarity. **(B)** *Adapted from (Trinh et al., 2021)*. The turgor pressure probe is a delicate instrument inserted directly into a cell to evaluate its osmotic pressure, using the pressure needed to keep cell contents out of the probe. **(C)** *Adapted from (Beauzamy et al., 2014)*. With a pressure chamber, the pressure exerted to see a drop appear at the cut section reveals the water potential in the sample. **(D)** *Adapted from (Pascut et al., 2021)*. Using Nuclear Magnetic Resonance and modelling, water fluxes can be monitored at the tissue scale.

(with sap and cell contents extractions followed by a test via an osmometer), the turgor pressure is deduced (Scholander et al., 1964).

For larger deformations, indentation techniques can also quantify the turgor pressure of a sample, using *k*, *E*, the thickness of the cell wall, and the local topography of the cell (Figure 4C). The rationale is that at larger indentation, the deformation also integrates the larger geometry and becomes less sensitive to local mechanical properties. To take an analogy, to measure the pressure of a car tyre, a large indentation will be necessary and will not give any information of the stiffness of the rubber.

Recently, a technique to observe water fluxes *in vivo* has been developed using Raman spectrometry. Raman spectrometry relies upon Raman scattering of light: when photons encounter components with molecular vibrations, the energy of the photons is shifted depending on the vibrational energy level of each component. In this technique, each molecule has its own signature and can be identified without the need for labelling, but analysing Raman spectrometry results is a challenge increased by the lack of repeatability. By associating it with modelling, water fluxes at cellular resolution were imaged in living *A. thaliana* roots (Pascut et al., 2021) (Figure 5D). This example is still however an exception and water fluxes remain rarely observed.

To quantify other mechanical properties, several fluorescent probes have been designed to be associated with optic microscopy (Colin et al., 2022). For example, the crowding in a cell is a measure of the concentration of molecules and how they interact with each other, affecting the viscosity and the diffusion of molecules. Crowding usually correlates with osmolarity and as such can be used as a proxy. Several crowding sensors have been designed using Förster resonance energy transfer (FRET) techniques: disordered sensors fluoresce at a certain wavelength and their crowding-induced folding modulate this fluorescence by interaction of two fluorophores (Boersma et al., 2015; Cuevas-Velazquez et al., 2021) (Figure 6A). Such sensors have been shown to be sensitive to osmolarity but certain cell characteristics (e.g. vacuole size) could also affect the measure. A range of tools to measure microviscosity has also been developed recently, for use in several plant structures (cytosol, vacuole, plasma membrane, cell wall) (Michels et al., 2020). The rotation of boron-dipyrromethene (BODIPY)-based molecular rotors depends on the viscosity of their surroundings and modulate their fluorescence lifetime (Figure 6B). Combined with Fluorescence lifetime imaging (FLIM), they

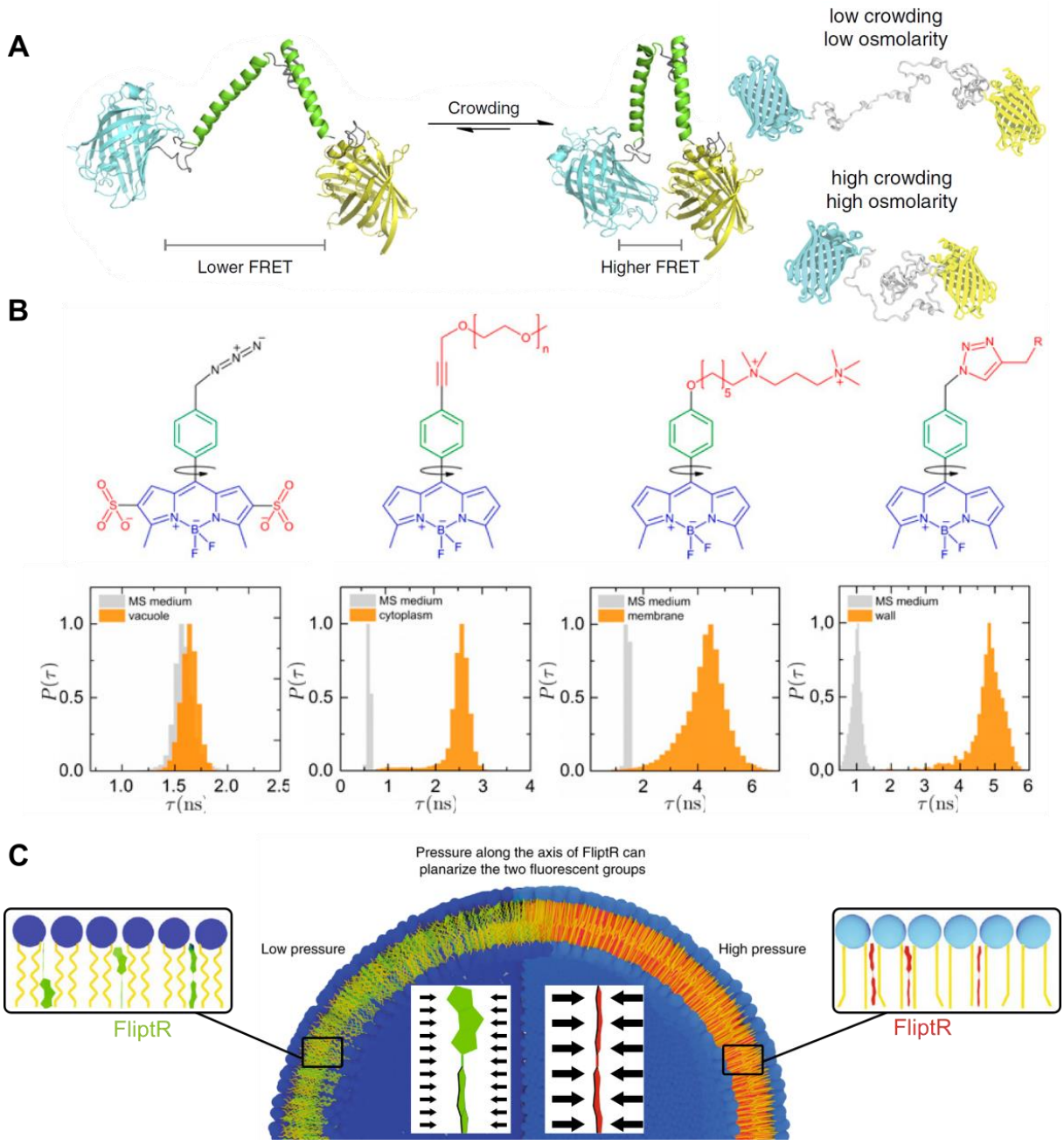

Figure 6: Molecular probes for mechanical stress. **(A)** *Adapted from (Boersma et al., 2015) (left), (Cuevas-Velazquez et al., 2021) (right)*. Molecular sensors for crowding rely on the crowding-dependent folding of a domain, which brings together two fluorophores interacting with FRET. **(B)** *Adapted from (Michels et al., 2020)*. Four different molecular sensors of microviscosity have been developed for use as a dye specific of different cell parts. The speed of their rotation (up) depends on the viscosity of their surroundings and affects their fluorescence lifetime τ (down). **(C)** *Adapted from (Colom et al., 2018)*. The planarization of the FliptR fluorophore is caused by membrane pressure, with an effect on its fluorescence lifetime.

can be used to detect properties linked to microviscosity such as membrane and cell wall tension. Another probe based on fluorescence lifetime provides a measurement of membrane tension: the membrane pression triggers the planarization of the Fluorescent lipid tension reporter (FliptR) protein, which changes its fluorescent lifetime linearly with membrane tension (Colom et al., 2018) (Figure 6C).

Another possibility to visualize mechanical forces in plant cells is to target the plant responses to mechanical stress. There is no fluorescent sensor derived from mechanosensors yet (Colin et al., 2022), but the cellular response to a mechanical stress includes a local influx of Ca^{2+}, a pH change, a microtubule reorientation or the expression of mechanosensitive genes. These reactions can be studied to investigate the response to mechanical forces.

Each of these techniques is biased and give different measures of the same parameter. For example, in the same set of experiments, a pressure probe inserted in a lily pollen tube gave a turgor pressure around 0.21MPa whereas measuring the turgor pressure of similar pollen tubes by plasmolysis produced a result around 0.79MPa (Benkert et al., 1997). It is thus best to use different techniques to have a range of behaviours, and keep the idea that all these measurements retain a large margin of error.

Open questions:

- Can molecular stretch sensors be used to deduce wall properties?
- Is it possible to develop a molecular sensor of osmolarity and turgor pressure?
- Knowing that different techniques give different measures of a same parameter, what are the values closest to real life mechanical characteristics?
- How to distinguish dynamic features from stable ones, e.g. wall modification under enzyme action vs. passive wall deformation)?

I.3◦ How do cells resist to turgor pressure?

As discussed in the previous paragraphs, a high concentration of solutes leads to water intake in plant cells, which triggers a pressure, called turgor pressure, pushing against the stiff cell wall. This results in a tensed cell wall resisting turgor pressure. That model is considering inert materials but what happens in growing cells, with sensing and feedback response? How

do cells maintain their mechanical integrity? Here we will focus the discussion on cells with a primary cell wall, which are the cells most susceptible to grow.

I.3.1◦ Controlling water influx

A cell increases its volume only thanks to an influx of water. According to Fick's law of diffusion (equation 3), out of equilibrium (during growth), this means either that the diffusion coefficient *L* increases (case A in Figure 7), or that $\Psi_{in} < \Psi_{out}$ with Ψ_{in} the water potential in the cell of interest and Ψ_{out} the water potential outside (case B in Figure 7).

Case A (the diffusion coefficient *L* increases): First, the diffusion coefficient can be affected by the two pathways through which water enters into a cell: (i) the symplasmic pathway, i.e. a continuum of cytoplasm between cells, and (ii) the apoplastic pathway, i.e. all intercellular spaces (including the cell wall, gas and water pockets).

(i) Symplasmic transport occurs through "pipes" across the cell wall joining two cells called plasmodesmata. Water and solutes (hormones, proteins, sugars, ions, RNAs, etc) smaller than the size exclusion limit can all travel through plasmodesmata, but plasmodesmata can still be highly selective in cell-to-cell transport in a process remaining unclear (Li et al., 2020; Zambryski and Crawford, 2000). The synthesis and degradation of callose polysaccharides in the cell wall seems essential to regulate plasmodesmata opening, and is controlled by biotic and abiotic stress as well as developmental cues (Amsbury et al., 2018; De Storme and Geelen, 2014). Other cell wall components such as pectins and cellulose, as well as cytoskeleton elements (Holdaway-Clarke et al., 2000) also seem to be involved in this process (Amsbury et al., 2018). However, whether the closing and opening of plasmodesmata affects water fluxes or not is still up for debate. Plasmodesmata have indeed been proposed to modulate water fluxes between cells in a process linked with osmotic pressure (Anisimov and Egorov, 2002) and affecting the turgor pressure (Hernández-Hernández et al., 2020). This is notably the case for cotton fibres, which rapid growth has been associated with a transient closure of plasmodesmata allowing a build-up of turgor pressure (Ruan et al., 2001). Plasmodesmata are even thought to act as mechanosensors, since they become closed upon pressure differentials (Oparka and Prior, 1992; Park et al., 2019). Such regulation may be instrumental to understand why neighbouring cells connected symplasmically through plasmodesmata can show different turgor pressures in tissues

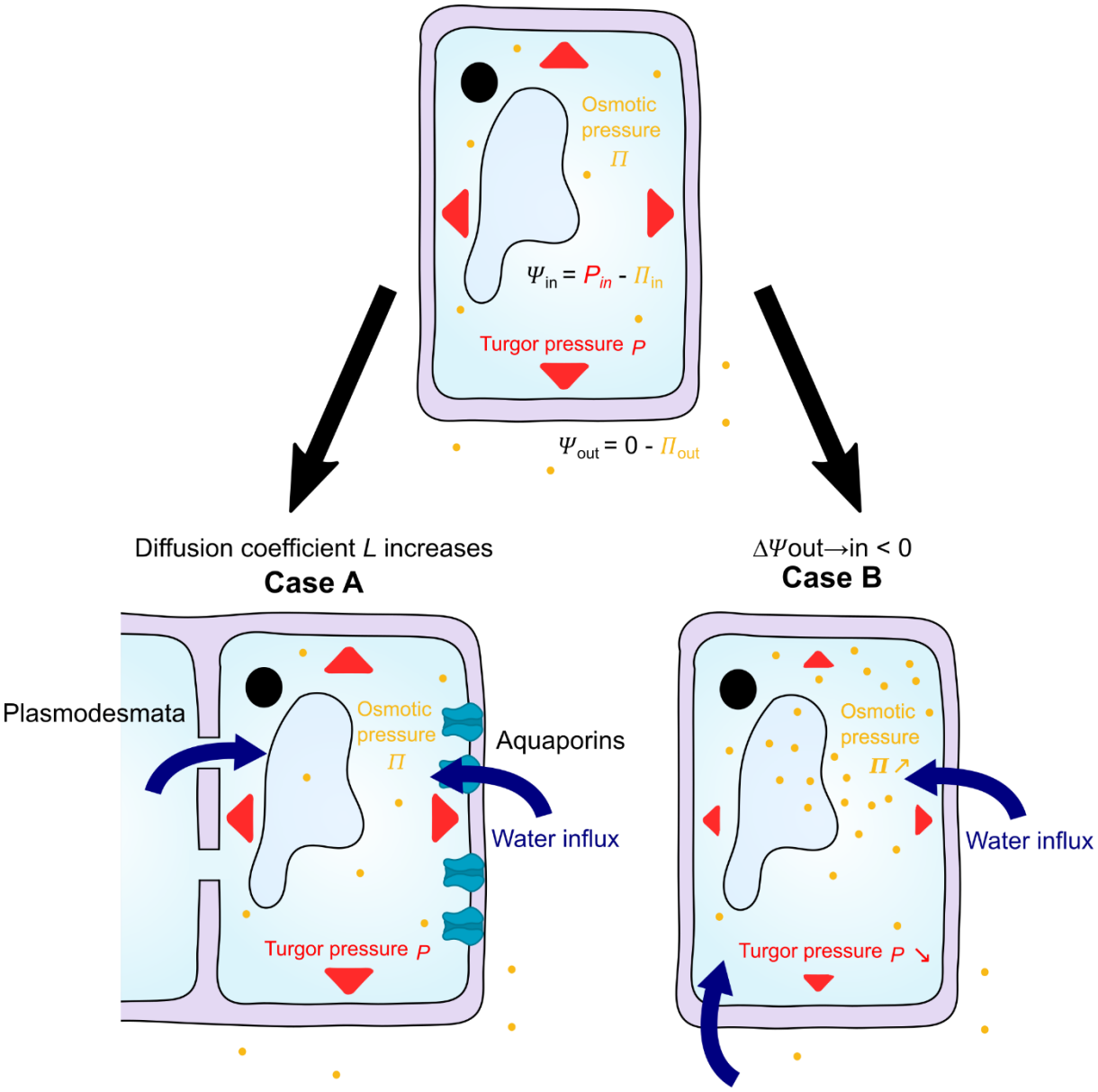

Figure 7: The regulation of water fluxes. Water influxes can be increased by: **(case A)** increasing the diffusion coefficient *L* through plasmodesmata opening or aquaporin regulation, or by **(case B)** reaching a negative difference in water potentials between the cell and the outside $\Delta\Psi_{out\rightarrow in} < 0$ through a decrease of the turgor pressure *P* or an increase of the difference of osmotic pressures $\Delta\Pi_{out\rightarrow in}$.

(Long et al., 2020; Rygol et al., 1993).

(ii) For apoplastic transport, water is mostly thought to flow freely in the apoplast, the cell wall being highly porous. In the cell wall, water fluxes can be restricted through the control of the water uptake surface area, with the deposition of a callose plug (e.g. pollen tube (Dumais, 2021)), or hydrophobic lignin and suberin, sometimes in specific structures (e.g. Casparian strips (Naseer et al., 2012)) in differentiated cells. Water can pass membranes either through diffusion, or through water channels called aquaporins (Maurel et al., 1993; Maurel et al., 2015). This large family is present on both the plasma membrane and the vacuole membrane, and can allow passive diffusion of water in an out of the cellthrough osmosis in both directions. Even though water may pass through plant membranes without aquaporins (Hill et al., 2004), they have been shown to play a primary role in water uptake (Chaumont et al., 2005; Ramahaleo et al., 1999). In particular, two loss-of-function mutants of different aquaporin isoforms display a reduced water conductivity by a factor up to 30% (Javot et al., 2003; Postaire et al., 2010). Aquaporin-dependent water transport can be regulated in two ways: in the expression and localisation of aquaporins, and in their activity (Chaumont et al., 2005; Kapilan et al., 2018). Aquaporin expression as well as activity seems to be altered by abiotic stress (salinity, drought, …) as well as pathogens and hormonal levels. Aquaporin phosphorylation appears to modulate water influx and may be a way to regulate their trafficking, as for mammalian aquaporins (Brown, 2003). Their trafficking also seems to be regulated by methylation, heteromerization and protonation (Kapilan et al., 2018). Gating (closing/opening) of aquaporins seems to be regulated by phosphorylation (keeping aquaporins open), by the formation of homomeres/heteromeres, by the second messenger calcium (Ca^{2+}), by pH, by protonation or by Reactive Oxygen Species (ROS) (Kapilan et al., 2018). Mechanical forces also appear to impact aquaporin activity, since aquaporins can close in the presence of high concentrations of solutes or pulses of turgor pressure (Wan et al., 2004; Ye et al., 2004). This may be due to tensile stress in the channel or conformational change due to water flow-linked energy. This would provide another function to aquaporins: detecting osmotic and pressure gradients (Hill and Shachar-Hill, 2015; Hill et al., 2004).

Case B ($\Psi_{in} < \Psi_{out}$): To reach $\Psi_{in} < \Psi_{out}$, plants can decrease the water potential Ψ_{in}. It is unclear whether plants can also affect the external water potential Ψ_{out} or not, for example by modulating the properties of the cell wall or even of the medium through the

transport of solutes. As little is known about this process, only Ψ_{in} will be considered in the rest of the paragraph. According to the water potential relation to osmotic pressure and turgor pressure (equation 2), decreasing the water potential Ψ_{in} means increasing the osmotic pressure Π or decreasing the turgor pressure P in the cell. Adjusting the cytosolic and vacuolar concentrations of osmotically active solutes (osmoregulation) can directly impact the concentration of solutes, which is directly proportional to the osmotic pressure (equation 1). For osmoregulation, plant cells mostly regulate the production and localisation of ions, sugars and amino acids in addition to the influx of water. Na^+, H^+ and K^+ and their counter-ions are transported through ion transporters proteins, which requires the consumption of ATP in the case of osmotic regulation. In addition to the transport of sucrose, production and breaking down of polysaccharides can modify the osmolarity of a cell. This mechanism is tightly regulated for photosynthesis regulation, cell growth, cell wall production, phloem transport and turgor control, in particular in case of a drought stress (Ozturk et al., 2021). Other cases of osmoregulation by combining several molecules have been observed, such as calcium oxalate crystals. The amino acid-dependent osmotic response to abiotic stress such as drought and salinity response seems to rely on proline regulation (Delauney and Verma, 1993; Hayat et al., 2012), which production is controlled by environmental stress (Szabados and Savouré, 2010). Note that vacuole storage of osmolytes does not create real differences in osmotic pressure between the cytoplasm and the vacuole because the membrane of the vacuole cannot sustain important turgor pressure. It is however an available reservoir of osmolytes and water for osmotic regulation.

In order for plant cells to regulate their osmolarity, they must first detect a change in osmolarity, i.e. have osmosensing capabilities. While the cell response to osmotic stress is well known, such sensing is poorly documented (Nongpiur et al., 2020). The sensors proposed would sense cell parameters changing in case of an osmotic stress: cell turgor, membrane deformation, protein hydration, composition of the membrane, cytoskeleton deformation, ion concentration, molecules interacting with a protein, etc (Poolman et al., 2002). Among osmosensors, we can cite the highly conserved two component systems formed of a histidine kinase (ARABIDOPSIS HISTIDINE KINASE) and a response receptor, able to complement osmoregulation mutants in *Saccharomyces cerevisiae* (Tran et al., 2007; Urao et al., 1999). Known or postulated mechanosensors have also been proposed to act as osmosensors due to

the mechanical deformations resulting from an osmotic stress (see Introduction ◦ III). Some possibilities include aquaporins, plasmodesmata, mechanosensitive channels and Receptor-Like Kinase (RLK) wall sensors. Finally, phospholipases C, which hydrolyses phospholipids and mediate lipid signaling, seem to be upstream of the mechanical stress-induced Ca^{2+} influx observed in response to water deficit (Li et al., 2017). This mechanism would follow several abiotic stresses linked with water availability and lead to membrane modifications and widespread signaling (Sagar and Singh, 2021). Such responses are present in tissues undergoing drought due to environmental (heat, wind, cold, etc.) or internally induced (dormant seeds) factors.

Finally, to decrease Ψ_{in} out of equilibrium, another possibility is to decrease the turgor pressure P. In the case of an influx of water, this can only happen through a decrease of cell wall mechanical properties with a deformation of the cell (growth).

Open questions:

- How can pressure gradients happen in symplasmic fields, with open plasmodesmata?
- Is it possible for cells to regulate Ψ_{out}, and if so, how do they do it?
- Is membrane tension sensed in the case of an osmotic stress?

I.3.2◦ Controlling cell wall mechanical properties

Since water intake drives growth, the cell wall properties control it by resisting deformation, both in intensity (growth rate) and orientation (growth direction). The cell wall properties thus have ambiguous roles: the wall stiffness allows the build-up of pressure, while the modulation of wall properties triggers cell expansion and growth.

The deformation behaviour of a cell wall can be compared to a viscoelastic material for low deformations: following a water intake, it resists deformation, can deform elastically and comes back to its original shape once the pressure decreases. If the deformation reaches a threshold called the yield pressure Y, the cell wall starts getting deformed plastically and the cell irreversibly grows (Dumais, 2021). This is summarized in Lockhart law (see Introduction ◦ I.3.3).

The mechanical properties of the wall relies on the organization of its components, as described in a recent and thorough review (Cosgrove, 2022). Cellulose microfibrils (CMFs) are generally thought to be the load bearing element of the cell wall, i.e. the main players to restrict growth rate and direction (Zhang et al., 2021a). They are stiff structures considered inextensible in the context of cell wall mechanical stress, resisting both bending and stretching (Cosgrove, 2022). CMFs are synthetized directly as a chain of glucose units at the surface of the cell by the transmembrane CELLULOSE SYNTHASE (CESA). Once deposited, the microfibrils form non-covalent Van der Waals (also called London) interactions as well as intra and inter-chains hydrogen bonds. Intra-chain hydrogen bonds lead to the formation of a rigid form of cellulose called crystalline cellulose (Nishiyama, 2018), by opposition to the rest of the cellulose, labelled amorphous cellulose. The mechanical difference between crystalline and amorphous CMFs seems to depend on the hydration level (Renuart and Viney, 2000) and seems to be characterized by a lower elastic modulus for amorphous CMF (see Box 1) (Kulasinski et al., 2014). The direction of CMFs determines the growth direction: if CMFs are oriented isotropically (i.e. in all direction with no particular bias), growth will be equally restricted in all direction. In contrast, with anisotropic CMFs orientation (i.e. oriented with a directional bias), growth will be reduced in the direction that is parallel to the CMFs (Figure 8A) (Baskin, 2005).

Because CMFs are thought to be relatively stable within the wall, at least locally, the directionality of CMFs is generally thought to emerge as they are synthesized. A directional bias can be induced by pre-existing CMFs in the wall (Chan and Coen, 2020; Emons and van Maaren, 1987), and more dynamically by cortical microtubules (CMTs). Indeed, CESAs are linked to a complex of proteins including the intracellular CESA INTERACTIVE PROTEIN 1 (CSI1), which binds to cortical microtubules (Paredez et al., 2006). In this scenario, the CESA complex is then propelled by cellulose synthesis along CMTs, and CMFs are synthetized in the same direction. CMT orientation itself is not random and often follows the maximal tensile stress axis in epidermal tissues, whether it be at the supracellular scale or at the cellular one (Hamant et al., 2008; Sampathkumar et al., 2014; Verger et al., 2018). Consequentially, CMFs are mostly aligned along the maximal tensile stress axis following CMTs.

Note that CMFs may also align in a given direction by default, because of their high persistence length (2.5µm) (Usov et al., 2015). In particular, a parallel orientation of newly

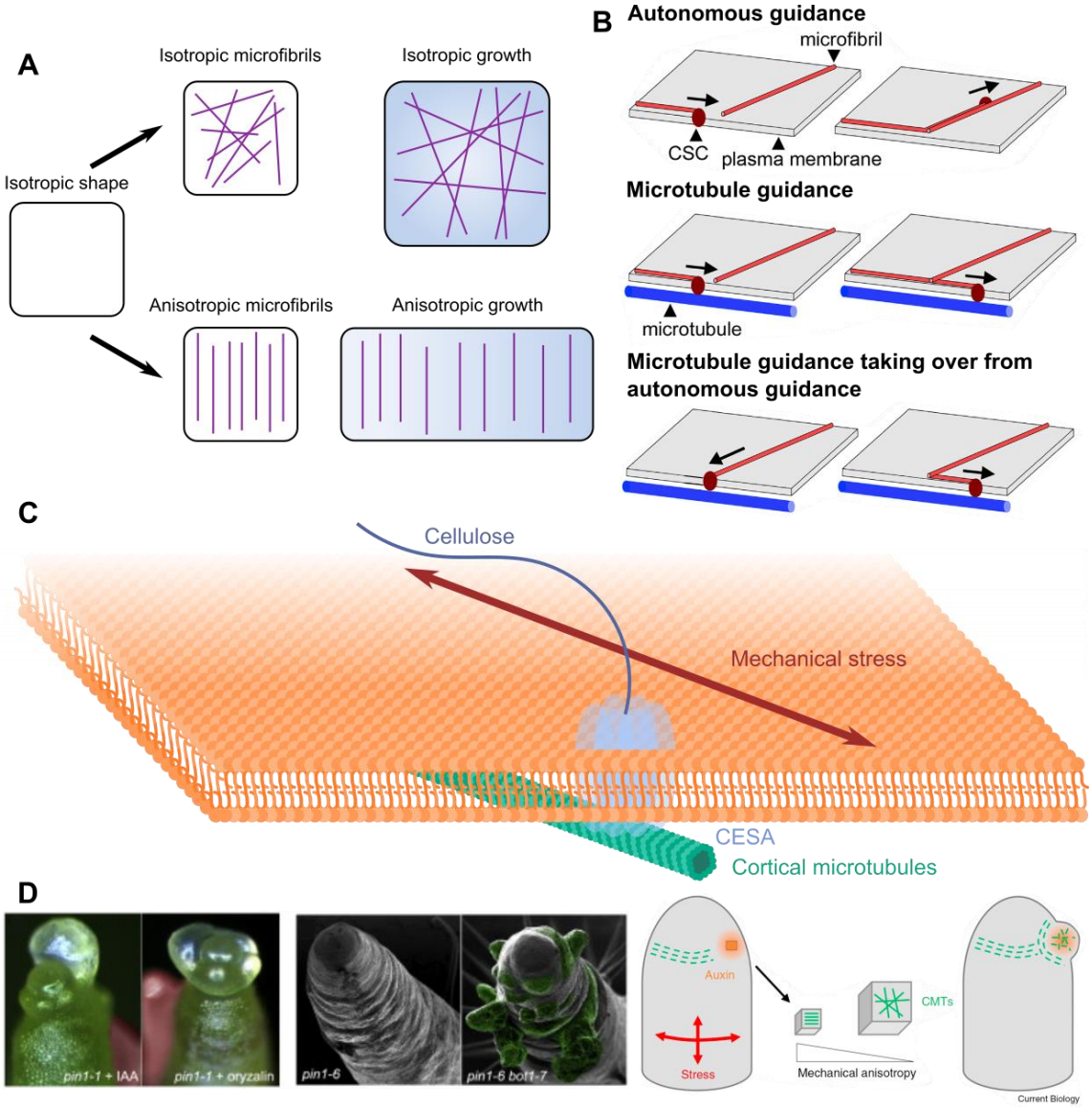

Figure 8: Cellulose orientation directs growth. **(A)** An isotropic orientation of cellulose microfibrils will lead to an isotropic growth, whereas an anisotropic orientation of cellulose microfibrils will restrict growth in that direction and lead to anisotropic growth. **(B)** *Adapted from (Chan and Coen, 2020)*. Three examples of precedence in cellulose synthase complexes (CSCs) guidance. When a free CSC encounters a pre-existing cellulose microfibril, the CSC aligns with the direction of the cellulose microfibril. When a CSC following a microtubule encounters a pre-existing cellulose microfibril, the CSC keeps following the microtubule. When a free CSC (or following a pre-existing microfibril) encounters a microtubule, microtubule guidance takes the lead. **(C)** Microtubules guide the deposition of cellulose microfibrils along the maximal tensile stress axis. **(D)** *Adapted from (Sassi et al., 2014) (left) and (Trinh et al., 2021) (right).* Microtubule anisotropy (by oryzalin depolymerisation or in microtubule dynamics mutants as *botero1*-7) triggers organ formation in PIN meristems.

synthetized CMFs has been observed in tissues with disturbed CMTs and disordered CMFs (Himmelspach et al., 2003). Other factors may also be involved in CMF alignment, such as the non-covalent links between them. Whenever CESA autonomous complexes cross the path of CMTs, microtubule guiding takes precedence (Figure 8B) (Baskin, 2001). Therefore, CMFs are mostly aligned and resist in the same direction on the same cell wall layer. This direction can change between two layers, creating a cross-ply or helicoidal pattern, and often is the one of the maximal tensile stress axis, when following CMTs (Sampathkumar et al., 2014) (Figure 8C). The process of cellulose deposition in addition to the non-covalent forces binding them leads to the creation of bundles of CMFs, able to transmit mechanical forces directly with no intervention of other cell wall components (Cosgrove, 2022).

The role of the orientation of CMFs in growth can be observed when microtubules are depolymerized, e.g. with an oryzalin or colchicine treatment: cells behave geometrically like soap bubbles and organs become spherical, two markers of isotropic properties (Corson et al., 2009; Green, 1962). The impact of growth direction can also impact morphogenesis in other ways. For instance, in plants treated with the auxin transport inhibitor naphtylphtalamic acid (NPA), shoot apical meristem (SAM) become unable to initiate new organs. The meristem is “naked”. In these meristems, CMTs are aligned circumferentially around the SAM, matching the predicted tensile stress pattern, and guide the deposition of cellulose circumferentially too, forcing growth in the perpendicular direction (Hamant et al., 2008; Sampathkumar et al., 2019). When applying the microtubule depolymerizing drug oryzalin locally in the peripheral zone, CMFs are thought to become isotropic locally, and the conflict between neighbouring anisotropically growing cells leads to bulging event (Figure 8D). Such a response can be mimicked in a mutant with disorganized microtubules (*katanin*, (Sassi et al., 2014), Figure 8D).

In conclusion, we are left with a model in which parallel CMFs are forming laterally bonded bundles in cell wall layers, are carrying most of the stress and are responsible for most of cell wall stiffness and tensile response (Zhang et al., 2021a).

Other cell wall components also affect cellulose deposition, organization and mechanical behaviour (Crowe et al., 2021; Xiao et al., 2016). CMFs are embedded in a matrix of pectins and hemicellulose. These components are synthesized in the Golgi apparatus and secreted into the cell wall (Dardelle et al., 2010). Pectins, and in particular homogalacturonan (HG) are synthetized in a highly methylesterified form, i.e. with methylester groups $COOCH_3$

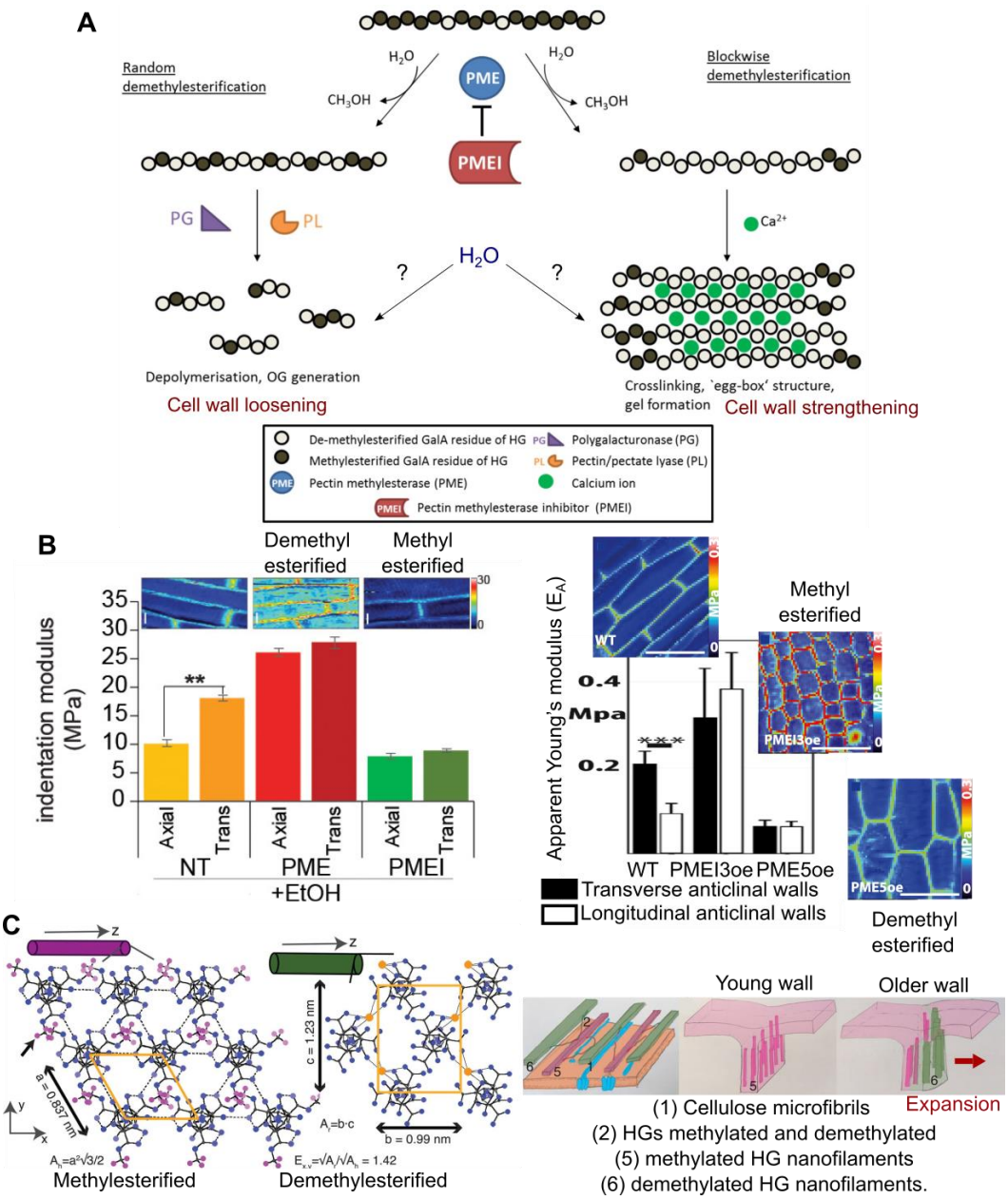

Figure 9: Mechanical consequences of pectin demethylesterification. **(A)** *Adapted from (Wormit and Usadel, 2018)*. Pectin demethylesterification is mediated by PME, which are inhibited by PMEIs. Depending on the mode of demethylesterification (random or blockwise), the demethylesterified pectins can be cut by PG and PL, leading to a loose cell wall, or crosslink with Ca2+, leading to a strengthened cell wall. The role of water in this process is poorly known for now. **(B)** *Adapted from (Bou Daher et al., 2018) (left) and (Peaucelle et al., 2015) (right)*. In vivo pectin demethylesterification returns contradictory mechanical results on the hypocotyl. **(C)** *Adapted from (Haas et al., 2020)*. Totally methylesterified and demethylesterified pectins adopt different 3D conformations, leading to nanofilaments of different thickness. This finding led to a new cell wall model with pectin demethylesterification generating wall expansion.

along the polymer chain. Over time, HGs can be de-methylesterified, i.e. the methylester group being turned into a carboxyl group COOH, often deprotonated (Sénéchal et al., 2015) (Figure 9A). The PECTIN METHYLESTERASE (PME) enzymes are responsible for this process and are inhibited by PME INHIBITORS (PMEIs). Demethylesterified HGs usually exhibit exposed chains of negative charges that can be crosslinked together through Ca^{2+} binding in an "eggbox" shape, depending on the tensile stress applied (Peaucelle et al., 2012; Proseus and Boyer, 2008). When demethylesterified, HGs change their conformation (Haas et al., 2020) and with Ca^{2+} present are supposed to create a dense, inextensible, gel. One would expect this to create a stiffer cell wall (Al-Qsous et al., 2004) and indeed *in vitro* HG gels exposed to PMEs appear stiffer (Williams, 2020). These results were reproduced *in vivo* in *A. thaliana* pollen tubes, which cell walls are particularly rich in pectins (Chebli et al., 2012; Zerzour et al., 2009) and hypocotyls (Bou Daher et al., 2018) (Figure 9B). However, other *in vivo* nanoindentation experiments seem to point to the opposite conclusion in *A. thaliana* SAMs and hypocotyls, where more PMEs (so more demethylesterified pectins) lead to a lower elastic modulus *E*, and consistently increased growth rate and organogenesis (Peaucelle et al., 2011; Peaucelle et al., 2015) (Figure 9B). This result may be due to the difference in tissues studied (for the pollen tube with a tip growth in particular), and in particular to a potential enzymatic action, explaining the difference with *in vitro* HGs. Supporting this hypothesis, an addition of polygalacturonase (PG) enzyme (which action is triggered by demethylesterification (Moustacas et al., 1991)) on *in vitro* demethylesterified HGs can soften them (Touzard, 2019). PGs could then soften the cell wall by hydrolysing demethylesterified HGs (Figure 9A). However, treatments with PMEs in isolated onion epidermis where PGs were neutralized also exhibited cell wall softening (Wang et al., 2020c). In addition to the action of PGs and other enzymes, the softness measured in demethylesterified HGs has been attributed to cell wall swelling and electrostatic repulsion. Indeed, pectins demethylesterification change their conformation from a hexagonal structure to a loose rectangular net taking up more space, which results in pectin nanofilament swelling (Haas et al., 2020) (Figure 9C). This result may be due to pectin hydration since along with ions, negatively charged demethylesterified HGs also attract water, which most certainly changes the hydromechanical properties of the cell wall in a way that lacks *in vivo* descriptions up to now (Zsivanovits et al., 2004). It then seems that demethylesterified pectins can appear softer or stiffer than methylesterified ones, depending on Ca^{2+}, water, and PG (Micheli, 2001) (Figure 9A).

The putative role of hemicellulose is to crosslink CMFs together, creating a strong net that can be directly affected by enzymes. In this model, called the tethered network, cell wall tension could be relaxed by the action of expansins, which would break the non-covalent bond (hydrogen bonds and London interactions) between hemicellulose and cellulose to allow CMFs sliding before reattachment in a manner called cell wall creep (Cosgrove, 1993) (Figure 10A). The most studied hemicelluloses, which are also the dominant ones in most land plants, are xyloglucans (Scheller and Ulvskov, 2010). This flexible polysaccharide is composed of a backbone of glucose with branches of xylose to which other sugars can attach (Schultink et al., 2014). The sidechains are important for xyloglucan architecture and interactions with water and other cell wall components. Despite this general picture highliting a putative central role of xyloglucans in wall properties, several recent studies have challenged this model.

First, recent imaging of xyloglucans with nanogold labelling and field-emission scanning electron microscopy in onion epidermis showed that xyloglucans binding to CMFs were not all extended, as previously thought, but some were also in a coiled conformation, similar to what happens in solution (Zheng et al., 2018). Upon secretion, xyloglucans bind to each other, pectins and CMFs with the help of XYLOGLUCAN ENDOTRANSGLUCOSYLASES (XTH). However, it seems that these enzymes have little effect on mechanical properties of cell walls (Cosgrove, 2022). In general, defects in xyloglucans synthesis only lead to shockingly mild phenotypes (Cavalier et al., 2008; Kim et al., 2020), which does not seem coherent with the tethered network model. Digesting xyloglucans also has negligible biomechanical effects on cell walls (Park and Cosgrove, 2012a; Zhang et al., 2019). In addition, NMR spectroscopy studies showed that only a small fraction of cell wall xyloglucans interact with CMFs (Pérez García et al., 2011). Xyloglucans would then not be a necessary CMF tether. Nonetheless, a digestion with the CELLULASE FAMILY-12A (CEL12A) enzyme, which hydrolyses both xyloglucans and cellulose, showed different biomechanical actions than using either a cellulose-specific or xyloglucan-specific digestion enzyme (Park and Cosgrove, 2012b), proving that some xyloglucans do have a contribution to cell wall properties (Figure 10B). One explanation would be that only a minority of xyloglucans, in regions inaccessible to most enzymes called “biomechanical hotspots”, would act as load-bearing junctions between CMFs (Cosgrove, 2014; Park and Cosgrove, 2015). In this model, under mechanical tension, EXPANSINS (EXP) would detach hemicellulose from CMFs in biomechanical hotspots, which

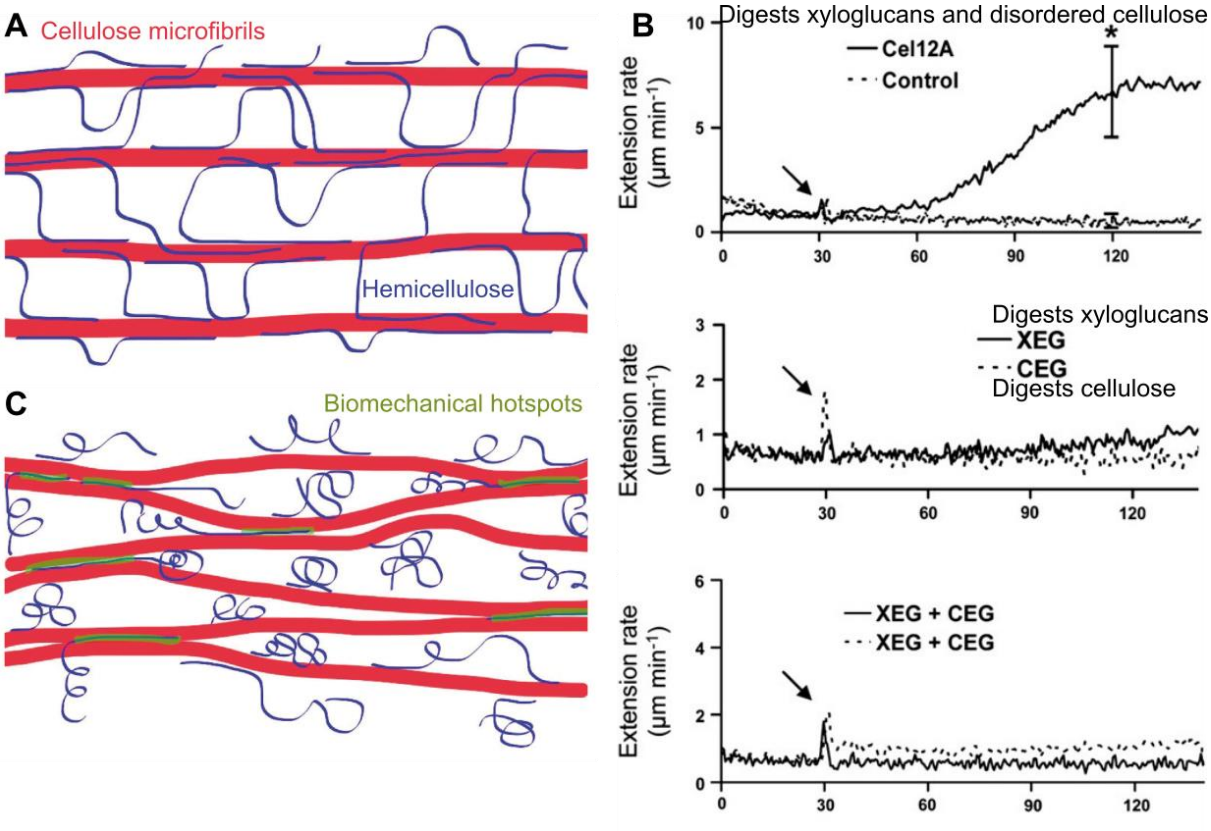

Figure 10: Models about the role and placement of hemicellulose in the cell wall are evolving. **(A)** *Adapted from* (*Cosgrove, 2016b)*. The tethered model predicted a crosslink of cellulose microfibrils effected by xyloglucans. **(B)** *Adapted from (Park and Cosgrove, 2012b)*. Extensometer assays with the use of different enzymes (addition indicated by arrow): Cel12A digests both xyloglucan and discorded cellulose, while XEG digests xyloglucans and CEG digests cellulose. Adding Cel12A induced a higher wall creep than adding XEG and CEG, separated or together. **(C)** *Adapted from (Cosgrove, 2016b)*. The biomechanical hotspot model, in which xyloglucans are more coiled than in the tethered model and only the action of some of them in spaces difficult to access by enzymes (accessible to Cel12A) would join cellulose microfibrils together.

would allow CMFs to slide along one another (Figure 10C). This would relax cell wall stress and create an irreversible cell wall creep. Biomechanical hotspots are still a relatively new concept, but they offer the interesting possibility of controlled wall expansion in selective subcellular, and even subparietal, zones.

Finally, structural glycoproteins with no enzymatic activity such as the ARABINOGALACTAN PROTEIN (AGP) play a mechanical role as AGP create crosslinks between pectins and xyloglucans (Tan et al., 2013). Another example is the glycoprotein EXTENSIN (EXT), which self-assemble to form a crosslinked network of EXTs and reinforce the cell wall (Marzol et al., 2018). Their role in cell wall mechanics is still under study.

Cell wall hydration must also be considered in cell wall mechanics as we saw for pectins. Water is incompressible and attracted by demethylesterified pectins and ions. Its presence changes the non-covalent bonds between cell wall elements to favour hydrophobic effects. Cell wall properties may then be controlled by water attractivity to the cell wall. This may also involve water influx since decreasing the water potential of the cell wall by increasing its osmotic pressure may limit water intake by plant cells (Castilleux et al., 2021). However, the role of cell wall hydration on mechanical properties, water retention and cell growth still need further clarification, notably because water content and distribution in cell walls remains an open research frontier.

Another mechanism that could be responsible for cell wall mechanical properties would be cell wall tension itself, as cell walls have been postulated to experience strain stiffening. Indeed, as in any elastic material, a cell wall under tension appears mechanically stiffer than when the tension is relaxed (Kierzkowski et al., 2012). One consequence of this stiffening would be its restriction of growth in the SAM, through mechanical forces.

As described in this part, the primary cell wall is a dynamic compartment and is generally modified to modulate cell growth, in relation with the plant status and its environment (Figure 11). In addition to the synthesis of new cell wall material, a certain number of secreted enzymes can change cell wall material properties and binding, as shown with PMEs and PMEIs for pectin methylesterification status, as well as EXP and XTH for xyloglucan binding. Ion secretion/internalization can also modify the cell wall mechanical properties: we saw the example of Ca^{2+} crosslinking demethylesterified pectins. In addition

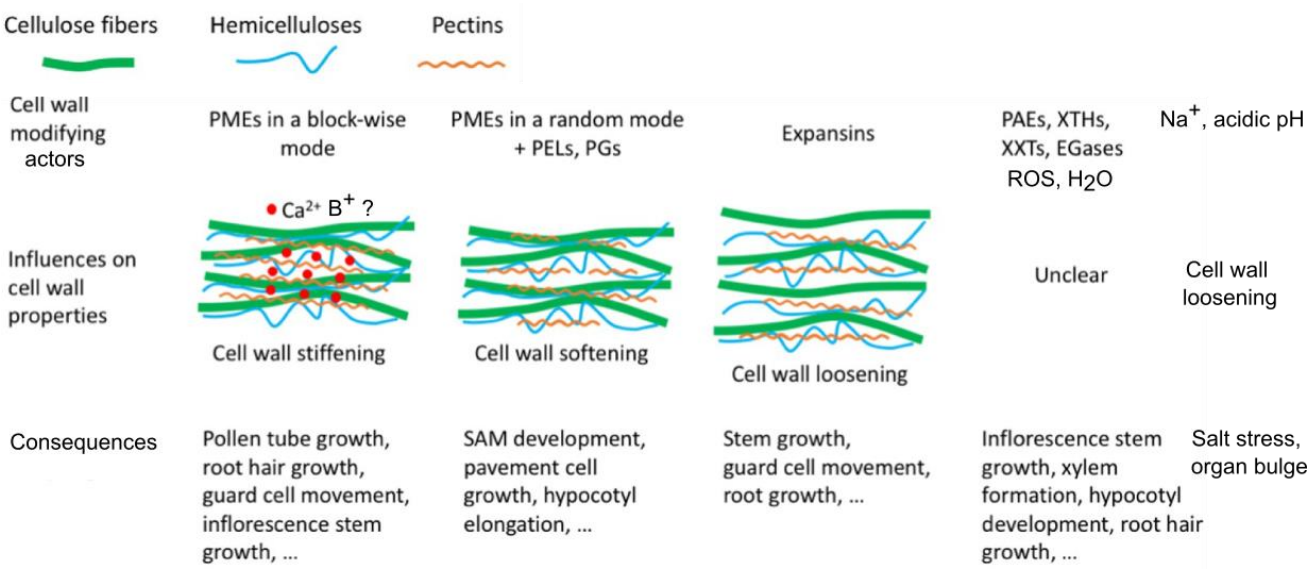

Figure 11: *Adapted from (Qiu et al., 2021)*. Cell wall modification actors and their consequences.

boron ion (B^+) has a structural role in the cell wall by crosslinking pectins (González-Fontes et al., 2008), and sodium ion (Na^+) seems to soften the cell wall likely through the disruption of load-bearing ionic interactions (Feng et al., 2018). The production of Reactive Oxygen Species (ROS) can also modify cell wall crosslinking and affect the cell wall mechanical properties, in particular in response to biotic and abiotic stress (Kärkönen and Kuchitsu, 2015). Finally, pH affects cell wall organization and mechanical status through cellulose hydration as well as pectin charges, leading to a loosened cell wall in acidic conditions (Phyo et al., 2019).

All these modifications are triggered by signaling pathways sensing and integrating both environmental cues and cell wall status. Sensors and signaling pathways ensure cell wall homeostasis: wall modifications and/or mechanical stress modify stress levels and chemical signatures in the wall; in turn, the cell expresses wall modifiers and synthesize new wall components. For example, unique cell walls are formed when plants are growing on a cellulose synthesis inhibitors, with pectins compensating for the lack of cellulose (Shedletzky et al., 1990). A vast number of putative sensors have been proposed to be involved in cell wall sensing, and in particular RLKs (Wolf, 2022). These transmembrane proteins display an extracellular domain that could be able to sense cell wall modifications (e.g. presence of a protein or carbohydrate deformation), and an intracellular kinase domain that could transmit an intracellular signal activating cell wall synthesis and remodelling (Wolf, 2017). It has also been proposed for tip-grown cells like pollen tubes that new material deposition itself would cause crosslink modifications and thus help modulate cell wall mechanical properties at a higher scale in a process independent from sensors (Rojas et al., 2011).

The “classical” model commonly accepted is that, while cell wall can restrict and direct growth, the propelling force for growth is the water influx. In this model, cell wall creep could lead to cell expansion along with other plastic deformations of the cell wall, triggered by cell wall tension (Figure 12A). An elegant metaphor describing this process would be the glassblower of D’Arcy Thompson (1942) (Dumais, 2021; Thompson, 1942). The air blown by the glassblower would correspond to the turgor pressure, pushing uniformly on the viscous glass paste representing the cell wall. The directed heat on the glass paste softens a certain place on the structure, similarly to cell wall modifications, and directs deformation in consequence (Figure 12B).

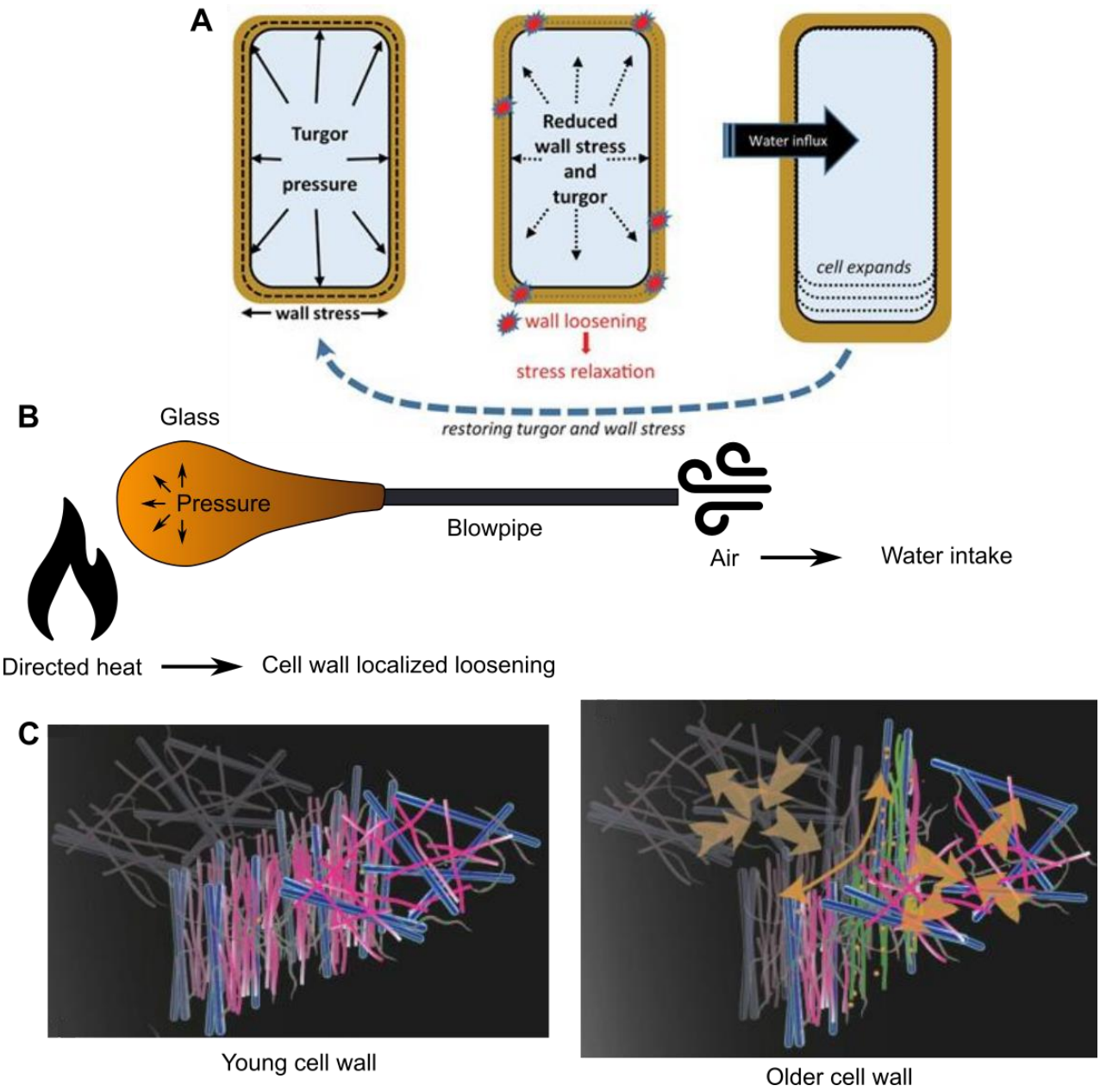

Figure 12: Cell growth models. **(A)** *Adapted from (Cosgrove, 2016a)*. In this model, turgor pressure causes a mechanical stress in the cell wall, and the directed loosening of the cell wall ensuing reduces the turgor pressure and allows a water influx, which expands the cell. **(B)** The analogy of the glassblower compares the turgor pressure caused by a water influx to the air blown by a glassblower. The directed heat shaping the glass object is equivalent to a directed cell wall loosening. **(C)** *Adapted from (Haas et al., 2021)*. In the expanding beam model, the total demethylesterification of pectins in older cell walls would cause their swelling and consequently cell wall expansion and growth without any action of the turgor pressure. Cellulose microfibrils are represented in blue, methylesterified HGs in pink, demethylesterified HGs in green, and stress created by cell wall expansion by orange arrows.

Challenging this model, there has been some postulations that part of cell wall extension could be driven by a swelling of the cell wall (Borowska-Wykręt and Kwiatkowska, 2018; Hejnowicz, 2011). More recently, single-molecule nanoscopy has revealed the presence of pectins forming aligned nanofilaments, both *in vitro* and *in vivo* perpendicular to the cell surface in the epidermis (Haas et al., 2020). These nanofilaments would be arranged as a hexagonal structure upon pectin synthesis but would then rearrange into a loose rectangular net upon total demethylesterification under high hydration, into a structure with a higher filament diameter. This would lead to cell wall expansion by the thickening of cell wall components, with no intervention of turgor pressure (Haas and Peaucelle, 2021). In this model, named the expanding beam model, the cell wall would then not only limit growth through its stiffness, but could also drive it through polymer rearrangement (Figure 12C). Pectin rearrangement has only been tested with a high hydration and a high concentration of Ca^{2+} up to now, so we can only postulate roles for water and Ca^{2+} in the expansion of nanofilaments. However, a mechanical stress induces an influx of Ca^{2+} in cells, i.e. a depletion of Ca^{2+} in the apoplast, so pectin rearrangement could be linked to mechanical stress. In fact, such autonomous pectin deformation may be instrumental to understand how cells perceive wall deformations (rather than acting as a major trigger of wall extension). For now, this model raises questions (see open questions). Cell wall composition and modifications still need to be studied more to fully understand how a cell resists to turgor pressure.

Open questions:

- What are the other mechanisms responsible for cellulose microfibril orientation?
- What is the quantitative contribution of biomechanical hotspots in cell wall deformation?
- How are biomechanical hotspots distributed in the cell wall?
- How are the hydromechanical properties of the cell wall (in particular matrix potential and osmotic pressure) altered with cell wall modifications and hydration?
- Is the apoplastic osmotic pressure actively controlled? Could the gradient of osmotic pressures between the cell and the cell wall control growth?
- In the expanding beam model, what are the links between cell wall tension, pectin methylesterification status, cell expansion, water and Ca^{2+}?

- How is the pectin deposition controlled to obtain these nanofilaments perpendicular to the cell surface?
- Could mechanical forces control pectin methylesterification status, as well as nanofilament expansion?
- What is the role of water in this expanding beam model?
- How significant could pectin rearrangement be for cell expansion considering the difference in volumes of the cell and the cell wall?

I.3.3◦ Growth as a function of water uptake and cell wall mechanical properties

As early as 1965, Lockhart linked water intake and cell wall properties. He developed a theoretical model to mathematically explain growth with simple parameters (Lockhart, 1965). In this model, he focused on a growing cylindrical cell with a constant radius (Figure 13A), and defined the volumetric expansion *r* (equation 6) as the resultant of water uptake (equation 4) and wall expansion (equation 5).

When considering the water uptake only, *r* can be defined as follows:

$$r = L\Delta\Psi = L(\Delta\Pi - P) \qquad \text{(equation 4)}$$

with *L*, hydraulic conductance, *P*, turgor pressure in the cell and $\Delta\Pi$, the difference in osmotic pressure between the outside compartment and the inside compartment (adapted from (Cosgrove, 1993)) (Figure 13B). With this, increasing the difference in water potentials (i.e. increasing the inner osmotic pressure (e.g. increase solute concentration) or decreasing the inner turgor pressure (e.g. weaken the cell wall)) or increasing the hydraulic conductance (i.e. the ability for water to enter into the cell) leads to an increase in growth rate.

When considering the plastic wall expansion, we have:

$$r = \phi(P - Y) \qquad \text{(equation 5)}$$

with ϕ, the cell wall extensibility, i.e. the rate at which the cell wall will deform plastically and *Y*, the yield pressure, i.e. the threshold that the turgor pressure *P* must exceed to observe a plastic extension (adapted from (Cosgrove, 1993)) (Figure 13B). With this, turgor pressure

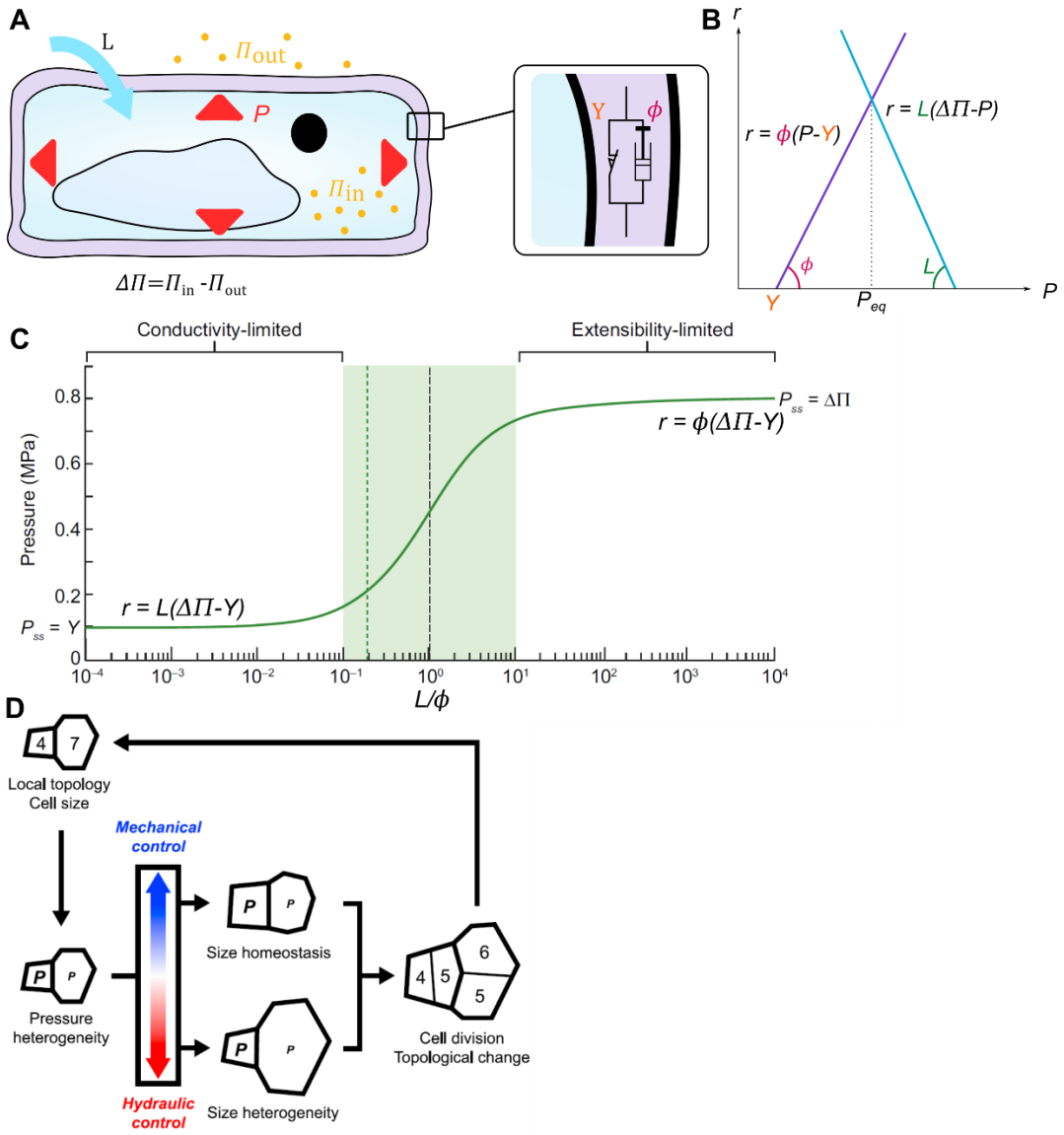

Figure 13: The Lockhart model mechanically explains growth. **(A)** The growth of a cell can be described mechanically using the following parameters: the turgor pressure *P*, the difference in osmotic pressure between out of the cell and in the cell $\Delta\Pi$, the hydraulic conductance *L*, the extensibility of the cell wall ϕ (represented as a hydraulic piston) and Y the yield pressure (represented as a threshold switch). **(B)** The turgor pressure *P* plays an ambivalent role on growth depending on the phenomenon considered (hydraulics or cell wall mechanical properties). **(C)** *Adapted from (Dumais, 2021)*. Two regimes of growth can be considered depending on the comparative values of the hydraulic conductance *L* and of the cell wall extensibility ϕ. When *L* is higher, growth is extensibility limited whereas when *L* is lower, growth is conductivity limited. **(D)** *Adapted from (Long et al., 2020)*. Emerging properties are generated when applying Lockhart's model to a tissue with non-homogeneous turgor pressure between cells. These properties are observed in the *A. thaliana* SAM.

leads to an increase in the growth rate and must exceed a threshold for growth to be observed.

In equations 4 and 5, it appears that turgor pressure plays opposing role on cell growth. This dual role (restricting water intake vs. deforming the cell wall) is at the core of growth control and homeostasis in plant cells. The two equations can be combined to obtain a growth rate for steady states:

$$r = \frac{\phi * L}{\phi + L}(\Delta\Pi - Y) \qquad \text{(equation 6)}$$

where all previous comments apply (Cosgrove, 1993). Equation 6 combines water intake and cell wall deformation to explain cell growth: ϕ the cell wall extensibility (the ability of the cell wall to be deformed), *L* the hydraulic conductance (the ability of the cell to let water flow in or out), and $\Delta\Pi$ the difference between the inside osmotic pressure and the outside one (proportional to the relative concentration of solutes in the cell) all increase the cell growth rate, while Y the yield pressure opposes growth. From equations 4 and 6 we can also extract turgor pressure for steady states:

$$P = \frac{L * \Delta\Pi + \phi * Y}{\phi + L} \qquad \text{(equation 7)}$$

and understand mathematically how it can increase with both cell wall properties and water intake (adapted from (Dumais, 2021)).

From equation 6, we can define two regimes of growth (Figure 13C). When the hydraulic conductance *L* is very low compared to the cell wall extensibility ϕ, water intake is limiting growth (rather than the cell wall properties) and growth is “conductivity limited”. The growth rate depends mostly on the hydraulic conductance *L*, and turgor pressure reduces to the yield pressure Y. In contrast, when the hydraulic conductance *L* is very high compared to the cell wall extensibility ϕ, the cell wall properties are restricting growth (rather than water intake) and growth is “extensibility limited”. The growth rate thus depends mostly on the cell wall extensibility ϕ, and turgor pressure can be reduced to the osmotic pressure $\Delta\Pi$.

For an example in real tissues, there is evidence that pollen tube growth is conductivity limited (Beauzamy et al., 2014; Dumais, 2021): turgor pressure does not seem correlated with growth rate in these tissues (especially not with the oscillation pattern), the concentration of

ions seems in antiphase with growth, and in a model representing pollen tube growth the conductivity term was calculated to be lower than the extensibility term. The predominant regime in plant cells undergoing diffuse growth in tissues is more debated (Boyer, 1988; Cosgrove, 1993). The distinction between the different scenarios may be particularly interesting to study as the growth regime seems to influence the dynamics of cell growth (Cheddadi et al., 2019).

One of the most interesting things about the Lockhart model, and its different variations, is how simple and general it is. Yet, it does not necessarily represent the reality. In particular, it focusses on the case of an undividing cylindrical cell, i.e. only growing in one direction and with a fixed radius, with a uniform cell wall, and with fixed values of L, $\Delta\Pi$, ϕ and Y. Therefore, it does not accurately describe certain growth behaviours such as the pulsatile growth observed in tip-growing cells (e.g. in pollen tubes (Dumais, 2021)), or dynamically changing ϕ and Y (Green and Cummins, 1974; Okamoto et al., 1990). Note that, these simplifications hold some truth, as cell wall microscopical behaviour seems sufficient to explain the properties of a macroscopically uniform cell wall, and thus of a set of parameters describing the whole cell wall (Veytsman and Cosgrove, 1998).

Since its formalisation, this model has been extended and adapted, notably to include the elastic properties of the cell wall (Ortega, 1985), a more detailed cell wall representation (Chakraborty et al., 2021), time (Bassel et al., 2014; Boudon et al., 2015), or 2D growth (Cheddadi et al., 2019). One model in particular added time variability as well as delays from a feedback mechanisms in the parameters L, $\Delta\Pi$, ϕ and Y (Dumais, 2021). This is particularly interesting in a biological context where plants seem to maintain homeostasis through sensing and altering their biochemical and biomechanical properties. In general, those model refinements often revealed real life properties (such as pulsatile growth (Dumais, 2021)) by adding elements more representative of the biological mechanisms to the Lockhart model.

One limitation of the original Lockhart model is its single cell basis. This has been tackled several times (Boudon et al., 2015) and in particular recently in a model where a 2D tissue with adjacent cells display heterogeneous properties and are able to exchange water symplasmically or apoplasmically through their shared edge (Cheddadi et al., 2019). In this model turgor pressure P is not treated as a constant but as a variable which is adjusted to the other constraints, consistent with the hypothesis that turgor pressure would not be controlled

on its own, but would be the result of a control of other parameters (Dumais, 2021). Several emergent properties appear from simulations of this model: as observed in real SAM, turgor pressure is heterogeneous in a tissue and varies with cell wall stiffness (lower for a softer cell wall), cell size (higher for a smaller cell) and cell neighbour number (lower when a high number of neighbours) (Long et al., 2020) (Figure 13D). A growth inhibition due to water fluxes from neighbouring cells also becomes apparent. This last property could be consistent with observations in meristem boundaries, where growth (in area) can become negative as the organ emerges (Kwiatkowska and Dumais, 2003).

In this part, we highlighted the central role of water and hydraulics to understand the mechanical properties of the cell (in parallel to the relatively more well-known role of cell walls). However, this may give the impression that turgor pressure and wall properties are simply the passive output of gene networks. Can mechanical stress also play an instructive role in development?

Open questions:

- How to code and integrate the contribution of specific genetic regulators to cell mechanics?
- How different are cell wall modifications and turgor pressure adjustments in diffuse growth vs. tip growth?
- What could be the status of a cell undergoing negative growth?

II◦ Mechanical stress as an instructive cue for plant development

II.1◦ Mechanical stress patterns in plants

As discussed above, the turgor pressure pushing on the membranes of a cell generates a tension in the membrane and the cell wall. A similar process happens at the tissue scale where a pressure is applied to an enveloping layer which does not deform easily. Indeed, the cell layer at the surface of all aerial tissues (the epidermis) is usually under tension while the inner tissues are under compression (Figure 14A). These forces can be visualised by peeling the epidermis of a sunflower hypocotyl: after peeling i.e. when the pattern of stress relaxes,

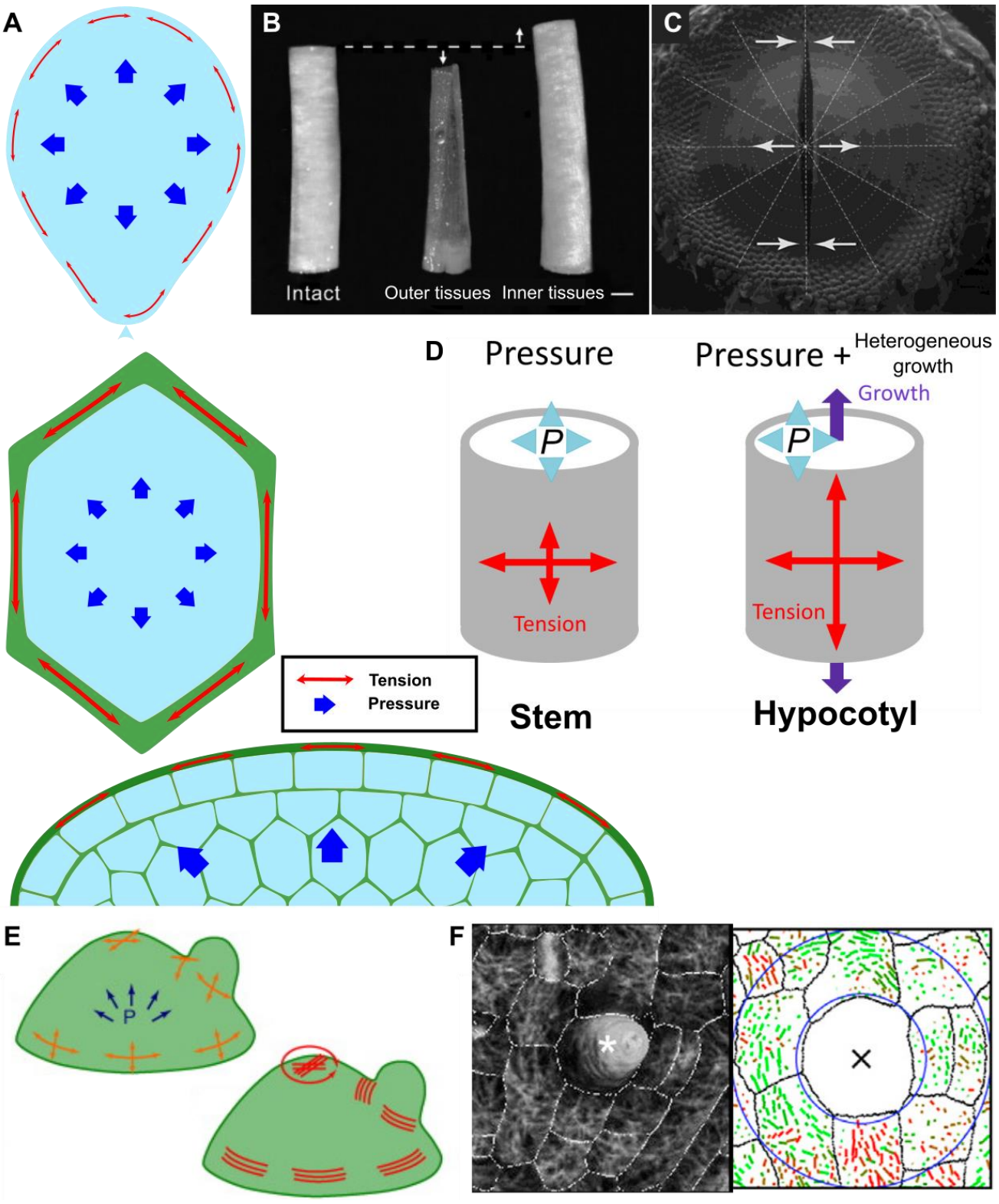
A
B
Intact
Outer tissues
Inner tissues
C
D
Pressure
Pressure +
Heterogeneous growth
Growth
P
Tension
Tension
Pressure
Stem
Hypocotyl
E
P
F

Figure 14: (A) The pattern of mechanical forces is similar in an inflated balloon, a cell and a tissue: an inner force (respectively caused by the air, water influx or the growth of inner tissues) is applied on a structure that does not deform easily (respectively the membrane of the balloon, the cell wall, the epidermis). This structure is thus under tension and the inner material under compression. **(B)** *Adapted from (Kutschera and Niklas, 2007)*. Peeling the epidermis of sunflower seedlings reveal the pattern of stress at play: the epidermis contracts, meaning it was under tension in the intact segment, whereas the inner tissue extends, meaning that it was under compression. **(C)** *Adapted from (Dumais and Steele, 2000)*. White arrows represent the forces, dashed lines the direction of radial stress and dotted lines the direction of circumferential stress. The behaviour of the edges of a cut in a sunflower capitulum highlight the compressive forces in the generating region (bringing the edges together) and the tensile forces in the centre of the capitulum (taking the edges apart). **(D)** *Adapted from (Verger et al., 2018)*. In a grown stem and in an epidermis the forces affecting the stress are different, leading to a different stress pattern. The pressure from inner tissues prescribe a circumferential stress in stems, whereas differential growth between inner and outer tissues overtop this stress and establish an axial tensile stress in growing hypocotyls. **(E)** *Adapted from (Boudaoud, 2010)*. The pattern of stress (orange arrows) in a meristem is revealed by the orientation of microtubules (red lines). **(F)** *Adapted from (Hervieux et al., 2017)*. The growth of a trichome (star, cross) redistributes the pattern of stress into a stress circumferential to the trichome (right) as evidenced by the orientation of microtubules (left).

the epidermis contracts compared to its original size, meaning that it was under tension before peeling (Figure 14B) (Kutschera and Niklas, 2007). Similarly, cuts on most part of the epidermis tend to keep the gap open due to the tensed nature of the epidermis (e.g. when cutting the skin of a tomato). As we will see later, this does not apply when shapes become more complex, and folds may instead lead to local compression events, as in the SAM boundary discussed previously (Hamant et al., 2008), or in young sunflower capitulum (Dumais and Steele, 2000) (Figure 14C).

More recently, the use of the *quasimodo1* (*qua1*) line, with defects in tissue adhesion leading to cracks in the epidermis helped reveal the stress pattern in different tissues (Verger et al., 2018). Those cracks played the role of the cuts in the epidermis seen previously and gaped in the direction of the maximal tensile stress axis. This experiment validated predictions concerning the tensile stress pattern: in the stem, the stress pattern is mainly shape-driven so circumferential (like in an elongated balloon), whereas the hypocotyl stress is mainly growth-derived and thus axial (particularly so in dark-grown hypocotyls) (Figure 14D).

From a biophysical point of view, as an hyperosmotic treatment reduces turgor pressure (through a reduction of the difference in osmotic pressure between the cell and the environment) and the gaping width in epidermal cuts, the turgor pressure of the inner tissues pushing on the epidermis would be responsible for epidermal tension (Dumais and Steele, 2000). This way, inner tissues that are inflated with turgor would be compressed by the slow growth of the epidermis, which in turn would be under tension (Galletti et al., 2016) (Figure 14A).

This scenario is supported by several genetic studies. Some mutants impaired in the synthesis or perception of brassinosteroid can be rescued by expressing the wild-type gene in the epidermis alone (Savaldi-Goldstein et al., 2007), showing that the epidermis restricts growth. Similar results have been obtained using this time ethylene as a target (Vaseva et al., 2018). More recently, the combination of extra inner cell production (*clavata3* (*clv3*) mutant) and weaker epidermal walls (de-etiolated3 (*det3*) mutant) led to cracks in epidermis, not only validating the presence of epidermal tension, but also mimicking the direction of cracks obtained in the *qua1* mutant, and thus the stress pattern in stems (Asaoka et al., 2021).

If the epidermis is generally under tension, it follows that the geometry of the organ prescribes a pattern of mechanical stress. For a simple shape like a sphere, the stress pattern in isotropoic. For a cylinder, tensile stress would be twice higher along the transverse direction, than along the axial direction. For more complex shapes, some tissue folding and specific cell and organ shapes can alter the paradigm. For example, it was shown that while cuts at the centre of sunflower SAMs gaped, they remained closed in the regions producing cells (generating regions) (Dumais and Steele, 2000) (Figure 14C). This means that those generating regions are under compression, which could explain the buckling shape, i.e. the bending observed in the SAM. A similar phenomenon occurs in *A. thaliana*, where a boundary marks the limit between the SAM and primordia. This boundary displays a folding of the tissues due to differential growth between the organ and the meristem, which induces a putative compression of the epidermis visualized by CMT alignment along the boundaries (Burian et al., 2013; Fal et al., 2021; Hamant et al., 2008) (Figure 14E).

With the SAM example, it appears that the final stress pattern is a combination of shape-derived stress and growth-derived stress. In the boundary, both stresses are synergic, which likely explains why the CMT alignment is so clearcut in that domain: tensile stress is likely very high. In other cases, growth-derived stress can be isolated. This is the case of socket cells surrounding trichomes. The epidermis of Arabidopsis is flat, at a local scale, and thus shape does not provide a strong bias in any direction. However, the young trichome cell growing much faster than its neighbours, it is predicted to induce circumferential tensile stress in the adjacent socket cells. Consistently, CMTs in socket cells become transiently circumferential in the period of fast trichome growth (Hervieux et al., 2017) (Figure 14F).

Experimentally, epidermal cellular ablations (with a laser or a needle) are routinely used in labs to modify the pattern of stress into one circumferential to the ablation, and observe CMT reorientation among other phenotypes (Hamant et al., 2008; Malivert et al., 2021; Sampathkumar et al., 2014) (Figure 15). Other mechanical perturbations have been tested, notably compression (Hamant et al., 2008; Hernandez and Green, 1993) or wall weakening with drugs or wall modifiers (Fleming et al., 1997; Heisler et al., 2010).

Interestingly, the shape-derived stress pattern that is observed in tissues can also be applied to single cells, in theory. Typically, a pressurized cylindrical cell would have maximal tensile stress in the transverse direction, matching the frequently observed transverse CMTs.

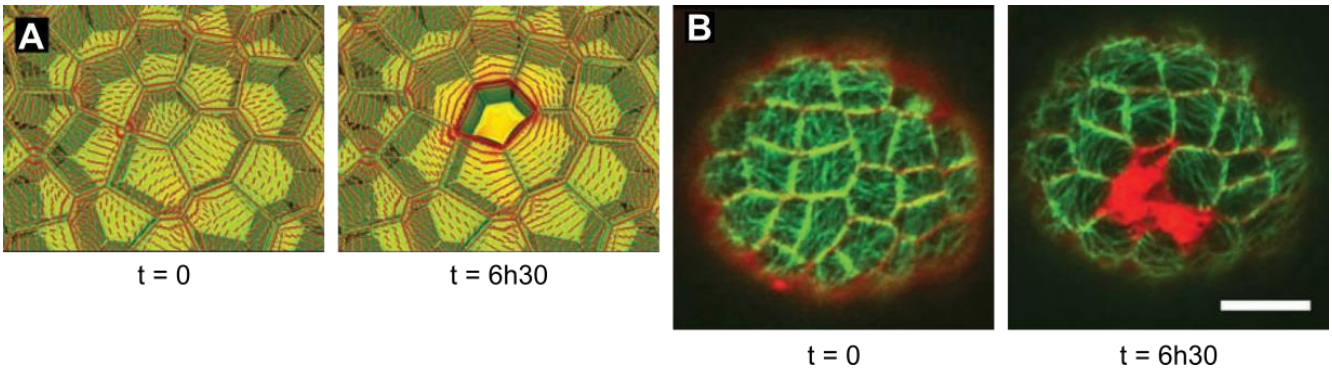

Figure 15: *Adapted from (Hamant et al., 2008)*. A cellular ablation in the epidermis (here of the SAM) induces a reorientation **(A)** or the pattern of stress circumferentially around the ablation, and **(B)** of cortical microtubules circumferentially around the ablation.

This is particularly striking in pavement cells, which are epidermal leave and cotyledon cells with a distinctive puzzle piece shape in lobes and necks (Figure 16A): this shape associated with epidermal tension and turgor pressure-induced inflation creates a strereotypical pattern of stress, with maximal tensile stress anisotropy in the necks (Figure 16B-C) (Sampathkumar et al., 2014). Again, CMT alignments appear in necks, where the mechanical tension is the highest (Sampathkumar et al., 2014; Sapala et al., 2018). Note that this kind of pattern of cellular stress can be overridden by arguably higher supracellular stress, e.g. when performing an ablation (Sampathkumar et al., 2014). Altogether, this means that "a shape is a diagram of force" (Thompson, 1942). Could these patterns of stress trigger certain responses, beyond cell wall reinforcement and water fluxes regulation?

Open questions:

- Are cellular and supracellular mechanical stresses sensed the same way?
- How are cellular and supracellular mechanical stresses integrated together?
- What is the contribution of supracellular tension and compression to water fluxes and cell wall reinforcement?

II.2◦ Mechanical stress controls cell shape, cell division and cell fate

Several putative sensors have been proposed to establish the link between mechanical forces and microtubules, such as RLKs, mechanosensitive channels, microtubule-associated proteins and even the plasma membrane (see Introduction ◦ III). Microtubule arrays have been suggested to self-organize their orientation in reaction to tension on their own (Hamant et al., 2019b). This hypothesis would be consistent with the *in vitro* observations that microtubules tend to autonomously reorient together in the same direction when the substrate they are fixed on is stretched (Inoue et al., 2016). Individual microtubules also polymerise faster when placed under tension with an optical trap (Trushko et al., 2013). Moreover, microtubules align with predicted maximal tension even in the absence of cell walls (Colin et al., 2020). This could mean that the network of microtubules, and their interactions, is sufficient to place microtubules under tension and bias their self-organization. More likely, CMTs are attached to the plasma membrane and may integrate their own mechanical status and other extracellular cues. Note that the actin cytoskeleton has been less studied in plants. Yet, actin

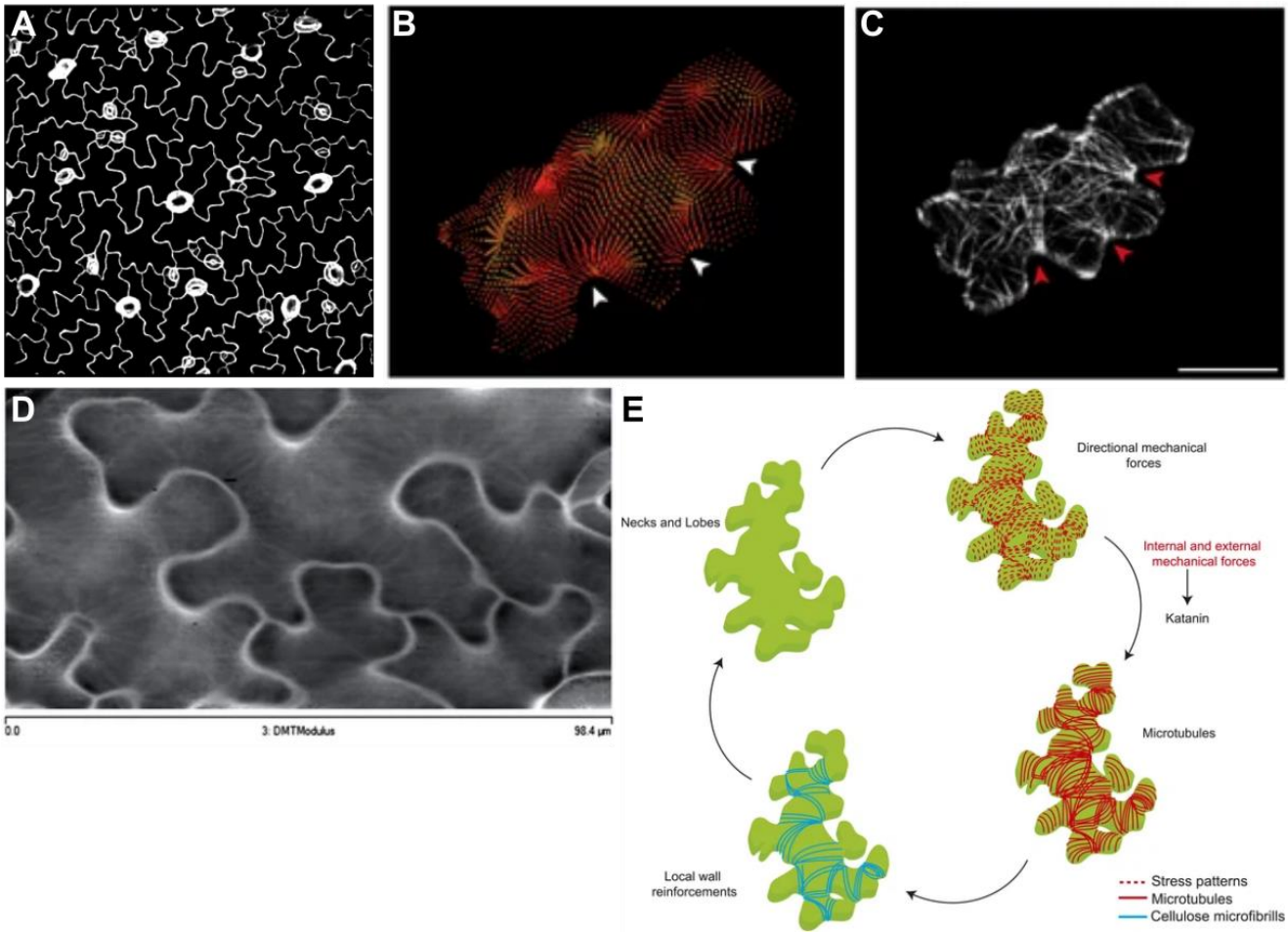

Figure 16: Pavement cell shape is reinforced by a mechanical stress feedback loop. **(A)** *Adapted from (Malivert et al., 2021)*. Pavement cells present a typical puzzle shape with lobes and necks. **(B-E)** *Adapted from (Sampathkumar et al., 2014)*. **(B)** Mechanical stress is particularly high (red) in necks (white arrowheads). **(C)** The orientation of cortical microtubules in pavement cells follows the direction of maximal mechanical stress. **(D)** Establishing an AFM stiffness map of the cell wall of pavement cells reveals a pattern of stiff fibrils in the same orientation as the maximal tensile stress and cortical microtubules. A likely origin for these structures would be cellulose microfibrils. **(E)** A mechanical feedback loop intensifies the shape of pavement cells: the mechanical stress pattern caused by turgor pressure applied to the cell shape guides the orientation of cortical microtubules, which mediate the deposition of cellulose microfibrils. Cellulose microfibrils then restricts growth in the direction they are deposited and the cell grows perpendicularly, reinforcing its shape.

filaments seem to orient with maximal tension too (Goodbody and Lloyd, 1990) consistent with results obtained in animal cells and *in vitro*. It appears to polymerise faster under tension and to branch more under compression (Risca et al., 2012; Yu et al., 2017).

The link between the orientation of the CMTs and mechanical stress has consequences on cell and organ shape. As discussed earlier (see Introduction ◦ I.3.2), CESAs can be guided by microtubules and thus tend to follow the maximal tensile stress axis. Since CMFs limits growth depending on their alignment, the pattern of mechanical stress influences the direction of growth. This results in highly determined shapes as can be seen with pavement cells (Figure 16A): the pattern of stress dictated by the cell shape inflated by turgor pressure reorients microtubules between necks, CMTs guide the deposition of cellulose in the same axis (Figure 16D) and CMFs restrict growth in this axis. This leads to cell growth mainly in the orthogonal direction to the mechanical stress, which reinforces the shape and thus the pattern of tensile stress in a feedback loop (Sampathkumar et al., 2014) (Figure 16E). The role of CMT orientation on cell shape can be demonstrated by looking at defects in the shape of pavement cells of microtubule dynamics mutants. For example, the *bot1* (*botero*) mutant for the microtubule severing protein KATANIN (KTN) exhibits a slower microtubule self-organization, and thus a reduced response to stress (Uyttewaal et al., 2012). Consistently, *bot1* pavement cells are more circular and with narrower lobes than the WT (Malivert et al., 2021). In this model, if the mechanism for amplification is clear, the origin of the shape of pavement cells is still unknown. While the role of the growth hormone auxin in pavement cell shape initiation is debated (Belteton et al., 2018; Xu et al., 2010), it has been postulated that a polarity of several cell wall elements including demethylesterified pectins would be responsible for the initial mechanical imbalance. This small mechanical heterogeneity would then be amplified through the CMT mechanical feedback loop, with an eventual implication for cell buckling (Belteton et al., 2021; Bidhendi et al., 2019; Majda et al., 2017). The pavement cell shape formed this way through cell mechanics seems to reduce the tensile stress levels for a wider cell area and potentially prevent cell bursting (Sapala et al., 2018). For an example of pavement cell bursting that may be due to geometry-linked mechanical stress, see Annexe 1 (Mylan Ansel's internship report).

At the organ scale, the response of microtubule to stress is thought to channel organ shape, with other indirect effects. For example, in mutants with a failing cell response to

stress, the defects in cell shape tend to add up and can lead to higher scale phenotypes. For example, the *csi1* mutant causes CESAs to be detached from CMTs and thus to move autonomously, with no response to mechanical stress. In this mutant, CMFs are tilted and induce a torsion of the stem leading to defects in the final position of organs along the stem (phyllotaxis) (Landrein et al., 2013). In the case of the *bot1* mutant, in which microtubules display a weak stress response, cell growth is more isotropic (as expected) and more counterinuitively, growth is also more homogeneous in the SAM than in the WT. It was proposed that WT cells over-react to stress, and the hyper-alignment of CMTs would trigger increased growth heterogeneity in the WT (Uyttewaal et al., 2012).

Growth arrest may also be controlled by mechanical forces in plants (Trinh et al., 2021). Reactive Oxygen Species (ROS) are expressed in case of most stresses and in particular in case of a mechanical stress (Martinière et al., 2019). As a higher ROS expression seems to promote growth arrest, possibly through cell wall reinforcement (Hong et al., 2016), mechanical stress could contribute to the definition of final organ shapes, by defining when the organ must stop its growth.

The CMT response to mechanical stress also seems to have a role in the orientation of the division plane in symmetric divisions (Robinson, 2021). The first hypothesis for the direction of symmetric cell division was a geometric one, issued from a comparison with soap bubbles (Errera, 1886): plant cells appear to divide like soap bubbles. This means that the new membrane divides the cell into two cells of equal size while minimizing its area (Figure 17A). While the analogy with soap bubble was wrongly reduced to a division along the shortest path in following works, the original Errera's model was more recently revisited to account for its probabilistic power: several local energy minima could be obtained for different division plane orientations (Besson and Dumais, 2011). The probability of observing a certain division plane orientation in the cell would depend on the energy linked with the plane area. To rephrase it, several division plane orientations would be possible, with a higher probability for the lowest areas of the division plane (Figure 17B). While this rule is observed in many tissues, exceptions have been noted. In particular, the SAM boundary region which is predicted to be under highly anisotropic tensile stress (as discussed in Introduction ◦ II.1) exhibits an enrichment of long division planes, i.e. the ones with a low probability according to the geometric rule (4^{th} most probable plane and higher). Such bias matches the maximal tensile stress axis (Figure 17C). A

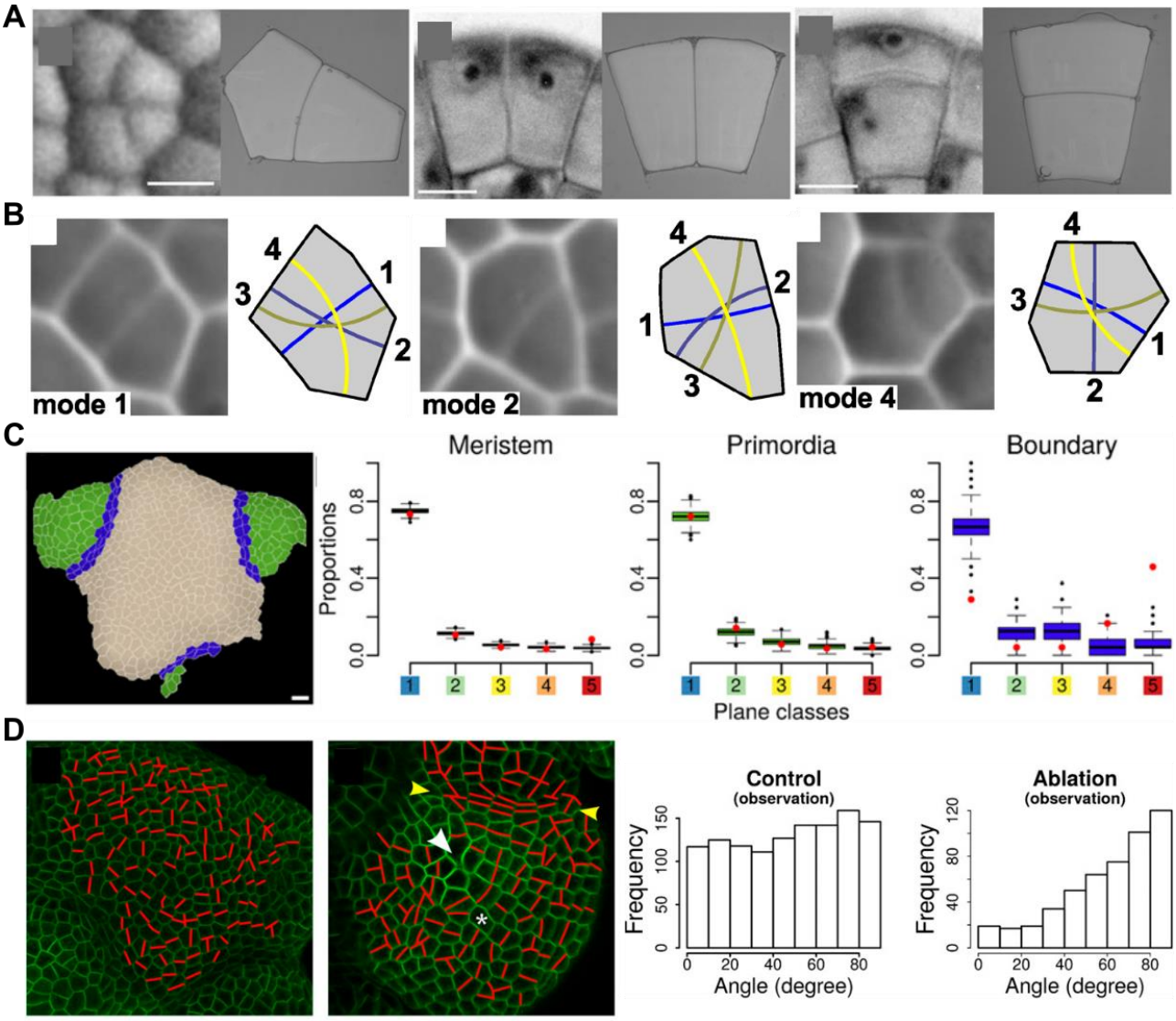

Figure 17: Cell division is also mediated by mechanical stress. **(A-B)** *Adapted from (Besson and Dumais, 2011)*. **(A)** Errera's model compares the division plane of a cell (left one on each pair) to the one of a soap bubble (right one on each pair). **(B)** Applying statistics to Errera's model can predict several possible division planes in a cell, and the probability for each one to be seen in real life. **(C-D)** *Adapted from (Louveaux et al., 2016).* **(C)** The SAM boundary (blue zone) presents a higher number of less probable division planes than other zones. This may be due to the high mechanical stress in this zone. **(D)** Mechanical perturbations in the form of cellular ablations (white arrowhead) create a pattern of divisions circumferential to the ablation (aligned with the mechanical stress).

mechanical perturbation in the form of an ablation also led division planes to be oriented circumferentially around an ablation, in the axis of the maximal tensile stress (Louveaux et al., 2016)(Figure 17D). However, this new addition adds determinism (through mechanical stress) into a probabilistic behaviour and may need further studies to be integrated into the probabilistic model.

Mechanical stress may also be used as a cue to contribute to cell fate definition. As mentioned earlier, thigmomorphogenesis is accompanied by the modification of the transcriptome (Braam, 2005). A more direct link to master regulators of development was also explored. In particular, SHOOT MERISTEMLESS (STM), a key protein responsible for stem cell fate in the SAM and responsible for organ separation, is highly expressed in the boundaries (Heisler et al., 2005) where tensile stress is proposed to be highly anisotropic (Hamant et al., 2008) with radial compression appearing in older boundaries (Fal et al., 2021). More precisely, the expression of *STM* has been shown to be correlated with the curvature of the SAM, and so with the pattern of stress (Landrein et al., 2015) (Figure 18A). With compression and ablation experiments, as well as a modification of cell wall mechanical properties, the expression of *STM* can be induced in what seems a dose-dependent manner (Figure 18B). Therefore, STM expression and thus cell fate may be regulated by mechanical stress. Note however, that this regulation seems very indirect since it takes more than 8 hours to detect a change in STM expression after mechanical perturbation. If cell fate regulation by mechanical forces during development is still relatively unstudied in plants, some occurrences of this mechanism are well known in animal systems (Roeder et al., 2021). One such example would be the one of joint progenitor maintenance by the *in utero* contraction of muscles, shaping the future limb (Kahn et al., 2009).

The activation of certain genes by mechanical stress may involve more largescale chromatin modification. Indeed, in old SAM boundaries, nuclei are compressed and become elongated (Fal et al., 2021) (Figure 18C). This correlates with the compression-triggered expression of the DNA organizing histone H1.3 (Figure 18D) and with a chromatin rearrangement that could lead to differential expression of some genes in the boundaries.

In the following section, we will discuss the specific case of the epidermis, which is under tension (as mentioned above), and which displays several specificities, which may in part be due to a response to this tension.

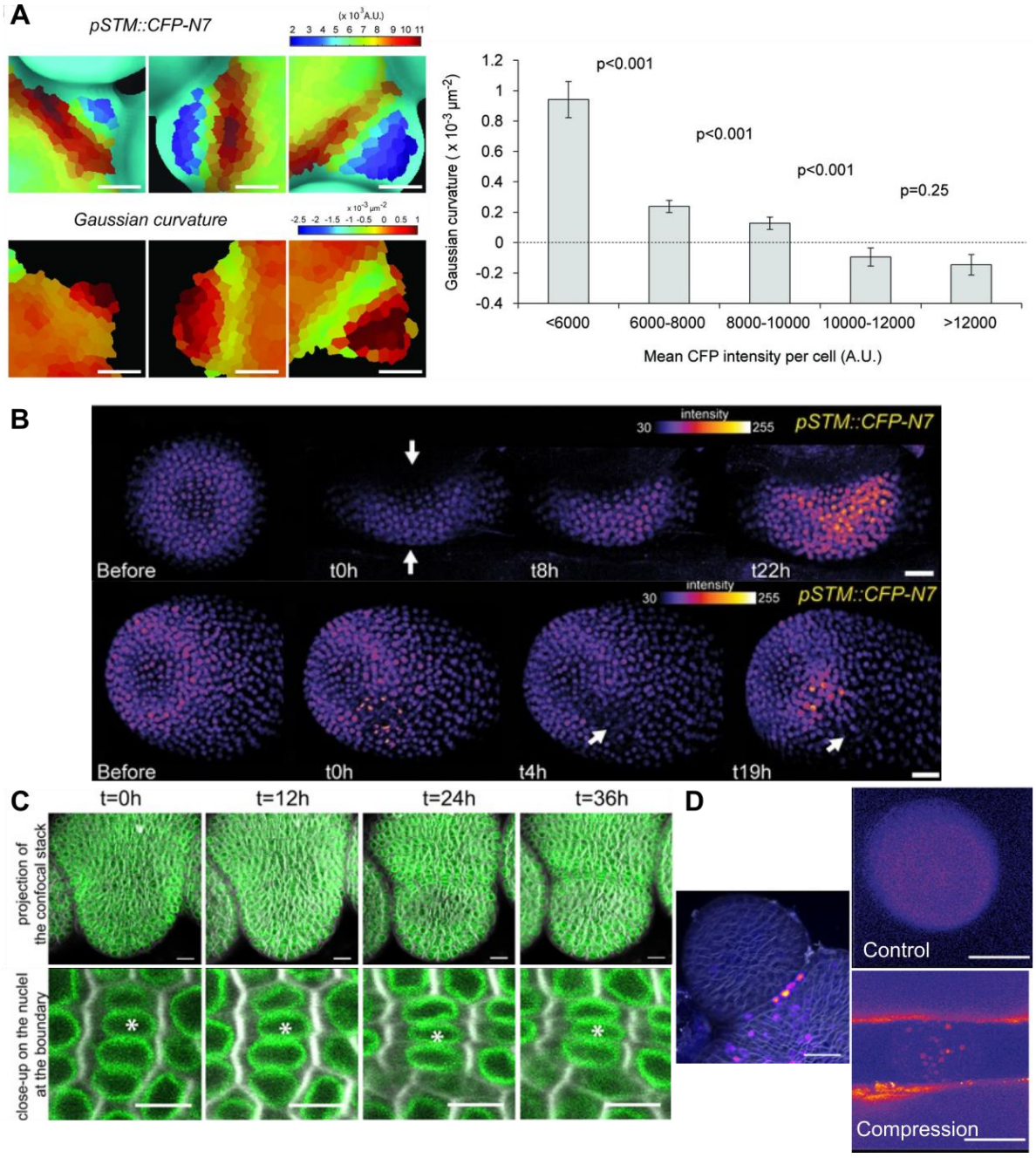

Figure 18: Cell fate seems linked with mechanical forces through the expression of STM, in the case of the SAM boundaries. **(A-B)** *Adapted from (Landrein et al., 2015)*. **(A)** The expression of STM is correlated with the curvature in the SAM, and so to be particularly high in the boundaries. **(B)** The expression of STM can be induced by mechanical constraints: compressions (up, in the direction of the two white arrows) and ablations (down, ablation at the white arrow) induce higher fluorescence intensity levels in *pSTM::CFP-N7*. **(C-D)** *Adapted from (Fal et al., 2021).* **(C)** The nucleus shape gets distorted in the boundaries of the SAM, increasingly with time and thus folding. **(D)** The histone H1.3 expression is particularly high in the boundaries (left) and can be induced by compressing a meristem (right).

Open questions:

- How is stress sensed for microtubule reorientation?
- Is there a mechanical stress threshold to overcome Errera's rule or is Errera's rule already involving a more local pattern of stress?
- Can the compression in inner tissues and tension in the epidermis lead to differential gene expression between tissue layers?
- How can the cell distinguish tension and compression?
- Is the expression of STM the result of a chromatin rearrangement due to the action of H1.3?

II.3◦ The formation of the epidermis: cell fate controlled by mechanical cues?

The following part has been published as a review I wrote with Olivier Hamant and Gwyneth Ingram (Malivert et al., 2018). The text is included in the published format.

Available online at www.sciencedirect.com

ScienceDirect

Current Opinion in Genetics & Development

The contribution of mechanosensing to epidermal cell fate specification

Alice Malivert[1,2], Olivier Hamant[1] and Gwyneth Ingram[1]

In land plants, the aerial epidermis is essential for growth control, protection and environmental interactions. Epidermal cell fate is specified early during embryogenesis and maintained throughout plant life. Molecular actors of epidermal specification have been characterized, but how epidermal fate is maintained during growth remains unclear. DEFECTIVE KERNEL 1 (DEK1) is required for epidermal cell fate maintenance during both embryonic and post-embryonic plant development. The activation of a mechanosensitive Ca^{2+} channel was recently shown to depend on DEK1, suggesting that the interpretation of mechanical cues could be critical for maintaining epidermal cell fate. Here, we integrate these findings into the epidermal specification network and propose a model explaining why epidermal specification may depend upon the sensing of epidermal tension.

Addresses
[1] Laboratoire Reproduction et Développement des Plantes, Univ Lyon, ENS de Lyon, UCB Lyon 1, CNRS, INRA, F-69342 Lyon Cedex 07, France
[2] Master de Biologie, École Normale Supérieure de Lyon, Université Claude Bernard Lyon I, Université de Lyon, F-69342 Lyon Cedex 07, France

Corresponding author: Ingram, Gwyneth (Gwyneth.Ingram@ens-lyon.fr)

Current Opinion in Genetics & Development 2018, **51**:52–58

This review comes from a themed issue on **Developmental mechanisms, patterning and evolution**

Edited by **Lance A Davidson** and **Gwyneth C Ingram**

For a complete overview see the Issue and the Editorial

Available online 4th July 2018

https://doi.org/10.1016/j.gde.2018.06.011

The epidermis: a layer under tension

The aerial epidermis is a continuous tissue localized at the surface of all land plants. In most cases it covers all young above-ground organs with one layer of cells [1••]. Since it forms the interface with the environment, the epidermis has evolved to play a protective role against external challenges (such as UV irradiation and pathogens) and acts as a surface for regulated exchanges between the internal tissue of the plant and the environment [2–6]. Most epidermal cells are given the generic name 'pavement cells' and adhere strongly to each other to form the epidermal monolayer. The aerial epidermis also hosts specialized cells, such as guard cells in stomata (regulating gas exchange, [7••]), trichomes (protecting the plant against biotic and abiotic aggression), or stigmatic papillae (involved in sexual reproduction) [6,8]. Some epidermal functions depend upon the polar secretion of a protective hydrophobic polymer known as the cuticle onto the plant surface. This structure can have dramatically different properties depending on cell and organ types [9].

Beyond its role at the interface with the environment, the epidermis also plays a prominent role in development. For instance, at the shoot apical meristem, auxin is distributed within this layer, ultimately generating local auxin peaks that drive the formation of new organs and associated vasculature [10]. Furthermore cytokinin is thought to diffuse from the epidermis to control the size of the pool of stem cells [11•]. Strikingly, dwarf brassinosteroid synthesis or signaling mutants, can be almost fully rescued when the wild-type gene is expressed only in the epidermis [12]. Similar restoration of normal root and shoot growth were recently obtained by modulating ethylene signaling in the epidermis [13]. Although these findings are based on genetics and biochemistry, the growth-controlling role of the epidermis entails a clear mechanical component: the continuous outer epidermal cell wall is generally thicker, and stiffer, than that of cells in underlying tissues, meaning that the turgor-driven expansion of internal cells is constrained by the epidermis (or more precisely the outer epidermal cell wall), which itself is under tissue level tension [14]. Note that epidermal outer wall thickening was mainly reported in hypocotyls, stems or leaves; yet, it seems to hold true for more undifferentiated tissues such as the shoot apical meristem ([15], Cloarec and Traas, unpublished data) or the embryo (unpublished data). Epidermal tension can be revealed in peeling experiments [16], by slicing open the epidermis [17], or by measuring the tissue response to compression [18]. Cell–cell adhesion defects in pectin synthesis mutants also reveal the presence of tension in the epidermis, and the resulting gaping patterns were recently used to deduce the principal orientation of tensile stress in aerial plant organs [19••]. In turn, epidermal cells respond to such tension. For instance, anisotropy in epidermal tension prescribes the orientation of the anticlinal divisions within the epidermis of the shoot apex in Arabidopsis [20]. Although the interplay between epidermal fate, function and tension are likely multiple, they remain

ill-described, notably because the control of epidermal tension is poorly understood.

The outer epidermal cell wall: a unique structure with a unique ontogeny

Both epidermal integrity and epidermal tension depend on the outer epidermal cell wall, which covers the entire aerial surface of the adult plant. Understanding the origin of this wall may clarify how epidermal tension develops and can be maintained.

During embryogenesis, the plant zygote divides to produce a population of outer cells (i.e. in contact with the original zygote cell wall) and inner cells (i.e. not in contact with the outer cell wall). Based upon the expression patterns of known epidermal markers, it appears that embryonic cells acquire an epidermal-precursor cell fate (protoderm fate) at a very early stage in embryo development, before the inner and outer cell populations form [21,22]. Protoderm fate is then maintained in 'outer' cells in a position dependent fashion. In Arabidopsis, where embryonic cell division patterns vary little, the sixteen cell (dermatogen) stage embryo is composed of eight 'outer' (protodermal) cells and eight 'inner' cells. Because plant cells usually do not move relative to each other, all epidermal cells in the adult plant derive ultimately from anticlinal divisions of the 'outer' cells of the dermatogen embryo and furthermore, because the extracellular matrix of dividing plant cells is not completely remodeled at each division, the outer epidermal cell wall covering the entire plant is, in ontogenetic terms, inherited directly from of the zygote cell wall. What are the consequences for the texture, composition and mechanics of this outer wall?

Cellulose microfibrils are the main load-bearing components of plant cell walls; they are embedded and tethered by a matrix of hemicelluloses, pectins and structural proteins, which play an important role in determining wall properties ([23•,24], see also [25••]). Epidermal cells divide like other plant cells: new walls form via the centrifugal growth of a 'cell plate (phragmoplast)', which ultimately inserts within the existing wall of the parent cell. At this stage, a middle lamella, which is strongly enriched in pectins, allows cell–cell adhesion [23•,26••]. Whereas cytokinesis in varying planes generates discontinuities in the network of most cell walls, the outer part of the outer epidermal wall only stretches during growth. In other words, the outer epidermal wall maintains a supracellular texture and mechanical continuity throughout development. From this point of view, the outer epidermal cell wall presents striking analogies with the mammalian basement membrane which acts as a supracellular support underlying epithelial monolayer ([27], see e.g. [28]). This has potentially important consequences for the coordination of signals across the epidermal layer. In fact, epidermal continuity was recently shown to be required for the propagation of mechanical signals [19].

To summarise, the structural role of the epidermis during development is associated with the unique continuity and stiffness of the outer wall. However, beyond mechanics and geometry, epidermal identity is also under tight genetic control.

The genetic basis of epidermal fate specification

De novo epidermal fate specification is a unique event. Epidermal ablation in *Citrus* showed that, when wounded, the late embryonic protoderm cannot regenerate [29]. Similar results from ablations in the meristems and organs of various other species during post-embryonic development [30] have led to the conclusion that protodermal cell fate is specified *de novo* only once, during early embryogenesis, and then inherited through divisions at the surface of developing meristems and organs during the whole life of the plant. Given this, the hypothesis that a chemical signal localized in the zygote cell wall is required for epidermal fate specification during early embryogenesis seems plausible, although the nature of this signal remains unclear. Nonetheless, several key proteins necessary for epidermal cell fate specification have been identified in plants, including members of the HD-ZIPIV family of transcription factors such as ARABIDOPSIS THALIANA MERISTEM L1 (ATML1) and PROTODERMAL FACTOR 2 (PDF2) [31–33] and receptor kinases including ABNORMAL LEAF SHAPE 2 (ALE2) and ARABIDOPSIS THALIANA HOMOLOGUE OF CR4 (ACR4) [33–37]. In Arabidopsis, genetic analysis suggests that feedback regulation between ACR4 and the functionally redundant ATML1 and PDF2 proteins is required to maintain epidermal cell fate [33,38]. As this may involve a mobile intercellular apoplastic signal, epidermal continuity seems essential for cell–cell signaling.

The specification and/or maintenance of epidermal identity in the early embryo, as marked by *ACR4*, *ATML1* and *PDF2*, also depends upon the gene *DEFECTIVE KERNEL 1* (*DEK1*) [39–41]. *DEK1* encodes an integral membrane protein composed of 23 transmembrane (TM) domains interrupted by a large cytosolic loop, as well as a C-terminus intracellular tail bearing a linker and a calpain-like domain (CALPAIN domain) – homologous to a family of cytoplasmic Ca^{2+}-dependent proteases found in animals and protists and involved in Ca^{2+} signaling cascades [42–45] (Figure 1). Similar to animal calpains, the activation of the DEK1 CALPAIN domain appears to involve an autocatalytic cleavage event upstream of the CALPAIN domain that may depend on the presence of Ca^{2+} [46,42]. Expression of the cytoplasmic CALPAIN domain of DEK1 alone is sufficient to complement loss of function mutations in the *DEK1* gene, suggesting that the DEK1 CALPAIN domain is the active form of the protein. This idea is also borne out by the inability of catalytically inactive versions either of the full length DEK1 protein, or the CALPAIN domain, to complement mutants [42].

Figure 1

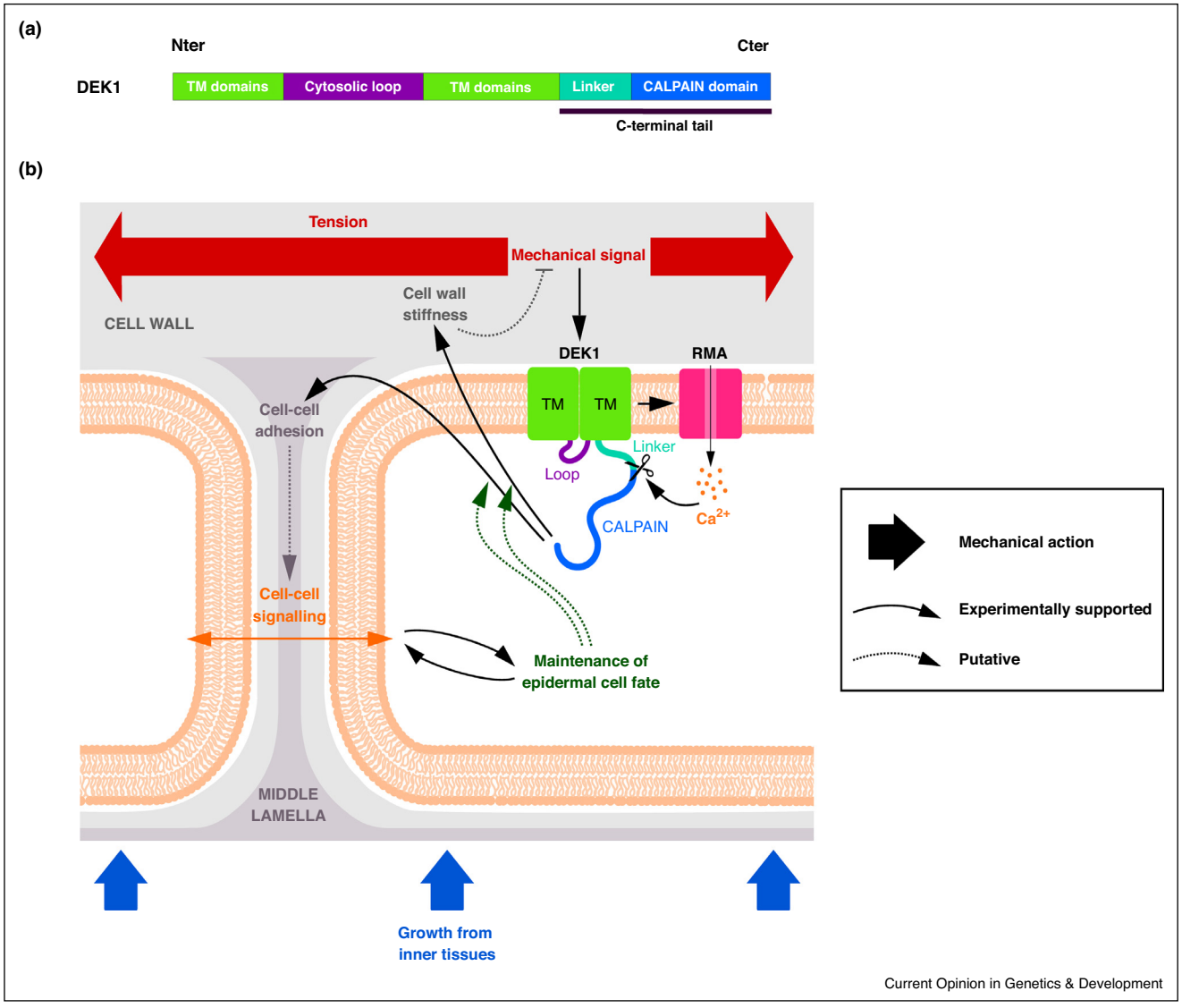

DEK1 function links mechanical cues to epidermal cell fate maintenance and development. **(a)** Schematic representation of the structural domains of the DEK1 protein. **(b)** Epidermal cell identity is maintained by cell–cell signalling (orange arrows) between epidermal cells, and is thus dependent upon epidermal integrity. However, the epidermal cell layer is placed under tension, as a result of the growth of underlying cells, and this tension tends to pull epidermal cells apart (physical forces are denoted by red arrows). The DEK1 protein translates membrane tension (a mechanical signal) into the cytoplasm through a mechanism involving the influx of Ca^{2+} via the RMA channel. Given current knowledge of CALPAIN activation mechanisms and DEK1 function, we propose that the RMA-mediated Ca^{2+} influx promotes the autolytic activation of DEK1 through cleavage of the CALPAIN domain. CALPAIN activation in turn leads to the modification of cell wall composition and thickness, most notably through the modification of pectin accumulation. This particular response to CALPAIN activation appears to be epidermis specific, and may therefore itself depend upon epidermal identity, although the underlying mechanism is unknown. Pectins influence the mechanical properties of the cell wall and are necessary for efficient cell–cell adhesion. Their accumulation ensures epidermal integrity, and thus maintains epidermal identity. In addition, by altering the mechanical properties of the cell wall, pectin accumulation may also modify (potentially attenuate) the mechanical stimulus perceived by DEK1. Note that the structural elements of the cells are not to scale.

Although DEK1 function is necessary for the expression of L1 fate regulators, over-expression of the DEK1 CALPAIN domain in a *dek1* mutant background does not cause over-expression of epidermal markers [42], suggesting that the dependence of the expression of epidermal regulators on DEK1 may be indirect.

Whereas these findings help us elucidate the genetic bases of epidermis specification, they do not integrate mechanics, and thus do not help us understand the potential interplays between epidermal specification and tension. The recent demonstration that DEK1 is required for the transduction of mechanical signals

(qualifying DEK1 as a mechanosensor in the broadest sense) [47••] provides a unique opportunity to revisit epidermis specification from a more integrated standpoint.

DEK1: the missing link between epidermal tension and fate maintenance

Mutants or mutant combinations in which early epidermal identity is seriously compromised (such as *atml1 pdf2* double null mutants and *dek1* null single mutants) show early embryo lethality, producing 'blobby' embryos, in which the smooth surface profile of the wild-type embryo is lost, cell adhesion at the embryo cell surface appears compromised and cell division patterns become disorganized [33,41,48]. This phenotype suggests that the mechanical properties of the outer cell wall, and indeed its integrity, are compromised, and that the build-up of epidermal tension is likely lost, in these mutants. This idea is also supported by mutants and mutant combinations with weaker phenotypes (such as lines with reduced DEK1 function, or mutant combinations including hypermorphic alleles of HD-ZIPIV encoding genes), which produce seedlings with defects in epidermal integrity [40,32]. These observations are consistent with the hypothesis that epidermal cell fate specification and the maintenance of epidermal integrity may both require, and likely promote, specific responses to the perception of epidermal tension. Analogous roles for tension in epithelial fate are currently emerging in animal development (see e.g. [49•,1••]).

How is tension perceived in the epidermis? In plant cells, mechanical stimulations have long been known to provoke a rapid influx of Ca^{2+} [50]. Several Ca^{2+} mechanosensitive channels have been identified [51,52•], but they seem to display minor roles in development, and have not been related to epidermal fate specifically. Recently, the DEK1 protein was shown to be required for the rapid activation of a Ca^{2+} channel activity — the Rapid Mechanically Activated (RMA) channel activity — in *Arabidopsis* protoplasts [53]. Given the established developmental role of DEK1 [39,41], this provides a formal link between mechanosensitive channel activity, calcium influx, and epidermal fate and maintenance. This is based on a scenario in which tension could be perceived by DEK1, activating the RMA channel, and leading to a rapid Ca^{2+} influx, cleaving and activating the CALPAIN domain of DEK1 (Figure 1).

The analysis of lines with different levels of DEK1 activity goes some way to elucidating how DEK1 activity leads to epidermal maintenance and mechanical integrity, notably by suggesting a role for DEK1, and its targets, in modulating epidermal wall structure [54••]. The constitutive over-expression of DEK1 CALPAIN domain leads to a specific thickening of outer epidermal cell walls with more cellulose and pectin than in the WT [54••]. Conversely, adhesion defects observed in the epidermis of hypomorphic *dek1* alleles are potentially explained by thinner epidermal cell walls and changes in the expression of genes involved in cell wall synthesis and remodeling [55]. Although wall thickness cannot be used as a proxy of wall stiffness, the modulation of wall thickness can result from mechanical defects. For instance, cell wall weakening with the cellulose synthase inhibitor isoxaben results in thicker walls [56].

Thus, the perception of epidermal tension, via DEK1, may trigger the reinforcement of the outer epidermal outer wall and/or cell–cell contacts, thereby consolidating epidermis continuity and allowing intercellular signaling to maintain epidermal identity [57] (Figure 1).

Although evidence is lacking, other putative mechanosensors may also be involved in epidermal specification, such as members of the *Catharanthus roseus* RECEPTOR-LIKE KINASE 1-LIKE (CrRLK1L) subfamily, which have been implicated in the control of cell wall integrity [58]. The mechanosensor FERONIA was also shown to regulate a Ca^{2+}-mediated mechanotransduction pathway in roots [59,60]. If this is the case, epidermal fate regulators (e.g. ACR4 and HD-ZIP IV transcription factors) are likely to genetically interact with mechanosensors (e.g. FERONIA, THESEUS) and analyzing these interactions may further refine our views on epidermal specification.

Conclusion

The formation of the epidermis is a crucial biological event impacting growth, development and survival. While the genetic control of epidermal specification is relatively well documented, the contribution of epidermal tension has only been recently integrated within the developmental gene network. Building on two decades of molecular genetics revealing the role of DEK1 in epidermal specification, the recent identification of DEK1 as a mechanosensor suggests that epidermal identity is maintained through the perception of tension within the epidermis. Growth in underlying tissues tends to pull epidermal cells apart. This tension would be perceived by mechanosensors such as DEK1. Mechanically induced DEK1 activation would lead to the opening of the RMA channel, provoking a fast Ca^{2+} influx and the cleavage of the DEK1 CALPAIN domain. Although the list of targets of CALPAIN remain to be identified, this response induces outer epidermal cell wall reinforcement ensuring cell-to-cell adhesion and thus epidermal continuity in a feedback loop (Figure 1).

Note that for this scenario to be fully confirmed, the presence of tension in the protoderm should be formally demonstrated; so far, protoderm tension has only been inferred from studies on seedlings (e.g. [14] or from

mechanical analogies (e.g. [61]). Furthermore, we propose that epidermal identity maintenance is dependent upon continuity, although how epidermal identity itself affects epidermal mechanics and responses to mechanical stimuli remains to be clarified. Last, this scenario holds for aerial organs; further mechanical analysis of roots would be required to extend this conclusion to underground organs.

Importantly, the identity of the DEK1-activated RMA channel protein remains to be discovered, and the scenario where DEK1 itself has a channel activity cannot be excluded [43]. Alternatively, the observed Ca^{2+} influx could be mediated by the PIEZO protein, for which a homolog has been identified in plants but still needs to be characterized. From an evolutionary point of view, this is a particularly pertinent hypothesis, considering the established roles of PIEZO1 and PIEZO2 in animal epithelia [62•,63–66]. These mechanosensitive Ca^{2+} channels have also been shown to act upstream of cytosolic calpains in animals [65,63,67], opening the possibility of conservation in epithelial/epidermal fate specification in both kingdoms.

Funding

This work was supported by a European Research Council (ERC) grant [#615739] 'MechanoDevo'.

Conflict of interest statement

Nothing declared.

References and recommended reading

Papers of particular interest, published within the period of review, have been highlighted as

- • of special interest
- •• of outstanding interest

1. •• Galletti R, Verger S, Hamant O, Ingram GC: **Developing a "thick skin": a paradoxical role for mechanical tension in maintaining epidermal integrity?** *Dev Camb Engl* 2016, **143**:3249-3258.
The authors highlight the tight connections between epidermal tension, integrity and fate in both plant and animals.

2. Serrano M, Coluccia F, Torres M, L'Haridon F, J-P Métraux: **The cuticle and plant defense to pathogens**. *Front Plant Sci* 2014, **5**:274.

3. Sieber P, Schorderet M, Ryser U, Buchala A, Kolattukudy P, Métraux J-P, Nawrath C: **Transgenic Arabidopsis plants expressing a fungal cutinase show alterations in the structure and properties of the cuticle and postgenital organ fusions**. *Plant Cell* 2000, **12**:721-737.

4. Wang Z-Y, Xiong L, Li W, Zhu J-K, Zhu J: **The plant cuticle is required for osmotic stress regulation of abscisic acid biosynthesis and osmotic stress tolerance in Arabidopsis**. *Plant Cell* 2011, **23**:1971-1984.

5. Engineer CB, Ghassemian M, Anderson JC, Peck SC, Hu H, Schroeder JI: **Carbonic anhydrases, EPF2 and a novel protease mediate CO_2 control of stomatal development**. *Nature* 2014, **513**:246-250.

6. Zeiger E, Farquhar GD, Cowan IR: *Stomatal Function*. Stanford University Press; 1987.

7. •• Carter R, Woolfenden H, Baillie A, Amsbury S, Carroll S, Healicon E, Sovatzoglou S, Braybrook S, Gray JE, Hobbs J *et al.*: **Stomatal opening involves polar, not radial, stiffening of guard cells**. *Curr Biol CB* 2017, **27**:2974-2983 e2.
The authors revisit the mechanical bases of stomata opening and show that the widespread inner wall thickening in guard cell is not correlated to the ability of stomata to open and close. Instead, using AFM, modeling and biochemical assay, they identify the stomata pole stiffening as a key requirement for stomata opening.

8. Sato Y, Kudoh H: **Herbivore-mediated interaction promotes the maintenance of trichome dimorphism through negative frequency-dependent selection**. *Am Nat* 2017, **190**:E67-E77.

9. Yeats TH, Rose JKC: **The formation and function of plant cuticles**. *Plant Physiol* 2013, **163**:5-20.

10. Reinhardt D, Pesce E-R, Stieger P, Mandel T, Baltensperger K, Bennett M, Traas J, Friml J, Kuhlemeier C: **Regulation of phyllotaxis by polar auxin transport**. *Nature* 2003, **426**:255-260.

11. • Gruel J, Landrein B, Tarr P, Schuster C, Refahi Y, Sampathkumar A, Hamant O, Meyerowitz EM, Jönsson H: **An epidermis-driven mechanism positions and scales stem cell niches in plants**. *Sci Adv* 2016, **2**e1500989.
Combining modelling and experimental work, the authors propose that the size of gene expression domains scale to tissue size through a cytokinin-gradient diffusing from the epidermis.

12. Savaldi-Goldstein S, Peto C, Chory J: **The epidermis both drives and restricts plant shoot growth**. *Nature* 2007, **446**:199-202.

13. Vaseva II, Qudeimat E, Potuschak T, Du Y, Genschik P, Vandenbussche F, Van Der Straeten D: **The plant hormone ethylene restricts Arabidopsis growth via the epidermis**. *Proc Natl Acad Sci* 2018, **115**:E4130-E4139.

14. Kutschera U, Niklas KJ: **The epidermal-growth-control theory of stem elongation: an old and a new perspective**. *J Plant Physiol* 2007, **164**:1395-1409.

15. Kierzkowski D, Nakayama N, Routier-Kierzkowska A-L, Weber A, Bayer E, Schorderet M, Reinhardt D, Kuhlemeier C, Smith RS: **Elastic domains regulate growth and organogenesis in the plant shoot apical meristem**. *Science* 2012, **335**:1096-1099.

16. Kutschera U: **Determination of the longitudinal tissue stresses in the growing and non-growing regions of sunflower hypocotyls**. *J Plant Physiol* 1991, **138**:460-465.

17. Dumais J, Steele CR: **New evidence for the role of mechanical forces in the shoot apical meristem**. *J Plant Growth Regul* 2000, **19**:7-18.

18. Beauzamy L, Louveaux M, Hamant O, Boudaoud A: **Mechanically, the shoot apical meristem of Arabidopsis behaves like a shell inflated by a pressure of about 1 MPa**. *Front Plant Sci* 2015, **6**:1038.

19. •• Verger S, Long Y, Boudaoud A, Hamant O: **A tension-adhesion feedback loop in plant epidermis**. *eLife* 2018, **7**.
In a simple set-up, gaps in a cell cell adhesion mutant reveal the pattern of tensile stress in hypocotyls, cotyledons, stems and leaves, and impair the ability of cortical microtubules to generate consistent supracellular alignments.

20. Louveaux M, Julien J-D, Mirabet V, Boudaoud A, Hamant O: **Cell division plane orientation based on tensile stress in *Arabidopsis thaliana***. *Proc Natl Acad Sci U S A* 2016, **113**:E4294-4303.

21. Lu P, Porat R, Nadeau JA, O'Neill SD: **Identification of a meristem L1 layer-specific gene in Arabidopsis that is expressed during embryonic pattern formation and defines a new class of homeobox genes**. *Plant Cell* 1996, **8**:2155-2168.

22. Takada S, Jürgens G: **Transcriptional regulation of epidermal cell fate in the Arabidopsis embryo**. *Dev Camb Engl* 2007, **134**:1141-1150.

23. • Chebli Y, Geitmann A: **Cellular growth in plants requires regulation of cell wall biochemistry**. *Curr Opin Cell Biol* 2017, **44**:28-35.
This didactic review presents a rather exhaustive view of the different biochemical players acting at the cell wall, their interdependence and their coupling with mechanics.

24. Cosgrove DJ: **Re-constructing our models of cellulose and primary cell wall assembly**. *Curr Opin Plant Biol* 2014, **22**:122-131.

25. •• Zhang T, Vavylonis D, Durachko DM, Cosgrove DJ: **Nanoscale movements of cellulose microfibrils in primary cell walls**. *Nat Plants* 2017, **3**:17056.
Using atomic force microscopy on wet cell walls, in combination with an extensometer, the author observe and analyze the movement of individual microfibrils during mechanical stretching, visualizing for the first time how microfibrils change their orientation and connectivity in walls under directional tensile stress.

26. •• Verger S, Chabout S, Gineau E, Mouille G: **Cell adhesion in plants is under the control of putative O-fucosyltransferases**. *Dev Camb Engl* 2016, **143**:2536-2540.
Building on a suppressor screen of cell–cell adhesion mutants, the authors show that pectin content is not the sole parameter behind adhesion defects, but that it also involves pectin signaling, thus adding another layer of complexity in the regulation of epidermis integrity.

27. Alberts B: *Molecular Biology of the Cell*. Garland Science, Taylor and Francis Group; 2015.

28. Evans MJ, Fanucchi MV, Miller LA, Carlson MA, Nishio SJ, Hyde DM: **Reduction of collagen VII anchoring fibrils in the airway basement membrane zone of infant rhesus monkeys exposed to house dust mite**. *Am J Physiol-Lung Cell Mol Physiol* 2010, **298**:L543-L547.

29. Bruck DK, Walker DB: **Cell determination during embryogenesis in *Citrus jambhiri*. II. Epidermal differentiation as a one-time event**. *Am J Bot* 1985, **72**:1602-1609.

30. Reinhardt D, Frenz M, Mandel T, Kuhlemeier C: **Microsurgical and laser ablation analysis of interactions between the zones and layers of the tomato shoot apical meristem**. *Dev Camb Engl* 2003, **130**:4073-4083.

31. Takada S, Takada N, Yoshida A: **ATML1 promotes epidermal cell differentiation in Arabidopsis shoots**. *Dev Camb Engl* 2013, **140**:1919-1923.

32. Abe M, Katsumata H, Komeda Y, Takahashi T: **Regulation of shoot epidermal cell differentiation by a pair of homeodomain proteins in Arabidopsis**. *Dev Camb Engl* 2003, **130**:635-643.

33. San-Bento R, Farcot E, Galletti R, Creff A, Ingram G: **Epidermal identity is maintained by cell–cell communication via a universally active feedback loop in *Arabidopsis thaliana***. *Plant J Cell Mol Biol* 2014, **77**:46-58.

34. Gifford ML, Dean S, Ingram GC: **The Arabidopsis ACR4 gene plays a role in cell layer organisation during ovule integument and sepal margin development**. *Dev Camb Engl* 2003, **130**:4249-4258.

35. Tanaka H, Watanabe M, Sasabe M, Hiroe T, Tanaka T, Tsukaya H, Ikezaki M, Machida C, Machida Y: **Novel receptor-like kinase ALE2 controls shoot development by specifying epidermis in Arabidopsis**. *Dev Camb Engl* 2007, **134**:1643-1652.

36. Tanaka T, Tanaka H, Machida C, Watanabe M, Machida Y: **A new method for rapid visualization of defects in leaf cuticle reveals five intrinsic patterns of surface defects in Arabidopsis**. *Plant J Cell Mol Biol* 2004, **37**:139-146.

37. Tanaka H, Onouchi H, Kondo M, Hara-Nishimura I, Nishimura M, Machida C, Machida Y: **A subtilisin-like serine protease is required for epidermal surface formation in Arabidopsis embryos and juvenile plants**. *Dev Camb Engl* 2001, **128**:4681-4689.

38. Moussu S, San-Bento R, Galletti R, Creff A, Farcot E, Ingram G: **Embryonic cuticle establishment: the great (apoplastic) divide**. *Plant Signal Behav* 2013, **8**e27491.

39. Becraft PW, Li K, Dey N, Asuncion-Crabb Y: **The maize dek1 gene functions in embryonic pattern formation and cell fate specification**. *Dev Camb Engl* 2002, **129**:5217-5225.

40. Galletti R, Johnson KL, Scofield S, San-Bento R, Watt AM, Murray JAH, Ingram GC: **DEFECTIVE KERNEL 1 promotes and maintains plant epidermal differentiation**. *Dev Camb Engl* 2015, **142**:1978-1983.

41. Johnson KL, Degnan KA, Ross Walker J, Ingram GC: **AtDEK1 is essential for specification of embryonic epidermal cell fate**. *Plant J Cell Mol Biol* 2005, **44**:114-127.

42. Johnson KL, Faulkner C, Jeffree CE, Ingram GC: **The phytocalpain defective kernel 1 is a novel Arabidopsis growth regulator whose activity is regulated by proteolytic processing**. *Plant Cell* 2008, **20**:2619-2630.

43. Kumar SB, Venkateswaran K, Kundu S: **Alternative conformational model of a seed protein deK1 for better understanding of structure–function relationship**. *J Proteins Proteomics* 2013, **1**.

44. Lid SE, Gruis D, Jung R, Lorentzen JA, Ananiev E, Chamberlin M, Niu X, Meeley R, Nichols S, Olsen O-A: **The defective kernel 1 (dek1) gene required for aleurone cell development in the endosperm of maize grains encodes a membrane protein of the calpain gene superfamily**. *Proc Natl Acad Sci* 2002, **99**:5460-5465.

45. Demko V, Perroud P-F, Johansen W, Delwiche CF, Cooper ED, Remme P, Ako AE, Kugler KG, Mayer KFX, Quatrano R *et al.*: **Genetic analysis of DEFECTIVE KERNEL1 loop function in three-dimensional body patterning in *Physcomitrella patens***. *Plant Physiol* 2014, **166**:903-919.

46. Wang C, Barry JK, Min Z, Tordsen G, Rao AG, O-A Olsen: **The calpain domain of the maize DEK1 protein contains the conserved catalytic triad and functions as a cysteine proteinase**. *J Biol Chem* 2003, **278**:34467-34474.

47. •• Tran D, Galletti R, Neumann ED, Dubois A, Sharif-Naeini R, Geitmann A, Frachisse J-M, Hamant O, Ingram GC: **A mechanosensitive Ca^{2+} channel activity is dependent on the developmental regulator DEK1**. *Nat Commun* 2017, **8**:1009.
The authors demonstrate the mechanosensitivity of DEK1, integrating the role of mechanical tension in epidermal specification, and incidentally, reveal that plant development beyond embryogenesis requires the perception of tension.

48. Liang Z, Brown RC, Fletcher JC, Opsahl-Sorteberg H-G: **Calpain-mediated positional information directs cell wall orientation to sustain plant stem cell activity, growth and development**. *Plant Cell Physiol* 2015, **56**:1855-1866.

49. • Hatte G, Prigent C, J-P Tassan: **Tight junctions negatively regulate mechanical forces applied to adherens junctions in vertebrate epithelial tissue**. *J Cell Sci* 2017 http://dx.doi.org/10.1242/jcs.208736.
In animals the mechanical integrity of epithelia is maintained by the mechanoresponsive reinforcement of adherens junctions. Here the authors show an important role for tight junctions at cytokinesis, in protecting adherens junctions from the imposition of excessive tension caused by the formation of the contractile ring, which can cause defects in cytokinesis. The work highlights the critical role of mechanical forces in the regulation of epithelial biology.

50. Chehab EW, Eich E, Braam J: **Thigmomorphogenesis: a complex plant response to mechano-stimulation**. *J Exp Bot* 2009, **60**:43-56.

51. Hamant O, Haswell ES: **Life behind the wall: sensing mechanical cues in plants**. *BMC Biol* 2017, **15**:59.

52. • Hamilton ES, Schlegel AM, Haswell ES: **United in diversity: mechanosensitive ion channels in plants**. *Annu Rev Plant Biol* 2015, **66**:113-137.
The authors review the different classes of mechanosensitive ion channels in plants, transducing a mechanical signal into a biochemical one, and raise the issue of assigning an ionic activity to a gene and a protein structure.

53. Tran D, Galletti R, Neumann ED, Dubois A, Sharif-Naeini R, Geitmann A, Frachisse J-M, Hamant O, Ingram GC: **A mechanosensitive Ca^{2+} channel activity is dependent on the developmental regulator DEK1**. *Nat Commun* 2017, **8**:1009.

54. •• Amanda D, Doblin MS, Galletti R, Bacic A, Ingram GC, Johnson KL: **DEFECTIVE KERNEL1 (DEK1) regulates cell walls in the leaf epidermis**. *Plant Physiol* 2016, **172**:2204-2218.
The authors analyse the effects of changing levels of DEK1 activity on leaf cell walls and pinpoint a key role for DEK1 in promoting the deposition of pectins and cellulose in the outer epidermal cell wall.

55. Amanda D, Doblin MS, Galletti R, Bacic A, Ingram GC, Johnson KL: **Regulation of cell wall genes in response to DEFECTIVE KERNEL1 (DEK1)-induced cell wall changes**. *Plant Signal Behav* 2017, **12**e1345405.

56. Manfield IW, Orfila C, McCartney L, Harholt J, Bernal AJ, Scheller HV, Gilmartin PM, Mikkelsen JD, Paul Knox J, Willats WGT: **Novel cell wall architecture of isoxaben-habituated Arabidopsis suspension-cultured cells: global transcript profiling and cellular analysis**. *Plant J Cell Mol Biol* 2004, **40**:260-275.

57. Galletti R, Ingram GC: **Communication is key: reducing DEK1 activity reveals a link between cell–cell contacts and epidermal cell differentiation status**. *Commun Integr Biol* 2015, **8**e1059979.

58. Wolf S: **Plant cell wall signalling and receptor-like kinases**. *Biochem J* 2017, **474**:471-492.

59. Haruta M, Sabat G, Stecker K, Minkoff BB, Sussman MR: **A peptide hormone and its receptor protein kinase regulate plant cell expansion**. *Science* 2014, **343**:408-411.

60. Shih H-W, Miller ND, Dai C, Spalding EP, Monshausen GB: **The receptor-like kinase FERONIA is required for mechanical signal transduction in Arabidopsis seedlings**. *Curr Biol CB* 2014, **24**:1887-1892.

61. Thompson DW: **Cambridge University Press**. *On Growth and Form*. 1917.

62. • Gudipaty SA, Lindblom J, Loftus PD, Redd MJ, Edes K, Davey CF, Krishnegowda V, Rosenblatt J: **Mechanical stretch triggers rapid epithelial cell division through Piezo1**. *Nature* 2017, **543**:118-121.

The authors demonstrate a critical role for the mechanosensitive channel PIEZO1 in maintaining epithelial homeostasis through the calcium-dependent stretch-activated promotion of mitosis in epithelial regions where cell density is sparse.

63. Hyman AJ, Tumova S, Beech DJ: **Piezo1 channels in vascular development and the sensing of shear stress**. *Curr Top Membr* 2017, **79**:37-57.

64. Li J, Hou B, Tumova S, Muraki K, Bruns A, Ludlow MJ, Sedo A, Hyman AJ, McKeown L, Young RS *et al.*: **Piezo1 integration of vascular architecture with physiological force**. *Nature* 2014, **515**:279-282.

65. Li J, Hou B, Beech DJ: **Endothelial Piezo1: life depends on it**. *Channels Austin Tex* 2015, **9**:1-2.

66. Ranade SS, Qiu Z, Woo S-H, Hur SS, Murthy SE, Cahalan SM, Xu J, Mathur J, Bandell M, Coste B *et al.*: **Piezo1, a mechanically activated ion channel, is required for vascular development in mice**. *Proc Natl Acad Sci U S A* 2014, **111**:10347-10352.

67. Bagriantsev SN, Gracheva EO, Gallagher PG: **Piezo proteins: regulators of mechanosensation and other cellular processes**. *J Biol Chem* 2014, **289**:31673-31681.

Mechanical stress is then sensed and used as a cue for mechanical reinforcement (to resist stress) and for other developmental processes. This implies that cells can indirectly monitor mechanical forces (mechanosensing) and then integrate this signal into biochemical pathways (mechanotransduction).

Open questions:

- What is the Ca^{2+} channel activated by DEK1? Is DEK1 this channel?
- How does DEK1 affect cell wall synthesis/modification?
- Does DEK1 play a role in water influx regulation?
- How would mechanical signaling be integrated with inner signals into the developmental pathway for epidermis specification?
- Is epidermis integrity (cell wall integrity) perceived as part of epidermis mechanical status (cell wall mechanical state)?

III◦ Mechanosensing and mechanotransduction: how is mechanical stress perceived and transduced?

Maybe the best evidence that plant cells do sense the mechanical status of their cell wall is compensation. Indeed, mutants impaired in a cell wall regulator often exhibit the molecular signature of the overexpressor of that regulator. For example, a *pme* mutant often exhibits the wall signature of a PME overexpressor (Sowinski et al., 2022). This means that the cell wall biochemical state and/or its mechanical status are closely monitored and taken into account for the subsequent cell wall production.

The following part has been published as part of a review I wrote along with the rest of Olivier Hamant's team during the course of my PhD (Trinh et al., 2021). I wrote this part of the review with particular help and feedback from Olivier Hamant, Duy-Chi Trinh and Juan Alonso-Serra. As such, the paragraph was placed between quotation marks with the relevant references replaced.

"The Lockhart equation describes the coupling between turgor pressure and cell wall (CW) properties during growth, and we have seen that this involves water flux control, CW synthesis and remodeling, cell geometry and tissue topology. As we will argue below, there is

growing evidence that these processes depend on the indirect perception of mechanical forces through mechanotransduction pathways, like wall sensors, mechanosensitive channels, the cytoskeleton, and even the cell nucleus (Figure 19).

There are different cell compartments where mechanical forces can be translated into biochemical cues. At the cell surface, the deformation of the CW may feed into downstream signaling events by liberating wall components. Under high tension, CW stretching may de-sequester signaling factors. For instance, demethylesterified pectin crosslinks in CWs could get distorted and release calcium (Proseus and Boyer, 2007). Although this would require more biophysical insight, tension in CW could also affect the distribution of other signaling molecules, such as peptides and oligosacharides.

The deformation and remodeling of CW can also transduce mechanical signals to the cell through conformational changes in downstream factors. At the interface between CW and plasma membrane, wall sensors monitor the integrity of the CW (Ringli, 2010). This notably includes RECEPTOR-LIKE KINASES (RLKs), a large family of membrane proteins with an extracellular domain and a cytosolic protein kinase domain (Dievart et al., 2020; Wolf, 2017). A well characterized member, FERONIA, binds to pectins in vitro (Feng et al., 2018). It is involved in a wide range of pathways, including calcium signaling and expression of touch-responsive genes, to maintain CW integrity (Feng et al., 2018; Shih et al., 2014). The closest homologs of FERONIA, ANXUR1 and ANXUR2, may sense CW integrity via extracellular maltose-binding domains (Li et al., 2016a). THE1 is another wall sensor only activated when CW properties are compromised (e.g., reduced cellulose biosynthesis) (Hématy et al., 2007). Similarly, WALL ASSOCIATED KINASES (WAKs) can bind to pectin and pectin derived molecules from pathogens, and are implicated in CW sensing (Brutus et al., 2010). As in animals, none of these sensors are strictly mechanosensors, as they also monitor the chemical properties of the wall. They probably rather sense chemical signatures in the CW that are derived from mechanical inputs (e.g., damage, unmasked motifs), also integrating other molecular cues, such as peptide ligands (e.g., RALF).

At the plasma membrane, mechanosensitive (also called stretch-activated) ion channels are transmembrane proteins mediating ion flux of, for example, Ca^{2+}, K^{+} and Cl^{-} through changes in protein conformation, following the thinning of the membrane when under tension (Haswell et al., 2011). Some, like MSL10, exhibit high conductance for anion

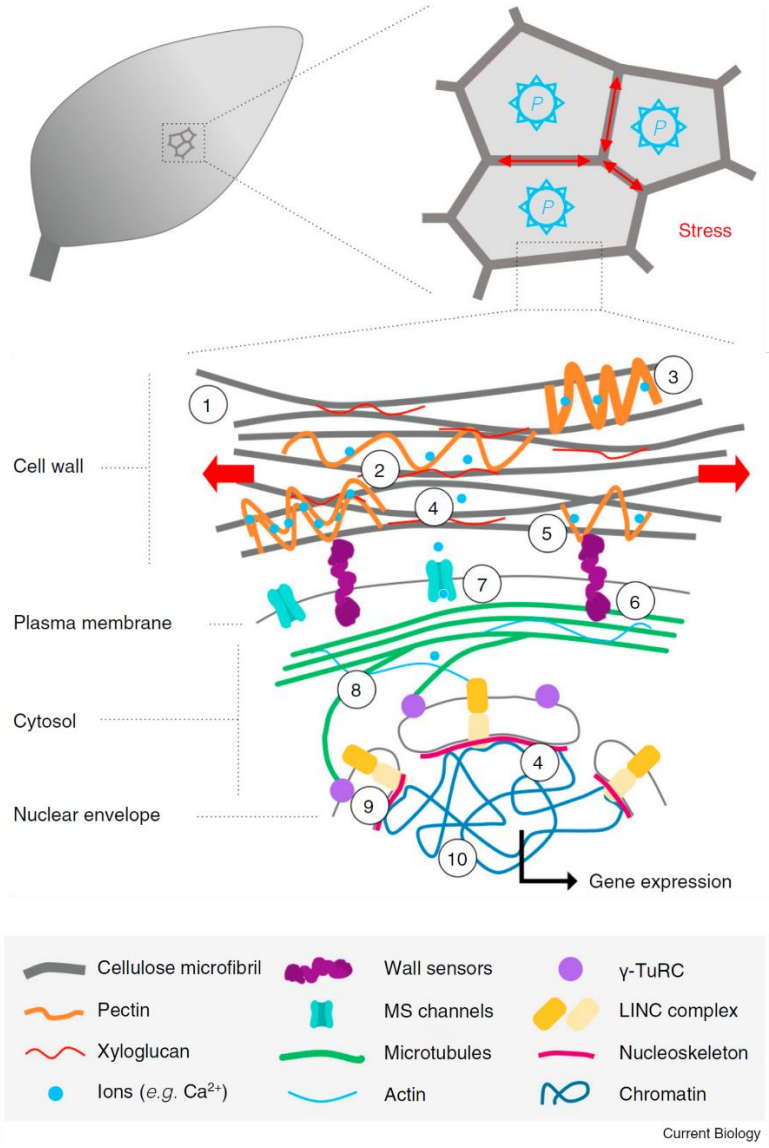

Figure 19: Putative events in a plant cell under mechanical stress: mechanical signaling through stress-induced nanostrains. **(1)** Nanoscale cellulose microfibril displacements (Zhang et al., 2017); **(2)** wall pectate distortion (Proseus and Boyer, 2007); **(3)** pectin nanofilament expansion (Haas et al., 2020); **(4)** (de)sequestration of signaling molecules or peptides (Muncie and Weaver, 2018; Proseus and Boyer, 2007); **(5)** unmasking of cryptic binding sites in wall components (polysaccharides and structural proteins) and/or changes in binding affinity (Roca-Cusachs et al., 2012); **(6)** protein conformation changes (Roca-Cusachs et al., 2012; Wang et al., 1993); **(7)** mechanosensitive channel opening (Haswell et al., 2011; Olesen et al., 1988); **(8)** biased cytoskeleton self-organization (Hamant et al., 2008; Heath and Dunn, 1978; Riveline et al., 2001); **(9)** stress propagation through stiff linkers, e.g., the g-tubulin ring complex (g-TuRC) or linker of nucleoskeleton and cytoskeleton (LINC) (Hampoelz and Lecuit, 2011); **(10)** chromatin conformation changes (Fal et al., 2017; Shivashankar, 2019).

release without inactivation and thus can serve as pressure valves to relax membrane tension, for example, in response to turgor increase (Hamilton et al., 2015a; Peyronnet et al., 2014). Others, like DEK1-dependent RMA, show low conductance for Ca^{2+} and high inactivation, and may rather serve as second-messenger providers (Guerringue et al., 2018). Ca^{2+} is involved in the response of many mechanical stimuli, such as gravity, touch, osmotic stress and bending (Hamilton et al., 2015a), with implications for organ morphogenesis, notably through its impact on auxin transport (Li et al., 2019).

Tension at the plasma membrane may have other effects. Although the content of phosphatidylinositol-4,5-bisphosphate is correlated with the pattern of tensile stress at the SAM (Stanislas et al., 2018), the impact of forces on membrane composition remains to be explored in plants (Ackermann and Stanislas, 2020). The link between tension and vesicle trafficking is better known — increasing plasma membrane tension promotes exocytosis and the secretion of wall materials, which, in turn, would reduce tension by reinforcing the CW (Fricke et al., 2000; Zonia and Munnik, 2007). It was reported that a 1.6-fold increase in turgor pressure is correlated with 4-fold increase in CW thickness in the SAM (Long et al., 2020). Through the control of vesicle trafficking, membrane tension may have other signaling consequences. For example, membrane tension may channel the trafficking of the auxin-efflux carrier PIN1 (Heisler et al., 2010; Nakayama et al., 2012). Osmotic stress also affects the generation of reactive oxygen species (ROS), which, together with Ca^{2+}, are often considered as second messengers of mechanical signals in plants (Shih et al., 2014). In turn, these factors may affect wall properties, turgor pressure and thus stress levels. In particular, ROS may weaken the wall through polysaccharide cleavage, or stiffen the wall through crosslinking (Tenhaken, 2015), they can induce the clustering and removal of aquaporin from the plasma membrane (Martinière et al., 2019) and they can affect cytoskeleton dynamics, and thus wall synthesis (Livanos et al., 2014).

At the cell cortex, the cytoskeleton is also sensitive to mechanical forces. For instance, actin filaments branch upon compression-induced bending (Risca et al., 2012). Stabilized microtubules can reorient upon stretching the surface on which they are attached in vitro (Inoue et al., 2015; Inoue et al., 2016). Both actin filaments and microtubules polymerize faster when under tension in vitro (Trushko et al., 2013; Yu et al., 2017). Interestingly, CMTs align along the maximal tensile stress direction in plant tissues; in turn, they guide the deposition

of CMFs and reinforce CWs in that orientation (Green and King, 1966; Hamant et al., 2008; Hejnowicz et al., 2000). This supports the view that microtubules may spontaneously orient with maximal tension in tissues. In that scenario, CMTs would be active mechanosensors relaying mechanical cues back to the CW (Hamant et al., 2019b).

Mechanosensing may also extend to the nucleus. Indeed, in animal cells, the cytoskeleton bridges the plasma membrane to the nuclear envelope, and participates in sensing mechanical deformations coming from the extracellular matrix. This form of nuclear mechanotransduction directly modulates the 3D architecture of the genome, resulting in differential gene expression (Uhler and Shivashankar, 2017). Plant nuclei are also deformed in response to hyperosmotic stress, and this correlates with an induction of mechanosensitive genes (Goswami et al., 2020). Whether this form of mechanotransduction provides transcriptional specificity to the response remains to be explored. Given the diversity of developmental and physiological status of plant cells, it is likely that mechanotransduction integrates signals from nuclear-cytoskeleton deformations (Fal et al., 2017), membrane mechanosensing (Basu and Haswell, 2017), and surveillance mechanisms of CW integrity (Vaahtera et al., 2019).”

As discussed in this part, RLKs have been proposed in many settings to be cell wall sensors, and in particular mechanosensors. Among them, FERONIA is a puzzling candidate as it is involved in a wide range of cellular processes.

Open questions:

- How to distinguish between direct and indirect (e.g. compensation) effects?
- At what spatial and temporal scale is strain sensing relevant as a proxy for stress sensing?
- Do mechanosensors transmit a specific signal for mechanical stress or is it an extension of stress sensing?
- How can we distinguish mechanosensors and other components of the mechanical signaling pathway?
- How do broad secondary messengers (ROS, Ca^{2+}) elicit a specific response for mechanical stress?

IV◦ Why is FERONIA pleiotropic?

The following part is a review in preparation I wrote during my PhD, with help and feedback from Olivier Hamant.

Since their emergence, cells had to face mechanical stress. The evolutive strategy adopted by plant cells is to produce a stiff cell wall to resist such stress. More specifically, this composite layer of polysaccharides and proteins resist mechanically the cell's turgor pressure and external stresses, while being plastic enough to adapt to cell growth in an ever-changing environment. This is achieved through the monitoring of the cell wall status, leading through signaling cascades, to dynamic cell wall production and modification. Many transmembrane proteins have been proposed as candidate cell wall sensors (Wolf, 2017; Wolf, 2022). Among them, the vast Receptor-Like Kinase (RLK) family contains more than 600 members (Morris and Walker, 2003). RLKs are composed of an intracellular kinase domain and a variable N-terminal extracellular domain used to classify them into subfamilies (Shiu and Bleecker, 2003). RLKs of the Catharanteus roseus receptor-like kinases (CrRLK) subfamily possess a malectin-like extracellular domains, similar to the conserved animal malectin binding carbohydrates (di-glucose motifs of N-linked oligoglycans, (Schallus et al., 2008; Wolf, 2017)). As such, the 17 members of this subfamily are good candidates for cell wall binding and sensing. Among them FERONIA (FER) is the most studied CrRLK, but its high number of interactors and the variety of phenotypes of its mutants may blur its core function.

IV.1◦ FERONIA is involved in many biological functions

FER is expressed in most plant organs, with the exception of mature anthers and pollen (Escobar-Restrepo et al., 2007). At the cell scale, the FER protein localizes to the plasma membrane without any detectable polarity (Duan et al., 2010; Escobar-Restrepo et al., 2007; Guo et al., 2009) , except for an accumulation at the filiform apparatus in synergids (Escobar-Restrepo et al., 2007; Hématy and Höfte, 2008).

FER was originally identified in a genetic screen in 2003, revealing its role in fertility (Huck et al., 2003; Rotman et al., 2003). The name FERONIA comes from the Etruscan goddess of fertility because of the role the protein plays in female fertility. In the *fer* and *srn* mutants,

defects in female signaling cause the pollen tube to continue growing instead of breaking upon reception (Dresselhaus et al., 2016; Duan et al., 2014; Escobar-Restrepo et al., 2007; Huck et al., 2003; Kessler et al., 2010; Rotman et al., 2003), leading to a high rate of polyspermy (Huck et al., 2003). Note that this function in fertility can be extended to other CrRLK members. In particular, close homologs of FER (ANXUR1/ANXUR2) are involved in male fertility, in the burst of the pollen tube (Boisson-Dernier et al., 2009; Miyazaki et al., 2009).

Other mutant alleles of *FER* have been studied, revealing additional developmental functions (Figure 20, Table 1). FER is indeed involved in a much wider range of biological functions beyond fertility, i.e. flowering, immunity, growth and morphogenesis. More specifically, several *fer* mutant alleles exhibit a delay in flowering, measured both in days after germination and in number of leaves (Wang et al., 2020a). *fer* mutants also develop bigger seeds than the wild type (WT) because of an increased elongation of the integument cells (Yu et al., 2014). Loss of function of the rice *FER* homolog also leads to smaller seed yield (Li et al., 2016b).

At the global phenotypic scale, all *fer* mutant alleles display stunt growth and many other developmental defects. In aerial parts, this includes smaller hypocotyls and cotyledons, leading to smaller plants at any developmental stage (Guo et al., 2009; Malivert et al., 2021; Yeats et al., 2016), partly due to reduced cell elongation (Guo et al., 2009) and partly due to reduced final number of growing cells (bursting cells) (Keinath et al., 2010; Malivert et al., 2021). Several mutants also display misshaped trichomes (Duan et al., 2010; Li et al., 2015b) and cyanosed leaves (Li et al., 2015b). The cotyledons of *fer-4* and *fer-2* are vitreous (Malivert et al., 2021) and exhibit pavement cells with a more circular shape, i.e. with larger and fewer lobes than in the WT (Li et al., 2015b; Malivert et al., 2021). Roots are affected too, as shown with the presence of collapsed root hairs (Duan et al., 2010; Li et al., 2015b; Zhu et al., 2020a), reduced root length (Haruta et al., 2014) and increased lateral root branching in *fer* mutants (Dong et al., 2019).

Last, FER functions have also been revealed in response to biotic and abiotic cues. More specifically, FER as other CrRLKs, was shown to upregulate the plant immune response (Ortiz-Morea et al., 2022), with different alleles of *fer* mutants displaying a low reactive oxygen

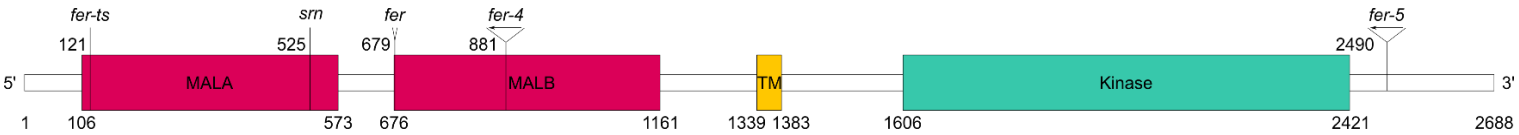

Figure 20: FERONIA structure and localization of different mutations. Positions are for base pairs.

Mutant name	Line name	Type	Mutation domain	Mutation precise place	Comment	First publication
fer	x	4–base pair (bp) insertion	MALB	Tyrosine 226	Frameshift, stop at beginning MALB domain, Leucine 228 (gene starts with MALA domain and ends with kinase domain)	(Escobar-Restrepo et al., 2007)
srn	x	single base pair deletion	MALA	Threonine 174	Frameshift, stop at Valine 191 right after MALA domain	(Escobar-Restrepo et al., 2007)
fer-2	x	tandem insertion of the activation-tagging vector, pSK015 (tDNA insertion)	x	x	KO mutant	(Deslauriers and Larsen, 2010)
fer-3	x	tDNA insertion	x	x	x	(Deslauriers and Larsen, 2010)
fer-4	GABI_GK 106A06	tDNA insertion	MALB	Methionin 293	KO mutant	(Duan et al., 2010)
fer-5	Salk_ 029056c	tDNA insertion	Kinase	Aspartic Acid 830	No K domain but Ex domain, weaker than *fer-4*	(Duan et al., 2010)
fer-ts	x	EMS single base pair substituation	MALA	Glycine 41	Temperature-sensitive mutant (unaffected at 20°C, enhanced protein turnover at 30°C)	(Kim et al., 2021)

Table 1: FER mutant alleles description.

species (ROS) response. The immune response in *fer* is in fact more complex. In particular, *fer* mutants exhibit a reduced bacterial infection, a powdery mildew resistance, and a hyposensitivity to several pathogen-associated molecular patterns but the mutant remains susceptible to other pathogens, in a stage-dependent manner (Guo et al., 2018; Keinath et al., 2010; Kessler et al., 2010; Masachis et al., 2016; Stegmann et al., 2017; Xiao et al., 2019; Zhang et al., 2020a). This correlates with constitutively high transcript levels of immunity marker genes in *fer-4* (Masachis et al., 2016). The FER protein was also recovered in a screen identifying proteins associated with membrane rafts following an exposition to bacterial peptides (flg22), along with other RLKs (Keinath et al., 2010). The FER immune response can be finely tuned in response to environmental cues to accommodate for root microbiome improving phosphate uptake (Tang et al., 2022). Abiotic stress resistance is also under the control of FER, as *fer* mutants display a cold, heat, and salt stress hypersensitivity (Chen et al., 2016; Feng et al., 2018; Yu and Assmann, 2018; Zhao et al., 2018). In contrast, *fer-4* growth is less sensitive to hyper osmotic stress (Chen et al., 2016; Malivert et al., 2021). In the hypocotyl, *fer-4* growth resistance to nickel is impaired, while resistance to cadmium, lead, copper and zinc is enhanced. Root growth however is more sensitive to copper and zinc and less sensitive to lead (Richter et al., 2017). Last, FER exhibits circadian expression dynamics, clock genes upregulating its mRNA levels, and in turn FER modulates clock genes expression (Wang et al., 2020a).

Beyond genetics, the involvement of FER in different biological functions can also be retrieved through *in silico* approaches, and notably through co-expression analysis. *FER* is co-expressed with *CELLULOSE SYNTHASE (CESA)* and other CrRLKs such as *THE1* (Ruprecht et al., 2014). On the BAR expressolog tree (http://bar.utoronto.ca/expressolog_treeviewer/cgi-bin/expressolog_treeviewer.cgi), *FER* appears to be co-expressed with other CrRLKs, in particular *CURVY1 (CVY1)* and *HERCULES RECEPTOR KINASE 1 (HERK1).* Taken together, these data suggest that FER may have a broader role in cell wall sensing and integrity. Yet the associated biological functions may have varied long-term implications. For instance, a *FER* deficiency leads to ectopic starch accumulation and an abnormal response to sucrose (Yang et al., 2015; Yeats et al., 2016).

We are thus left with a picture in which FER is involved in many, apparently unrelated, functions (Figure 21). One can thus wonder why and how FER can be so pleiotropic

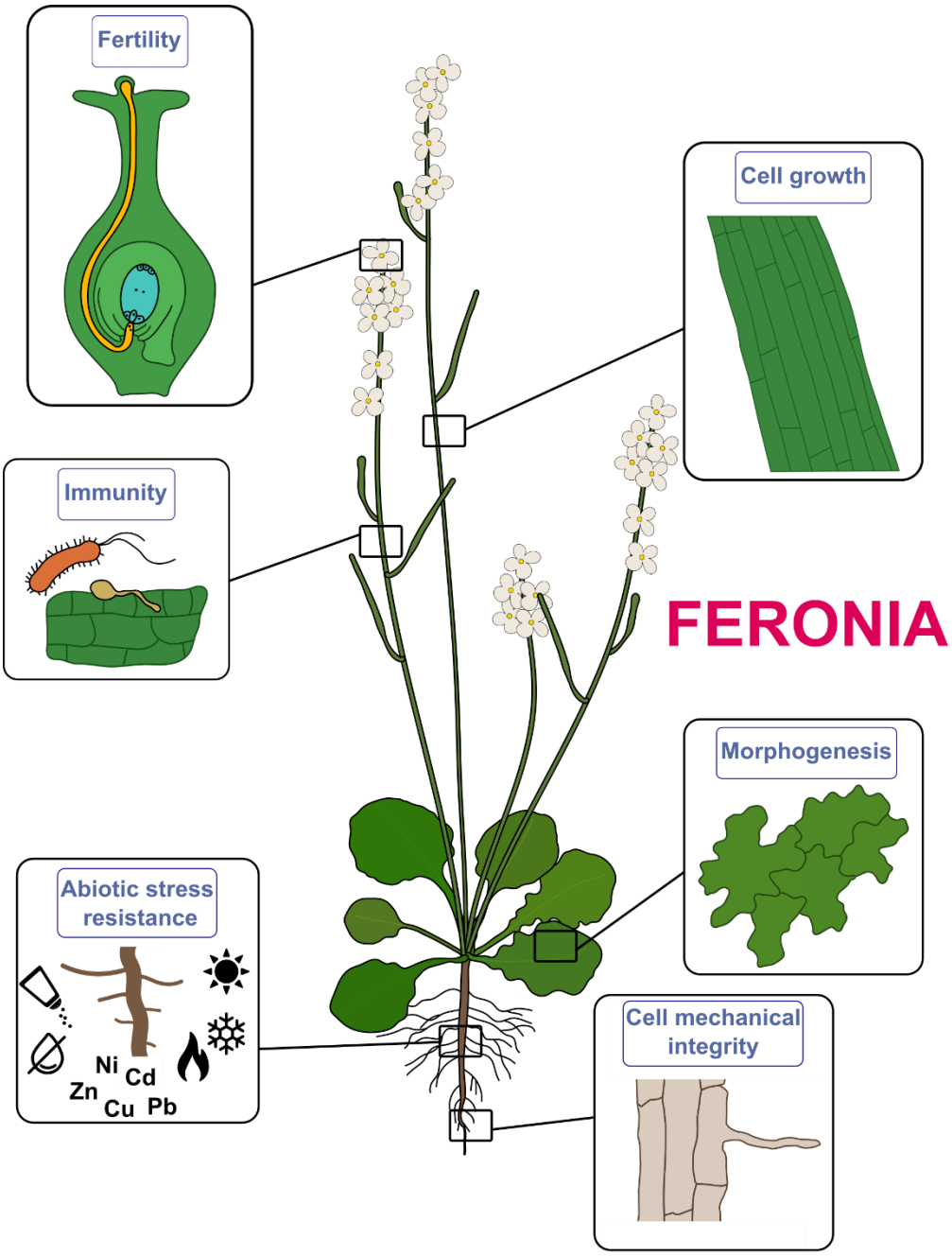

Figure 21: The pleiotropic role of FERONIA. FERONIA is involved in a wide range of functions in the whole organism: fertility, cell growth and mechanical integrity, morphogenesis, biotic and abiotic stress resistance.

(Solis-Miranda and Quinto, 2021). The biochemical characterization of FER partners may bring more mechanistic insight.

IV.2◦ FERONIA interacts with many cell wall partners

IV.2.1◦ Extracellular domains binding

As the two extracellular malectin-like domains in FER (Figure 20) are thought to bind carbohydrates, FER is a good candidate for cell wall binding and sensing. Note that the conserved malectin-like domains in the close homologs ANXUR1 and ANXUR2 lack some important residues required for carbohydrate binding in animal malectin (Du et al., 2018; Moussu et al., 2018). Thus, we cannot exclude that the interaction ability of the malectin domain may have functionally diverged between animals and plants (and between CrRLK members).

Beyond these predictions based on protein sequence, there is experimental evidence supporting carbohydrate binding ability for FER. In particular, the two FER malectin-like domains were shown to bind highly demethylesterified pectins (polygalacturonic acid PGA) in a dose-dependent manner *in vitro* (Feng et al., 2018). In a semi *in-vivo* pull down assay (after transient expression of FER in protoplasts), it was further shown that only the MALA domain is able to bind to both methylesterified and demethylesterified pectins, with a significantly higher affinity for demethylesterified pectins (PGA) (Lin et al., 2021). The binding of FER to pectins was also integrated in larger signaling pathways, and notably through the activation of the GTPase ROP6 (Lin et al., 2021).

In addition to carbohydrate binding, the FER extracellular domain can also bind to a large range of ligands and coreceptors. One of FER coreceptors is the glycosylphosphatidylinositol-anchored protein (GPI-AP) LORELEI (LRE), expressed exclusively in the ovule, where it plays a role in female fertility (Capron et al., 2008; Li et al., 2015b). FER can also bind to LRE-LIKE-GPI AP 1 (LLG1) and LLG2, necessary for the plasma membrane localization of FER in several tissues (Li et al., 2015b; Xiao et al., 2019). Immunoprecipitation experiments have also shown that FER forms complexes with some LEUCINE RICH REPEAT EXTENSINS (LRXs), and the other coreceptors FLAGELLIN-SENSING 2 (FLS2), BRASSINOSTEROID INSENSITIVE 1–ASSOCIATED KINASE 1 (BAK1) (Dünser et al., 2019; Stegmann et al., 2017),

while GST assays have revealed a complex formed by FER and RPM1-INDUCED PROTEIN KINASE (RIPK). The presence of numerous extracellular partners of FER further reinforces the position of FER as a wall sensor, but it does not elucidate FER pleiotropy. Instead, FER gains even more function, notably in hormonal signaling.

IV.2.2◦ RALF interactions

Like THE1 (Gonneau et al., 2018), FER has been shown to bind to several members of the family of RAPID ALKALINIZATION FACTOR (RALF) peptides (among a family of 34 members in *Arabidopsis* with a wide range of developmental and signaling functions, sometimes even with opposing roles e.g. in immunity, where RALF-like peptides mimicked by parasites instead downregulate the immune response (Blackburn et al., 2020)). Beyond immunity, RALF have much more genetic roles in the cell wall and may appear as an important clue to elucidate the mystery of pleiotropic FER functions (Zhang et al., 2020b).

Among the different RALFs interacting with FER, RALF1 is one of the most studied. It binds to FER and promotes its phosphorylation (Haruta et al., 2014). While *fer* roots and leaves exhibit defective cell expansion, overexpressing RALF1 leads to the same phenotype and silencing RALF1 promotes cell growth (Bergonci et al., 2014; Cheung and Wu, 2011; Du et al., 2016; Haruta et al., 2014). This suggests that RALF1 may act as a negative regulator of FER. This scenario is further consolidated by the observation that upon binding to RALF1, FER induces the opposite response for stomatal aperture and salt tolerance as well (Yu and Assmann, 2018; Yu et al., 2018). Similarly, treating plants with ectopic RALF1 also negatively regulates flowering time (thus mimicking *fer* loss-of-function) by modulating the transcript accumulation and more importantly the mRNA alternative splicing of flowering genes through GLYCINE-RICH RNA BINDING PROTEIN 7 (GRP7) phosphorylation (Wang et al., 2020a; Wang et al., 1). As often in biology, the situation is not so clear-cut, notably because of other feedback loops. In particular, RALF1 can also upregulate the expression of FER, as it does in the response to carbone/nitrogen (C/N) ratios. RALF1 induces the FER-mediated phosphorylation of the E3 ubiquitin ligase ARABIDOPSIS TÓXICOS EN LEVADURA 6 (ATL6) which leads to 14-3-3 proteins degradation and reduces C/N sensitivity (Xu et al., 2019). RALF1 promotes the kinase activity of FER on ERBB3-BINDING PROTEIN 1 (EBP1) as well, leading to its nuclear localization and the subsequent inhibition of RALF1-regulated gene transcription (Li et al., 2018, 1). This may be

amplified by the promotion of EBP1 translation among other genes by the FER-RALF1 complex (Li et al., 2018) through the upregulation of FER mediated phosphorylation of the translation initiation factor eIF4E1 (Zhu et al., 2020a; Zhu et al., 2020b). This last mechanism leads to a negative feedback loop reducing RALF1 levels as well as an opposite overall role for EBP1 and FER in seed size and root hair size.

FER also binds RALF23, notably in the context of immunity and salt stress. The decreased ROS levels in *fer* indicate a positive role of FER in ROS production, whereas the inhibition of ROS production afters a RALF23 treatment. This suggests that the immune response is hindered by the binding of RALF23 to FER (Stegmann et al., 2017). This would involve the disruption of a complex composed of the receptor kinases EF-TU RECEPTOR (EFR), FLS2 and BAK1 upon RALF23 binding to FER. RALF23 binds to LLG1 and FER to associate them as heterodimers and to regulate membrane nanodomain organisation (Gronnier et al., 2022; Shen et al., 2017; Xiao et al., 2019). In addition, RALF23 binding to FER negatively contributes to plant immunity by preventing FER from phosphorylating and destabilizing MYC2, an upregulator of the jasmonic acid stress hormone (Guo et al., 2018). RALF23 also disassociates from LEUCINE-RICH REPEAT EXTENSINS (LRX) 3/4/5 under a salt stress and it associates with FER, leading to FER internalization and an inhibition of plant growth (Zhang et al., 2021b; Zhao et al., 2021).

Interestingly, FER-RALF binding seems to be independent from glycolysation since it occurs with bacterially-produced recombinant proteins (Haruta et al., 2014), suggesting that the binding mechanism is different from that of carbohydrate binding. The high number of FER ligands and coreceptors may thus imply various domains for different binding types involving the extracellular domain. RALF binding seems to modulate FER function depending on the RALF peptide and the FER coreceptors involved, sketching FER as a potential RALF-modulated hub integrating various signals (Li et al., 2015b; Xiao et al., 2019; Zhang et al., 2020a). In that scenario, FER would rather act as a platform aggregating signaling receptors and ligands, rather than being a specific receptor by itself (Figure 22). Whereas the upstream FER interactions rather suggest that FER core function is its pleiotropic role as a signaling hub, the downstream signaling cascade may help us to shed some light on more specific biochemical functions.

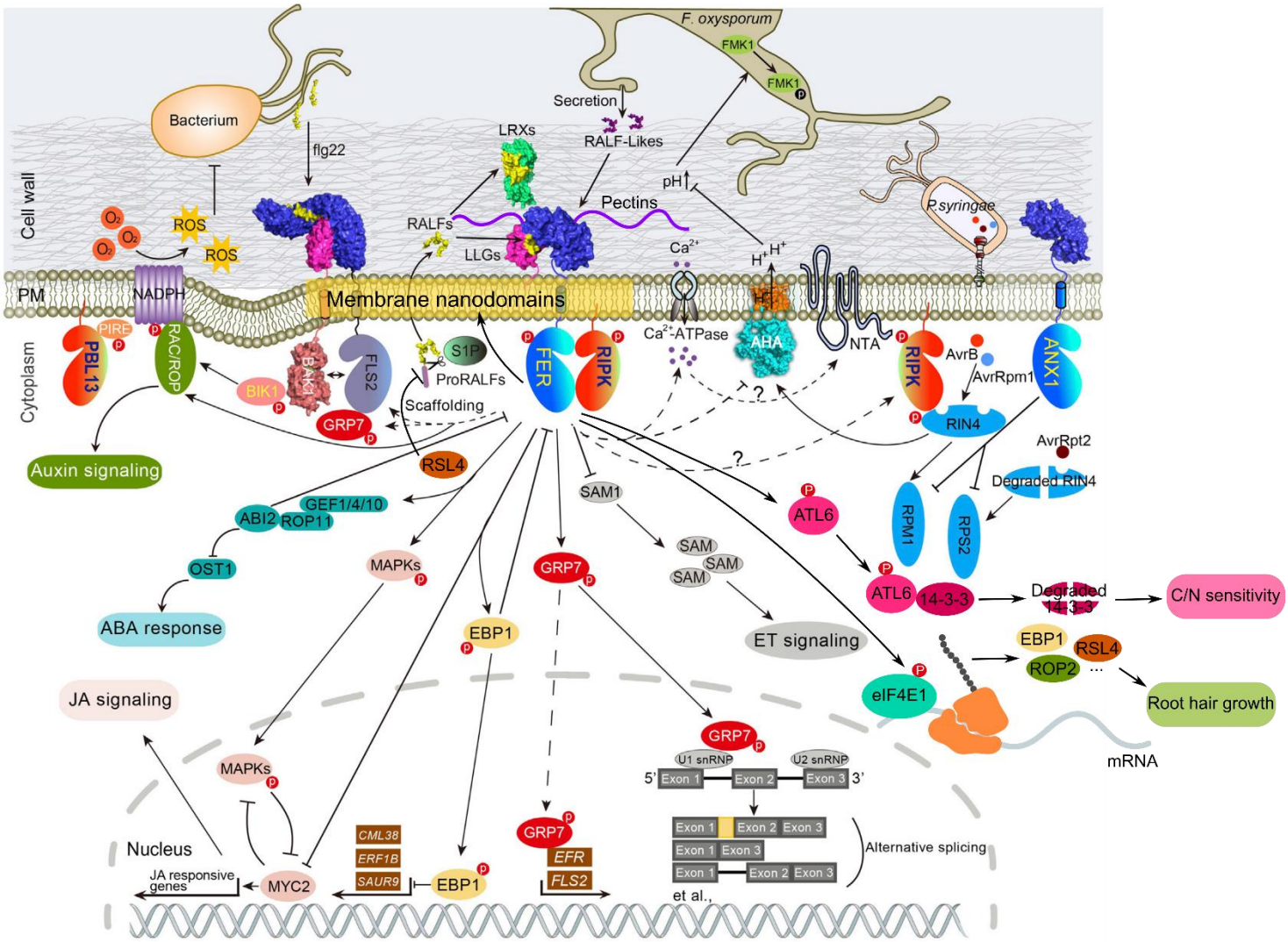

Figure 22: *Adapted from (Zhang et al., 2020a)*. FERONIA is involved in a multitude of signaling pathways. FERONIA interacts with numerous actors, both in the cell and in the apoplast, and thus acts as a hub for different signaling pathways.

IV.3◦ The FERONIA signaling pathway converges to shared secondary messengers

IV.3.1◦ ROS pathway

As mentioned above, several *fer* mutant alleles exhibit decreased ROS levels in various tissues (Duan et al., 2014; Keinath et al., 2010). An associated molecular mechanism has been identified. Indeed, FER binds to the guanine nucleotide exchange factor ROP-GEF, which then activates the RAC/ROPs plant RHO GTPases. This mechanism is dependent on LLG1 binding to FER and leads to the RAC/ROP activation of the NADPH oxidase RBOH, and a subsequent localized burst of ROS (Duan et al., 2010; Duan et al., 2014; Li et al., 2015b).

ROS production in response to FER signaling partly explains the FER role in fertility since ROS modulate compatible pollination on stigmata and can induce pollen tube rupture (Duan et al., 2014; Zhang et al., 2021b). The local, polarized production of ROS also leads to cell polarity, mediating fertility, immunity and root hair production (Duan et al., 2010; Kessler et al., 2010; Lee et al., 2020).

Even if FER generally promotes ROS production, this action can be modulated by other factors. RALF23 binding to FER inhibits ROS production upon bacterial pathogen associated molecular patterns (PAMPs) treatments (Gronnier et al., 2022), and ABA presence leads to the same response in guard cells (Yu et al., 2012).

IV.3.2◦ Ca2+ signaling

FER is required to trigger the production of a burst of calcium (Ca^{2+}) in roots following mechanical stress or salt stress (Feng et al., 2018; Shih et al., 2014). This is consistent with cell integrity and mechanical response defects in *fer* mutants. In particular, RALF1 binding is responsible for this FER-dependent Ca^{2+} signaling in roots (Haruta et al., 2014). FER is also required for initiating the Ca^{2+} influx responsible for a ROS increase leading to pollen tube rupture, and thus sperm release (Duan et al., 2014; Ngo et al., 2014). Despite the clear association of FER and Ca^{2+}, the precise mechanism for FER action on Ca^{2+} influxes, and in particular the channel involved still needs to be determined (Liao et al., 2017).

With ROS and Ca^{2+}, it appears that FER activates two classic secondary messengers that are involved in most biological functions. This could also explain why FER displays such pleiotropic functions (Figure 22). However, many other proteins also trigger such downstream signals, without having the pleiotropy level of FER. Is the plethora of cell wall binding partners and shared downstream factors sufficient to explain FER pleiotropy?

IV.4◦ FER at the crossroads of hormonal signaling pathways

There is increasing evidence of widespread crosstalk between FER and hormones (Figure 22). FER is a downstream effector in the auxin signaling pathways, consistent with its role in cell growth: auxin does not trigger root hair elongation in several *fer* mutant alleles (Duan et al., 2010; Kim et al., 2021; Li et al., 2015b). More precisely, FER is responsible for a transient alkalization of the apoplast following auxin level increase, inhibiting root cell growth (Barbez et al., 2017). Moreover, FER seems to be involved in the polar localization of the PIN-FORMED2 (PIN2) auxin transporter, and thus in the polarization of auxin transport (Dong et al., 2019). FER role in cell growth may also be due to FER involvement in ethylene biosynthesis regulation (Mao et al., 2015), leading to a hypersensitive hypocotyl length phenotype to ethylene exposition (Deslauriers and Larsen, 2010) and fruit ripening defects in crops (Jia et al., 2017a; Jia et al., 2017b) in *fer* mutants. Cell elongation is also controlled by brassinosteroids (BRs), which act on FER in several ways (Höfte, 2015). BRs induce FER expression (Guo et al., 2009), and FER contributes to the BR signaling cascade (Deslauriers and Larsen, 2010) by binding to the brassinosteroid receptor BR INSENSITIVE3 (BRI3) (Fàbregas et al., 2013).

FER is also involved in stress hormones pathways (Xie et al., 2022). Several *fer* mutants exhibit a hypersensitive growth arrest in response to abscisic acid (ABA), a response that is also triggered by LLG1 (Li et al., 2015b; Yu et al., 2012). FER suppresses ABA signaling by activating the ABA INSENSITIVE 2 (ABI2) phosphatase through the ROP-GEF/RAC pathway which, in turn inhibits the ABA response (Yu et al., 2012). As ABI2 dephosphorylates FER, this creates a negative feedback loop regulating different aspects of the stress response (stomata closure, immune response, …) (Chen et al., 2016). The role of FER in immunity, salt resistance and plant growth is also due to its link with ABA, Jasmonic Acid (JA) and Salicylic Acid (SA). As mentioned above, while FER activates the phosphorylation and destabilization of the

transcription factor MYC2, a master regulator of JA and SA signaling, RALF23 association with FER – and in at least some of these processes LRXs - counters this effect, which increases JA and downregulates immunity (Guo et al., 2018; Zhao et al., 2021). Interestingly, the role of FER in immunity through ROS production is also linked to its role in ethylene signaling , as the accumulation of FLS2 relies on ethylene signaling (Mersmann et al., 2010), and to its role in ABA signaling (Zhao et al., 2021).

Because of the multiple FER interactions – with cell wall components, RALF peptides, downstream factors and hormones – it can be conceptualized as a scaffold, a structural component where multiple signaling pathways could cross and potentially interact (Stegmann et al., 2017). This could explain the pleiotropy of FER. However, this catalogue may mask another, non-exclusive, hypothesis. At the nexus between the genotype and the phenotype, one finds the essential contribution of mechanics: genes control shape via their indirect impact on the mechanical properties of cells; conversely, shape and growth prescribe mechanical stress fields that coordinate cell growth and gene expression (Trinh et al., 2021). In other words, the mechanical status of the cell integrates all signaling outputs into one coherent parameter. Could cell wall mechanics contribute to explain FER pleiotropy?

IV.5◦ Is FERONIA a mechanosensor?

IV.5.1◦ fer mutants are unable to maintain the mechanical integrity of their cells

FER was first proposed to be involved in mechanotransduction based on studies in roots. The loss of FER causes defects in the ability of the root to probe its environment when encountering an impenetrable medium (root barrier response) (Shih et al., 2014). These defects are partially rescued when roots are grown on a lower density agar medium before meeting the barrier, suggesting that the phenotype is due to a lower mechanical strength in the mutant. This is confirmed by the decreased ability in *fer* roots to penetrate stiffer mediums. In addition, several elements of the touch response are lost in *fer*: the Ca^{2+} influx, acidification, and *TOUCH* genes expression induction observed following root bending or a hypoosmotic stress. All of these match a defective mechanoperception in *fer*. Finally, *fer* mutants also present a root skewing, i.e. a progressive growth deviation from the gravity axis

normally absent in the WT (Shih et al., 2014). This last phenotype is accompanied by a delayed gravitropic response which seems to be linked to auxin transport through the polarity of PIN2 following gravistimulation (Dong et al., 2019).

The response to touch or gravity is not sufficient to make mechanosensing the primary role of FER. Following these pioneering studies, there is now evidence that *fer* growth and development defects rely on mechanics. In particular, *fer* mutants are unable to maintain the mechanical integrity of their cells in various tissues: their root hairs show defects ranging from dwarfism to collapsing associated with a cytoplasm discharge (Duan et al., 2010). In rosette leaves infiltrated with a PAMP in solution, or simply with $MgCl_2$, *fer* displays tissue collapse and aberrant cell death revealed by Trypan blue, exhibiting *fer* sensitivity to mechanical stress (Keinath et al., 2010). In a recent study, dead cells were also reported in *fer-4* and *fer-2* aerial tissues in normal *in vitro* growth conditions. These cells first swell, then burst and deflate, and the number of burst cells keeps increasing over time (Figure 23A) (Malivert et al., 2021). This burst cell phenotype can explain organ growth defects in *fer*, as it correlates with smaller cotyledons (Figure 23B).

Interestingly, the burst cell phenotype depends on the mechanical environment of the seedling. When increasing the agar concentration in the growth medium, the water potential is lowered (meaning that the water availability for the plant is reduced) and this decreases cell wall tension (Verger et al., 2018). Strikingly, in such conditions, the burst cell phenotype in *fer-4* and *fer-2* is almost completely rescued (Malivert et al., 2021)(Figure 23A). Consistently, cotyledon growth is also largely rescued in these conditions, further confirming the link between burst cells and growth defects (Figure 23B). Therefore, most of the morphogeneic *fer* defects may depend on a single core variable: the magnitude of cell wall tension. Note that only the bursting of root hair cells do not seem to be rescued on 2.5% agar in *fer*, possibly because of the specificities of tip-growth development.

Before going further in that functional dissection, one must ask whether such mechanical defects should be considered as first order causes of FER pleiotropy. The burst cell phenotype is extremely rare among Arabidopsis mutants. To our knowledge there are only two other lines with potentially collapsed cells. One is a double mutant of the other CrRLKs HERK1 and THE1, which displays similar transcriptome profile than a line with FER defects

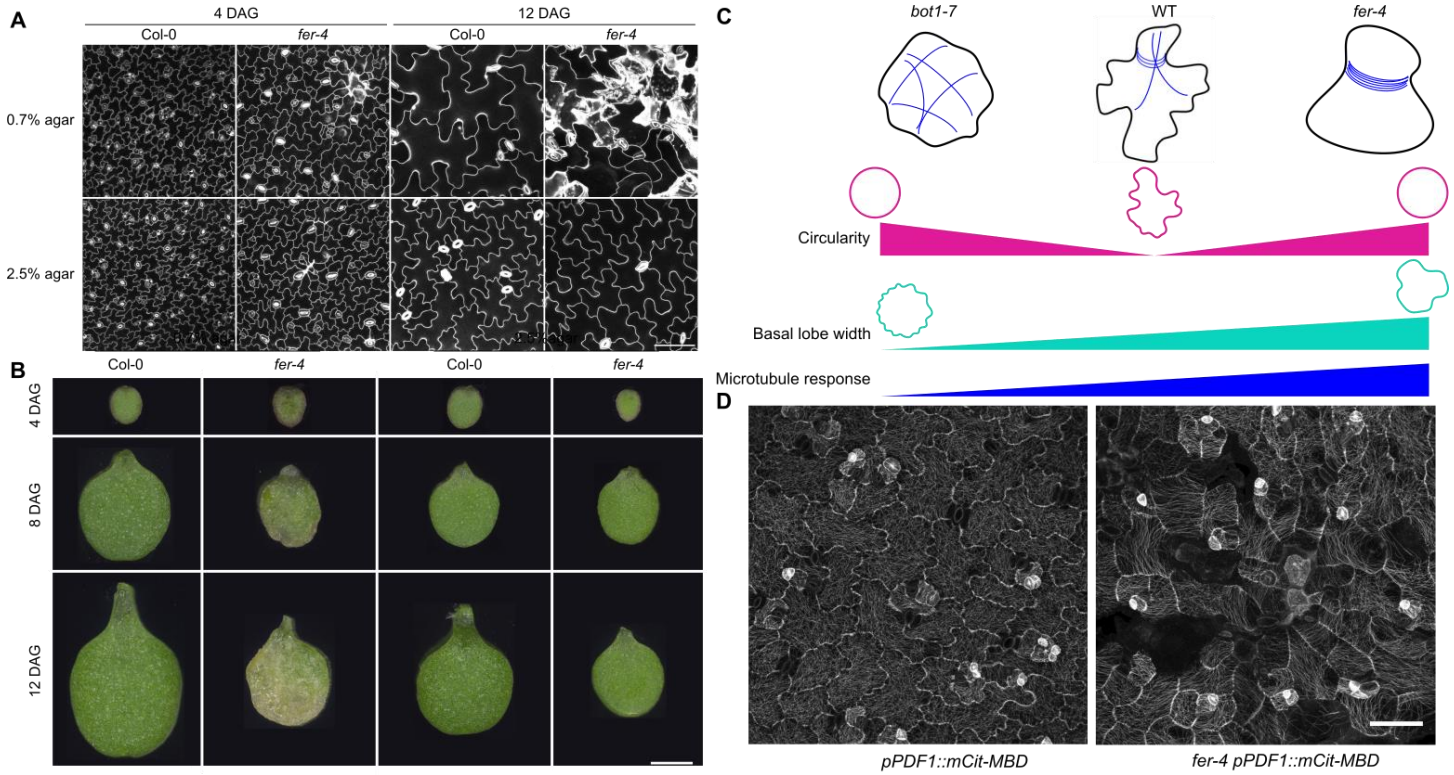

Figure 23: FERONIA is responsible for cell mechanical integrity. **(A)** *Adapted from (Malivert et al., 2021)*. *fer-4* pavement cells burst when the cell wall tension is high (on 0,7% agar). This phenotype is partially rescued by decreasing cell wall tension (2,5% agar). Representative confocal images of *Col-0* and *fer-4* pavement cells, from seedlings grown on a medium containing 0.7% or 2.5% agar at t = 4 DAG and t = 12 DAG (propidium iodide staining). Scale = 100 µm. **(B)** *Adapted from (Malivert et al., 2021). fer-4* cotyledons are small and vitreous when the cell wall tension is high (0,7% agar). This phenotype is partially rescued by decreasing cell wall tension (2,5% agar). Representative images of *Col-0* and *fer-4* cotyledons, grown on a medium containing 0.7% or 2.5% agar at t = 4 DAG, t = 8 DAG, and t = 12 DAG. Scale = 1 mm. **(C)** Several descriptors can be used to quantify pavement cell shape. If the circularity is a good proxy for defects in the response to stress, it is not a parameter as good as the basal lobe width to describe the microtubule response to stress. In *bot1-7* and *fer-4* both the circularity is higher but pavement cells in *bot1-7* present a low basal lobe width, coherent with a low microtubule response, while the ones in *fer-4* display a high basal lobe width, signs of a hyper-reponse of microtubules to stress. **(D)** *Adapted from (Malivert et al., 2021).* Microtubules are hyperaligned in *fer-4* on 0,7% agar, sign of a high tensile stress. Representative confocal images of *pPDF1*::*mCit-MBD* and *fer-4 pPDF1*::*mCit-MBD* pavement cells from seedlings grown on a medium containing 0.7% agar. Note the presence of circumferential cortical microtubules around dead cells, matching the predicted maximal tensile stress direction.

(Guo et al., 2009) and a similar salt stress response (Gigli-Bisceglia et al., 2021). The other is *pSTM:CDKA;1.N146*, a negative dominant allele of A-type cyclin-dependent kinase under the *SHOOTMERISTEMLESS* promoter, with likely defects in delivery of cell wall components (Borowska-Wykręt et al., 2013). More generally, this analysis reveals that behind the apparent pleiotropy of the *fer* phenotype, there is instead a quasi unique and specific feature in the mutant: the cell bursting phenotype. Furthermore, when rescuing it (in hyperosmotic conditions), the larger *fer* phenotype is also rescued (Figure 23A-B). Although this would need to be verified for the other FER functions (in particular for immunity and other abiotic stresses), this suggests that mechanical integrity is a primary contributor to FER pleiotropy.

IV.5.2◦ FER could play a key role in matrix reinforcement

One could wonder if the mechanical failure, i.e. the burst cell phenotype, is primarily due to cell wall defects in *fer* mutants (Li et al., 2015b). Cellulose microfibrils being the main load-bearing components of the wall, does FER maintain cell integrity through cellulose-dependent wall reinforcement? *fer* does exhibit an overall cellulose level deficiency (Yeats et al., 2016). However, this is not sufficient to explain the *fer* phenotype. Massive cellulose defects in mutants do not necessarily lead to bursting cells (Gu et al., 2010). This suggests that we are still missing a piece of the puzzle.

In a scenario where the pleiotropic role of FER would be due to a shared role in mechanical sensing, one should find quantitative proxy of defective mechanosensing in *fer* shapes. This can be illustrated with the case of pavement cells in cotyledon epidermis, which jigsaw puzzle shape (e.g. measured by circularity) scales with the amplitude of mechanical stress (Sapala et al., 2018),. Mechanistically, the maintenance of necks is determined by the microtubule response to tensile stress (Sampathkumar et al., 2014). Like the microtubule-associated mutant *bot1-7*, *fer-4* and *fer-2* exhibit an increased pavement cell circularity, suggesting a reduced response to stress in *fer* (Malivert et al., 2021). However, a more careful analysis of the pavement cell shape brings a more pertinent insight. Indeed, circularity integrates different shape descriptors and does not necessarily scale with the number or size of necks. In particular, increased circularity can be triggered by many small necks (consistent with reduced microtubule response to stress) or by few large necks (consistent with increased microtubule response to stress). This means that lobe or neck width is a better proxy for the

microtubule response to stress. Interestingly, *bot1-7* pavement cells exhibit lower basal lobe width than the WT, consistent with a reduced microtubule response to stress, whereas *fer* pavement cells exhibit higher basal lobe width, consistent with higher microtubule response to stress (Figure 23C). This is confirmed when visualizing hyperaligned microtubules in *fer-4* on 0.7% agar or in response to local mechanical perturbations (Figure 23D). Thus, FER is not necessary for the cortical microtubule response to stress. This does not exclude a contribution of FER in the modulation of microtubule organization, via the GTPase ROP6 for example (Tang et al., 2021), but rather suggests that FER is not the primary mechanosensor responsible for microtubule reorganization. In fact, when depolymerizing microtubules, the burst cell phenotype becomes even more severe further showing that FER and microtubule-dependent cellulose deposition can be uncoupled (Malivert et al., 2021). Together with the burst cell phenotype, this rather suggests that *fer* cells attempt to resist mechanical stress through the microtubule response to stress, yet unsuccessfully. This would narrow down FER mechanosensing defect to a subset of wall responses.

There is evidence that FER binds pectin. One could imagine that FER is a matrix tension sensor or matrix status sensor. In turn, FER does not rely on the pathway of microtubules/cellulose microfibrils to reinforce the wall, but may rather involve elements of the wall matrix, and more specifically pectins and xyloglucans. The content in matrix monosaccharides is altered in *fer* (Yeats et al., 2016). In particular, the lack of a pectin cross-linking mediated by FER through Ca^{2+} transients seems responsible for *fer* root burst cells after a salt treatment (Feng et al., 2018; Gigli-Bisceglia et al., 2021). Pectin demethylesterification (or maintenance in a demethylesterified state) also appears to be modulated by FER at the filiform apparatus (Duan et al., 2020). These results associated with the Ca^{2+} depletion in *fer* apoplasts may lead to possible changes in cell wall stiffness and loosening mediated by FER (Codjoe et al., 2022). This is also an opportunity to explore the link between ROS and cell wall mechanical state because FER is involved in ROS production (Duan et al., 2014; Keinath et al., 2010) and ROS may both loosen and stiffen the cell wall through cleavage and cross-linking of polysaccharides (Kärkönen and Kuchitsu, 2015). Changes in the production or in the alteration (methylation) of some cell wall elements could also explain mechanical defects in *fer*. Indeed, the *shaven3* (*shv3*) mutant exhibits root hairs collapse as well as small hypocotyls, similarly to *fer*, linked to a reduced cellulose content and decreased pectin cross-linking (Hayashi et al.,

2008; Yeats et al., 2016). Pectin delivery in the cell wall could also be altered since it is a mechanism dependent on vesicle transport along the actin cytoskeleton (Toyooka et al., 2009), which seems to be impaired in *fer-4* roots (Dong et al., 2019).

The FER contribution to cell wall properties (both sensing the wall and triggering its mechanical reinforcement) could play the role of a functional integrator, explaining its pleiotropic contributions to many biological functions. Interpretation is supported by results obtained in animal systems where core mechanosensors (e.g. integrins) also bind ligands and are involved in many biochemical pathways. Yet, this is only one side of the coin. The mechanical integrity of the cell depends on wall properties as well as turgor pressure (Figure 24). Following the observation of the explosive pollen tube discharge observed immediately after Ca^{2+} channels opening, the hypothesis of the rupture of an equilibrium between turgor pressure and cell wall strength has been proposed (Duan et al., 2014). In that scenario, FER would thus also, and possibly mainly, act as a pressure sensor.

IV.6◦ Is FERONIA a pressure sensor?

Essentially, cell wall tension and rupture is caused by the high turgor pressure building up in plant cells following water absorption (Beauzamy et al., 2014). In growing cells from small plants such as *A. thaliana*, differences in turgor pressure are mainly linked to (i) cell wall properties (a stiffer wall increasing turgor pressure (Cheddadi et al., 2019)), (ii) solute concentration in the cell setting the osmotic pressure (a higher solute concentration increasing turgor pressure) and (iii) the ability to channel water (a high connectivity and conductivity with adjacent cells increasing turgor pressure) (Figure 24).

To avoid mechanical failure, the equilibrium between cell turgor pressure and cell wall properties must be closely monitored. Cells can then regulate their turgor pressure by reinforcing vs loosening their cell wall (wall sensing and reinforcement, see above) or adapting their water intake (osmoregulation). During growth, water intake can be modulated through aquaporin and plasmodesmata regulation as well as adjustment of the cytosolic and vacuolar solutes. Directly measuring the turgor pressure in plants is challenging and can only be done by using an invasive pressure probe (Javot et al., 2003). Nevertheless, several methods have been developed to measure the wall stiffness as a proxy of pressure (with large indentation), the water potential (pressure chamber, psychrometer) or the

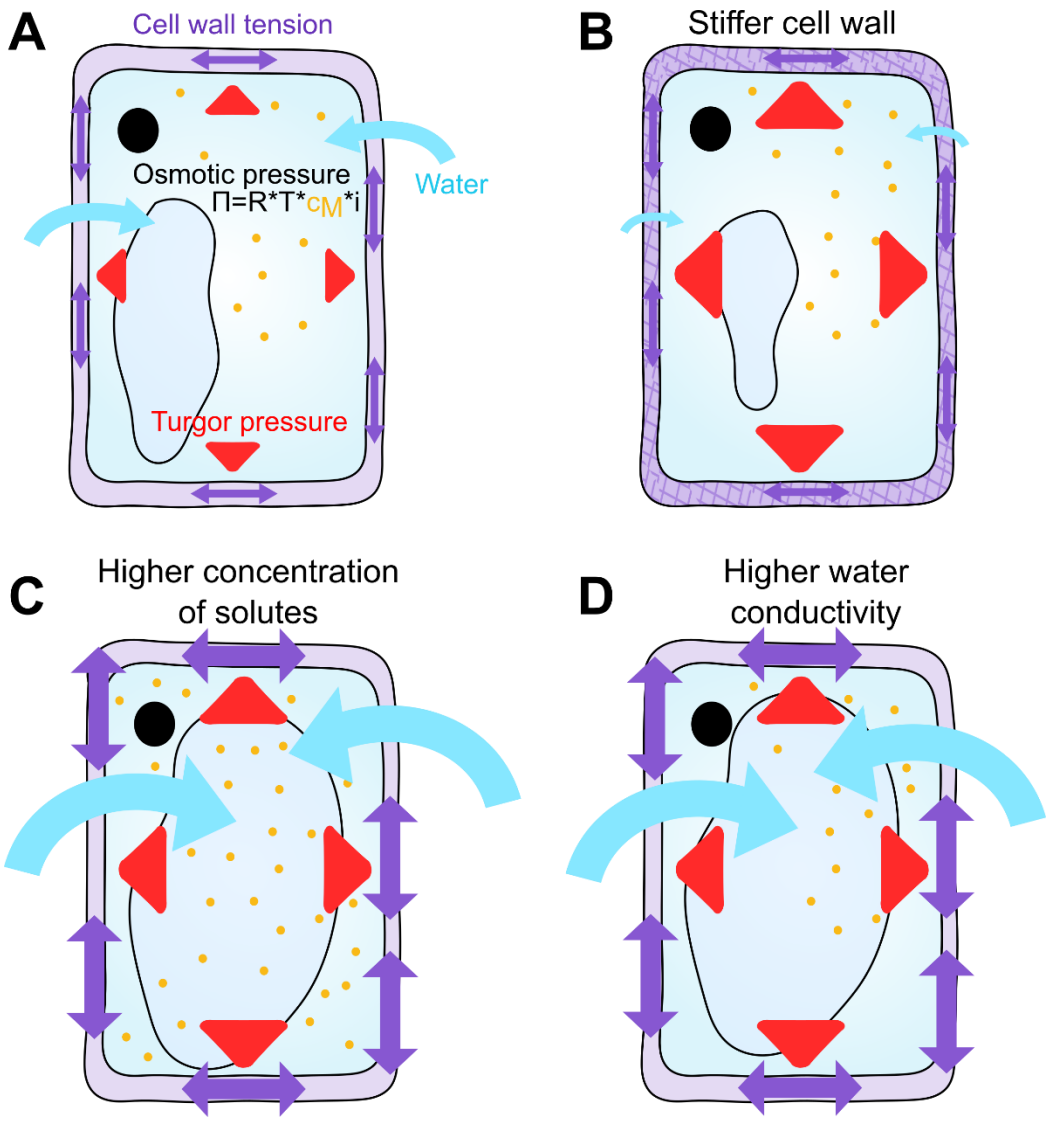

Figure 24: Mechanical forces in plant cells. **(A)** The osmotic pressure depends on the concentration of solutes: $\Pi = R \times T \times c\_m \times i$ with R the molar gas constant at 8.32 J·K−1·mol−1, T the temperature (in K), cM the molar concentration of solute (in mol.L-1), and i the Van't Hoff index, which takes into account the actual number of particles when a substance is dissolved (e.g. 1 for sucrose, 2 for NaCl). It drives water intake, which creates a force pushing on the cell wall: the turgor pressure. The cell wall, resisting this force and the deformation that goes along, becomes tensed. **(B)** A stiffer cell wall increases the turgor pressure (the wall has a higher resistance to deformation), which decreases water intake without changing the osmotic pressure nor the tension in the cell wall. **(C)** A higher concentration of solutes increases the osmotic pressure, which increases water intake, turgor pressure and consequently cell wall tension. **(D)** A higher water conductivity increases water intake, which increases the turgor pressure without changing the osmotic pressure, and consequently increases cell wall tension.

osmotic pressure (successive plasmolysis) of a cell or a tissue and deduce a turgor pressure from it (Beauzamy et al., 2014).

In *fer*, no measurement, direct or indirect of the turgor pressure has been published yet but three elements may support the hypothesis of FER being involved in the regulation of the osmotic or turgor pressure. First, FER regulates stomatal aperture (Chen et al., 2016; Yu et al., 2018), which is directly linked with transpiration and thus water potential and osmotic and turgor pressures. Second, FER downregulates vacuole expansion in association with LRXs during cell growth, in a mechanics-dependent manner (Dünser et al., 2019; Herger et al., 2019). This might lead to a higher water content in *fer* cells coherent with the rescue of cell burst in seedlings when limiting water availability on high agar media.

Finally, FER was shown to physically bind to two aquaporins (namely, plasma membrane intrinsic protein (PIP) 1;2 and PIP2;1), in a close enough manner to be able to act on at least PIP2;1 (Bellati et al., 2016). FER is a kinase and the activity of aquaporins as well as their regulation seems to be regulated by their phosphorylation status (Kapilan et al., 2018). A link between FER and aquaporins seems even more likely since FER is related to several pathways affecting aquaporins: FER coreceptor BAK1 can phosphorylate PIP2;1 in response to ROS (Rodrigues et al., 2017); FER is involved in Ca2+ signaling and apoplastic pH (Shih et al., 2014), both of which may regulate aquaporin activity (Kapilan et al., 2018); RALF1 binding to FER increases the degradation of 14-3-3 proteins (Xu et al., 2019), proteins that may regulate phosphorylated PIP2;1 (Prado et al., 2019).

To conclude, to understand the pleiotropy of FER, a future avenue may be to consider the role of FER in mechanosensing, possibly through matrix tension and/or turgor pressure perception. Some biological functions associated with FER would then ensue, due to their own link to mechanics. For instance, the hormones Auxin and ABA, as well as JA are also involved in mechanical stress and the regulation of plant water status (Mielke et al., 2021; Popko et al., 2010). FER may then be a pleiotropic regulator of many functions via its action on turgor pressure, integrating environmental signals through water influx and cell wall mechanics (Figure 25).

One can also wonder whether FER could directly sense mechanical stresses (and thus be considered a mechanosensor) or if it is simply involved in the transduction of a mechanical

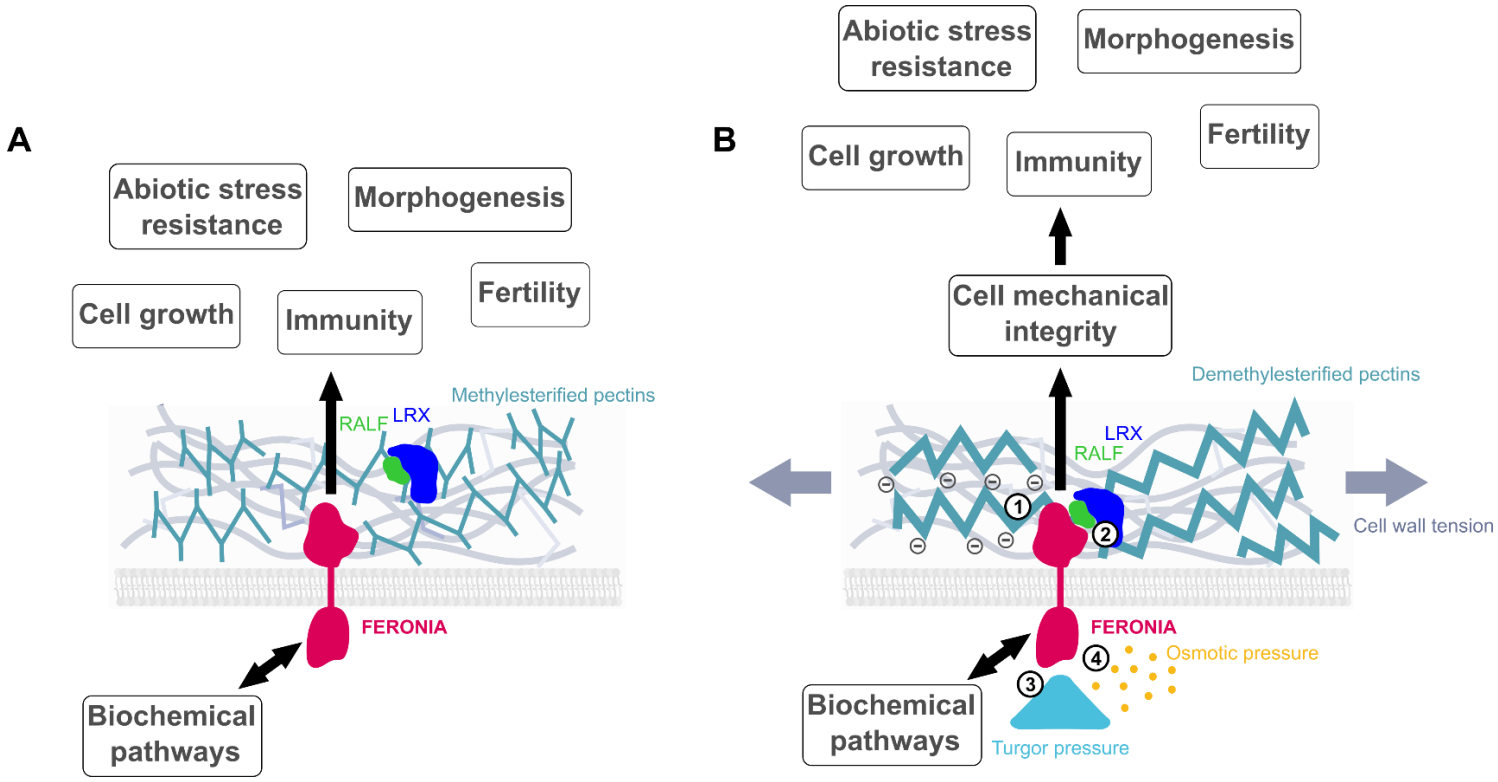

Figure 25: The pleiotropy of FERONIA may reside in its action on the turgor pressure. **(A)** FERONIA acts through biochemical pathways on a wide range of functions. **(B)** In addition to these biochemical pathways, FERONIA role appears to be modulated by mechanical stress. FERONIA could sense mechanical stress through (1) the demethylesterification of pectins (perhaps because of their expansion), (2) a release of RALFs linked to cell wall tension, (3) the turgor pressure, or/and (4) the osmotic pressure. FERONIA could then modulate the cell mechanical integrity, which would be a way to affect several signaling pathways.

signal following sensing by another cell element (and thus be considered a mechanotransducer). For now, no experiment has proven nor refuted that FER could directly sense a mechanical stress, but a parallel can be drawn to animal receptor-mediated mechanosensors such as integrins (Chen et al., 2017). These animal transmembrane mechanosensors can bind to an unmasked RGD sequence from a protein in the extracellular matrix (e.g. fibronectin) upon stretching. This leads to the sensing and signaling of mechanical stress (Choquet et al., 1997), and affects various cellular processes such as cell migration, adhesion, proliferation, differentiation and spreading. Interestingly, FER seems to share with integrins their ability to act upon the actin cytoskeleton (Dong et al., 2019) in addition to their binding to extracellular matrix material and involvement in many signaling pathways through hubs (focal adhesions for integrins). This parallel suggests a role of FER in mechanosensing through the sensing of cell wall deformation. Moreover, integrins seem to be responsible for both outside-in and inside-out signaling because of their reversible conformational changes, an ability which could partially explain the role of FER both on intracellular signaling and cell wall modifications.

The analogy with fibronectin-binding and pectin-binding may also let us speculate on the exact role of FER in pectin sensing. More specifically, FER is supposed to bind demethylesterified pectins more strongly than methylesterified ones, perhaps due to their difference in filament width (Haas et al., 2020). Concurrently, demethylesterified pectins seem to be more present in cell walls with a high tensile stress such as pavement cell necks (Galletti et al., 2016; Haas et al., 2020; Sapala et al., 2018). Therefore, FER might be able to sense pectins expanding due to mechanical stress, similarly to integrins sensing unfolding fibronectins in a stretched extracellular matrix. Going one step further, pectin deformation also depends on water status (Haas et al., 2020), opening the possibility that pectin status also represents a proxy for water content and osmotic pressure. In that scenario, FER would act as a pressure sensor. The observed bias towards pectins may open a new avenue of research on wall hydration, and the role of pectins in that process. For instance, FER may sense the water status of the cell (as a proxy of turgor pressure) through the binding to pectins. And the signaling cascade would only involve a feedback on pectins. Needless to say, pressure sensing would involve other actors beyond FER. For instance, RALF peptides are thought to usually be

sequestered by LRXs (Gronnier et al., 2022; Zhao et al., 2018), and might be released by cell wall tension or wall hydration for FER sensing.

More generally, the question of FER pleiotropy, and its many connection to environmental cues (water, salt, temperature, etc.) opens the larger research field of mecano-eco-sensing, in which plants could perceive changes in the environment through mechanical forces to adapt their growth accordingly.

Open questions:

- How much of FER role can be explained by its involvement with mechanical forces?
- Is FER a mechanosensory or a mechanotransducer?
- If FER is able to sense a mechanical signal, which one would it be?
- Can plants really use mechanical forces as cues for environmental sensing?
- Why do *fer* cells burst?

V◦ Objectives

In this introduction, we saw that turgor-driven mechanical stress is an essential element to explain many aspects of plant development: size, shape, identity, etc. As such mechanical stress is constantly monitored by plants and, in turn, molecular processes are induced, usually to reduce its magnitude (e.g. through cell wall reinforcement or osmoregulation). The regulation of water influx and wall properties has been studied to a great extent. However, the nature of the signal detected (stress, cell wall deformation, membrane tension, etc.) and how it is sensed remains unknown. In particular, cortical microtubules have been found to reorient along the direction of maximal tensile stress, but how they could detect stress changes in the wall is still unclear. Similarly, despite the identification of proteins with wall binding abilities, how the mechanical integrity of plant cells is controlled is largely unknown. Recently, some transmembrane proteins called RECEPTOR-LIKE KINASES (RLKs) have been postulated to be involved in the cell stress response and in particular in microtubule reorientation and/or cell wall integrity. **Are RLKs involved in mechanoperception?**

If so, which ones? In the first part, I have screened 11 RLK mutants to investigate the role of the corresponding proteins in the response to mechanical stress. This screen has singled out FERONIA (FER) as a primary contributor to the cell response to turgor-derived mechanical stress. In *fer* loss-of-function mutants, cell wall tension leads to wall failure, i.e. epidermal cells swell and ultimately burst.

Is FERONIA involved in microtubule reorientation? Strikingly, I found that the microtubule response to stress does not require FER, and that microtubules and FER have additive contribution to the mechanical integrity of plant cells.

Why do *fer* cells burst? In the second part, I have tried to better characterize the role of FER in the response to stress. I have studied the mechanical characteristics of *fer* and tried to link them to the bursting cell phenotype. I have shown that, in *fer*, cell walls are less deformable and thinner than in the WT, consistent with strain-stiffening leading to more brittle cell walls. I also found that the aerial parts display a higher water content associated with a higher osmotic pressure. This provides a scenario in which FER may have a more integrative role in mechanotransduction (wall properties and water status), independent of the microtubule response to stress. This also provides new hypotheses to explain the role of FER in the cellular response to a mechanical stress, as well as new experimental ideas to test them.

Results

I◦ FERONIA and microtubules independently contribute to mechanical integrity in the *Arabidopsis* shoot

I.1◦ Preamble

If the reorientation of microtubules along maximal tensile stress direction seems to be a crucial mechanism to shape cells and organs, how stress in the cell wall would be transmitted to them is still unknown. Among the many candidates proposed for the indirect detection and transduction of mechanical stress, RLKs appear as good candidates. They have an extracellular domain, which could sense a stress as a cell wall deformation, and an intracellular kinase domain, which could activate intracellular signaling pathways, possibly including the reorientation of microtubules. Experimental investigations have suggested that several RLKs may be cell wall integrity sensors (Wolf, 2022).

To select RLKs that could be involved in the microtubule response to stress, we devised and implemented two reverse genetic screens for the cellular response to mechanical stress. The first screen took advantage of the specific puzzle shape exhibited by pavement cells: this shape in lobes and necks is reinforced by the microtubule response to stress, and defects in pavement cell shape could thus mean defects in the cellular response to mechanical stress. We thus analysed the pavement cell shape of 11 RLK mutants using the ImageJ plugin PaCeQuant (Möller et al., 2017), which returns 27 shape descriptors. To determine which descriptor to use when comparing the 11 mutants, we performed a Principal Component Analysis (PCA) to identify the descriptors with the most variability between the different mutants. We also analysed the shape of known microtubule dynamics mutants with PaCeQuant and chose to keep the descriptors with the most variability between mutants while showing significant differences in the microtubule dynamics mutants compared to the WT. As the first descriptor fitting these criteria (nonlobe area) showed a significant difference between most of the 11 RLKs used and the WT, we decided to use the next one (circularity) as a descriptor with more discriminating power. Using circularity, we found out that *fer-4*, *the1-*

6, *mik2-1* and *wak2-1* mutants displayed a pavement cell shape significantly different from the WT, with *fer-4* displaying cell shapes most different from the WT cells.

For the second genetic screen, we added isoxaben in the growth medium of the 11 CrRLK mutants and looked at the length of their etiolated hypocotyl. Isoxaben inhibits the deposition of cellulose (Scheible et al., 2001), which triggers mechanical perturbations in the cell wall. This screen uncovered significant results for all CrRLKs tested, with a difference particularly important for *fer-4*. Surprisingly, all of the other CrRLK mutants displayed a relatively longer hypocotyl than the WT after an isoxaben treatment while *fer-4* displayed a shorter one. We looked at *fer-4* at the cellular scale and found dead cells in the hypocotyl epidermis, explaining the shorter hypocotyls. This phenotype seems consistent with a severely impaired wall sensing in *fer-4*.

We also found burst cells in the epidermis of *fer-4* cotyledons in absence of isoxaben treatment. A more in-depth analysis revealed that they corresponded to cells which first swelled, then burst and deflated. The number of burst cells in cotyledons increased with time during development, and affected organ size. To evaluate if this phenotype was due to mechanical causes, we tried to reduce tensile stress levels in the epidermis by increasing the concentration of agar (and thus decreasing the water potential) in the growth medium (Verger et al., 2018). Doing so rescued the burst cell phenotype, and almost fully rescued the size of cotyledons in *fer-4*. These results are consistent with a scenario in which the burst cell phenotype is due to defects in the sensing or more generally in the response to mechanical stress in *fer-4*. We thus focused on FER as a candidate RLK required for the microtubule response to mechanical stress.

We wanted to directly observe the dynamics of microtubules in response to mechanical perturbation in *fer-4* and to do so, we realized ablation experiments in a *fer-4* line with a microtubule marker. After an ablation in the epidermis, microtubules usually reorient along the pattern of maximal tensile stress, i.e. circumferentially around the ablation (Hamant et al., 2008). In microtubule dynamics mutants, this reorientation is delayed (Uyttewaal et al., 2012). We were surprised to find that the microtubule reorientation to mechanical stress was not significantly different in *fer-4* than in the WT.

Based on these results, we propose that the cellular response to stress would then use (at least) two independent signaling pathways, one through FER and another one through microtubule orientation. To verify this, we looked at the additivity of phenotypes when disturbing both pathways: we depolymerised microtubules by adding oryzalin to the growth medium and used the *fer-4* mutant to affect the FER pathway. Oryzalin treatments can induce cell burst in fragile cells or when using high concentrations for a long period of time (Sapala et al., 2018). With this experiment, we observed a large increase of burst cells in the *fer-4* seedlings grown on oryzalin compared to the ones grown on a control medium. We thus concluded that (i) FER is not required for the microtubule response to stress, and (ii) that cell mechanical integrity is maintained through two distinct signaling pathways (FER and microtubules).

Stéphane Verger, Özer Erguvan (M1 internship) and Antoine Chevallier (L3 internship) started this project before I arrived for my Masters internship. When I took up the project, Stéphane had selected the list of RLKs to study, gathered the seeds, completed many crosses and had started planning the first experiments. Antoine had done a short internship aiming to use cell growth after an ablation as a proxy of microtubule response (data not shown) and thus had established a protocol for cotyledon ablation (Fig 4). Özer had set up a protocol for the pavement cell shape screen and completed the experiment and image analysis of the mutants displayed in the paper (Fig 1). For this figure, I completed Özer's results with double and triple mutants of RLKs (data not shown), and performed the PCA and statistical analysis for the pavement cell shape screen. For the rest of the experiments, I conducted most of the experiments, i.e. set up the protocol, did the experiments and analysed the images. I also co-supervised several students. For the isoxaben screen (Fig 2), I had some help from Antoine Dehem during his L3 internship for the double and triple RLK mutants (data not shown). I supervised Théophile Peyraud during his L3 internship and we established the oryzalin experiment protocol together (Fig 5). He also performed projections of *fer-4* and WT pavement cells at various developmental stages for about half of the data (Fig 3) (see Annexe 2). Mengying Liu and Marjolaine Martin were a great help for the genotyping of the lines we used, and Marjolaine also helped me measure the cotyledon area for half of the data (Fig 3). Rodrigue Friaud (L3 internship) replicated the pavement cell shape screen and the isoxaben screen with *fer-2* (S3) and other alleles of already studied RLK mutant (data not shown). I

wrote the paper and prepared all the figures with feedback from Stéphane Verger and Olivier Hamant.

I.2◦ Publication

The following part has been published as a research article I wrote with Özer Erguvan, Antoine Chevallier, Antoine Dehem, Rodrigue Friaud, Mengying Liu, Marjolaine Martin, Théophile Peyraud, Olivier Hamant and Stéphane Verger (Malivert et al., 2021). The text is included in the published format.

PLOS BIOLOGY

RESEARCH ARTICLE

FERONIA and microtubules independently contribute to mechanical integrity in the *Arabidopsis* shoot

Alice Malivert, Özer Erguvan¤, Antoine Chevallier, Antoine Dehem, Rodrigue Friaud, Mengying Liu, Marjolaine Martin, Théophile Peyraud, Olivier Hamant*, Stéphane Verger¤*

Laboratoire de Reproduction et Développement des Plantes, Université de Lyon, UCB Lyon 1, ENS de Lyon, INRAE, CNRS, Lyon, France

¤ Current address: Umeå Plant Science Centre, Department of Forest Genetics and Plant Physiology, Swedish University of Agricultural Sciences, Umeå, Sweden
* olivier.hamant@ens-lyon.fr (OH); stephane.verger@slu.se (SV)

OPEN ACCESS

Citation: Malivert A, Erguvan Ö, Chevallier A, Dehem A, Friaud R, Liu M, et al. (2021) FERONIA and microtubules independently contribute to mechanical integrity in the *Arabidopsis* shoot. PLoS Biol 19(11): e3001454. https://doi.org/10.1371/journal.pbio.3001454

Academic Editor: Mark Estelle, UCSD, UNITED STATES

Received: June 21, 2021

Accepted: October 22, 2021

Published: November 12, 2021

Data Availability Statement: All relevant data are within the paper and its Supporting Information files.

Funding: This work was supported by the European Research Council (ERC-2013-CoG-615739 'MechanoDevo' to O.H). The funders had no role in study design, data collection and analysis, decision to publish, or preparation of the manuscript.

Competing interests: The authors have declared that no competing interests exist.

Abstract

To survive, cells must constantly resist mechanical stress. In plants, this involves the reinforcement of cell walls, notably through microtubule-dependent cellulose deposition. How wall sensing might contribute to this response is unknown. Here, we tested whether the microtubule response to stress acts downstream of known wall sensors. Using a multistep screen with 11 mutant lines, we identify FERONIA (FER) as the primary candidate for the cell's response to stress in the shoot. However, this does not imply that FER acts upstream of the microtubule response to stress. In fact, when performing mechanical perturbations, we instead show that the expected microtubule response to stress does not require FER. We reveal that the *feronia* phenotype can be partially rescued by reducing tensile stress levels. Conversely, in the absence of both microtubules and FER, cells appear to swell and burst. Altogether, this shows that the microtubule response to stress acts as an independent pathway to resist stress, in parallel to FER. We propose that both pathways are required to maintain the mechanical integrity of plant cells.

Introduction

All living organisms use mechanical forces as instructive cues during their development [1,2]. They also share a common mechanical property: Cells are pressurized by osmotic pressure and thus experience cortical tension. Osmotic pressure in plants is several orders of magnitude higher than that of animal cells, and it is counterbalanced by stiff cell walls [3]. Regulating the mechanical properties of cell walls, through the perception of wall tension and integrity, is thus crucial for plant growth and development [4,5].

Plant cell walls are composed of load-bearing cellulose microfibrils, tethered by a matrix made of polysaccharides and structural proteins [6,7]. The deposition of cellulose microfibrils is generally guided by cortical microtubules [8]. Beyond the average stiffness, the orientation

Abbreviations: CrRLK, *Catharanthus roseus* Receptor-Like Kinase; *cvy1*, *curvy1*; FER, FERONIA; herk1, *hercules receptor kinase 1*; *mik2-1*, *mdis1-interacting receptor-like kinase2*; PI, propidium iodide; ROS, reactive oxygen species; *tfr1*, *theseus1/feronia-related1*; THE1, THESEUS1; *wak*, *wall-associated kinase*; WT, wild type.

of cellulose microfibrils controls the mechanical anisotropy of the wall. There is now ample evidence showing that cortical microtubules align with maximal tensile stress directions in the wall [9,10–13]. This provides a feedback loop in which shape and growth, whether at the individual cell or whole organ scale, prescribes a pattern of stress, to which cells resist by reinforcing their walls along maximal tensile stress directions [12,14].

Although they are significantly less stiff, other wall components contribute to wall properties. In particular, pectins can partially rescue defects in cellulose synthesis in young cell walls. For instance, isoxaben treatment, which inhibits cellulose deposition through the internalization of CESA complexes, leads to thicker walls that are enriched in pectin [15]. Similarly, in young hypocotyls, pectin polarities precede the formation of mechanically anisotropic walls [16]. In contrast to cellulose deposition, pectin, as well as all other matrix components, are secreted to the cell wall [6,7]. Therefore, in principle, this provides an alternative mechanism for the cell to resist wall tension or damage. As for microtubules, the related mechanotransduction pathway is largely unknown. Yet, over the past decade, *Catharanthus roseus* Receptor-Like Kinases (CrRLKs) have emerged as key players. Although the link with mechanical stress remains to be formally established, THESEUS1 (THE1) has been implicated in the wall integrity pathway [17–19]. Based on defective root growth behavior on stiff interface, calcium signaling, pH response, and *TOUCH* gene expression, FERONIA (FER) has emerged as a candidate mechanosensor [20]. FER can sense the status of the cell wall, notably when salinity rises, through pectin binding [21]. It was recently proposed that FER also monitors microtubule behavior through a cascade involving Rho GTPases (ROP6) and the microtubule severing protein katanin [22]. Here, through a reverse genetic screen on wall sensors and using a suite of mechanical tests, we show that our best wall sensor candidate FER is not required for the microtubule response to stress, further suggesting that the microtubule response to stress can be more autonomous than anticipated. We also reveal that FER-dependent wall integrity pathway depends on wall tension and that both FER and the microtubule response to stress contribute to wall integrity.

Results

Altered pavement cell shape as a proxy for defective response to mechanical stress

We first used a morphometric proxy to test the involvement of wall sensors in the microtubule response to stress. The jigsaw puzzle shape of *Arabidopsis* pavement cells has been proposed to be actively maintained and amplified by the microtubule response to mechanical stress. Indeed, necks in such cells prescribe highly anisotropic tensile stresses locally, to which microtubule arrays and thus cellulose deposition align [14,23,24]. We reasoned that the shape of pavement cells could be used in a mutant screen as a proxy for defects in that mechanical feedback loop. In past research, such screens have targeted the intracellular biochemical cues behind cell–cell coordination [25] and the contribution of cell wall properties in cell shape [26]. Whether wall sensors are involved in pavement cell shape remains ill described. Here, we focused on mutants impaired in receptor-like kinases that are highly expressed in the epidermis and aerial parts of the plant during early development and that exhibit an established link with the cell wall (and their closest homologs), namely *feronia (fer)*, *theseus1 (the1)*, *theseus1/feronia-related1* (*tfr1*; *at5g24010)*, *curvy1* (*cvy1)*, *hercules receptor kinase 1* (*herk1)*, *herk2*, *mdis1-interacting receptor-like kinase2 (mik2-1)*, *wall-associated kinase 1 (wak1)*, *wak2*, *wak3*, and *wak4* (see S1 Table). We imaged and quantified the pavement cell shapes in receptor-like kinase candidate mutants, with the aim to select the ones with the strongest cell shape defects (Fig 1A).

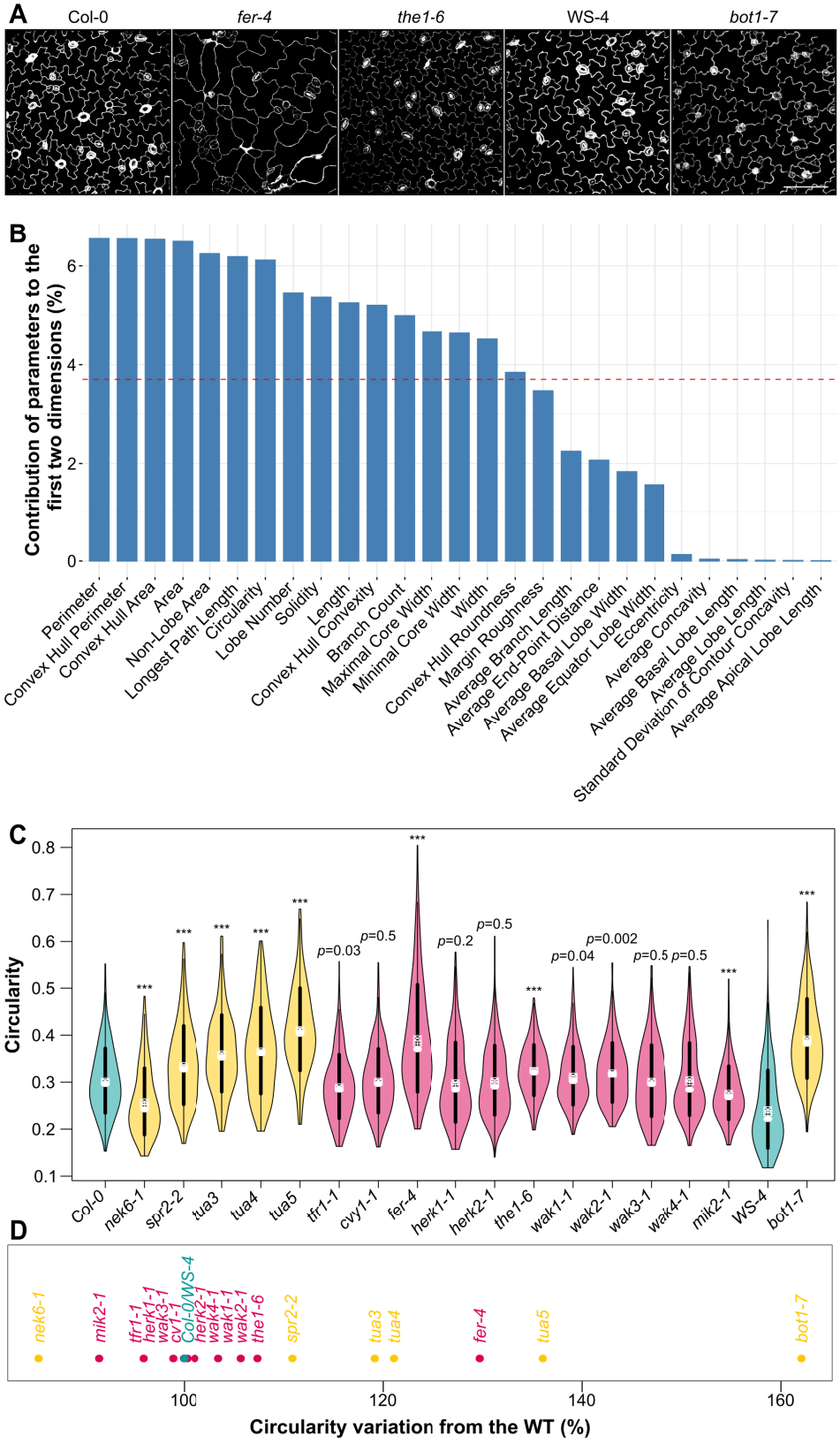
A
Col-0
fer-4
the1-6
WS-4
bot1-7
B
Contribution of parameters to the first two dimensions (%)
0
2
4
6
Perimeter
Convex Hull Perimeter
Convex Hull Area
Area
Non-Lobe Area
Longest Path Length
Circularity
Lobe Number
Solidity
Length
Convex Hull Convexity
Branch Count
Maximal Core Width
Minimal Core Width
Width
Convex Hull Roundness
Margin Roughness
Average Branch Length
Average End-Point Distance
Average Basal Lobe Width
Average Equator Lobe Width
Eccentricity
Average Concavity
Average Basal Lobe Length
Average Lobe Length
Standard Deviation of Contour Concavity
Average Apical Lobe Length
C
Circularity
0.1
0.2
0.3
0.4
0.5
0.6
0.7
0.8
***
p=0.03
p=0.5
p=0.2
p=0.5
p=0.04
p=0.002
p=0.5
p=0.5
Col-0
nek6-1
spr2-2
tua3
tua4
tua5
tfr1-1
cvy1-1
fer-4
herk1-1
herk2-1
the1-6
wak1-1
wak2-1
wak3-1
wak4-1
mik2-1
WS-4
bot1-7
D
nek6-1
mik2-1
tfr1-1
herk1-1
wak3-1
cv1-1
Col-0/WS-4
herk2-1
wak4-1
wak1-1
wak2-1
the1-6
spr2-2
tua3
tua4
fer-4
tua5
bot1-7
100
120
140
160
Circularity variation from the WT (%)

Fig 1. Pavement cell shape in receptor-like kinase mutants. (A) Representative images of *Col-0*, *WS-4*, *fer-4*, *the1-6*, and *bot1-7* pavement cells. Samples were PI stained, and cell contours were extracted with MorphoGraphX and projected in 2D. Scale = 100 μm. **(B)** Relative contribution of 27 shape descriptors to pavement cell shape, as assessed by principal component analysis. **(C)** Circularity (violin plots) of pavement cells and *p*-values of Dunn tests for the WT (in blue, *Col-0* and *WS-4*), for the microtubule regulator mutants (in orange, *nek6-1*, *spr2-2*, *tua3*, *tua4*, *tua5*, and *bot1-7*) and the receptor-like kinase mutants (in pink, *tfr1-1*, *cvy1-1*, *fer-4*, *herk1-1*, *herk2-1*, *the1-4*, *the1-6*, *wak1-1*, *wak2-1*, *wak3-1*, *wak4-1*, and *mik2-1*). **(D)** Percentage of increase or decrease in pavement cell circularity from the WT (in blue, *Col-0* and *WS-4*), for the microtubule regulator mutants (in orange, *nek6-1*, *spr2-2*, *tua3*, *tua4*, *tua5*, and *bot1-7*) and the receptor-like kinase mutants (in pink, *tfr1-1*, *cvy1-1*, *fer-4*, *herk1-1*, *herk2-1*, *the1-4*, *the1-6*, *wak1-1*, *wak2-1*, *wak3-1*, *wak4-1*, and *mik2-1*). All underlying data can be found in S1 Data. PI, propidium iodide; WT, wild type.

https://doi.org/10.1371/journal.pbio.3001454.g001

To do so, we extracted the epidermal signal and used PaCeQuant to segment pavement cells and measure 27 shape descriptors (see Materials and methods [27] (S1A Fig)). To select the most discriminating PaCeQuant shape descriptor, we first performed a principal component analysis on our data. We compared the contribution of each parameter to the 2 axes with the most variation (Fig 1B). The cell perimeter was first, followed by the convex hull perimeter, the convex hull area, the cell area, the nonlobe area, and the longest path length, then by circularity (for relevant definition, see S1B Fig).

To confirm that such shape descriptors are pertinent, and knowing that cortical microtubules are well-known pavement cell shape regulators, we used mutants with microtubule defects as positive controls. We performed the same analysis on 2 loss-of-function mutants: *nek6* is impaired in a tubulin kinase which depolymerizes microtubules, and the mutant exhibits an enhanced microtubule response to stress [28]; *bot1* is impaired in the microtubule severing protein katanin and exhibits a reduced response to stress [29]. We also included lines with tubulin mutations affecting microtubule dynamics ($tua3^{D205N}$, $tua4^{S178\Delta}$, and $tua6^{A281T}$ referred as *tua3*, *tua4*, and *tua5* in the following [30,31]) and *spr2* with a reported enhanced cortical microtubule response to stress [32] but also ambivalent regulatory role in microtubule severing depending on tissue [33–35]. We found that cell perimeter, convex hull perimeter, convex hull area, cell area, and the longest path length descriptors were not sufficient to discriminate the pavement cell shape phenotype of those microtubules regulators (cell perimeter: $p_{spr2\text{-}2} = 0.07$; $p_{tua3} = 0.018$; $p_{tua4} = 0.4$; convex hull perimeter: $p_{tua3} = 0.39$; $p_{tua5} = 0.011$; convex hull area: $p_{tua3} = 0.5$; $p_{tua5} = 0.03$; cell area: $p_{tua3} = 0.06$; $p_{tua5} = 0.07$; longest path length: $p_{tua3} = 0.28$; $p_{tua4} = 0.1$; $n_{spr2\text{-}2} = 262$; $n_{tua3} = 204$; $n_{tua4} = 230$; $n_{tua5} = 297$; $n_{Col\text{-}0} = 428$). By contrast, all microtubule regulator mutant lines tested exhibited a defect in nonlobe area and circularity (nonlobe area: $p_{nek6\text{-}1} = 0.009$; $p_{spr2\text{-}2} < 10^{-3}$; $p_{tua3} = 0.003$; $p_{tua4} < 10^{-3}$; $p_{tua5} < 10^{-3}$; $p_{bot1\text{-}7} < 10^{-3}$; circularity: $p_{nek6\text{-}1} < 10^{-3}$; $p_{spr2\text{-}2} < 10^{-3}$; $p_{tua3} < 10^{-3}$; $p_{tua4} < 10^{-3}$; $p_{tua5} < 10^{-3}$; $p_{bot1\text{-}7} < 10^{-3}$, $n_{nek6\text{-}1} = 183$; $n_{spr2\text{-}2} = 262$; $n_{tua3} = 204$; $n_{tua4} = 230$; $n_{tua5} = 297$; $n_{bot1\text{-}7} = 252$; $n_{Col\text{-}0} = 428$; $n_{WS\text{-}4} = 294$, Fig 1C, S1C Fig).

A total of 9 of the 11 receptor-like kinase mutants exhibited a nonlobe area significantly different from that of the wild type (WT). *tfr1-1*, *fer-4*, *herk1-1*, *herk2-1*, and *wak4-1* displayed a nonlobe area significantly higher than that of the WT ($p_{tfr1\text{-}1} < 10^{-3}$; $p_{fer\text{-}4} < 10^{-3}$; $p_{herk1\text{-}1} < 10^{-3}$; $p_{herk2\text{-}1} < 10^{-3}$; $p_{wak4\text{-}1} = 0.007$; $n_{tfr1\text{-}1} = 244$; $n_{fer\text{-}4} = 321$; $n_{herk1\text{-}1} = 225$; $n_{herk2\text{-}1} = 238$; $n_{wak4\text{-}1} = 204$; $n_{Col\text{-}0} = 428$, S1C Fig), while the nonlobe area of *cvy1-1*, *the1-6*, *wak1-*,*1* and *mik2-1* was significantly lower than that of the WT ($p_{cvy1\text{-}1} < 10^{-3}$; $p_{the1\text{-}6} < 10^{-3}$; $p_{wak1\text{-}1} < 10^{-3}$; $p_{mik2\text{-}1} < 10^{-3}$; $n_{cvy1\text{-}1} = 277$; $n_{the1\text{-}6} = 174$; $n_{wak1\text{-}1} = 295$; $n_{mik2\text{-}1} = 177$; $n_{Col\text{-}0} = 428$). Only *wak2-1* and *wak3-1* displayed nonlobe area values that were nonsignificantly different from that of the WT ($p_{wak2\text{-}1} = 0.1$; $p_{wak3\text{-}1} = 0.03$; $n_{wak2\text{-}1} = 271$; $n_{wak3\text{-}1} = 202$; $n_{Col\text{-}0} = 428$). Thus, nonlobe area is not a discriminant parameter in our screen. We decided to study the next most variable parameter with defects in known microtubule regulator lines—circularity—for the rest of the analysis, justifying a posteriori a common choice in the literature on pavement cell shape [36].

Among the receptor-like kinase mutants tested, the pavement cells in *fer-4*, *the1-6*, and *wak2-1* were significantly more circular than the WT supporting the hypothesis that the corresponding proteins could contribute to the microtubule response to stress in pavement cells ($p_{fer\text{-}4} < 10^{-3}$; $p_{the1\text{-}6} < 10^{-3}$; $p_{wak2\text{-}1} = 0.002$; $n_{fer\text{-}4} = 321$; $n_{the1\text{-}6} = 174$; $n_{wak2\text{-}1} = 271$; $n_{Col\text{-}0} = 428$; Fig 1C). *wak1-1* also exhibited increased pavement cell circularity, albeit much less significantly ($p_{wak1\text{-}1} = 0.04$; $n_{wak1\text{-}1} = 295$; $n_{Col\text{-}0} = 428$). Only *mik2*-1 exhibited a significantly decreased pavement cell circularity ($p_{mik2\text{-}1} < 10^{-3}$; $n_{mik2\text{-}1} = 177$; $n_{Col\text{-}0} = 428$), while *tfr1-1* exhibited a tendency toward a decreased pavement cell circularity ($p_{tfr1\text{-}1} = 0.03$; $n_{tfr1\text{-}1} = 244$; $n_{Col\text{-}0} = 428$). Pavement cells in all the other receptor-like kinase mutants (*cvy1-1*, *herk1-1*; *herk2-1*; *wak3-1*; *wak4-1*) displayed a circularity comparable to that of the WT ($p_{cvy1\text{-}1} = 0.5$; $p_{herk1\text{-}1} = 0.2$; $p_{herk2\text{-}1} = 0.47$; $p_{wak3\text{-}1} = 0.47$; $p_{wak4\text{-}1} = 0.5$; $n_{cvy1\text{-}1} = 277$; $n_{herk1\text{-}1} = 225$; $n_{herk2\text{-}1} = 238$; $n_{wak3\text{-}1} = 202$; $n_{wak4\text{-}1} = 204$; $n_{Col\text{-}0} = 428$). To distinguish the relative contributions of the most affected mutants, we quantified the deviation of circularity from the WT. Among all the receptor-like kinases tested, the candidate mutants with the largest defect in circularity when compared to the WT were *fer-4* (consistent with previously published results, [37]) and, to a lesser extent, *the1-6* (Fig 1D). *fer-4* cells were 30% more circular and *the1-6* cells were 7% more circular than the WT, values that were comparable to that of microtubule regulator mutants, such as *spr2-2* or *bot1-7* (Fig 1D).

Note that the same trend was obtained when considering solidity, another parameter often used to characterize lobe formation [38] (S1D Fig). Note also that while circularity and solidity can be impacted when stress response levels change, they do not necessarily directly scale with stress response level. Different shapes can lead to similar circularity and solidity values (e.g., see last figure); nevertheless, this cell shape-based screening allowed us to identify the RLK mutants with the most affected pavement cell shape, possibly through a defective microtubule response to stress. Because *fer-4* stands out, this first screening suggests that FER could play a role in the microtubule response to mechanical stress.

Differential response of receptor-like kinase mutants to isoxaben

To challenge the results from this initial screen, we next used a well-established protocol to mechanically perturb cell walls. Isoxaben inhibits the biosynthesis of cellulose [39], and thus weakens the wall. In past work, such treatment were shown to induce a hyperalignment of cortical microtubules at the shoot apical meristem and in cotyledon pavement cells [14,40], consistent with a response to increased tensile stress levels in the cell wall. Note that isoxaben can also trigger other responses, including reactive oxygen species (ROS) production, lignification, and changes in gene expression [17]. Thus, depending on time and dose, isoxaben may also ultimately reduce stress level [41]. Here, we use this drug as a screening tool, complementary to the pavement cell shape screen, to identify mutants insensitive or hypersensitive to mechanical perturbation and which are thus likely to be defective in mechanosensing.

We grew the seedlings in a medium containing 1 nM isoxaben or the same volume of DMSO, in the dark (Fig 2A). We then measured the length of the etiolated hypocotyls 4 days after germination. After isoxaben treatment, 4-day-old WT seedlings exhibited a shorter hypocotyl (by 41% for *Col-0*, 34% for *WS-4*, $n_{Col\text{-}0\ \mathrm{DMSO}} = 281$, $n_{Col\text{-}0\ \mathrm{iso}} = 271$, $n_{WS\text{-}4\ \mathrm{DMSO}} = 127$, $n_{WS\text{-}4\ \mathrm{iso}} = 129$). To compare WT and mutants, we normalized the obtained distribution of lengths to the same mean and standard deviation as the control, thus providing a hypocotyl length index (Fig 2B, S2 Fig). Treated mutants with a relatively shorter hypocotyl than the treated WT were labeled more sensitive to isoxaben, whereas treated mutants with a relatively longer hypocotyl than the treated WT were labeled less sensitive than the WT.

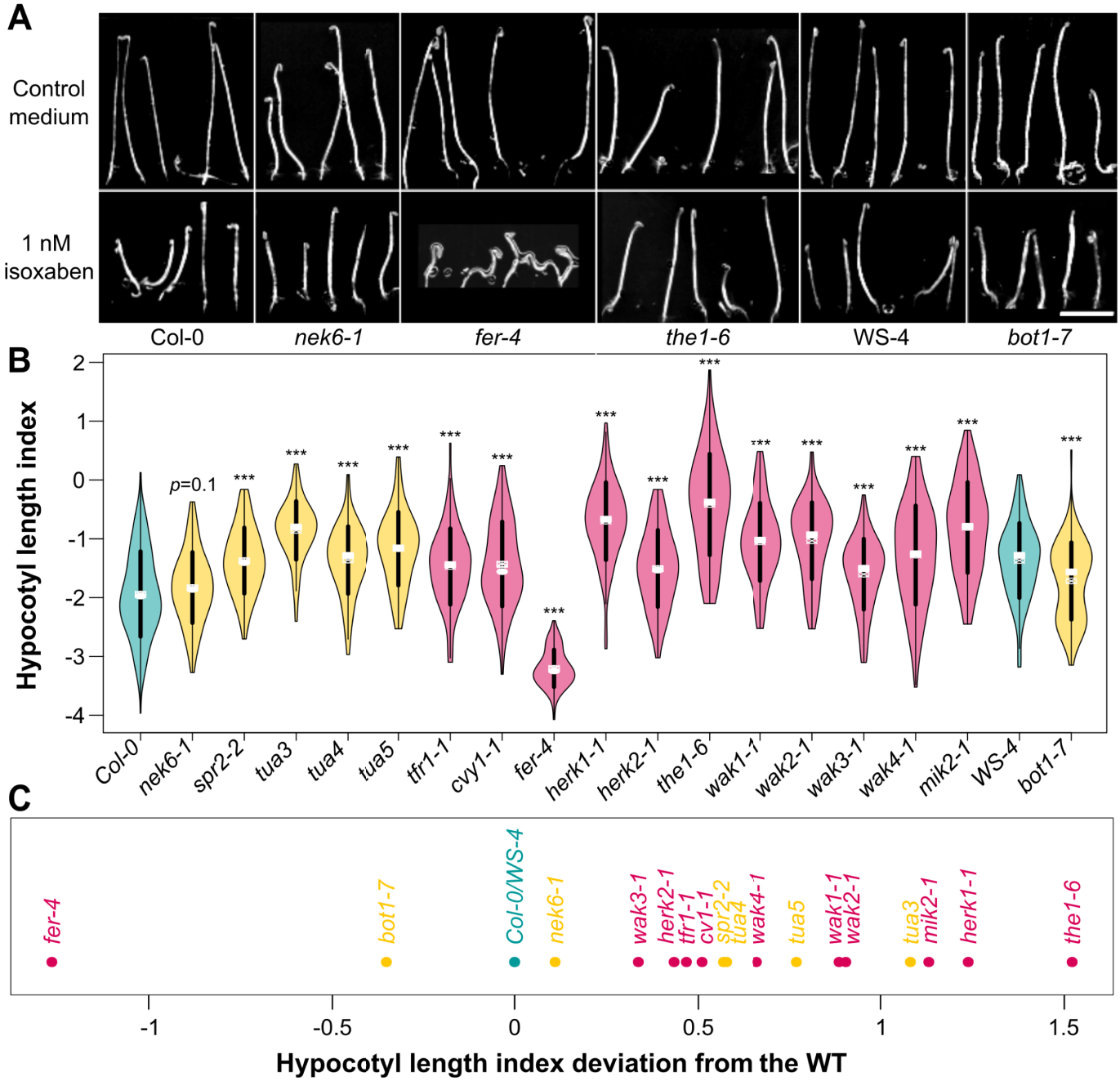

Fig 2. Impact of isoxaben on hypocotyl length in receptor-like kinase mutants. (A) Representative images of *Col-0*, *WS-4*, *fer-4*, *the1-*,*6* and *bot1-7* etiolated seedlings grown with or without 1 nM isoxaben. Scale = 1 cm. **(B)** Hypocotyl length index (violin plot): distribution of isoxaben-grown hypocotyl length, normalized relative to the DMSO-grown ones. *p*-values of Wilcoxon–Mann–Whitney test for the WT (in blue, *Col-0* and *WS-4*), the microtubule regulator (in orange, *nek6-1*, *spr2-2*, *tua3*, *tua4*, *tua5*, and *bot1-7*), and the receptor-like kinase mutants (in pink, *tfr1-1*, *cvy1-1*, *fer-4*, *herk1-1*, *herk2-1*, *the1-4*, *the1-6*, *wak1-1*, *wak2-1*, *wak3-1*, *wak4-1*, and *mik2-1*). **(C)** Deviation of hypocotyl length index. The WT accessions (*Col-0* and *WS-4*) are labeled in blue. The microtubule regulator mutants (*nek6-1*, *spr2-2*, *tua3*, *tua4*, *tua5*, and *bot1-7*) are labeled in orange. The receptor-like kinase mutants (*tfr1-1*, *cvy1-1*, *fer-4*, *herk1-1*, *herk2-1*, *the1-4*, *the1-6*, *wak1-1*, *wak2-1*, *wak3-1*, *wak4-1*, and *mik2-1*) are labeled in pink. All underlying data can be found in S2 Data. WT, wild type.

https://doi.org/10.1371/journal.pbio.3001454.g002

A total of 10 out of the 11 receptor-like kinase mutants studied were less sensitive than the WT (*tfr1-1*, *cvy1-1*, *herk1-1*, *herk2-1*, *the1-6*, *wak1-1*, *wak2-1*, *wak3-1*, *wak4-1*, *mik2-1*; $p_{tfr1\text{-}1} < 10^{-3}$; $p_{cvy1\text{-}1} < 10^{-3}$; $p_{herk1\text{-}1} < 10^{-3}$; $p_{herk2\text{-}1} < 10^{-3}$; $p_{the1\text{-}6} < 10^{-3}$; $p_{wak1\text{-}1} < 10^{-3}$; $p_{wak2\text{-}1} < 10^{-3}$; $p_{wak3\text{-}1} < 10^{-3}$; $p_{wak3\text{-}1} < 10^{-3}$; $p_{mik2\text{-}1} < 10^{-3}$; $n_{tfr1\text{-}1\ DMSO} = 80$; $n_{tfr1\text{-}1\ iso} = 83$; $n_{cvy1\text{-}1\ DMSO} = 109$; $n_{cvy1\text{-}1\ iso} = 115$; $n_{herk1\text{-}1\ DMSO} = 82$; $n_{herk1\text{-}1\ iso} = 70$; $n_{herk2\text{-}1\ DMSO} = 88$; $n_{herk2\text{-}1\ iso} = 106$; $n_{the1\text{-}6\ DMSO} = 57$; $n_{the1\text{-}6\ iso} = 91$; $n_{wak1\text{-}1\ DMSO} = 116$; $n_{wak1\text{-}1\ iso} = 89$; $n_{wak2\text{-}1\ DMSO} = 63$; $n_{wak2\text{-}1\ iso} = 78$; $n_{wak3\text{-}1\ DMSO} = 99$; $n_{wak3\text{-}1\ iso} = 89$; $n_{wak4\text{-}1\ DMSO} = 103$; $n_{wak4\text{-}1\ iso} = 86$; $n_{mik2\text{-}1\ DMSO} = 84$; $n_{mik2\text{-}1\ iso} = 96$; $n_{Col\text{-}0\ DMSO} = 281$; $n_{Col\text{-}0\ iso} = 271$), whereas *fer-4* was significantly more sensitive ($p_{\text{fer-4}} < 10^{-3}$; $n_{fer\text{-}4\ DMSO} = 104$; $n_{fer\text{-}4\ iso} = 90$) than the WT (Fig 2B). When plotting the deviation of each mutant from the WT phenotype, it appeared that among all the receptor-like kinase tested, *fer-4* and *the1-6* were the most affected mutants in their response to isoxaben, albeit in opposite trend: *fer-4* hypocotyl were more sensitive to isoxaben, whereas *the1*-6 were less sensitive to isoxaben (Fig 2C). These results indicate that all the receptor-like kinases tested might be involved in the cellular response to a mechanical stress, with *FER* and *THE1* having the most clear-cut, and opposing, response.

To check whether these defects could be related to the microtubule response to stress, we performed the same analysis on microtubule regulator mutants. *bot1-7* (in *WS-4* ecotype) was more sensitive to the isoxaben treatment than the WT ($p_{bot1\text{-}7} < 10^{-3}$; $n_{bot1\text{-}7\ DMSO} = 99$; $n_{bot1\text{-}7\ iso} = 96$; $n_{\text{WS-4 DMSO}} = 127$; $n_{\text{WS-4 iso}} = 129$) and thus fell in the same cluster as *fer-4*. The *nek6-1* mutant exhibited the same isoxaben sensitivity as the WT ($p_{nek6\text{-}1} = 0.1$; $n_{nek6\text{-}1\ DMSO} = 91$; $n_{nek6\text{-}1\ iso} = 104$; $n_{Col\text{-}0\ DMSO} = 281$; $n_{Col\text{-}0\ iso} = 271$) (Fig 2B). The *spr2-2* mutant was significantly less sensitive than the WT ($p_{spr2\text{-}2} < 10^{-3}$; $n_{spr2\text{-}2\ DMSO} = 99$; $n_{spr2\text{-}2\ iso} = 85$; $n_{Col\text{-}0\ DMSO} = 281$; $n_{Col\text{-}0\ iso} = 271$) and thus fell in the same cluster as *the1-6*. Last, *tua3*, *tua4*, and *tua5* were significantly less sensitive than the WT ($p_{tua3} < 10^{-3}$; $p_{tua4} < 10^{-3}$; $p_{tua5} < 10^{-3}$; $n_{tua3\ DMSO} = 93$; $n_{tua3\ iso} = 90$; $n_{tua4\ DMSO} = 83$; $n_{tua4\ iso} = 108$; $n_{tua5\ DMSO} = 72$; $n_{tua5\ iso} = 66$; $n_{Col\text{-}0\ DMSO} = 281$; $n_{Col\text{-}0\ iso} = 271$).

Altogether, our primary screening approach using both pavement cell shape analysis and isoxaben sensitivity test as a combined proxy for the microtubule response to mechanical stress highlights FER as a primary candidate. So far, our data are also consistent with the proposed scenario in which FER and katanin belong to the same pathway [22], but these remain primary screening approaches that do not directly test the involvement of our main candidate in the microtubule response to mechanical stress. Based on this screening, in the following we decided to focus on FER to investigate its involvement in the mechanical integrity of the shoot and to directly test its contribution to the microtubule response to mechanical stress.

Rescue test: Decreasing the matrix potential of the growth medium rescues the burst cell phenotype in *feronia*

We first decided to further investigate the isoxaben hypersensitivity phenotype of *fer-4*. It is commonly believed that WT seedlings display a shorter hypocotyl on isoxaben because cell wall defects are perceived and compensated through wall reinforcement, ultimately leading to reduced growth. Both wall reinforcement and reduced growth would prevent the cells from bursting. This notably builds on the analysis of *the1* mutant, which exhibits a longer hypocotyl than the WT on isoxaben because of the lack of wall sensing [17]. In *fer*, the hypocotyl is in contrast even shorter than the WT. Thus, either wall sensing is enhanced in *fer* thus strongly repressing growth, or, by contrast, wall sensing is impaired in *fer*, even more than in *the1*, and cells burst before walls can even be reinforced. In the rest of the article, we focus the analysis of the *fer-4* allele, but similar results could be obtained in *fer-2* (S3 Fig).

When looking closely at *fer-4* hypocotyls grown on isoxaben and stained with propidium iodide (PI), we observed many dead cells, as revealed by PI staining (Fig 3A). We calculated a bursting index, i.e., the percentage of burst cell area over total area of a field of epidermal cells in a given image. We found the bursting index to be more than one order of magnitude higher in *fer-4* isoxaben-grown hypocotyls (20 ± 18%) than in the WT (0 ± 1%, $p < 10^{-3}$; $n_{Col\text{-}0,iso,0.7\%agar} = 16$; $n_{fer\text{-}4,iso,0.7\%agar} = 16$, Fig 3B). This observation thus seems consistent with the latter scenario.

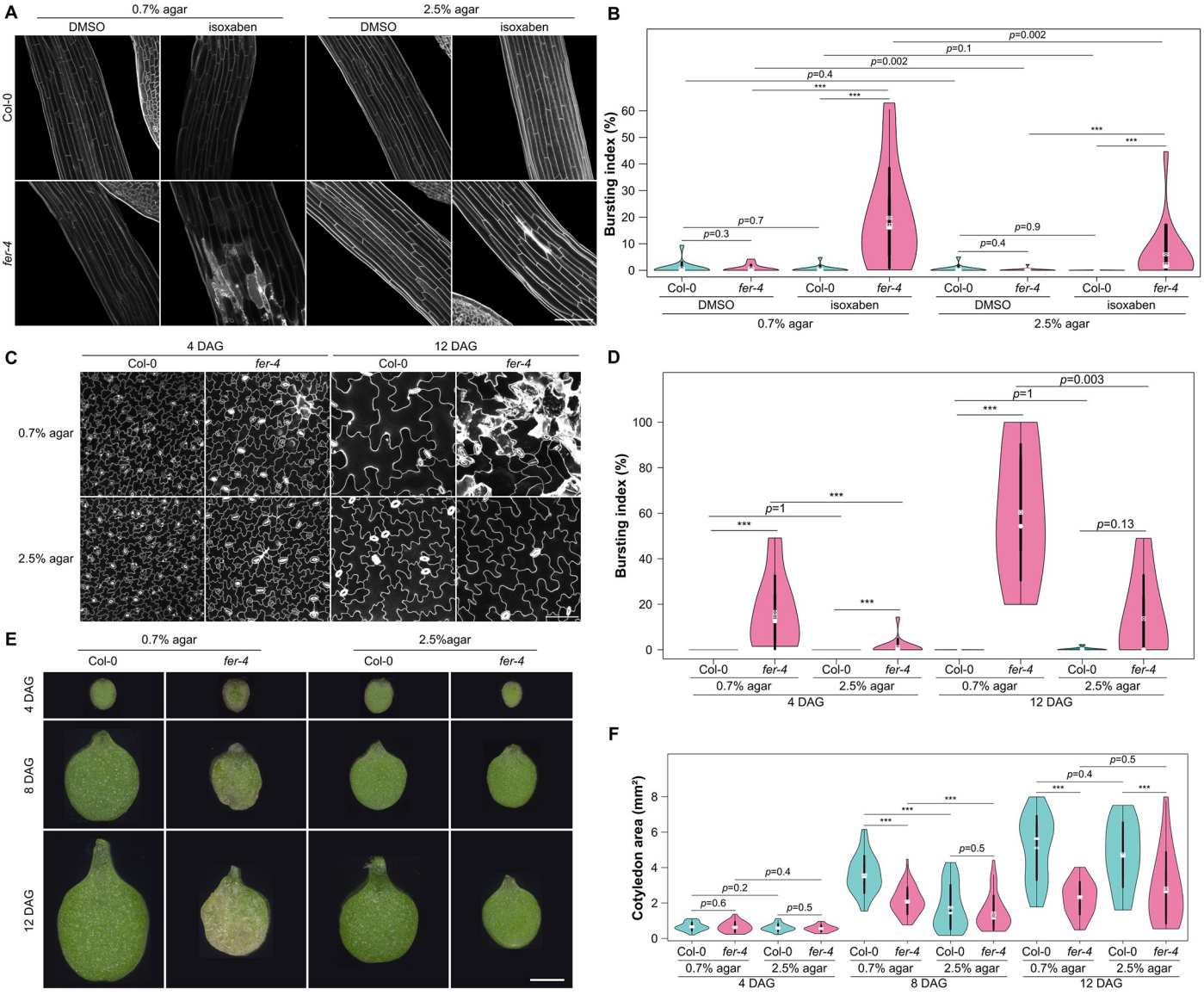

Fig 3. The *fer* phenotype can be partially rescued on 2.5% agar. (A) Representative confocal images of Col-0 and *fer-4* etiolated hypocotyls, from seedlings grown on a medium containing 1 nM isoxaben with 0.7% or 2.5% agar (propidium iodide staining). Scale = 100 μm. **(B)** Bursting index (violin plot) and *p*-values of Wilcoxon–Mann–Whitney tests in *Col-0* and *fer-4* etiolated hypocotyls grown on a medium containing 1nM isoxaben with 0.7% or 2.5% agar. **(C)** Representative confocal images of *Col-0* and *fer-4* pavement cells, from seedlings grown on a medium containing 0.7% or 2.5% agar at t = 4 DAG and t = 12 DAG (propidium iodide staining). Scale = 100 μm. **(D)** Bursting index (violin plot) and *p*-values of Wilcoxon–Mann–Whitney tests in *Col-0* and *fer-4* pavement cells, from seedlings grown on a medium containing 0.7% or 2.5% agar at t = 4 DAG and t = 12 DAG. **(E)** Representative images of *Col-0* and *fer-4* cotyledons, grown on a medium containing 0.7% or 2.5% agar at t = 4 DAG, t = 8 DAG, and t = 12 DAG. Scale = 1 mm. **(F)** Cotyledon area (violin plot) and *p*-values of Wilcoxon–Mann–Whitney tests in *Col-0* and *fer-4* seedlings, grown on a medium containing 0.35%, 0.7%, 1.25%, or 2.5% agar at t = 4 DAG, t = 8 DAG, and t = 12 DAG. All underlying data can be found in S3 Data.

https://doi.org/10.1371/journal.pbio.3001454.g003

To test this hypothesis further, we reasoned that lowering the water potential in the medium should reduce water intake for seedlings, reduce tensile stress level [13], and in the end, reduce the number of burst cells. We thus tested different agar concentration in the medium and analyzed the impact on *fer-4* phenotype. When increasing the agar concentration to 2.5%, the bursting index in hypocotyls was reduced by 70% in isoxaben-grown seedlings, supporting our hypothesis ($p = 0.002$; $n_{fer\text{-}4,isoxaben,0.7\%agar} = 16$; $n_{fer\text{-}4,isoxaben,2.5\%agar} = 16$, Fig 3A and 3B).

We then took a closer look at the pavement cells of *fer-4* cotyledons grown in a medium containing a standard concentration of agar (0.7%) and over time. When looking at orthogonal sections, the outer cell wall appeared very deformed, consistent with cell swelling in *fer-4*, when compared to WT (S4 Fig). This geometry echoes previously observed phenotypes and is consistent with increased wall stretch in *fer* [20,21,42].

In these growth conditions, the mechanical integrity of the cell was not maintained in *fer*: Many burst cells were present, as marked by a strong PI coloration (Fig 3C, S4 Fig). The bursting index increased over time, from 16 ± 16% at 4 DAG (days after germination) to 60 ± 30% at 12 DAG. At both time points, it was significantly higher to that of the WT ($p_{4DAG,0.7\%agar} < 10^{-3}$; $p_{12DAG,0.7\%agar} < 10^{-3}$; $n_{Col\text{-}0,4DAG,0.7\%agar} = 14$, $n_{Col\text{-}0,12DAG,0.7\%agar} = 9$, $n_{fer\text{-}4,4DAG,0.7\%agar} = 14$, $n_{fer\text{-}4,12DAG,0.7\%agar}$ 8; Fig 3D). To further confirm that burst cells appear in response to mechanical stress, we exposed cotyledon to an osmotic shock and monitored cell behavior. We transferred seedlings grown on 2.5% agar for 4 days to 0.35% agar, reasoning that this sudden change should challenge the *fer-4* cell walls. As predicted, many *fer-4* cells swelled and burst in the hours following the transfer (S5 Fig, S1 Movie).

Next, we reasoned that maintaining seedling on 2.5% agar might rescue the *fer-4* phenotype in cotyledons too. In these conditions, the bursting index in *fer-4* was still higher to that of the WT at 4 DAG ($p_{4DAG,2.5\%agar} < 10^{-3}$; $n_{Col\text{-}0,4DAG,2.5\%agar} = 15$; $n_{fer\text{-}4,4DAG,2.5\%agar} = 15$, Fig 3D). However, the bursting index was reduced to 1 ± 4% at 4 DAG ($p_{fer\text{-}4,4DAG} < 10^{-3}$) and to 14 ± 19% at 12 DAG ($p_{fer\text{-}4,12DAG} = 0.003$, Fig 3D), which made it not significantly different from the WT ($p_{12DAG,2.5\%agar} = 0.13$; $n_{Col\text{-}0,12DAG,2.5\%agar} = 9$, $n_{fer\text{-}4,12DAG,2.5\%agar} = 7$; Fig 3D). Once again, lowering the water availability for cells partially rescued the bursting cell phenotype in *fer-4*.

To check whether the apparent rescue could have a more global effect on organ shape, we measured *fer-4* cotyledon area over time on seedlings grown on media containing different agar concentrations (0.7%, 2.5%, Fig 3E and 3F). At a young stage (4 days of light), *fer-4* cotyledons had comparable area as WT ones for every agar concentration ($p_{4DAG,0.7\%agar} = 0.63$; $p_{4DAG,2.5\%agar} = 0.54$; $n_{Col\text{-}0,4DAG,0.7\%agar} = 38$; $n_{fer\text{-}4,4DAG,0.7\%agar} = 23$; $n_{Col\text{-}0,4DAG,2.5\%agar} = 35$; $n_{fer\text{-}4,4DAG,2.5\%agar} = 27$, Fig 3E and 3F). After 8 days of light, *fer-4* cotyledons were 41% smaller than the WT for seedling grown on a medium containing 0.7% agar ($p_{8DAG,0.7\%agar} < 10^{-3}$; $n_{Col\text{-}0,8DAG,0.7\%agar} = 45$; $n_{fer\text{-}4,8DAG,0.7\%agar} = 56$). Strikingly, *fer-4* cotyledons reached a size comparable to that of the WT for seedlings grown on 2.5% agar ($p_{8DAG,2.5\%agar} = 0.51$; $n_{Col\text{-}0,8DAG,2.5\%agar} = 55$; $n_{fer\text{-}4,8DAG,2.5\%agar} = 40$). However, this trend was not maintained after 12 days of light (Fig 3E and 3F).

Note that in all these experiments, the aerial phenotype is rescued, even though only the roots are in contact with a medium with different agar concentrations. This is consistent with the idea that the differences in matrix potential is the cause of the rescue (and not the contact with soft or stiff agar). This is also consistent with previous results obtained in other mutants with cell wall defects, such as the *quasimodo* mutants, where it was also confirmed, using atomic force microscopy, that growth on 2.5% agar medium significantly decreased the apparent tensions in the cotyledon's outer epidermal cell walls [13].

Thus, we find a correlation between the mechanical status of the *fer-4* cotyledons (as monitored by the bursting index) and growth. Taken together, these results suggest that the *fer-4*

mutant is unable to sense the mechanical status of the tissue and that the *fer-4* phenotype reflects a passive turgor-dependent wall defect.

Cortical microtubules orient with predicted maximal tensile stress after ablation in *fer-4*

So far, all the tests suggest that FER is a major player in the mechanical integrity the shoot, consistent with signaling and growth data obtained in the root [20] and with growth data in the hypocotyl [43]. However, it is not clear whether this involves the microtubule response to mechanical stress. To formally check this, we analyzed the behavior of cortical microtubules in response to local ablation in *fer-4*. From a mechanical standpoint, the sudden drop of turgor pressure in the ablated cells, together with epidermal tension [44], generates a circumferential tensile stress around the dead cells [12]. Such a perturbation causes the cortical microtubules to reorient in the new maximal tensile stress direction (circumferential) around the ablation [12,14]. We used the microtubule reporter *pPDF1*::*mCit-MBD* to monitor the microtubule response in *Col-0* and *fer-4* cotyledons. As a 0.7% agar medium triggers widespread cell death in *fer-4* (Fig 3C, S6A–S6D Fig), all tests were performed on 2.5% agar. We measured both the anisotropy and the average orientation of cortical microtubule arrays (relative to the ablation site) in cells surrounding the ablation (Fig 4, S7 and S8 Figs).

The anisotropy (a) of cortical microtubule arrays was low in the WT immediately after ablation ($a_{Col\text{-}0,t0} = 0.11$; $n_{Col\text{-}0,t0} = 248$). It increased by 50% 7 hours later, consistent with the co-alignment of cortical microtubules with tensile stress ($a_{Col\text{-}0,t7h} = 0.16$; $p < 10^{-3}$; $n_{Col\text{-}0,t7h} = 220$; Fig 4E). In *fer-4*, cortical microtubule arrays were slightly less anisotropic (by 30%) than the WT at t = 0 hour ($a_{fer\text{-}4,t0} = 0.075$; $p < 10^{-3}$; $n_{fer\text{-}4,t0} = 174$). After 7 hours, the anisotropy of cortical microtubule arrays increased by 129% and became comparable to that of the WT ($a_{fer\text{-}4,t7h} = 0.17$; $p = 0.26$; $n_{fer\text{-}4,t7h} = 203$, Fig 4E).

Immediately after the ablation, cortical microtubule arrays exhibited no preferred orientation (o) around the ablation, with an average angle of 47 ± 25˚ for the WT, which was not significantly different from that of *fer-4* ($o_{fer\text{-}4,t0} = 46 \pm 25$˚; $p = 0.69$; Fig 4F and 4H, S7B Fig). At t0, both distributions followed a uniform law on 0 to 90˚ ($p_{Col\text{-}0,t0} = 0.5$; $p_{fer\text{-}4,t0} = 0.8$; Kolmogorov–Smirnov test for uniformity). After 7 hours, cortical microtubules did not follow a uniform distribution anymore ($p_{Col\text{-}0,t7h} < 10^{-3}$; $p_{fer\text{-}4,t7h} < 10^{-3}$; Kolmogorov–Smirnov test for uniformity) and became more circumferential around the ablation in both *Col-0* and *fer-4*, with no significant difference between the genotypes ($o_{Col\text{-}0,t7h} = 28 \pm 23$˚, $o_{fer\text{-}4,t7h} = 31 \pm 25$˚; $p = 0.48$, Fig 4G and 4I, S7 and S8 Fig).

Similar trends could be observed when using the *p35S*::*GFP-TUB* microtubule marker line: cortical microtubule orientation appeared circumferential around ablations in both WT and *fer-4* (S9 Fig). However, the diffuse fluorescent signal hindered quantitative analysis with FibrilTool. Because the microtubule response to ablation is comparable in *fer-4* and in the WT, this formally shows that the microtubule response to stress can be independent from FER.

FER and microtubules independently contribute to the mechanical integrity of the shoot in response to mechanical stress

Our ablation results may seem at odds with the fact that *fer-4* and *bot1-7* belong to the same cluster when analyzing pavement cell circularity (see Fig 1D). We thus revisited our quantification of pavement cell shape to identify other shape descriptors amenable to discriminate *bot1-7* and *fer-4*. We focused on lobe size in pavement cells. In the katanin mutant *bot1-7*, which displayed a higher circularity than the WT (see Fig 1), the average basal lobe width was 3%

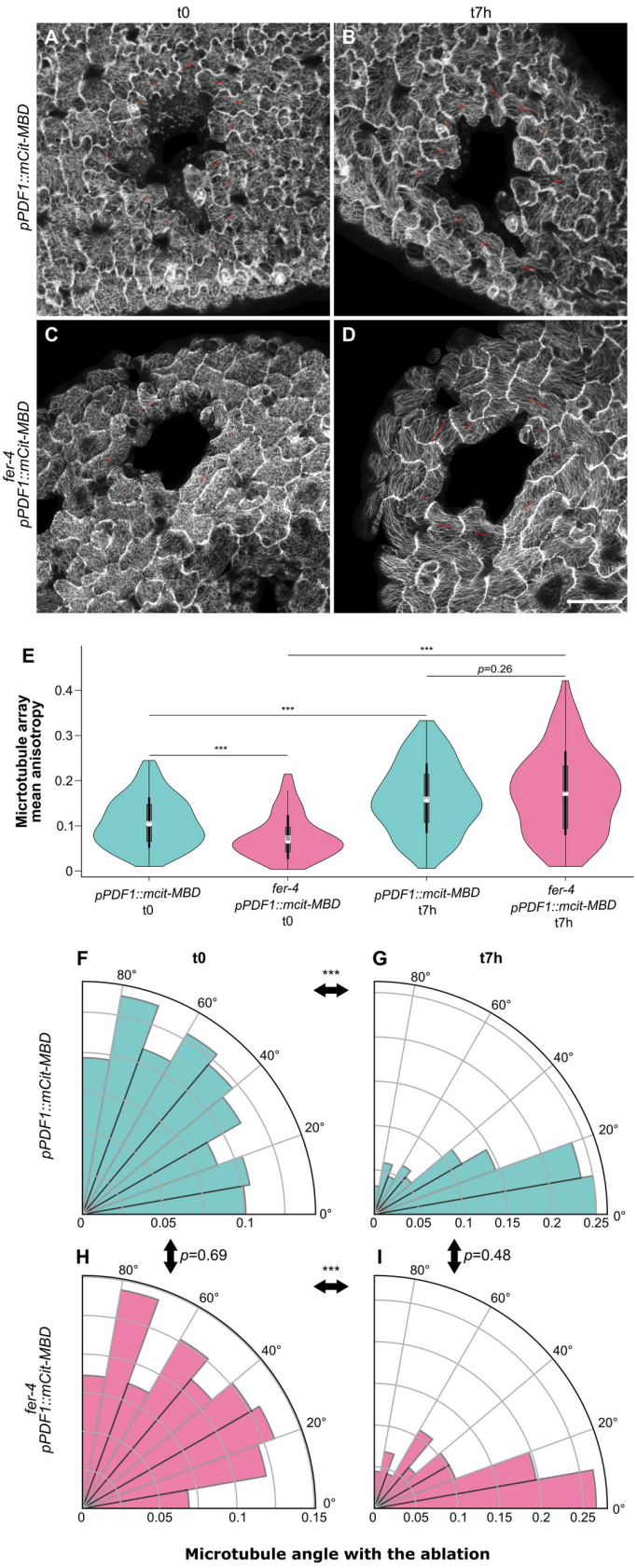
t0
t7h
A
B
C
D
pPDF1::mCit-MBD
fer-4
pPDF1::mCit-MBD
E
Micrtotubule array
mean anisotropy
0
0.1
0.2
0.3
0.4
***
***
***
p=0.26
pPDF1::mcit-MBD
t0
fer-4
pPDF1::mcit-MBD
t0
pPDF1::mcit-MBD
t7h
fer-4
pPDF1::mcit-MBD
t7h
F
t0
G
t7h
H
I
p=0.69
p=0.48
80°
60°
40°
20°
0°
0
0.05
0.1
0.15
0.2
0.25
Microtubule angle with the ablation

Fig 4. Cortical microtubule alignment in *fer* after ablation. All seedlings were grown on 2.5% agar. **(A–D)** Representative confocal images of *pPDF1*::*mCit-MBD* (A, B) and *fer-4 pPDF1*::*mCit-MBD* (C, D) pavement cells, immediately after an ablation (t0, A, C) and 7 hours later (t7h, B, D). The red bars indicate the average orientations of cortical microtubule arrays, and the length of the red bars is proportional to the anisotropy of the cortical microtubule arrays (using ImageJ FibrilTool). Scale = 50 μm. **(E)** Anisotropy (violin plot) of cortical microtubule arrays and *p*-values of Wilcoxon–Mann–Whitney tests in cells surrounding the ablation site in *pPDF1*::*mCit-MBD* and *fer-4 pPDF1*::*mCit-MBD* pavement cells, immediately after an ablation (t0) and 7 hours later (t7h). **(F–I)** Cortical microtubule orientations (polar plots) and *p*-values of Wilcoxon–Mann–Whitney tests in cells surrounding the ablation site in *pPDF1*::*mCit-MBD* (F, G) and *fer-4 pPDF1*::*mCit-MBD* (H, I) pavement cells, immediately after an ablation (t0, F, H)) and 7 hours later (t7h, G, I). All underlying data can be found in S4 Data.

https://doi.org/10.1371/journal.pbio.3001454.g004

smaller than that of the WT ($p < 10^{-3}$; $n_{WS\text{-}4} = 294$; $n_{bot1\text{-}7} = 252$; Fig 5A). Although this is a rather small difference, this is consistent with a reduced microtubule response to stress in the katanin mutant. By contrast, the average basal lobe width in *fer-4* was 12% larger than that of the WT ($p < 10^{-3}$; $n_{Col\text{-}0} = 428$; $n_{fer\text{-}4} = 321$; Fig 5A). Similar trends in basal lobe width were observed when seedlings were grown on 2.5% agar, albeit with lower values, also consistent with a reduced microtubule response to mechanical stress in such conditions (S10 Fig). Thus, both *fer-4* and *bot1-7* pavement cells exhibit higher circularity than the WT through different geometries. Pavement cell shape may thus reflect different responses to stress: Reduced microtubule dynamics in *bot1-7* would generate smaller lobes, whereas increased stress levels in *fer-4* would lead to hyperaligned cortical microtubules and larger lobes. Such hyperaligned cortical microtubules can be observed in *fer-4* pavement cells when seedlings are grown on 0.7% agar (S6C Fig). Alternatively, and nonexclusively, the presence of dead cells in *fer-4* may affect the stress pattern, and thus the cortical microtubule response, further increasing the circularity of pavement cells.

Treatment with the microtubule depolymerizing drug oryzalin has previously been shown to induce cell bursting events in the largest cells at the shoot apical meristem [23], mimicking the bursting cell phenotype we observe in hypocotyls and cotyledons in *fer-4*. If both pathways are truly independent, then one should expect additive behaviors. To test this prediction, we observed hypocotyl growth when both pathways are down, by applying oryzalin on *fer-4* mutants. On 0.7% agar, bursting cells appeared in both oryzalin-treated hypocotyls and control ones in *fer-4*. The bursting index increased by 192% in oryzalin-treated *fer-4* hypocotyls, consistent with an additive role of both pathways in wall integrity ($p_{fer\text{-}4,0.7\%agar} < 10^{-3}$; $n_{fer\text{-}4,DMSO,0.7\%agar} = 10$; $n_{fer\text{-}4,oryzalin,0.7\%agar} = 11$, Fig 5B and 5C). To relate this phenotype to stress levels, we performed the same experiment on 2.5% agar and found a reduction in the bursting cells in all conditions (by 71% on DMSO; $p_{fer\text{-}4,DMSO} = 0.002$; $n_{fer\text{-}4,DMSO,0.7\%agar} = 10$; $n_{fer\text{-}4,DMSO,2.5\%agar} = 9$; by 67% on oryzalin; $p_{fer\text{-}4,oryzalin} < 10^{-3}$; $n_{fer\text{-}4,oryzalin,0.7\%agar} = 11$; $n_{fer\text{-}4,oryzalin,2.5\%agar} = 10$; Fig 5B and 5C). This further confirms that FER and cortical microtubules independently contribute to the response to stress.

Discussion

From a reverse genetic screen, we show that FER plays a primary role in the mechanical integrity of the shoot (using both hypocotyl and cotyledons as model systems). We then find that FER prevents turgor-dependent cell bursting in the shoot. We also find that the microtubule response to stress does not require FER. This does not exclude the possibility that FER may modulate the microtubule response to stress, indirectly. Finally, we show that shutting down both FER and microtubule pathways has an additive effect on turgor-dependent cell bursting. This provides a scenario in which the mechanical feedback in the shoot that is required to maintain mechanical integrity, involves 2 largely independent modules, cortical microtubules and FER (Fig 5D).

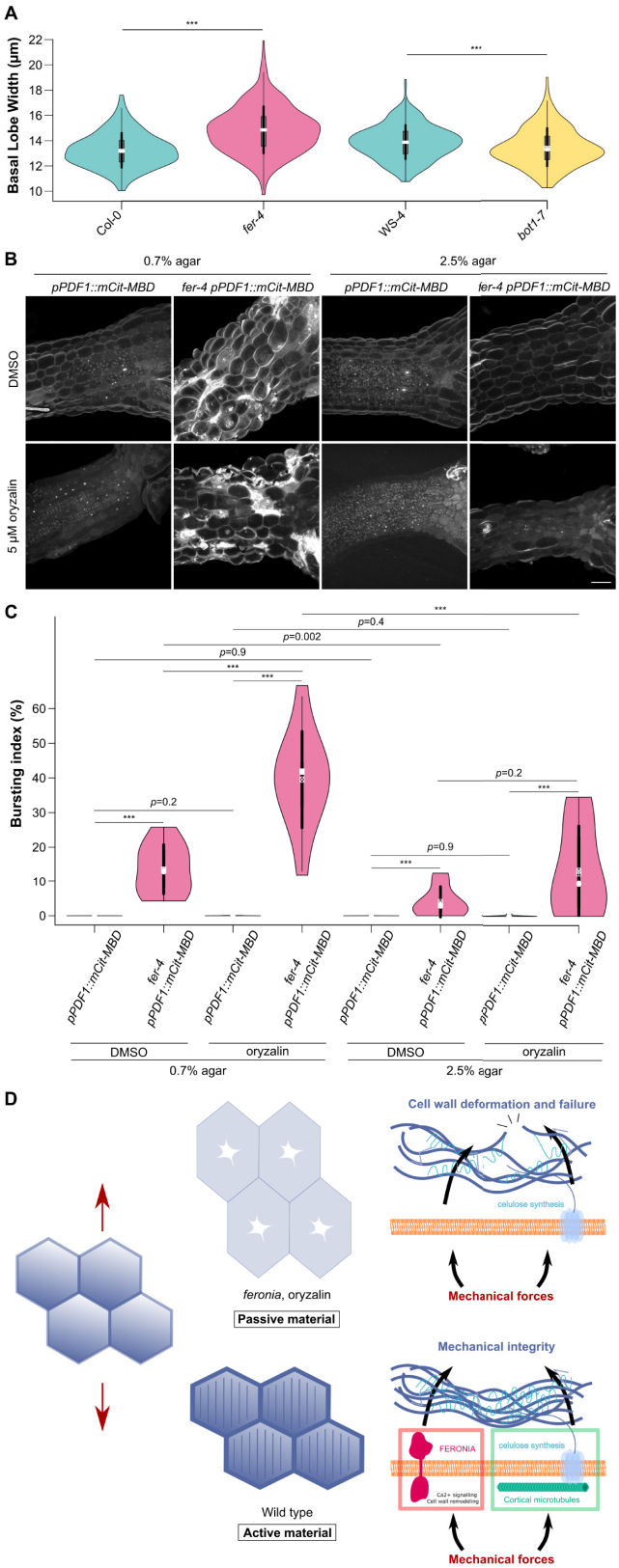
A
Basal Lobe Width (µm)
22
20
18
16
14
12
10
***
***
Col-0
fer-4
WS-4
bot1-7
B
0.7% agar
2.5% agar
pPDF1::mCit-MBD
fer-4 pPDF1::mCit-MBD
pPDF1::mCit-MBD
fer-4 pPDF1::mCit-MBD
DMSO
5 µM oryzalin
C
Bursting index (%)
60
50
40
30
20
10
0
***
p=0.4
p=0.002
p=0.9
***
***
p=0.2
***
p=0.9
***
p=0.2
***
pPDF1::mCit-MBD
fer-4 pPDF1::mCit-MBD
pPDF1::mCit-MBD
fer-4 pPDF1::mCit-MBD
pPDF1::mCit-MBD
fer-4 pPDF1::mCit-MBD
pPDF1::mCit-MBD
fer-4 pPDF1::mCit-MBD
DMSO
oryzalin
DMSO
oryzalin
0.7% agar
2.5% agar
D
feronia, oryzalin
Passive material
Wild type
Active material
Cell wall deformation and failure
celulose synthesis
Mechanical forces
Mechanical integrity
FERONIA
celulose synthesis
Ca2+ signalling
Cell wall remodeling
Cortical microtubules
Mechanical forces

Fig 5. FER and microtubules independently contribute to the response to mechanical stress. (A) Basal lobe width (violin plot) of pavement cells and *p*-values of Dunn tests for the WT (*Col-0*, *WS-4*), katanin mutant (*bot1-7*), and *fer-4*. Seedlings were grown on 0.8% agar. **(B)** Representative confocal images of *pPDF1*::*mCit-MBD* and *fer-4 pPDF1*::*mCit-MBD* hypocotyls grown on 0.7% and 2.5% agar with and without 5 μm of oryzalin. Scale bar = 50 μm. **(C)** Bursting index (violin plot) and *p*-values of Wilcoxon–Mann–Whitney tests in *pPDF1*::*mCit-MBD* and *fer-4 pPDF1*::*mCit-MBD* hypocotyls grown on 0.7% or 2.5% agar, with and without 5 μm of oryzalin. **(D)** In the WT (bottom), cells resist mechanical stress (red arrows) by 2 independent pathways (microtubule-dependent cellulose synthesis and FER-dependent wall reinforcement). In absence of both FER and microtubules (top), cells deform like passive matter and ultimately burst. All underlying data can be found in S5 Data. FER, FERONIA; WT, wild type.

https://doi.org/10.1371/journal.pbio.3001454.g005

This result is consistent with recent findings showing how pectin and cellulose deposition are controlled with largely disconnected networks: Pectins are important for the initiation of pavement cell formation, and the deposition of cellulose microfibril rather amplifies a preexisting mechanical pattern [24]. Similarly, mechanical polarities in growing hypocotyl cells precedes the cellulose-derived mechanical anisotropy in hypocotyl cells [16].

We also provide evidence that the *fer* mutant can be largely rescued through changes in the mechanical environment of the plant despite its central and somewhat pleiotropic role in plant development. This echoes recent findings where essential regulators are found optional, when challenged with different mechanical environments. This is the case for instance for key regulators of pectin synthesis, where decreasing tensile stress can rescue cell–cell adhesion defects in the *quasimodo* mutants [13]. This was also shown for the katanin mutant, where increasing tensile stress levels with isoxaben treatment can generate WT-like cortical microtubule arrays [29]. More recently, this was even extended to signaling in the context of apical hook formation: *arf7 arf19* auxin transduction mutant seedlings exhibit a WT phenotype when mechanically constrained [45].

If the microtubule response to stress does not depend on FER, what could be the most relevant mechanotransduction pathway? As shown with optical tweezers, pulling on microtubules promote their polymerization in vitro [46,47]. Cortical microtubules also align with predicted maximal tension when protoplasts are confined in rectangular microwells and pressurized by hypoosmotic conditions [48]. These data, together with the FER-independent microtubule response to stress, further support the hypothesis that microtubules may be their own mechanosensor [49].

Conversely, microtubule (and cellulose microfibril) alignment likely results from a combination of several cues, beyond tensile stress. Cell geometry can affect microtubule behavior, independent of cortical tension. In particular, due to their high persistence length, microtubules tend to become longitudinal in vitro [50] or in depressurized protoplasts [51]. Furthermore, cell edge factors can affect cortical microtubule behavior, leading to cell-scale aligned arrays [52–54]. Although microtubule, FER, stress, and cell geometry can be uncoupled in experiments, their interplay may provide synergies in vivo. In particular, the deposition of matrix material in the wall depends on exocytosis, which is also promoted by membrane tension. Conversely, affecting matrix deposition may weaken the wall and increase the tensile stress levels. Consistently, microtubule arrays exhibit an enhanced anisotropy when the cell edge GTPase Rab-A5c dependent trafficking is affected in roots [54].

All living organisms constantly sense and respond to mechanical stress. Interestingly, so far, all known mechanosensors at the extracellular matrix (e.g., integrins) also display ligand binding activity. FER may belong to this category as well, as FER also acts as a RALF peptide receptor. Whether this dual role provides synergistic activity for signaling remains to be investigated.

By impairing FER and microtubules, we reveal how plant cells behave when they become unable to respond to stress: They switch to a more passive mode, like a balloon or a soap

bubble, and because of turgor pressure, swell and ultimately die by bursting. Revisiting living systems with the lens of active matter physics is thus particularly suited to understand how cells manage to resist to stress, notably in their response to a fluctuating environment.

Materials and methods

Plant material and growth conditions

All plants were in the *Columbia-0* (*Col-0*) ecotype, except the *bot1-7* mutant, which was in the *Wassilewskija-4* (*WS-4*) ecotype (S1 Table).

Seeds were surface sterilized and individually sown on Murashige and Skoog medium (MS medium, Duchefa, Haarlem, the Netherlands) or *Arabidopsis* medium (custom-made Duchefa "*Arabidopsis*" medium (DU0742.0025, Duchefa Biochemie, The Netherlands) with different agar concentrations (see S2 Table for detailed description of the different media used). For drug treatments, media were supplemented with isoxaben (Sigma, Germany) or oryzalin (Chem Service, USA) from stock solutions in dimethyl sulfoxide (DMSO, Sigma). All plants were placed 2 days in the dark at 4˚C then transferred in a 20˚C long days growth chamber. When seedlings were maintained in the dark, petri dishes were covered with aluminum foil in the 20˚C long days growth chamber.

Image acquisition

Samples were imaged with either a SP8 confocal microscope (Leica Microsystems, Germany) equipped with a 25× long-distance water objective (NA = 0.95), an Epson Perfection 2400 scanner, or a Leica MZ12 microscope (as specified in S2 Table). Samples were stained for 10 minutes with a 1/10 propidium iodide solution (Sigma; PI stains wall pectins and thus marks cell contours). Ablations (Fig 4) were performed manually with a fine needle (Minutien pin, 0.15-mm rod diameter, 0.02-mm tip width, RS-6083–15, Roboz Surgical Instrument, USA) as described in [13]. In all confocal microscopy images, 0.5-μm thick optical slices were acquired.

For every experiment, 3 biological replicates or more were obtained. *Col-0* or *WS-4* seedlings were included as controls in all experiments and replicates. This also explains why the sample size of *Col-0* images used in Figs 1 and 2 is bigger than for the other genotypes. Note that some of the *Col-0* cotyledon data were previously used in our methodological article [55], as templates to introduce the SurfCut ImageJ tool (see below in Image analysis) for cell contour extraction.

Image analysis

Pavement cell shape were obtained by first processing confocal images with MorphoGraphX (http://www.mpipz.mpg.de/MorphoGraphX) [56] to obtain cell contours in a 2.5D epidermal surface (Figs 1 and 5A) or SurfCut (https://github.com/sverger/SurfCut) [55] to extract the flattened cell contours (Fig 3E). The cell contour images were then processed with PaCeQuant [27], an ImageJ plug-in quantifying up to 27 shape descriptors of pavement cells. Hypocotyl length (Fig 2) was measured manually with ImageJ (https://fiji.sc/). Cell burst area (Figs 3, 5C and 5D) was measured manually with ImageJ after extracting the flattened cell contours with SurfCut (https://github.com/sverger/SurfCut) [55]. Cotyledon area (Fig 3) was measured manually with ImageJ. Microtubule organization (Fig 4) was quantified with FibrilTool [57] after flattening the images with SurfCut and denoising them (ROF Denoise, Theta = 25) in ImageJ, as performed in [13]. After image analyses, the brightness and contrast of all images presented in this study were enhanced to help visualization.

Statistical analysis

Statistical analyses were performed with R software (https://www.R-project.org). The sample size is indicated in the main text. For pavement cell shapes (Figs 1 and 5A), we used PaCeQuantAna, the R script that accompanies the PaCeQuant analysis [27], and the FactoMineR and factoextra R libraries for the principal component analysis [58]. Violin plots were shown with the corresponding *p*-value of Kruskal–Wallis tests. For hypocotyl length (Fig 2), the control distribution of hypocotyl length was standardized and the same parameters (μ_{ctrl}, o'_{ctrl}) used to shift the isoxaben distribution similarly (S2 Fig). A Wilcoxon–Mann–Whitney test was then performed on the shifted distributions of the mutant and of the WT for each genotype. For the orientation of cortical microtubules, a Kolmogorov–Smirnov test was performed to compare the angle distributions to a uniform distribution between 0˚ and 90˚. All other quantitative measures were compared using Wilcoxon–Mann–Whitney tests. As a Wilcoxon–Mann–Whitney test can be directed or not, the *p*-value shown in all experiments with a Wilcoxon–Mann–Whitney test was that of a nondirected test for nonsignificant *p*-value (to ensure that neither distribution was higher than the other) and that of a directed test in the significant direction for a significant *p*-value. Differences with *p*-values that were under 1% were considered significant, and those between the commonly used thresholds of 5% and 1% were considered as tendencies. All ± values referred to the standard deviation of the distribution.

Supporting information

S1 Table. Accessions.
(DOCX)

S2 Table. Growth and imaging conditions.
(DOCX)

S1 Fig. Analysis of pavement cell shapes. (A) Pipeline for the extraction and analysis of pavement cell shape. Epidermal signal was first extracted with MorphoGrahX, then segmented with the PaCeQuant ImageJ plug-in, which extracted 27 pavement cell shape descriptors (parameters). Finally, the results were processed by PaCeQuantAna (the PaCeQuant R script). **(B)** Main shape descriptors of pavement cells. Nonlobe area (in μm^2) stands for the area of a cell without the lobes. Circularity is the area of a cell divided by its square perimeter, with a normalization to have a maximal circularity of 1 for a circle. Solidity is the area of a cell divided by the area of its convex hull (convex polygon with the smallest area including the whole cell). Average basal lobe width (μm) stands for the average length of the bases of a cell's lobes. **(C)** Nonlobe area (violin plots) of pavement cells and *p*-values of Dunn tests in the WT (in blue, *Col-0* and *WS-4*), in microtubule associated mutants (in orange, *nek6-1*, *spr2-2*, *tua3*, *tua4*, *tua5*, and *bot1-7*) and in receptor-like kinase mutants (in pink, *tfr1-1*, *cvy1-1*, *fer-4*, *herk1-1*, *herk2-1*, *the1-4*, *the1-6*, *wak1-1*, *wak2-1*, *wak3-1*, *wak4-1*, and *mik2-1*). **(D)** Solidity (violin plots) of pavement cells and *p*-values of Dunn tests in the WT (in blue, *Col-0*, *WS-4*), in microtubule associated mutants (in orange, *nek6-1*, *spr2-2*, *tua3*, *tua4*, *tua5*, and *bot1-7*) and in receptor-like kinase mutants (in pink, *tfr1-1*, *cvy1-1*, *fer-4*, *herk1-1*, *herk2-1*, *the1-4*, *the1-6*, *wak1-1*, *wak2-1*, *wak3-1*, *wak4-1*, and *mik2-1*). All underlying data can be found in S1 Data. WT, wild type.
(JPG)

S2 Fig. Definition of the hypocotyl length index. The continuous black and red lines represent the distribution of the actual measurement of hypocotyl lengths for the treated (red) and control (black) samples. In this example, the values are between 0 and 2 cm, and the average

values for the treated sample are lower. However, when comparing different genotypes, the average length of the untreated (control) mutant samples could already be lower or higher than the control WT samples, thus hampering a direct comparison of the effect of the treatment on the mutant. In order to allow statistical comparison between the samples we normalized the distribution of hypocotyl lengths in the presence of isoxaben according to the distribution of hypocotyl lengths in control conditions, following the standard score method. To do so, the parameters of the control distribution (DMSO, mean: μ_{ctrl}, standard deviation: o'_{ctrl}) are shifted around 0 (dashed black line) and are used to shift the isoxaben distribution to the same extent (dashed red line). With this method, the control samples for all genotypes have a value around 0, which then allows to reveal the effect of the treatment on the different mutants by comparing the means of the normalized treated samples (the hypocotyl length index; Fig 2B). To further ease the comparison, the differences between WT and mutants are then plotted as the hypocotyl length index deviation from the WT, which are the values obtained when subtracting the mutant treated normalized mean to the WT treated normalized mean. This generates a negative value in the hypocotyl length index for mutants being more sensitive to the treatment and a positive value for mutants less sensitive to the treatment (Fig 2C). WT, wild type.
(PNG)

S3 Fig. *fer-2* phenotypes. (A) Representative images of Col-0 and *fer-2* pavement cells. Samples were PI stained and cell contours were extracted with MorphoGraphX and projected in 2D. Scale = 100 μm. **(B)** Representative images of Col-0 and *fer-2* etiolated seedlings grown with or without 1 nM isoxaben. Scale = 1 cm. **(C)** Representative confocal images of *Col-0* and *fer-2* pavement cells, from seedlings grown on a medium containing 0.7% or 2.5% agar at t = 4 DAG and t = 12 DAG (propidium iodide staining). Scale = 100 μm. **(D)** Representative images of *Col-0* and *fer-2* cotyledons, grown on a medium containing 0.7% or 2.5% agar at t = 4 DAG, t = 8 DAG and t = 12 DAG. Scale = 1 mm. **(E)** Representative confocal images of Col-0 and *fer-2* hypocotyls grown on 0.7% and 2.5% agar with and without 5 μm of oryzalin. All underlying data can be found in Supporting information folder. Scale bar = 50 μm. PI, propidium iodide.
(JPG)

S4 Fig. Swelling pavement cells in *fer-4* on 0.7% agar. (A, B) Representative images of *Col-0 (A) and fer-4 (B)* pavement cells, from seedlings grown on a medium containing 0.7% agar at t = 4 DAG. Samples were PI stained and cell contours were extracted with SurfCut and projected in 2D. Orthogonal projections were also extracted with Fiji. Note the presence of curvy outer walls in some *fer-4* cells. All underlying data can be found in Supporting information folder. Scale = 100 μm. PI, propidium iodide.
(JPG)

S5 Fig. Bursting cells in *fer-4* upon switch from 2.5% to 0.35% agar conditions. (A, B) Representative confocal images of *fer-4* pavement cells, from seedlings grown on a medium containing 2.5% agar for 4 days, transferred on a medium containing 0.35% agar, stained with PI and imaged in water immediately after the transfer to a new medium (t0) and 1 to 16 hours later. Cell contours were extracted with SurfCut and projected in 2D. Orthogonal projections were also extracted with Fiji, focusing on the cell indicated with red arrows. See also S1 Movie. Scale = 100 μm.
(JPG)

S6 Fig. Cortical microtubule behavior in *fer-4* grown on 0.7% agar medium. Representative confocal images of *pPDF1*::*mCit-MBD* **(A)** and *fer-4 pPDF1*::*mCit-MBD* **(B)** pavement cells

from seedlings grown on a medium containing 0.7% agar. Quantification of the anisotropy of cortical microtubule arrays in both lines **(C)**. Note the presence of circumferential cortical microtubules around dead cells, matching the predicted maximal tensile stress direction. Representative confocal images of *pPDF1*::*mCit-MBD* **(D, E)** and *fer-4 pPDF1*::*mCit-MBD* **(F, G)** pavement cells from seedlings grown on a medium containing 0.7% agar, immediately after ablation (t0, D, F) and 7 hours later (t7h, E, G). Note the presence of many dead cells and the strong alignment of cortical microtubules at t0 in *fer-4*. All underlying data can be found in Supporting information folder. Scale = 50 μm.
(JPG)

S7 Fig. Ablations (full kinetics) on 2.5% agar medium (example 1). (A) Representative confocal images of *pPDF1*::*mCit-MBD* (top) and *fer-4 pPDF1*::*mCit-MBD* (bottom) pavement cells, from seedlings grown on a medium containing 2.5% agar, immediately after an ablation (t0) and 1 to 7 hours later. Scale = 50 μm. **(B)** Orientation to the ablation (violin plot) of cortical microtubule arrays and *p*-values of Wilcoxon–Mann–Whitney tests in cells surrounding the ablation site in *pPDF1*::*mCit-MBD* and *fer-4 pPDF1*::*mCit-MBD* pavement cells, immediately after an ablation (t0) and 7 hours later (t7h) (see Fig 4). All underlying data can be found in Supporting information folder.
(JPG)

S8 Fig. Ablations (full kinetics) on 2.5% agar medium (example 2). (A) Representative confocal images of *pPDF1*::*mCit-MBD* (A) and *fer-4 pPDF1*::*mCit-MBD* **(B)** pavement cells, from seedlings grown on a medium containing 2.5% agar, immediately after an ablation (t0) and 1 to 7 hours later. Scale = 50 μm.
(JPG)

S9 Fig. Microtubule response after ablation using the GFP-tubulin reporter. Representative confocal images of *p35S*::*GFP-TUB* (top) and *fer-4 p35S*::*GFP-TUB* (bottom) pavement cells from seedlings grown on a medium containing 2.5% agar, immediately after an ablation (t0) and 7 hours later (t7h). Scale = 50 μm.
(JPG)

S10 Fig. Basal lobe width according to genotype and growth conditions. Basal lobe width (violin plot) of pavement cells and *p*-values of Dunn tests for the WT (*Col-0*, *WS-4*), katanin mutant (*bot1-7*), and *fer-4*. Seedlings were grown on 0.8% or 2.5% agar. Data from Fig 5A (0.8% agar) are reproduced here to allow a full comparison of the results. All underlying data can be found in S7 Data. WT, wild type.
(PNG)

S1 Movie. Bursting cells in *fer-4* upon switch from 2.5% to 0.35% agar conditions. Animation of representative confocal images of *fer-4* pavement cells, from seedlings grown on a medium containing 2.5% agar for 4 days, transferred on a medium containing 0.35% agar, stained with PI and imaged in water immediately after the transfer to a new medium (t0) and 1 to 16 hours later. Cell contours were extracted with SurfCut and projected in 2D (same images as in S5 Fig) then aligned with the stackreg (Pyramid Registration) plug-in in Fiji. PI, propidium iodide.
(AVI)

S1 Data. Data related to Fig 1 (panels B, C, and D), Fig 5 (panel A), and S1 Fig (panels C and D).
(XLSX)

S2 Data. Data related to Fig 2 (panels B and C).
(XLSX)

S3 Data. Data related to Fig 3 (panels B, D, and F).
(XLSX)

S4 Data. Data related to Fig 4 (panels E–I) and S7 Fig (panel B).
(XLSX)

S5 Data. Data related to Fig 5 (panel C).
(XLSX)

S6 Data. Data related to S6 Fig (panel C).
(XLSX)

S7 Data. Data related to S10 Fig.
(XLSX)

Acknowledgments

We are thankful to our colleagues at the plant reproduction and development lab for their comments and feedback on this manuscript. We thank the Imaging and Microscopy Core Facility (Platim) for help with imaging.

Author Contributions

Conceptualization: Alice Malivert, Olivier Hamant, Stéphane Verger.

Data curation: Alice Malivert, Özer Erguvan, Antoine Chevallier, Antoine Dehem, Rodrigue Friaud, Mengying Liu, Marjolaine Martin, Théophile Peyraud.

Formal analysis: Alice Malivert, Özer Erguvan, Antoine Chevallier, Antoine Dehem, Rodrigue Friaud, Mengying Liu, Marjolaine Martin, Théophile Peyraud, Stéphane Verger.

Funding acquisition: Olivier Hamant.

Methodology: Alice Malivert, Özer Erguvan.

Supervision: Alice Malivert, Olivier Hamant, Stéphane Verger.

Writing – original draft: Alice Malivert, Olivier Hamant, Stéphane Verger.

Writing – review & editing: Alice Malivert, Olivier Hamant, Stéphane Verger.

References

1. Wolfenson H, Yang B, Sheetz MP. Steps in Mechanotransduction Pathways that Control Cell Morphology. Annu Rev Physiol. 2019; 81:585–605. https://doi.org/10.1146/annurev-physiol-021317-121245 PMID: 30403543
2. Hamant O, Saunders TE. Shaping Organs: Shared Structural Principles Across Kingdoms. Annu Rev Cell Dev Biol. 2020; 36:385–410. https://doi.org/10.1146/annurev-cellbio-012820-103850 PMID: 32628862
3. Schopfer P. Biomechanics of plant growth. Am J Bot. 2006; 93:1415–25. https://doi.org/10.3732/ajb.93.10.1415 PMID: 21642088
4. Bacete L, Hamann T. The Role of Mechanoperception in Plant Cell Wall Integrity Maintenance. Plan Theory. 2020; 9:574. https://doi.org/10.3390/plants9050574 PMID: 32369932
5. Trinh D-C, Alonso-Serra J, Asaoka M, Colin L, Cortes M, Malivert A, et al. How Mechanical Forces Shape Plant Organs. Curr Biol. 2021; 31:R143–59. https://doi.org/10.1016/j.cub.2020.12.001 PMID: 33561417

6. Cosgrove DJ. Growth of the plant cell wall. Nat Rev Mol Cell Biol. 2005; 6:850–61. https://doi.org/10.1038/nrm1746 PMID: 16261190

7. Anderson CT, Kieber JJ. Dynamic Construction, Perception, and Remodeling of Plant Cell Walls. Annu Rev Plant Biol. 2020; 71:39–69. https://doi.org/10.1146/annurev-arplant-081519-035846 PMID: 32084323

8. Paredez AR, Somerville CR, Ehrhardt DW. Visualization of cellulose synthase demonstrates functional association with microtubules. Science. 2006; 312:1491–5. https://doi.org/10.1126/science.1126551 PMID: 16627697

9. Green P, King A. A mechanism for the origin of specifically oriented textures in development with special reference to Nitella wall texture. Aust J Biol Sci. 1966:421–37.

10. Williamson R. Alignment of cortical microtubules by anisotropic wall stresses. Aust J Plant Physiol. 1990:601–13.

11. Hejnowicz Z, Rusin A, Rusin T. Tensile Tissue Stress Affects the Orientation of Cortical Microtubules in the Epidermis of Sunflower Hypocotyl. J Plant Growth Regul. 2000; 19:31–44. https://doi.org/10.1007/s003440000005 PMID: 11010990

12. Hamant O, Heisler MG, Jonsson H, Krupinski P, Uyttewaal M, Bokov P, et al. Developmental patterning by mechanical signals in Arabidopsis. Science. 2008; 322:1650–5. https://doi.org/10.1126/science.1165594 PMID: 19074340

13. Verger S, Long Y, Boudaoud A, Hamant O. A tension-adhesion feedback loop in plant epidermis. Elife. 2018; 7. https://doi.org/10.7554/eLife.34460 PMID: 29683428

14. Sampathkumar A, Krupinski P, Wightman R, Milani P, Berquand A, Boudaoud A, et al. Subcellular and supracellular mechanical stress prescribes cytoskeleton behavior in Arabidopsis cotyledon pavement cells. Elife. 2014; 3:e01967. https://doi.org/10.7554/eLife.01967 PMID: 24740969

15. Manfield IW, Orfila C, McCartney L, Harholt J, Bernal AJ, Scheller HV, et al. Novel cell wall architecture of isoxaben-habituated Arabidopsis suspension-cultured cells: global transcript profiling and cellular analysis. Plant J Cell Mol Biol. 2004; 40:260–75. https://doi.org/10.1111/j.1365-313X.2004.02208.x PMID: 15447652

16. Peaucelle A, Wightman R, Höfte H. The Control of Growth Symmetry Breaking in the Arabidopsis Hypocotyl. Curr Biol. 2015; 25:1746–52. https://doi.org/10.1016/j.cub.2015.05.022 PMID: 26073136

17. Hématy K, Sado P-E, Van Tuinen A, Rochange S, Desnos T, Balzergue S, et al. A receptor-like kinase mediates the response of Arabidopsis cells to the inhibition of cellulose synthesis. Curr Biol. 2007; 17:922–31. https://doi.org/10.1016/j.cub.2007.05.018 PMID: 17540573

18. Gonneau M, Desprez T, Martin M, Doblas VG, Bacete L, Miart F, et al. Receptor Kinase THESEUS1 Is a Rapid Alkalinization Factor 34 Receptor in Arabidopsis. Curr Biol. 2018; 28:2452–8.e4. https://doi.org/10.1016/j.cub.2018.05.075 PMID: 30057301

19. Engelsdorf T, Gigli-Bisceglia N, Veerabagu M, McKenna JF, Vaahtera L, Augstein F, et al. The plant cell wall integrity maintenance and immune signaling systems cooperate to control stress responses in *Arabidopsis thaliana*. Sci Signal. 2018; 11:eaao3070. https://doi.org/10.1126/scisignal.aao3070 PMID: 29945884

20. Shih H-W, Miller ND, Dai C, Spalding EP, Monshausen GB. The receptor-like kinase FERONIA is required for mechanical signal transduction in Arabidopsis seedlings. Curr Biol. 2014; 24:1887–92. https://doi.org/10.1016/j.cub.2014.06.064 PMID: 25127214

21. Feng W, Kita D, Peaucelle A, Cartwright HN, Doan V, Duan Q, et al. The FERONIA Receptor Kinase Maintains Cell-Wall Integrity during Salt Stress through Ca2+ Signaling. Curr Biol. 2018; 28:666–75.e5. https://doi.org/10.1016/j.cub.2018.01.023 PMID: 29456142

22. Lin W, Tang W, Anderson CT, Yang Z. FERONIA's sensing of cell wall pectin activates ROP GTPase signaling in *Arabidopsis*. bioRxiv. 2018 Feb. https://doi.org/10.1101/269647

23. Sapala A, Runions A, Routier-Kierzkowska A-L, Das Gupta M, Hong L, Hofhuis H, et al. Why plants make puzzle cells, and how their shape emerges. Elife. 2018; 7. https://doi.org/10.7554/eLife.32794 PMID: 29482719

24. Bidhendi AJ, Altartouri B, Gosselin FP, Geitmann A. Mechanical Stress Initiates and Sustains the Morphogenesis of Wavy Leaf Epidermal Cells. Cell Rep. 2019; 28:1237–50.e6. https://doi.org/10.1016/j.celrep.2019.07.006 PMID: 31365867

25. Fu Y, Gu Y, Zheng Z, Wasteneys G, Yang Z. Arabidopsis interdigitating cell growth requires two antagonistic pathways with opposing action on cell morphogenesis. Cell. 2005; 120:687–700. https://doi.org/10.1016/j.cell.2004.12.026 PMID: 15766531

26. Majda M, Grones P, Sintorn I-M, Vain T, Milani P, Krupinski P, et al. Mechanochemical Polarization of Contiguous Cell Walls Shapes Plant Pavement Cells. Dev Cell. 2017; 43:290–304.e4. https://doi.org/10.1016/j.devcel.2017.10.017 PMID: 29112850

27. Möller B, Poeschl Y, Plötner R, Bürstenbinder K. PaCeQuant: A Tool for High-Throughput Quantification of Pavement Cell Shape Characteristics. Plant Physiol. 2017; 175:998–1017. https://doi.org/10.1104/pp.17.00961 PMID: 28931626

28. Takatani S, Verger S, Okamoto T, Takahashi T, Hamant O, Motose H. Microtubule Response to Tensile Stress Is Curbed by NEK6 to Buffer Growth Variation in the Arabidopsis Hypocotyl. Curr Biol. 2020; S0960982220301974. https://doi.org/10.1016/j.cub.2020.02.024 PMID: 32169210

29. Uyttewaal M, Burian A, Alim K, Landrein B, Borowska-Wykret D, Dedieu A, et al. Mechanical stress acts via katanin to amplify differences in growth rate between adjacent cells in Arabidopsis. Cell. 2012; 149:439–51. https://doi.org/10.1016/j.cell.2012.02.048 PMID: 22500806

30. Ishida T, Kaneko Y, Iwano M, Hashimoto T. Helical microtubule arrays in a collection of twisting tubulin mutants of Arabidopsis thaliana. Proc Natl Acad Sci U S A. 2007; 104:8544–9. https://doi.org/10.1073/pnas.0701224104 PMID: 17488810

31. Matsumoto S, Kumasaki S, Soga K, Wakabayashi K, Hashimoto T, Hoson T. Gravity-induced modifications to development in hypocotyls of Arabidopsis tubulin mutants. Plant Physiol. 2010; 152:918–26. https://doi.org/10.1104/pp.109.147330 PMID: 20018592

32. Hervieux N, Dumond M, Sapala A, Routier-Kierzkowska A-L, Kierzkowski D, Roeder AHK, et al. A Mechanical Feedback Restricts Sepal Growth and Shape in Arabidopsis. Curr Biol. 2016. https://doi.org/10.1016/j.cub.2016.03.004 PMID: 27151660

33. Wightman R, Chomicki G, Kumar M, Carr P, Turner SR. SPIRAL2 determines plant microtubule organization by modulating microtubule severing. Curr Biol. 2013; 23:1902–7. https://doi.org/10.1016/j.cub.2013.07.061 PMID: 24055158

34. Fan Y, Burkart GM, Dixit R. The Arabidopsis SPIRAL2 Protein Targets and Stabilizes Microtubule Minus Ends. Curr Biol. 2018; 28:987–94.e3. https://doi.org/10.1016/j.cub.2018.02.014 PMID: 29526586

35. Nakamura M, Lindeboom JJ, Saltini M, Mulder BM, Ehrhardt DW. SPR2 protects minus ends to promote severing and reorientation of plant cortical microtubule arrays. J Cell Biol. 2018; 217:915–27. https://doi.org/10.1083/jcb.201708130 PMID: 29339437

36. Zhang C, Halsey LE, Szymanski DB. The development and geometry of shape change in Arabidopsis thalianacotyledon pavement cells. BMC Plant Biol. 2011; 11:27. https://doi.org/10.1186/1471-2229-11-27 PMID: 21284861

37. Li C, Yeh F-L, Cheung AY, Duan Q, Kita D, Liu M-C, et al. Glycosylphosphatidylinositol-anchored proteins as chaperones and co-receptors for FERONIA receptor kinase signaling in Arabidopsis. Elife. 2015;4. https://doi.org/10.7554/eLife.06587 PMID: 26052747

38. Vőfély RV, Gallagher J, Pisano GD, Bartlett M, Braybrook SA. Of puzzles and pavements: a quantitative exploration of leaf epidermal cell shape. New Phytol. 2019; 221:540–52. https://doi.org/10.1111/nph.15461 PMID: 30281798

39. Scheible WR, Eshed R, Richmond T, Delmer D, Somerville C. Modifications of cellulose synthase confer resistance to isoxaben and thiazolidinone herbicides in Arabidopsis Ixr1 mutants. Proc Natl Acad Sci U S A. 2001; 98:10079–84. https://doi.org/10.1073/pnas.191361598 PMID: 11517344

40. Heisler MG, Hamant O, Krupinski P, Uyttewaal M, Ohno C, Jönsson H, et al. Alignment between PIN1 Polarity and Microtubule Orientation in the Shoot Apical Meristem Reveals a Tight Coupling between Morphogenesis and Auxin Transport. PLoS Biol. 2010;8. https://doi.org/10.1371/journal.pbio.1000516 PMID: 20976043

41. Engelsdorf T, Kjaer L, Gigli-Bisceglia N, Vaahtera L, Bauer S, Miedes E, et al. Functional characterization of genes mediating cell wall metabolism and responses to plant cell wall integrity impairment. BMC Plant Biol. 2019; 19:320. https://doi.org/10.1186/s12870-019-1934-4 PMID: 31319813

42. Duan Q, Kita D, Li C, Cheung AY, Wu H-M. FERONIA receptor-like kinase regulates RHO GTPase signaling of root hair development. Proc Natl Acad Sci U S A. 2010; 107:17821–6. https://doi.org/10.1073/pnas.1005366107 PMID: 20876100

43. Bastien R, Legland D, Martin M, Fregosi L, Peaucelle A, Douady S, et al. KymoRod: a method for automated kinematic analysis of rod-shaped plant organs. Plant J Cell Mol Biol. 2016; 88:468–75. https://doi.org/10.1111/tpj.13255 PMID: 27354251

44. Kutschera U, Niklas KJ. The epidermal-growth-control theory of stem elongation: an old and a new perspective. J Plant Physiol. 2007; 164:1395–409. https://doi.org/10.1016/j.jplph.2007.08.002 PMID: 17905474

45. Baral A, Morris E, Aryal B, Jonsson K, Verger S, Xu T, et al. External mechanical cues reveal core molecular pathway behind tissue bending in plants. Plant Biol. 2020 Mar. https://doi.org/10.1101/2020.03.05.978296

46. Franck AD, Powers AF, Gestaut DR, Gonen T, Davis TN, Asbury CL. Tension applied through the Dam1 complex promotes microtubule elongation providing a direct mechanism for length control in mitosis. Nat Cell Biol. 2007; 9:832–7. https://doi.org/10.1038/ncb1609 PMID: 17572669

47. Trushko A, Schäffer E, Howard J. The growth speed of microtubules with XMAP215-coated beads coupled to their ends is increased by tensile force. Proc Natl Acad Sci U S A. 2013; 110:14670–5. https://doi.org/10.1073/pnas.1218053110 PMID: 23964126

48. Colin L, Chevallier A, Tsugawa S, Gacon F, Godin C, Viasnoff V, et al. Cortical tension overrides geometrical cues to orient microtubules in confined protoplasts. Proc Natl Acad Sci U S A. 2020; 117:32731–8. https://doi.org/10.1073/pnas.2008895117 PMID: 33288703

49. Hamant O, Inoue D, Bouchez D, Dumais J, Mjolsness E. Are microtubules tension sensors? Nat Commun. 2019; 10:2360. https://doi.org/10.1038/s41467-019-10207-y PMID: 31142740

50. Cosentino Lagomarsino M, Tanase C, Vos JW, Emons AMC, Mulder BM, Dogterom M. Microtubule organization in three-dimensional confined geometries: evaluating the role of elasticity through a combined in vitro and modeling approach. Biophys J. 2007; 92:1046–57. https://doi.org/10.1529/biophysj.105.076893 PMID: 17098802

51. Durand-Smet P, Spelman TA, Meyerowitz EM, Jönsson H. Cytoskeletal organization in isolated plant cells under geometry control. Proc Natl Acad Sci U S A. 2020; 117:17399–408. https://doi.org/10.1073/pnas.2003184117 PMID: 32641513

52. Ambrose C, Allard JF, Cytrynbaum EN, Wasteneys GO. A CLASP-modulated cell edge barrier mechanism drives cell-wide cortical microtubule organization in Arabidopsis. Nat Commun. 2011; 2:430. https://doi.org/10.1038/ncomms1444 PMID: 21847104

53. Chakrabortty B, Willemsen V, de Zeeuw T, Liao C-Y, Weijers D, Mulder B, et al. A Plausible Microtubule-Based Mechanism for Cell Division Orientation in Plant Embryogenesis. Curr Biol. 2018; 28:3031–43.e2. https://doi.org/10.1016/j.cub.2018.07.025 PMID: 30245102

54. Kirchhelle C, Garcia-Gonzalez D, Irani NG, Jérusalem A, Moore I. Two mechanisms regulate directional cell growth in Arabidopsis lateral roots. Elife. 2019; 8:e47988. https://doi.org/10.7554/eLife.47988 PMID: 31355749

55. Erguvan Ö, Louveaux M, Hamant O, Verger S. ImageJ SurfCut: a user-friendly pipeline for high-throughput extraction of cell contours from 3D image stacks. BMC Biol. 2019; 17:38. https://doi.org/10.1186/s12915-019-0657-1 PMID: 31072374

56. Barbier de Reuille P, Routier-Kierzkowska A-L, Kierzkowski D, Bassel GW, Schüpbach T, Tauriello G, et al. MorphoGraphX: A platform for quantifying morphogenesis in 4D. Elife. 2015; 4:05864. https://doi.org/10.7554/eLife.05864 PMID: 25946108

57. Boudaoud A, Burian A, Borowska-Wykręt D, Uyttewaal M, Wrzalik R, Kwiatkowska D, et al. FibrilTool, an ImageJ plug-in to quantify fibrillar structures in raw microscopy images. Nat Protoc. 2014; 9:457–63. https://doi.org/10.1038/nprot.2014.024 PMID: 24481272

58. Lê S, Josse J, Husson F. FactoMineR: An R Package for Multivariate Analysis. J Stat Softw. 2008; 25:1–18. https://doi.org/10.18637/jss.v025.i01

FERONIA and microtubules independently contribute to mechanical integrity in the Arabidopsis shoot

Alice Malivert[1], Özer Erguvan[1,2], Antoine Chevallier[1], Antoine Dehem[1], Rodrigue Friaud[1], Mengying Liu[1], Marjolaine Martin[1], Théophile Peyraud[1], Olivier Hamant[1,*], Stéphane Verger[1,2,*]

* Correspondence: olivier.hamant@ens-lyon.fr (OH), stephane.verger@slu.se (SV)

Supplementary information

Supplementary Table 1. Accessions

ID	Line	Full gene name	AGI	Ontology	Ecotype	Reference
nek6-1	SALK_152782	*NIMA (NEVER IN MITOSIS, GENE A)-RELATED 6*	AT3G44200	Tubulin kinase	Col-0	Motose *et al.,* 2008. Plant J Cell Mol Biol 54(5):829–844.
spr2-2	EMS CS6549	*SPIRAL2*	AT4T27060	MAP	Col-0	Shoji *et al.,* 2004. Plant Physiol 136(4):3933–3944.
tua3(D205N)	EMS CS68878	*TUBULIN ALPHA-3*	AT5G19770	Tubulin	Col-0	Ishida et al., 2007. Proc Natl Acad Sci U S A 104(20):8544–8549.
tua4(S178D)	EMS CS68881	*TUBULIN ALPHA-4*	AT1G04821	Tubulin	Col-0	Ishida et al., 2007. Proc Natl Acad Sci U S A 104(20):8544–8549.
tua5(D251N)	EMS CS68884	*TUBULIN ALPHA-5*	AT5G19780	Tubulin	Col-0	Ishida et al., 2007. Proc Natl Acad Sci U S A 104(20):8544–8549..
tfr1-1	GK649 – E11-67	*THESEUS-FERONIA-RELATED1*	AT5G24010	CrRLK	Col-0	This study, provided by H. Höfte
cvy1-1	SALK_018797	*CURVY1*	AT2G39360	CrRLK	Col-0	Gachomo *et al.,* 2014. BMC Plant Biol 14:221.
fer-4	GABI 106_A06	*FERONIA*	AT3G51550	CrRLK	Col-0	Duan et al., 2010. Proc Natl Acad Sci U S A 107(41):17821–17826.
fer-2	TAG insert	*FERONIA*	AT3G51550	CrRLK	Col-0	Deslauriers and Larsen, 2010. Molecular Plant 3, 626–640
herk1-1	SALK_008043	*HERCULES RECEPTOR KINASE 1*	AT3G46290	CrRLK	Col-0	Guo et al., 2009. Proc Natl Acad Sci U S A 106(18):7648–7653.
herk2-1	SALK_105055	*HERCULES RECEPTOR KINASE 2*	AT1G30570	CrRLK	Col-0	Guo et al., 2009. Proc Natl Acad Sci U S A 106(18):7648–7653.
the1-6	EMS (sup ctl1-2)	*THESEUS1*	AT5G54380	CrRLK	Col-0	Merz *et al.,* 2017. J Exp Bot 68(16):4583–4593.
wak1-1	SALK_107175	*CELL WALL-ASSOCIATED KINASE 1*	AT1G21250	WAK	Col-0	He *et al.,* 1996. J Biol Chem 271(33):19789–19793.

wak2-1	SAIL_286_E03	*CELL WALL-ASSOCIATED KINASE 2*	AT1G21270	WAK	Col-0	He *et al.,* 1996. J Biol Chem 271(33):19789–19793.
wak3-1	SALK_071999	*CELL WALL-ASSOCIATED KINASE 3*	AT1G21240	WAK	Col-0	He et al., 1999. Plant Mol Biol 39(6):1189–1196.
wak4-1	SAIL_1156_F08	*CELL WALL-ASSOCIATED KINASE 4*	AT1G21210	WAK	Col-0	He et al., 1999. Plant Mol Biol 39(6):1189–1196.
mik2-1	SALK_061769	*MDIS1-INTERACTING RECEPTOR LIKE KINASE2*	AT4G08850	LRR-RLK	Col-0	Wang *et al.,* 2016. Nature 531(7593):241–244.
bot1-7	deletion of 19 bp	*KATANIN 1*	AT1G80350	Katanin	WS-4	Bichet *et al.,* 2001. Plant J 25(2):137–148.
pPDF1::mCit-MBD	Translational fusion protein			Microtubule marker	Col-0	Armezzani *et al.,* 2018. Development 145.
fer-4 pPDF1::mCit-MBD	Translational fusion protein			Microtubule marker	Col-0	Cross, this study
p35S::GFP-TUB	Translational fusion protein			Microtubule marker	Col-0	Lin et al., 2018) BioRxiv. https://doi.org/10.1101/269647
fer-4 p35S::GFP-TUB	Translational fusion protein			Microtubule marker	Col-0	Lin et al., 2018) BioRxiv. https://doi.org/10.1101/269647

Abbreviations: MAP: Microtubule Associated Protein, CrRLK: Catharanthus Receptor-Like Kinase, WAK: Wall Associated Kinase, LRR-RLK: Leucin Rich Repeat Receptor-Like Kinase

Supplementary Table 2. Growth and imaging conditions

Figure	Panel	Medium	Growth conditions	Imaging
Figure 1	A-D	Medium A	Condition 1	Imaging a
Figure 2	A-C	Medium B	Condition 2	Imaging b
Figure 3	A-B	Medium C	Condition 2	Imaging c
Figure 3	C-D	Medium D	Condition 3	Imaging a
Figure 3	E-F	Medium D	Condition 3	Imaging f
Figure 4	A-I	Medium D	Condition 1	Imaging d
Figure 5	A	Medium A	Condition 1	Imaging a
Figure 5	B-C	Medium E	Condition 4	Imaging e

Growth medium	
Medium A	MS medium with 0.8% agar, 1% sucrose, and no vitamin
Medium B	MS medium with 0.8% agar, no sucrose, and no vitamin supplemented with 1 nM of isoxaben diluted in DMSO, or the same volume of DMSO (control)
Medium C	MS medium with 0.8% or 2,5% agar, no sucrose, and no vitamin supplemented with 1 nM of isoxaben diluted in DMSO, or the same volume of DMSO
Medium D	Arabidopsis medium with 0,7% or 2,5% agar and no vitamin
Medium E	Arabidopsis medium with 0,7% or 2,5% agar, no vitamin, and supplemented with 5 µM of oryzalin diluted in DMSO, or the same volume of DMSO
Growth conditions	
Condition 1	8 hours light, 3 days darkness, 3 days light
Condition 2	8 hours light, 4 days darkness
Condition 3	4 days light, 8 days light or 12 days light
Condition 4	5 days light
Imaging In all confocal microscopy image acquisition, optical sections were 0.5 µm thick.	
Imaging a	Samples were transferred to new medium plates, stained with a PI solution (dilution 1/10), and rinsed twice. Cotyledons were manually set in flat position with forceps under a binocular stereoscopic microscope and imaged with a long distance 25x objective (Leica SP8).
Imaging b	The petri dish lid was removed and the petri dish was scanned with an office scanner.
Imaging c	Samples were stained with PI (1/100 dilution), rinsed once, mounted in water between slides and coverslips, and imaged with a long distance 25x objective (Leica SP8).
Imaging d	Samples were transferred to new medium plates. Cotyledons were manually set in flat position with forceps under a binocular stereoscopic microscope, and imaged with a 25x long distance objective (Leica SP8).
Imaging e	Samples were stained with PI (1/100 dilution), rinsed once, mounted in medium and water between slides and coverslips, and imaged with a long distance 25x objective (Leica SP8).
Imaging f	Dissected cotyledons were mounted in water between slides and coverslips and imaged with a binocular stereomicroscope (Leica MZ12).

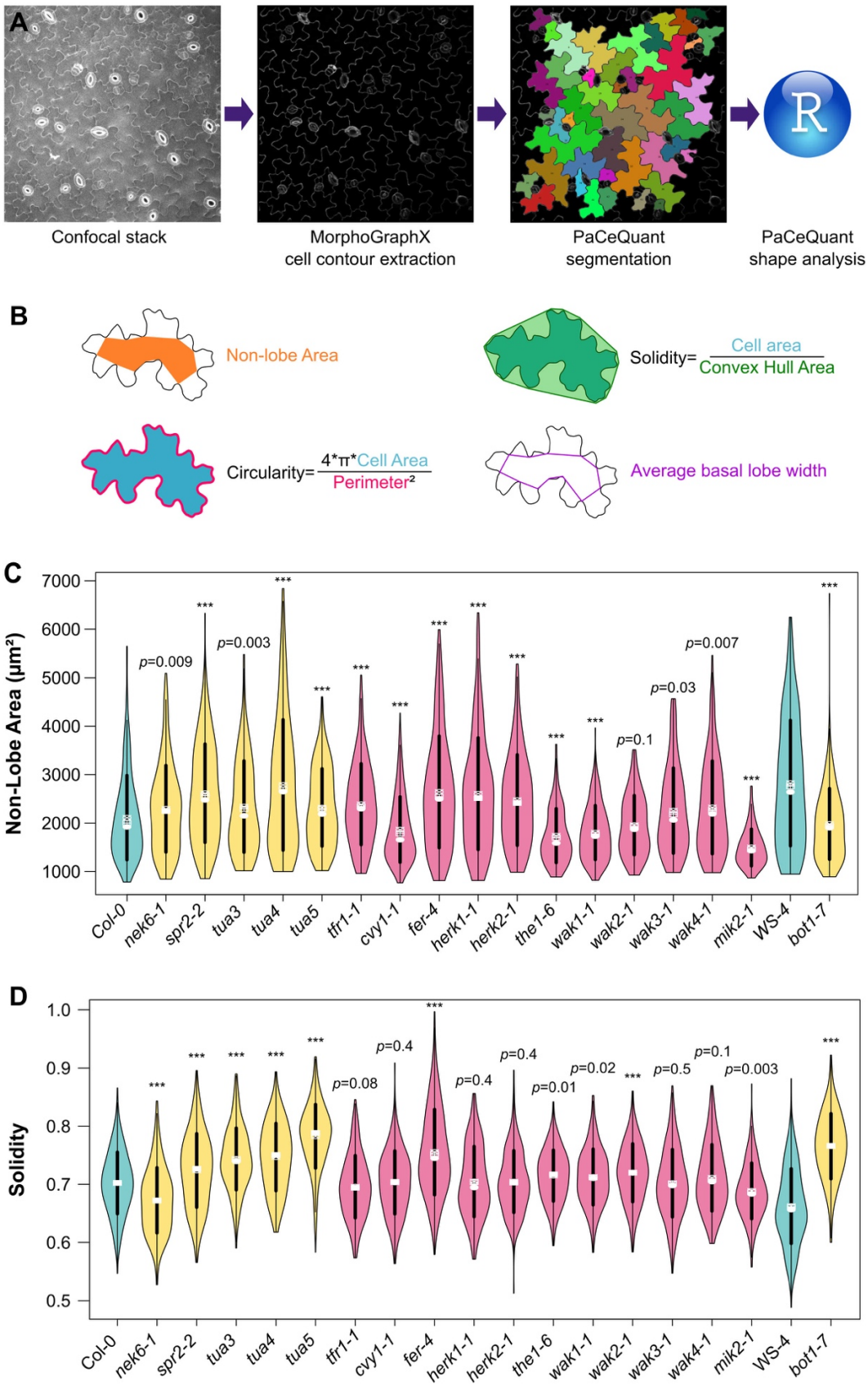

Supplementary Figure 1. Analysis of pavement cell shapes

Supplementary Figure 1. Analysis of pavement cell shapes

A. Pipeline for the extraction and analysis of pavement cell shape. Epidermal signal was first extracted with MorphoGrahX, then segmented with the PaCeQuant ImageJ plugin, which extracted 27 pavement cell shape descriptors (parameters). Finally, the results were processed by PaCeQuantAna (the PaCeQuant R script).

B. Main shape descriptors of pavement cells. Non-lobe area (in µm²) stands for the area of a cell without the lobes. Circularity is the area of a cell divided by its square perimeter, with a normalization to have a maximal circularity of 1 for a circle. Solidity is the area of a cell divided by the area of its convex hull (convex polygon with the smallest area including the whole cell). Average basal lobe width (µm) stands for the average length of the bases of a cell's lobes.

C. Non-lobe area (violin plots) of pavement cells and *p*-values (*p*) of Dunn tests in the WT (in blue, *Col-0, WS-4*), in microtubule associated mutants (in orange, *nek6-1, spr2-2, tua3, tua4, tua5, bot1-7*) and in receptor-like kinase mutants (in pink, *tfr1-1, cvy1-1, fer-4, herk1-1, herk2-1, the1-4, the1-6, wak1-1, wak2-1, wak3-1, wak4-1, mik2-1*).

D. Solidity (violin plots) of pavement cells and *p*-values (*p*) of Dunn tests in the WT (in blue, *Col-0, WS-4*), in microtubule associated mutants (in orange, *nek6-1, spr2-2, tua3, tua4, tua5, bot1-7*) and in receptor-like kinase mutants (in pink, *tfr1-1, cvy1-1, fer-4, herk1-1, herk2-1, the1-4, the1-6, wak1-1, wak2-1, wak3-1, wak4-1, mik2-1*).

All underlying data can be found in supporting information folder.

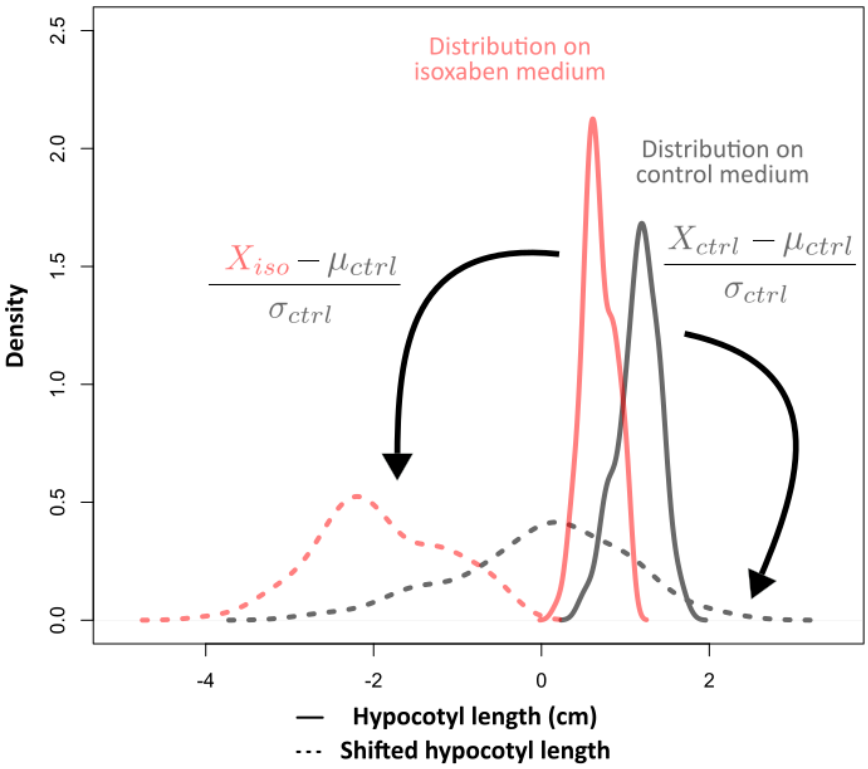

Supplementary Figure 2. Definition of the hypocotyl length index

The continuous black and red lines represent the distribution of the actual measurement of hypocotyl lengths for the treated (red) and control (black) samples. In this example, the values are between 0 and 2 cm and the average values for the treated sample are lower. However, when comparing different genotypes, the average length of the untreated (control) mutant samples could already be lower or higher than the control WT samples thus hampering a direct comparison of the effect of the treatment on the mutant. In order to allow statistical comparison between the samples we normalized the distribution of hypocotyl lengths in the presence of isoxaben according to the distribution of hypocotyl lengths in control conditions, following the standard score method. To do so, the parameters of the control distribution (DMSO, mean: μ_{ctrl}, standard deviation: σ_{ctrl}) are shifted around 0 (dashed black line) and are used to shift the isoxaben distribution to the same extent (dashed red line). With this method, the control samples for all genotypes have a value around 0, which then allows to reveal the effect of the treatment on the different mutants by comparing the means of the normalized treated samples (The hypocotyl length index; Figure 2B). To further ease the comparison, the differences between WT and mutants are then plotted as the Hypocotyl length index deviation from the WT, which are the values obtained when subtracting the mutant treated normalized mean to the WT treated normalized mean. This generates a negative value in the hypocotyl length index for mutants being more sensitive to the treatment and a positive value for mutants less sensitive to the treatment (Figure 2C).

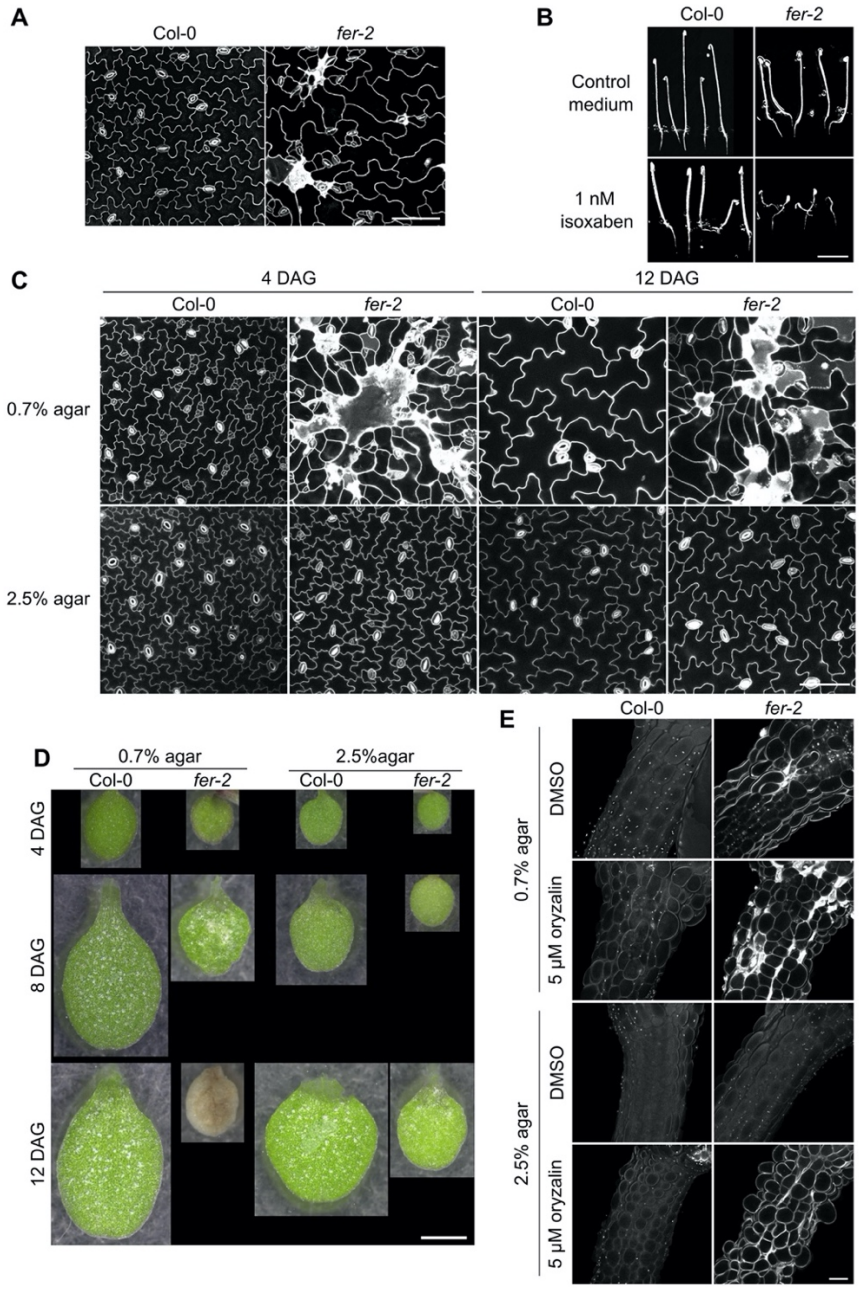

Supplementary Figure 3. *fer-2* phenotypes

A. Representative images of Col-0 and *fer-2* pavement cells. Samples were PI stained and cell contours were extracted with MorphoGraphX and projected in 2D. Scale=100µm. B. Representative images of Col-0 and *fer-2* etiolated seedlings grown with or without 1 nM isoxaben. Scale=1 cm. C. Representative confocal images of *Col-0* and *fer-2* pavement cells, from seedlings grown on a medium containing 0.7% or 2.5% agar at t=4 DAG and t=12 DAG (propidium iodide staining). Scale=100µm. D. Representative images of *Col-0* and *fer-2* cotyledons, grown on a medium containing 0.7% or 2.5% agar at t=4 DAG, t=8 DAG and t=12 DAG. Scale =1mm. E. Representative confocal images of Col-0 and *fer-2* hypocotyls grown on 0.7% and 2.5% agar with and without 5 µm of oryzalin. All underlying data can be found in supporting information folder. Scale bar=50µm.

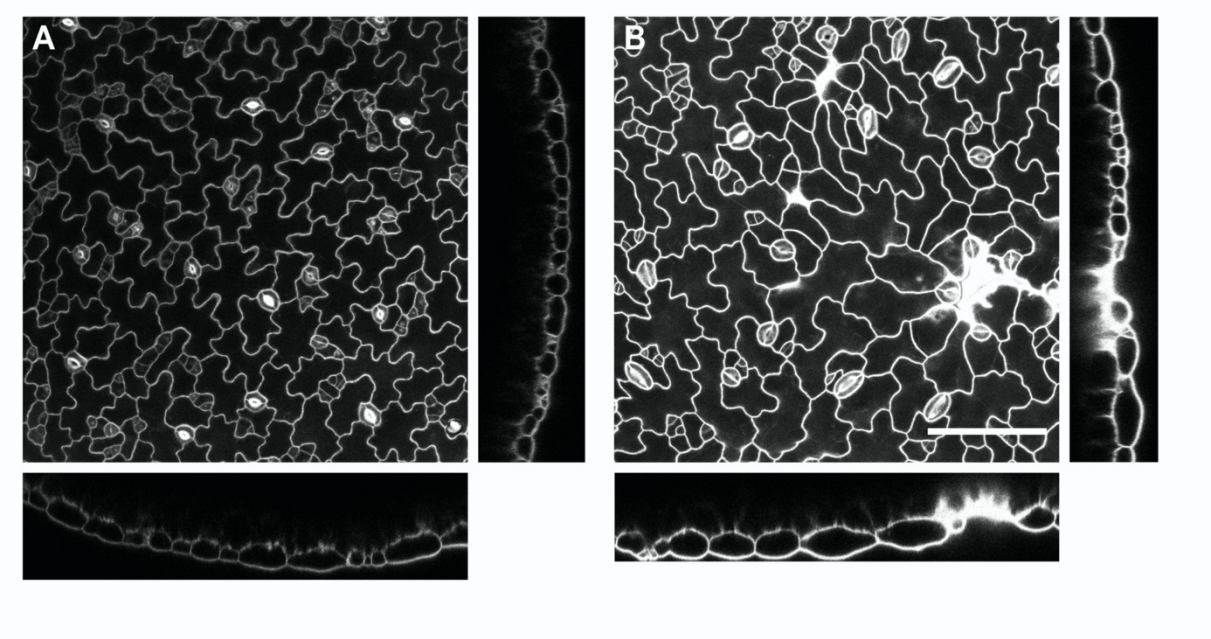

Supplementary Figure 4. Swelling pavement cells in *fer-4* on 0.7% agar

A-B**.** Representative images of *Col-0* (A) and *fer-4* (B) pavement cells, from seedlings grown on a medium containing 0.7% agar at t=4 DAG. Samples were PI stained and cell contours were extracted with SurfCut and projected in 2D. Orthogonal projections were also extracted with Fiji. Note the presence of curvy outer walls in some *fer-4* cells. All underlying data can be found in supporting information folder. Scale=100µm.

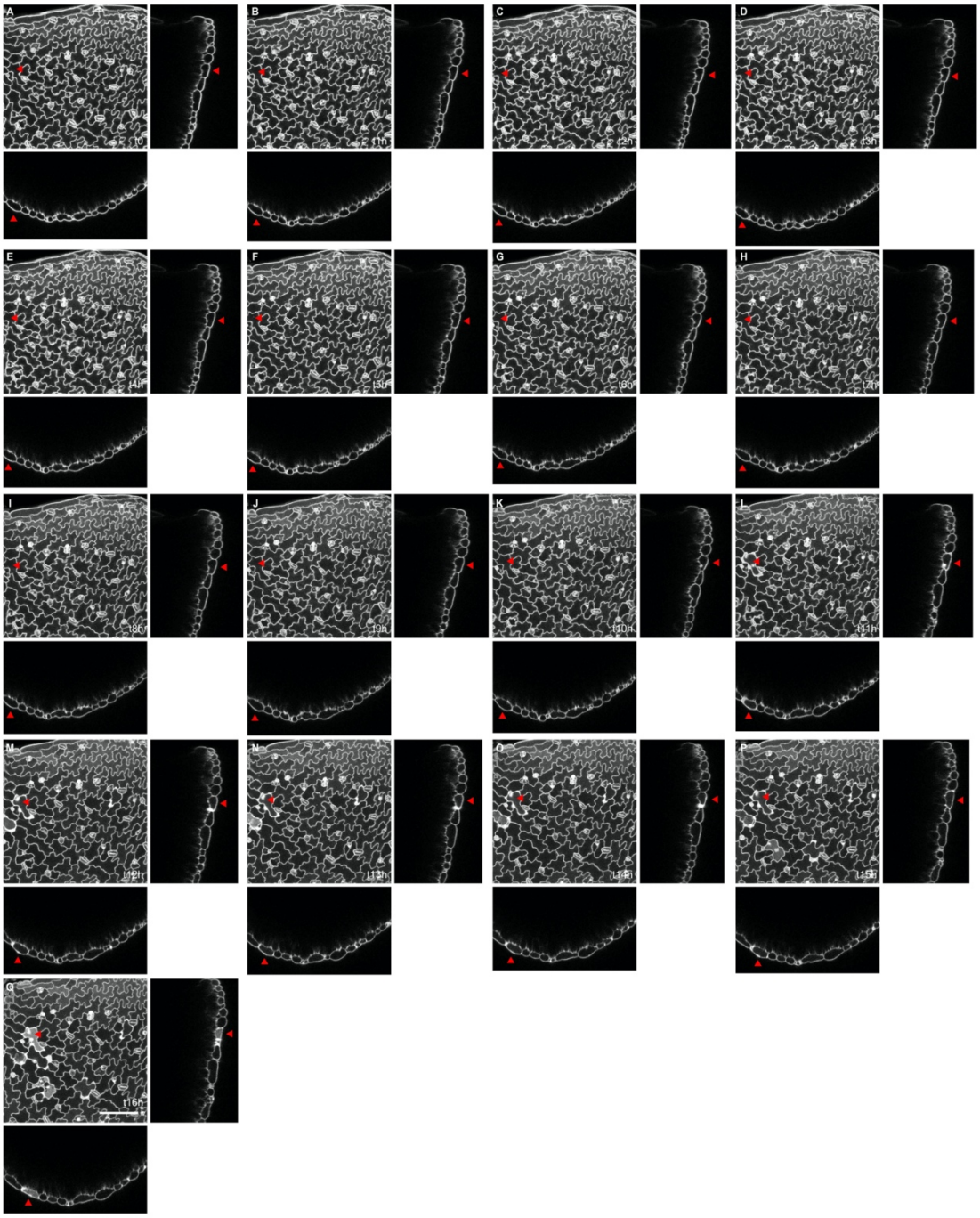

Supplementary Figure 5. Bursting cells in *fer-4* upon switch from 2.5% to 0.35% agar conditions

A-B**.** Representative confocal images of *fer-4* pavement cells, from seedlings grown on a medium containing 2.5% agar for four days, transferred on a medium containing 0.35% agar, stained with PI and imaged in water immediately after the transfer to a new medium (t0) and 1 to 16 hours later. Cell contours were extracted with SurfCut and projected in 2D. Orthogonal projections were also extracted with Fiji, focusing on the cell indicated with red arrows. See also Movie 1. Scale=100µm.

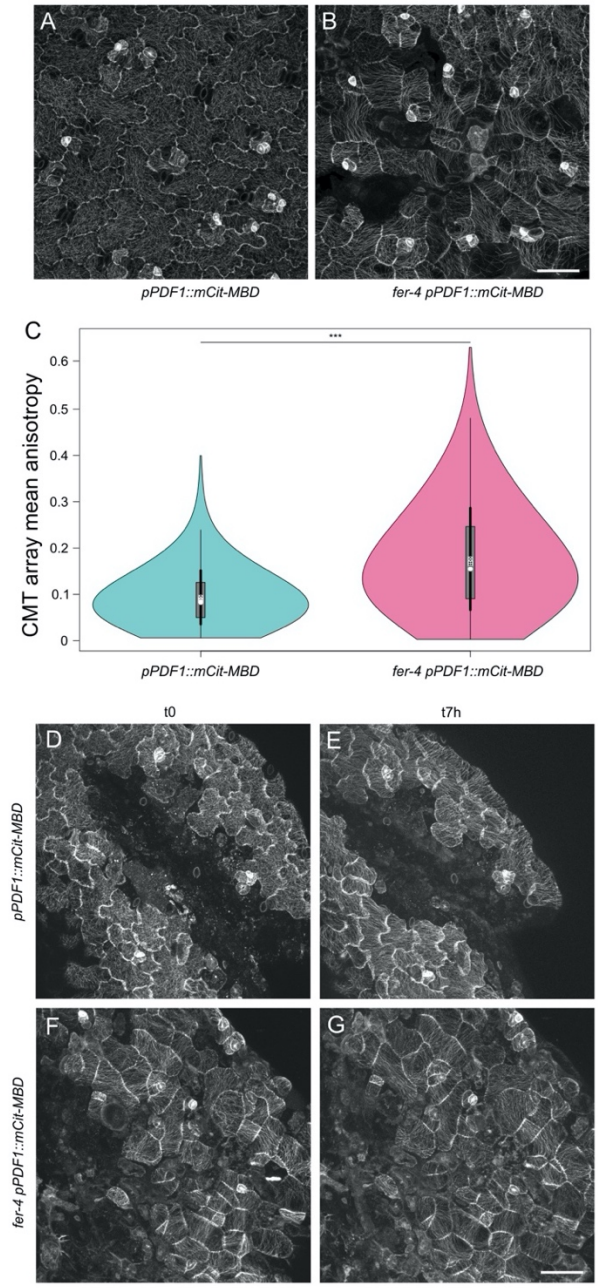

Supplementary Figure 6. Cortical microtubule behavior in *fer-4* grown on 0.7% agar medium

Representative confocal images of *pPDF1::mCit-MBD* (A) and *fer-4 pPDF1::mCit-MBD* (B) pavement cells from seedlings grown on a medium containing 0.7% agar. Quantification of the anisotropy of cortical microtubule arrays in both lines (C). Note the presence of circumferential CMTs around dead cells, matching the predicted maximal tensile stress direction. Representative confocal images of *pPDF1::mCit-MBD* (D, E) and *fer-4 pPDF1::mCit-MBD* (F, G) pavement cells from seedlings grown on a medium containing 0.7% agar, immediately after ablation (t0, D, F) and seven hours later (t7h, E, G). Note the presence of many dead cells and the strong alignment of cortical microtubules at t0 in *fer-4*. All underlying data can be found in supporting information folder. Scale=50µm.

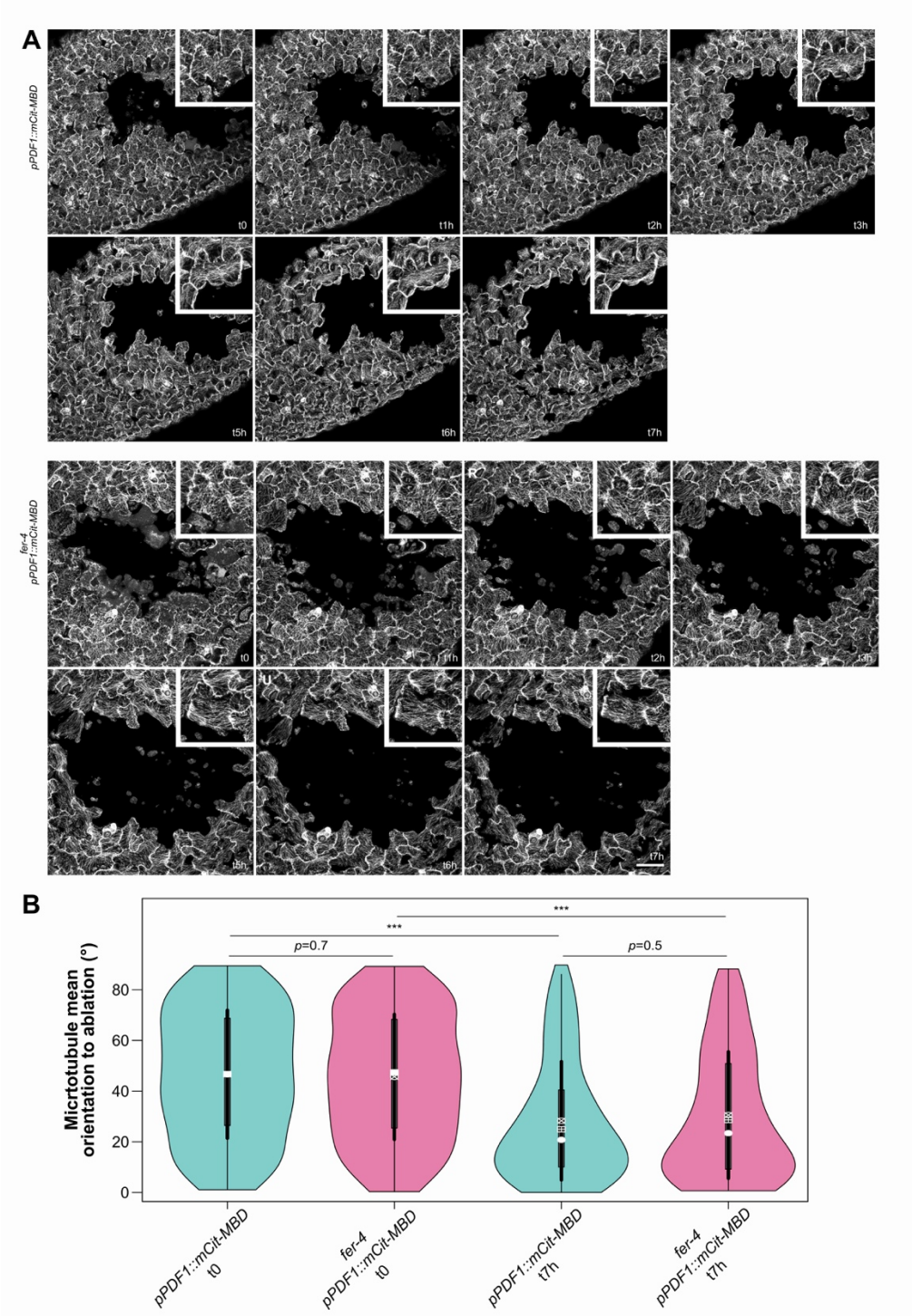

Supplementary Figure 7. Ablations (full kinetics) on 2.5% agar medium (example 1)

A. Representative confocal images of *pPDF1::mCit-MBD* (top) and *fer-4 pPDF1::mCit-MBD* (bottom) pavement cells, from seedlings grown on a medium containing 2.5% agar, immediately after an ablation (t0) and 1 to 7 hours later. Scale=50µm. **B.** Orientation to the ablation (violin plot) of cortical microtubule arrays and *p*-values (*p*) of Wilcoxon-Mann-Whitney tests in cells surrounding the ablation site in *pPDF1::mCit-MBD* and *fer-4 pPDF1::mCit-MBD* pavement cells, immediately after an ablation (t0) and 7 hours later (t7h) (see Figure 4). All underlying data can be found in supporting information folder.

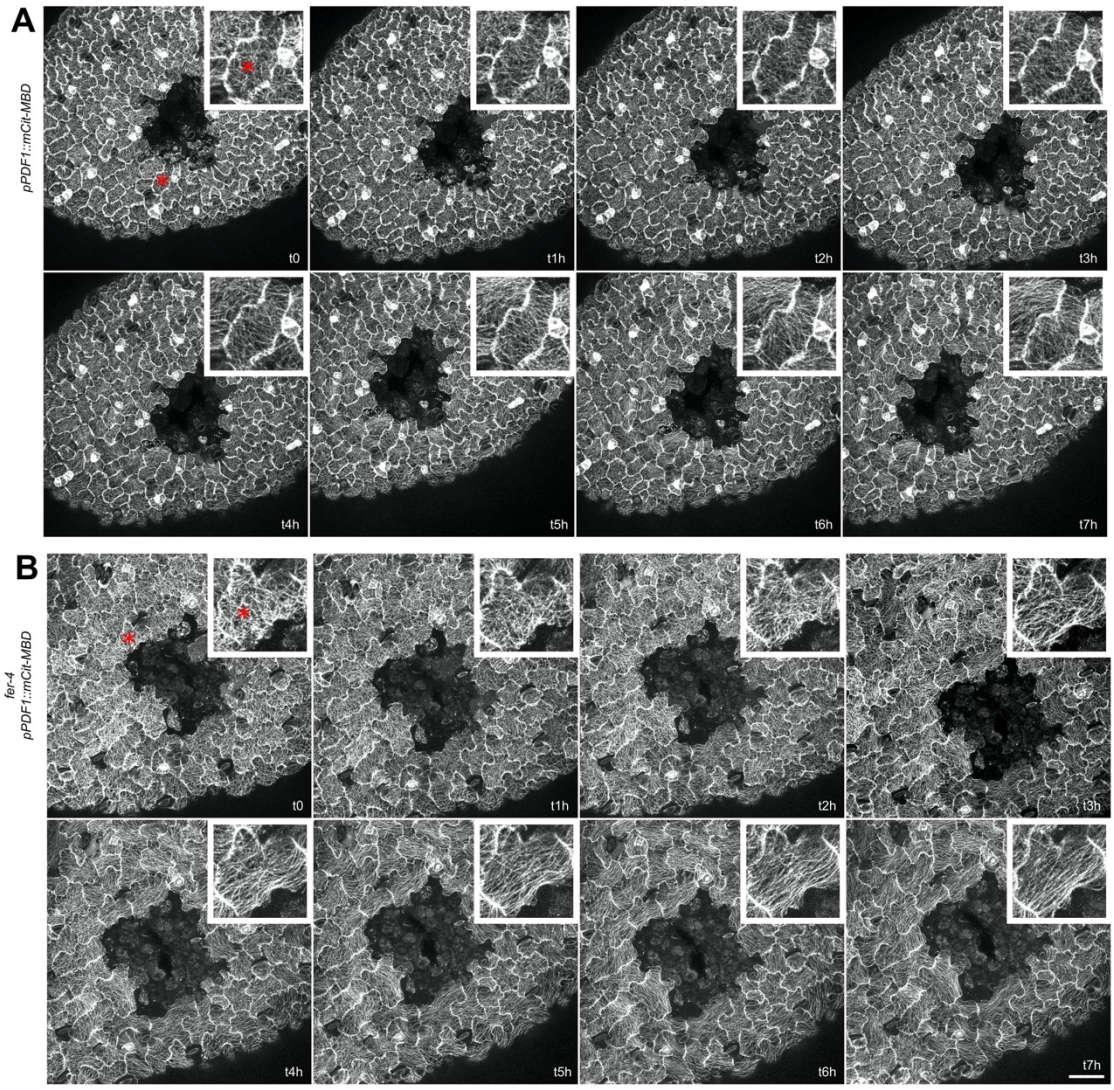

Supplementary Figure 8. Ablations (full kinetics) on 2.5% agar medium (example 2)

A. Representative confocal images of *pPDF1::mCit-MBD* (A) and *fer-4 pPDF1::mCit-MBD* (B) pavement cells, from seedlings grown on a medium containing 2.5% agar, immediately after an ablation (t0) and 1 to 7 hours later. Scale=50µm.

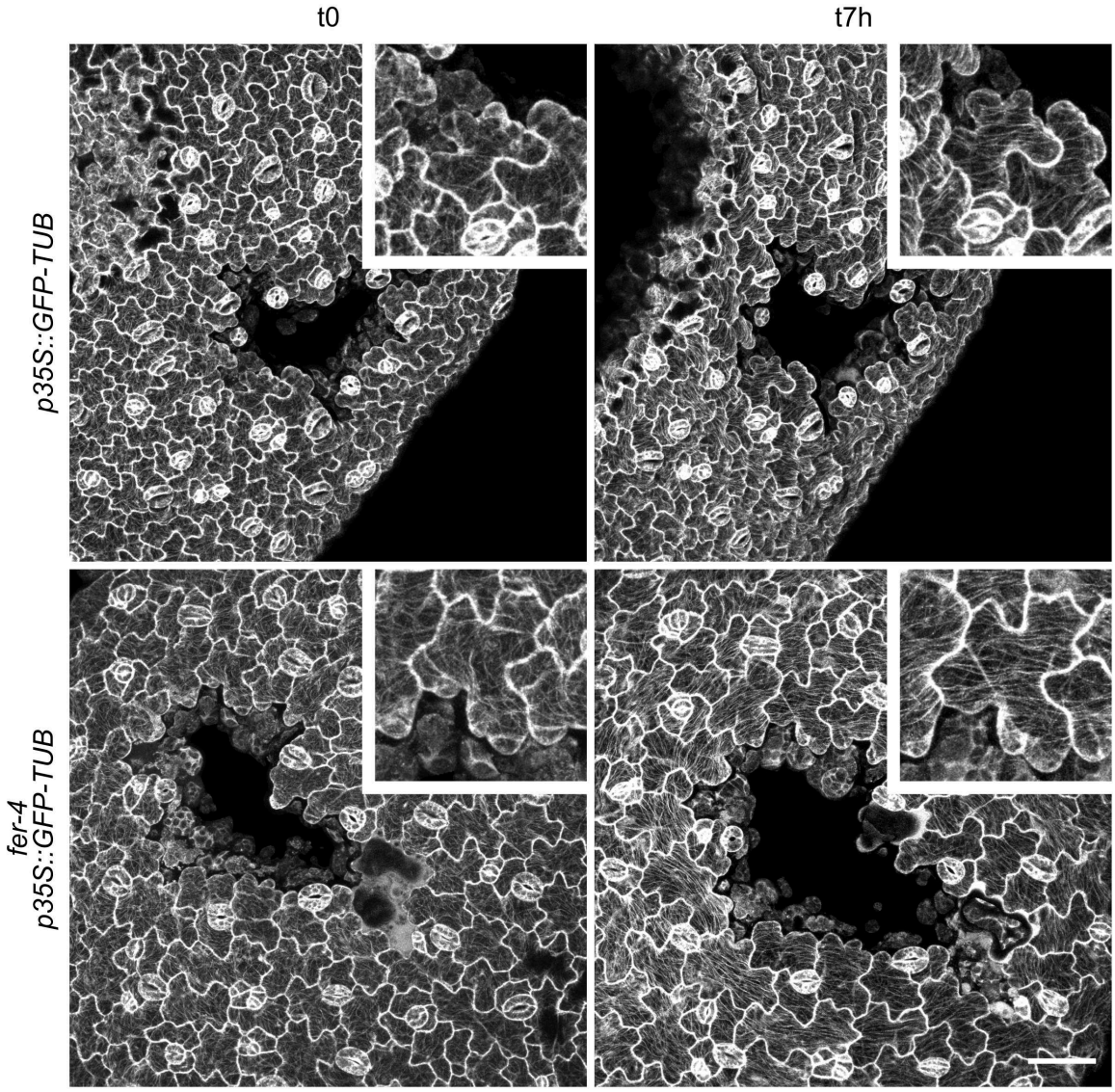

Supplementary Figure 9. Microtubule response after ablation using the GFP-tubulin reporter

Representative confocal images of *p35S::GFP-TUB* (top) and *fer-4 p35S::GFP-TUB* (bottom) pavement cells from seedlings grown on a medium containing 2.5% agar, immediately after an ablation (t0) and seven hours later (t7h). Scale=50µm.

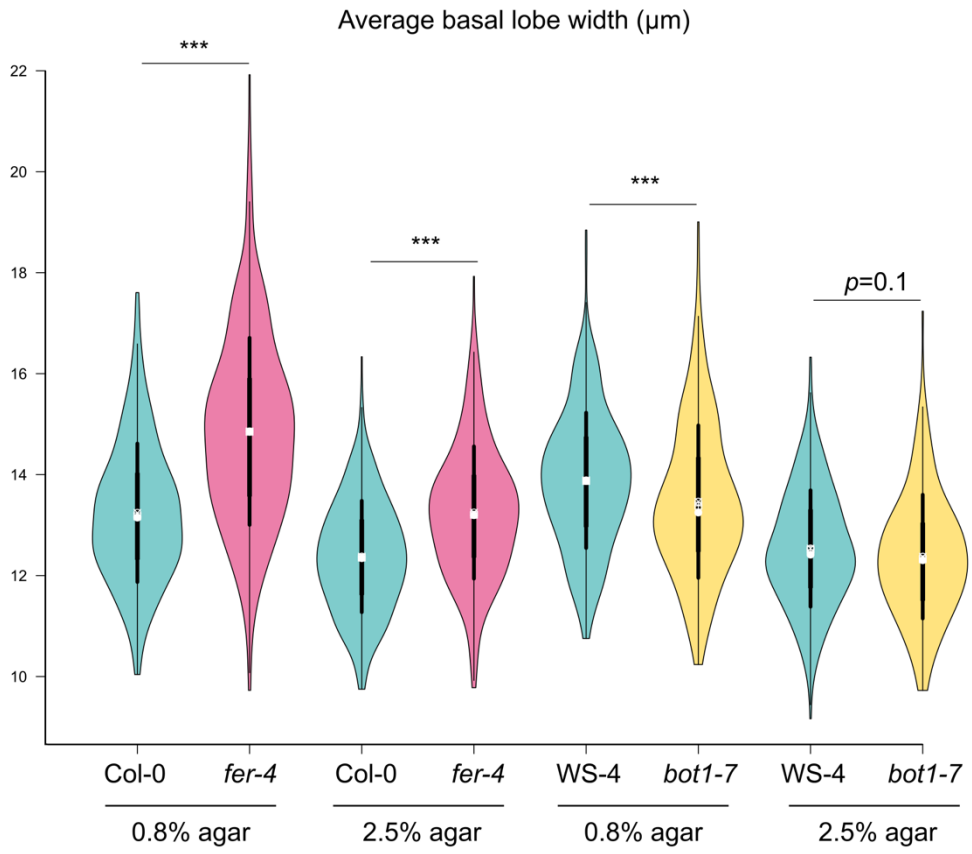

Supplementary Figure 10. Basal lobe width according to genotype and growth conditions.

Basal lobe width (violin plot) of pavement cells and *p*-values (*p*) of Dunn tests for the WT (*Col-0, WS-4*), katanin mutant (*bot1-7*), and *fer-4*. Seedlings were grown on 0.8% or 2.5% agar. Data from Figure 5A (0.8% agar) are reproduced here to allow a full comparison of the results. All underlying data can be found in supporting information folder.

Movie 1. Bursting cells in *fer-4* upon switch from 2.5% to 0.35% agar conditions

Animation of representative confocal images of *fer-4* pavement cells, from seedlings grown on a medium containing 2.5% agar for four days, transferred on a medium containing 0.35% agar, stained with PI and imaged in water immediately after the transfer to a new medium (t0) and 1 to 16 hours later. Cell contours were extracted with SurfCut and projected in 2D (same images as in Supplementary Figure 5) then aligned with the stackreg (Pyramid Registration) plugin in Fiji.

II◦ Why do *fer-4* cells burst?

II.1◦ Preamble

In this part, I investigated further the bursting cell phenotype in *fer* mutants (Malivert et al., 2021). I explored the cause of the phenotype, going deeper in the mechanics and hydraulics of cell growth. This raised more questions along the way, such as how many ways can cells resist mechanical stress? What is the role of mechanical sensing at the plant scale? How to measure the mechanical properties at the whole cell scale? To answer these questions, I involved several collaborators. Dorota Borowska-Wykręt (University of Silesia, Katowice) measured cell wall thicknesses using transmission electron microscopy (see Results ◦ II.4.2). Bertrand Muller, Myriam Dauzat and Alexis Bédiée (INRAE Montpellier) measured several hydric traits in plant grown *in terra* at various humidity levels (see Results ◦ II.4.4). I interacted with them to design experiments and interpret their results.

The establishment of a protocol for the successive plasmolyses experiments (see Results ◦ II.4.3), and of a model used to analyse the results, was done with help from Corentin Mollier and Mylan Ansel (an intern I co-supervised with Corentin Mollier, in a larger project aiming to investigate the compensation of stress caused by the loss of pavement cell shape, see Annexe 1). I then fully performed the data collection and the image analysis.

For the pavement cell growth experiment, I reused data I had collected and published in (Malivert et al., 2021). I did the experimental work and prepared projections of the images, and due to technical issues, Özer Erguvan ran the PaCeQuant ImageJ plugin.

In this whole part (Results ◦ II), I performed all the statistical analyses and the data presentation. I also asked some collaborators for some help in the data interpretation and the conceptual thinking: Yuchen Long and Ibrahim Cheddadi, who were a great help to better understand the physics of cell growth. Insightful ideas were offered by Richard Smith and Herman Höfte when I presented this work to them.

I also cosupervised another intern on this project: Amaya Richer (cosupervision with Leia Colin), who checked the robustness of the *fer-4* phenotype in different growth conditions (see Annexe 3).

II.2◦ Abstract

In contrast to animal cells, which burst when placed in a hypo-osmotic medium, plant cells do not generally burst even when placed in a hypo-osmotic environment, including pure water. The stiff cell wall surrounding every plant cell is responsible for this resistance, and as such is subject to high tensile stress levels. One notable exception to the mechanical integrity normally displayed by plant cells can be found in the loss-of-function mutant in the receptor-like kinase FERONIA: in hypo-osmotic conditions, epidermal cells in cotyledon and hypocotyl swell and burst. This mutant can be used to better understand how cells sense and resist mechanical stress. Here, through the measurement of cell mechanical properties, we establish that the cell wall is thinner, less deformable and the water content higher in *fer-4*. Based on available results, we propose that the cell bursting phenotype in *fer-4* is caused by a dual impairment in turgor control and wall properties. We also propose additional experiments to refine this model.

II.3◦ Introduction

Maintaining the mechanical integrity of plant cells involves molecular sensors able to detect mechanical stress and to trigger a signaling and response pathway. Several wall-integrity receptors have been identified either in specific cells (e.g. pollen tube, (Boisson-Dernier et al., 2009)) or in specific genetic contexts (e.g. when cellulose synthesis is impaired in hypocotyls, (Hématy et al., 2007)). Pressure valves, e.g. MSL channels, have also been identified, again in specific contexts (e.g. in pollen (Hamilton et al., 2015b), or chloroplasts (Veley et al., 2012)). Yet, no generic mechanosensor that would be responsible for cell mechanical integrity has been identified yet. We propose the receptor-like kinase FERONIA (FER) acts as such a sensor: in at least two *fer* loss of function mutant alleles, epidermal cells swell and eventually burst when cell wall tension is too high (Malivert et al., 2021). Consistently, decreasing the outer cell wall tension by increasing the agar concentration in the growth medium (Verger et al., 2018) largely rescues this burst cell phenotype (Malivert et al., 2021).

Although the mechanical integrity of plant cell has not been studied in depth from the biophysical point of view, one can find inspiration from the Lockhart model, which relates to

plant cell growth (Lockhart, 1965): it formalizes cell deformation by involving cell wall mechanical properties (*Y* and ϕ) as well as water uptake (*L* and Ψ) (see Introduction ◦ I.3.3, Figure 26A):

$$r = \frac{\phi * L}{\phi + L}(\Delta\Pi - Y) \qquad \text{(equation 6)}$$

with *r* the cell growth rate, *Y* the yield pressure, ϕ the cell wall extensibility, L the hydraulic conductance and $\Delta\Pi$ the difference in osmotic pressure between the cell and the medium. The origin of cell burst phenotype in *fer* may thus be due to defects in cell wall mechanical properties and/or in the regulation of water intake. To better understand why *fer-4* cells burst and get more insight into how mechanical integrity is sustained in plants, we analysed wall properties and hydraulic properties in *fer-4* and WT plants. We looked for indications of how the Lockhart equation parameters differ in the two genotypes by studying growth rate, cell wall geometrical and mechanical properties as well as water-related traits. In this process we also observed the burst cell phenotype *in terra* and thus confirmed its robustness.

II.4◦ Results

II.4.1◦ fer-4 epidermal cells in cotyledons exhibit a lower growth rate

fer-4 cotyledons are smaller than that of the WT (Malivert et al., 2021), and in the simplest scenario, this could be due to reduced cell size and growth. Yet, *fer* cells swell and burst, suggesting that *fer* cells may on the contrary be too large. To discriminate between these two scenarios, we analysed the differences of growth between *fer-4* and WT cotyledons. To do so, we imaged 4 DAG (days after germination) and 12 DAG cotyledons grown on mediums with a low water potential (0.7% agar) and stained with propidium iodide (PI) (Figure 26B).

We quantified the pavement cell area using PaCeQuant (Möller et al., 2017) (Figure 26C). At 4 DAG, there was no significant difference between pavement cell areas in *fer-4* and WT cotyledons grown on 0.7% agar (p = 0.4; $n_{Col\text{-}0,0.7\%agar,4DAG}$ = 119; $n_{fer\text{-}4,0.7\%agar,4DAG}$ = 212). However, at 12 DAG, the area of WT pavement cells was 128% larger than the one of *fer-4*

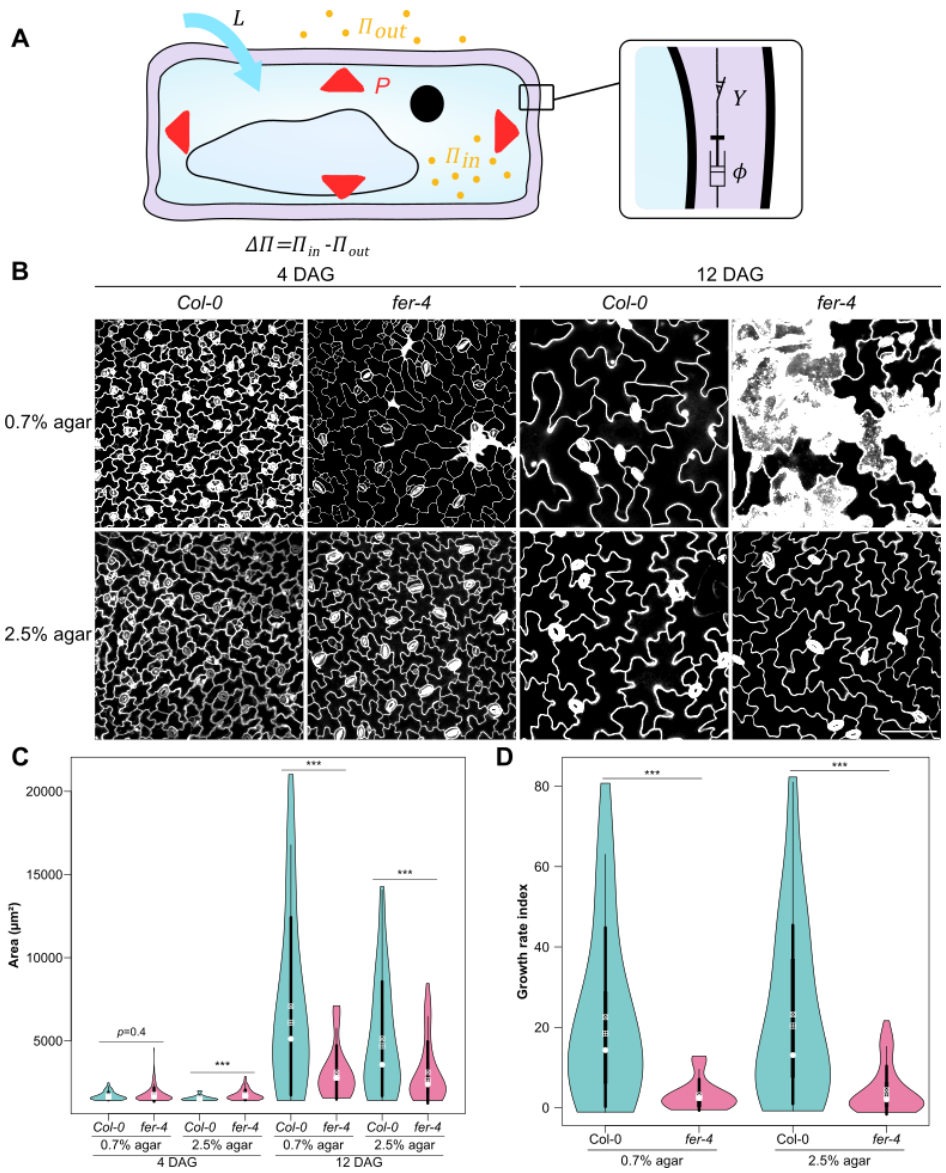

Figure 26: *fer-4* cotyledons display a lower growth rate than the WT. **(A)** For ease of reading, I reproduced Figure 13A here. Mechanical parameters used in the Lockhart model of growth rate. ϕ is for the cell wall extensibility (represented as a hydraulic piston), *L* the hydraulic conductance, *ΔΠ* the difference between the inside osmotic pressure and the outside one, and *Y* the yield pressure (represented as a threshold switch). **(B)** Representative confocal images of *Col-0* and *fer-4* pavement cells, from seedlings grown on a medium containing 0.7% or 2.5% agar at t = 4 DAG and t = 12 DAG (propidium iodide staining). Scale = 100 µm. **(C)** Cell area (violin plot) and *p*-values of Wilcoxon–Mann–Whitney tests in *Col-0* and *fer-4* pavement cells, from seedlings grown on a medium containing 0.7% or 2.5% agar at t = 4 DAG and t = 12 DAG. **(D)** Growth rate index (violin plot) and *p*-values of Wilcoxon–Mann–Whitney tests in *Col-0* and *fer-4* pavement cell, from seedlings grown on a medium containing 0.7% or 2.5% agar at t = 4 DAG and t = 12 DAG.

ones for cotyledons grown on 0.7% agar ($p < 10^{-3}$; $n_{Col\text{-}0,0.7\%agar,12DAG} = 27$; $n_{fer\text{-}4,0.7\%agar,12DAG} = 32$).

However, the presence of burst cells on 0.7% agar may induce other indirect effects on growth. To challenge this conclusion, we performed the same analysis using seedlings grown on high water potential (2.5% agar). At 12 DAG the higher concentration of agar (2.5%), the number of burst cells was dramatically reduced (as previously shown) but the cell size defects were only partially rescued in *fer-4*, with the WT displaying cells 65% larger than *fer-4* ($p < 10^{-3}$; $n_{Col\text{-}0,2.5\%agar,12DAG} = 49$; $n_{fer\text{-}4,2.5\%agar,12DAG} = 85$). *fer-4* pavement cells thus seem to grow more slowly than the WT.

As we imaged different cotyledons at 4 DAG and 12 DAG, we could not calculate a relevant growth rate. Instead, we normalized the distribution of areas at 12 DAG for each condition (*Col-0* 0.7% agar, *fer-4* 0.7% agar, *Col-0* 2.5% agar and *fer-4* 2.5% agar) using the mean and standard deviation of each condition at 4 DAG, and called the result growth rate index (see Results ◦ II.6.5, Supplementary figure 1). Using this approach, we could confirm that the growth rate index in cotyledons is significantly lower in *fer-4* than in the WT both on 0.7% agar and on 2.5% agar (by 86% for 0.7% agar and 81% for 2.5% agar, $p_{0.7\%agar} < 10^{-3}$; $p_{2.5\%agar} < 10^{-3}$; $n_{Col\text{-}0,0.7\%agar,4DAG} = 119$; $n_{fer\text{-}4,0.7\%agar,4DAG} = 212$; $n_{Col\text{-}0,0.7\%agar,12DAG} = 27$; $n_{fer\text{-}4,0.7\%agar,12DAG} = 32$; $n_{Col\text{-}0,2.5\%agar,4DAG} = 25$; $n_{fer\text{-}4,2.5\%agar,4DAG} = 177$; $n_{Col\text{-}0,2.5\%agar,12DAG} = 49$; $n_{fer\text{-}4,2.5\%agar,12DAG} = 85$; Figure 26D). Surprisingly, there was no significant difference in growth rate indexes between the 0.7% and 2.5% agar growth conditions, for either of the genotype ($p_{Col\text{-}0} = 0.9$; $p_{fer\text{-}4} = 0.9$; $n_{Col\text{-}0,0.7\%agar,4DAG} = 119$; $n_{fer\text{-}4,0.7\%agar,4DAG} = 212$; $n_{Col\text{-}0,0.7\%agar,12DAG} = 27$; $n_{fer\text{-}4,0.7\%agar,12DAG} = 32$; $n_{Col\text{-}0,2.5\%agar,4DAG} = 25$; $n_{fer\text{-}4,2.5\%agar,4DAG} = 177$; $n_{Col\text{-}0,2.5\%agar,12DAG} = 49$; $n_{fer\text{-}4,2.5\%agar,12DAG} = 85$). Altogether, these results demonstrate a lower growth rate for *fer-4* than for the WT.

II.4.2◦ fer-4 outer cell walls are significantly thinner than in the WT

The growth defects in *fer-4* pavement cells must reflect impaired mechanical properties. More specifically, in the Lockhart model, growth rate depends on ϕ the cell wall extensibility, L the hydraulic conductance, $\Delta\Pi$ the difference between the inside osmotic pressure and the outside one, and Y the yield pressure (Figure 26A, see equation 6). From equation 6, we can postulate that the lower growth rate r could be due to a lower hydraulic conductance L, a lower cell wall extensibility ϕ, a lower difference of osmotic pressures $\Delta\Pi$ and/or a higher yield

pressure *Y* for *fer-4* than for the WT. As cell wall tension seems an essential component in the burst cell phenotype, we started by investigating cell wall properties.

From the cell wall perspective, a lower growth rate would be associated with lower cell wall extensibility. Biochemically, this could be achieved through stiffer walls (e.g. more wall materials and/or more crosslinks) or through strain-stiffening (i.e. getting closer to the maximum of deformation). Little is known about the composition of the cell wall in *fer-4*, and even less for mechanical properties. There is evidence of a decrease in cellulose content (Yeats et al., 2016), and a decrease in pectin demethylesterification (Duan et al., 2020) and crosslinking (Feng et al., 2018; Gigli-Bisceglia et al., 2021) in *fer*. However, other mutants with more dramatic reduction cellulose content or defective pectin properties do not exhibit burst cells (e.g. *csi1* and *procuste1* (Gu et al., 2010), *quasimodo1* (Bouton et al., 2002)) Thus, these defects do not seem sufficient to explain the presence of burst cells in *fer*. We thus studied the geometrical properties of the cell wall by imaging the outer epidermal cell wall of 8 DAG cotyledons with transmission electronic microscopy (Figure 27A).

We manually measured the thickness of the outer epidermal wall on the adaxial side and on the abaxial side, in *fer-4* and WT cotyledons grown on 0.8% or 2.5% agar mediums. On the adaxial side as on the abaxial side, the outer epidermal cell wall appeared to be thinner in *fer-4* than in the WT for cotyledons grown on 0.8% agar (48% thinner for the adaxial side; 50% thinner for the abaxial side; $p_{0.8\%agar,adaxial} < 10^{-3}$; $p_{0.8\%agar,abaxial} < 10^{-3}$; $n_{Col-0,0.8\%agar,adaxial} = 1053$; $n_{fer-4,0.8\%agar,adaxial} = 998$; $n_{Col-0,0.8\%agar,abaxial} = 865$; $n_{fer-4,0.8\%agar,abaxial} = 709$; Figure 27B,C). Decreasing the matrix potential by increasing the agar concentration did not change the WT outer epidermal wall thickness on the abaxial side but increased it slightly, by 4%, on the adaxial side ($p_{Col-0,abaxial} = 0.1$; $p_{Col-0,adaxial} < 10^{-3}$; $n_{Col-0,0.8\%,adaxial} = 1053$; $n_{Col-0,2.5\%,adaxial} = 692$; $n_{Col-0,0.8\%,abaxial} = 865$; $n_{Col-0,2.5\%,abaxial} = 337$). However, it increased the thickness of *fer-4* cell walls (25% thicker for both sides; $p_{fer-4,abaxial} < 10^{-3}$; $p_{fer-4,adaxial} < 10^{-3}$; $n_{fer-4,0.8\%agar,adaxial} = 998$; $n_{fer-4,2.5\%agar,adaxial} = 378$; $n_{fer-4,0.8\%agar,abaxial} = 709$; $n_{fer-4,2.5\%agar,abaxial} = 409$). Consistently, this partially rescued the thinner cell wall phenotype in *fer-4* (38% thinner than the WT for the adaxial side; 35% thinner than the WT for the abaxial side; $p_{2.5\%agar,adaxial} < 10^{-3}$; $p_{2.5\%agar,abaxial} < 10^{-3}$; $n_{Col-0,2.5\%agar,adaxial} = 692$; $n_{fer-4,2.5\%agar,adaxial} = 378$; $n_{Col-0,2.5\%agar,abaxial} = 337$; $n_{fer-4,2.5\%agar,abaxial} = 409$).

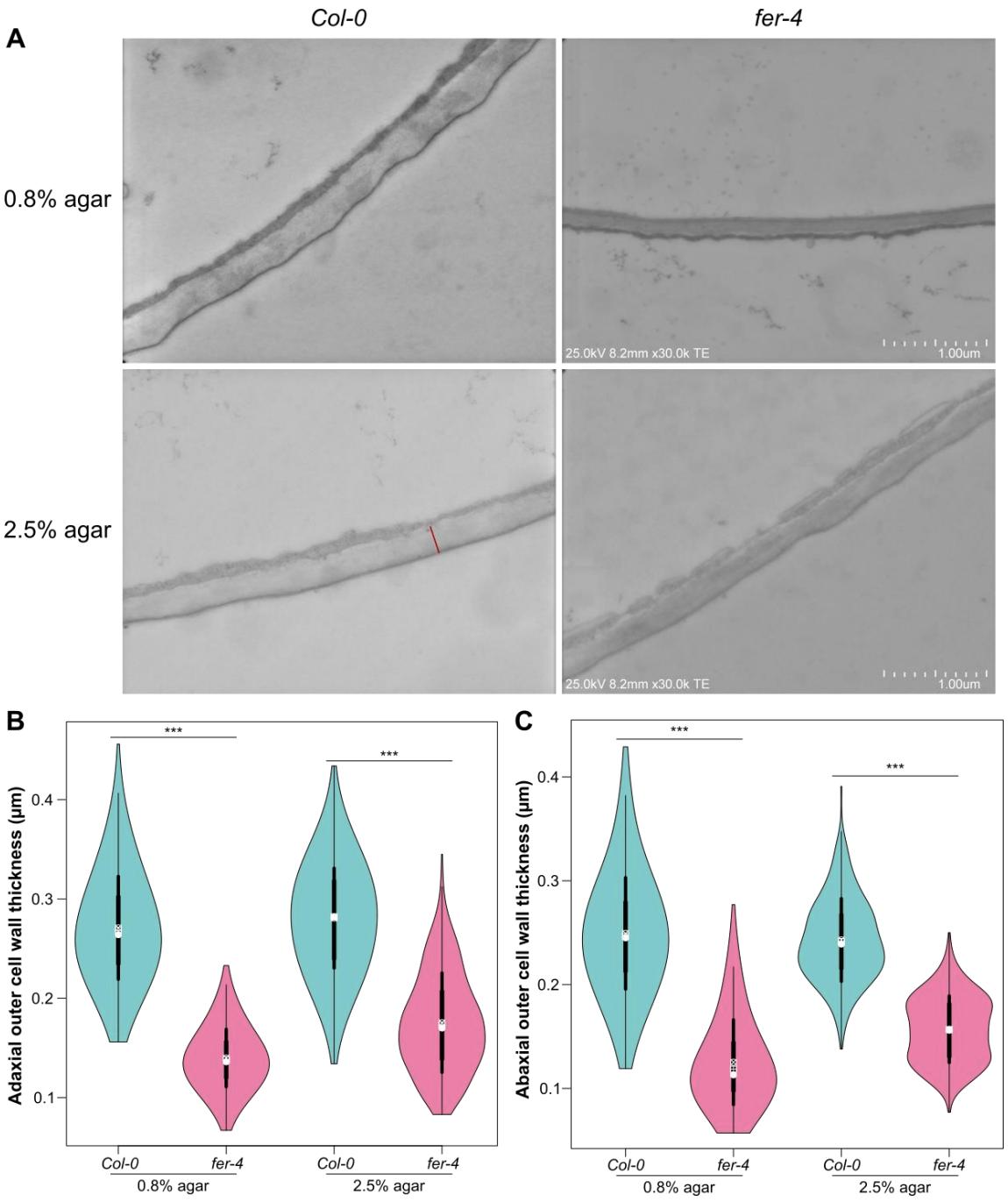

Figure 27: *fer-4* cell walls are thinner than the WT. **(A)** Representative transmission electron microscopy images of *Col-0* and *fer-4* pavement cells adaxial out cell walls, from seedlings grown on a medium containing 0.8% or 2.5% agar at t = 8 DAG. Red line is an example of thickness measurement. **(B)** Adaxial cell wall thickness (violin plot) and *p*-values of Wilcoxon–Mann–Whitney tests in *Col-0* and *fer-4* pavement cells, from seedlings grown on a medium containing 0.8% or 2.5% agar at t = 8 DAG. **(C)** Abaxial cell wall thickness (violin plot) and *p*-values of Wilcoxon–Mann–Whitney tests in *Col-0* and *fer-4* pavement cells, from seedlings grown on a medium containing 0.8% or 2.5% agar at t = 8 DAG.

We performed the same experiment on *fer-2* and obtained similar results (Supplementary figure 2). Therefore, cotyledon outer cell walls are thinner in *fer-4* than in the WT.

Together with the reports of reduced cellulose content and defective matrix crosslinking, the finding that *fer* cell walls are thinner suggests that the lower growth rate and burst cell phenotype emerge from cell walls that have reached their maximum deformation. Indeed, the thinning of the *fer* cell walls could be seen as a defect in wall deposition/synthesis. As the rescue when decreasing the cell wall tension is not total, other factors are probably involved in cell wall thinning in *fer-4*, and in particular the defects in cell wall biosynthesis.

II.4.3◦ Successive plasmolyses confirm the reduced elasticity of the fer-4 cell wall and also suggest osmotic defects

The presence of thinner outer cell walls in *fer* is a first indication of a more global cell wall defect in *fer*. Yet, it is not sufficient to explain the *fer-4* phenotype. Indeed, other mutants with thinner cell walls do not seem to exhibit burst cells (e.g. *repressor of lrx1 1* in the root (Liu et al., 2019; Ringli et al., 2008)). Furthermore, defects in cellulose biosynthesis usually lead to thicker cell walls instead, because of compensation (Manfield et al., 2004). To test for cell wall mechanical properties in a more integrative way, we performed successive plasmolyses of 8 DAG *fer-4* and WT cotyledons grown on 0.7% or 2.5% agar (Sapala and Smith, 2020). For each condition, we dissected cotyledons and immersed them for 18 minutes into a water solution of sorbitol of known osmotic pressure before imaging them and starting over with a solution of higher concentration (Figure 28A). We measured the area of the cotyledon at each plasmolysis step and calculated a relative area of the cotyledon for each measurement by dividing it with the area of the cotyledon at step 0, i.e. in pure water (Figure 28B).

When immersing the cotyledon in solutions with a lower water potential than the cells, water moves to the medium and the cotyledon decreases in size, i.e. in relative cotyledon area (see red outline in Figure 28A). After reaching a certain osmolarity in the medium (named here the inflexion point), the protoplast detaches from the cell wall and the relative cotyledon area reaches a plateau (blue line, model cotyledon in Figure 28C). This behaviour can be modelled

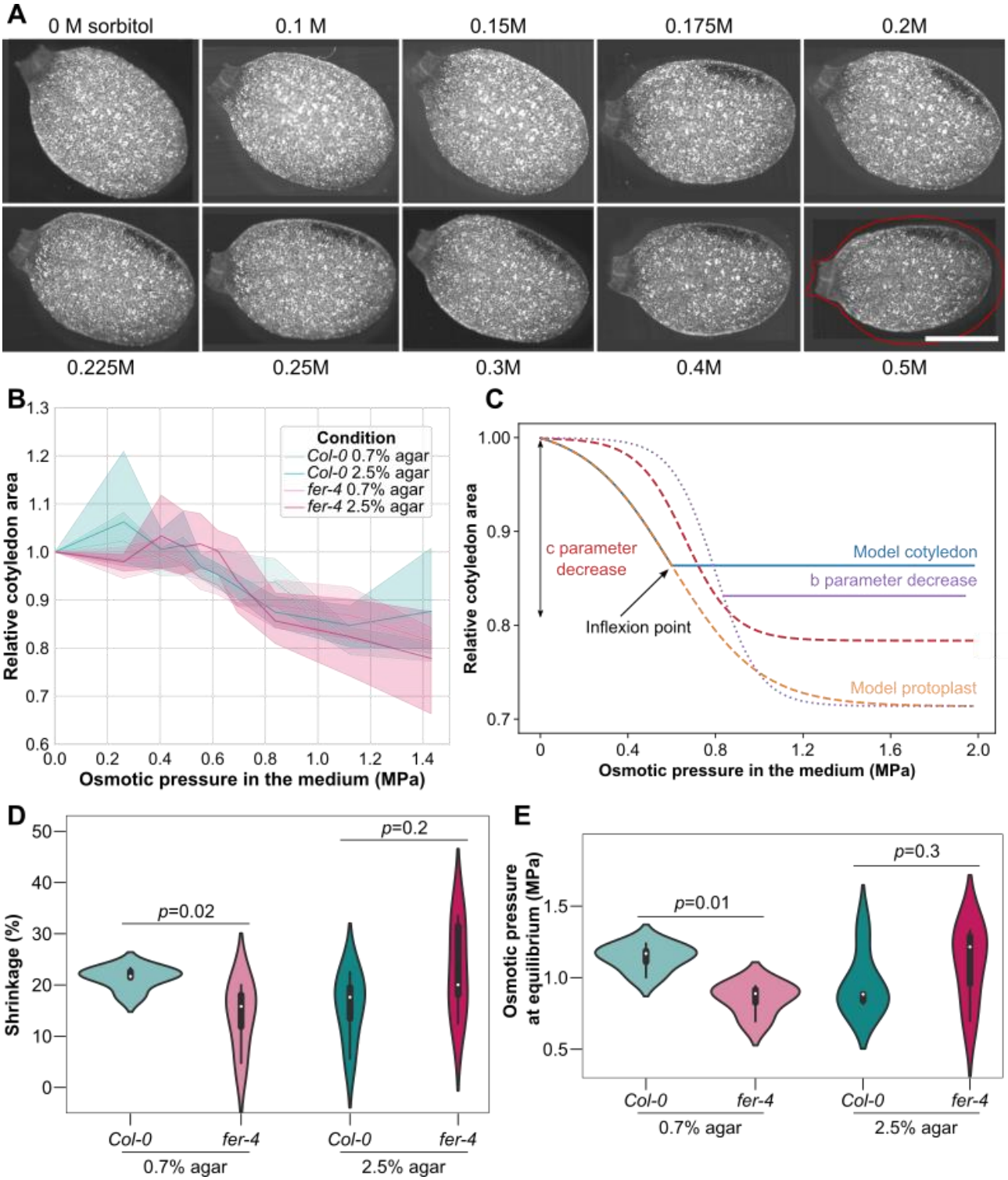
A
0 M sorbitol
0.1 M
0.15M
0.175M
0.2M
0.225M
0.25M
0.3M
0.4M
0.5M
B
Relative cotyledon area
Osmotic pressure in the medium (MPa)
Condition
Col-0 0.7% agar
Col-0 2.5% agar
fer-4 0.7% agar
fer-4 2.5% agar
C
Relative cotyledon area
Osmotic pressure in the medium (MPa)
c parameter decrease
Inflexion point
Model cotyledon
b parameter decrease
Model protoplast
D
Shrinkage (%)
p=0.02
p=0.2
Col-0
fer-4
0.7% agar
2.5% agar
E
Osmotic pressure at equilibrium (MPa)
p=0.01
p=0.3
Col-0
fer-4
0.7% agar
2.5% agar

Figure 28: In *fer-4*, cell walls are less deformable and the osmotic pressure is lower than in the WT. **(A)** Representative optic microscopy images of *Col-0* and *fer-4* cotyledons, from seedlings grown on a medium containing 0.7% or 2.5% agar at t = 8 DAG in successive plasmolysis with sorbitol solutions at 0 MPa (ultrapure water), 0.26 MPa, 0.41 MPa, 0.49 MPa, 0.55 MPa, 0.62 MPa, 0.84 MPa, 1.12 MPa and 1.43 MPa. **(B)** Average relative cotyledon area (compared to area in ultrapure water) for *Col-0* and *fer-4* seedlings grown on a medium containing 0.7% or 25% agar at t = 8 DAG in successive plasmolysis with sorbitol solutions. **(C)** Model of the evolution of the relative cotyledon area for successive plasmolysis. When the osmotic pressure of the surrounding medium increases, the relative area of the cotyledon decreases. At the inflexion point, the plasma membrane does not touch the cell wall anymore, leading to a plateau in the cotyledon relative area (whereas the protoplast keeps decreasing in size). Equation 9 describes the curve of the model. In this equation, the parameter b (purple curve) describes the inflexion point, where the turgor pressure is null, and so gives an estimation of the osmotic pressure in the cotyledon. The parameter *c* (red curve) describes the amplitude of the curve and so the deformation of the cotyledon during these successive plasmolyses. **(D)** Parameter *c* representing the shrinkage of the cotyledon (violin plot) and *p*-values of Wilcoxon–Mann–Whitney tests in *Col-0* and *fer-4* pavement cells, from seedlings grown on a medium containing 0.7% or 2.5% agar at t = 8 DAG in successive plasmolysis with sorbitol solutions. **(E)** Parameter *b* representing the osmotic pressure at equilibrium (violin plot) and *p*-values of Wilcoxon–Mann–Whitney tests in *Col-0* and *fer-4* pavement cells, from seedlings grown on a medium containing 0.7% or 2.5% agar at t = 8 DAG in successive plasmolysis with sorbitol solutions.

with an equation (equation 9) with three parameters (*a*, *b* and *c*) that can be adjusted to fit the measured relative cotyledon area. In particular, the parameter *c* is a marker of the shrinkage of the cotyledon (of the amplitude of the relative area curve). When the parameter *c* is high, the cotyledon is less deformed (red line, parameter *c* increases in Figure 28C), which can be the sign either of a less elastic cell wall, or of less turgid cells. Although the shrinkage of the cotyledon was not significantly different for *fer-4* than for the WT at any growth medium agar concentration, there was a tendency for a lower shrinkage in *fer-4* than in the WT on 0.7% agar (26% lower than the WT; $p_{0.7\%agar} = 0.02$; $p_{2.5\%agar} = 0.2$; $n_{Col\text{-}0,0.7\%agar} = 5$; $n_{fer\text{-}4,0.7\%agar} = 4$; $n_{Col\text{-}0,2.5\%agar} = 5$; $n_{fer\text{-}4,2.5\%agar} = 5$). However, determining whether this lower shrinkage came from cell wall properties or turgor at origin would require additional experiments, which can be reflected in the two other parameters *a* and *b*.

Parameter *b* can help discriminate the cell wall mechanical properties from the hydraulic properties in *fer-4*. Indeed, it is a marker of the osmotic pressure reached at the inflexion point in the model (purple line, parameter *b* increases in Figure 28C): a higher *b* reflects a higher osmotic pressure in the medium needed to reach the equilibrium, i.e. to attain a null turgor pressure. At this stage, the osmotic pressure is the same in the cotyledon and in the medium. Using this approach, we deduced a 25% decrease in the osmotic pressure at equilibrium in *fer-4* compared to the WT for seedlings grown on 0.7% agar, with a full rescue of the phenotype for seedlings grown on 2.5% agar ($p_{0.7\%agar} = 0.01$; $p_{2.5\%agar} = 0.3$; $n_{Col\text{-}0,0.7\%agar} = 5$; $n_{fer\text{-}4,0.7\%agar} = 4$; $n_{Col\text{-}0,2.5\%agar} = 5$; $n_{fer\text{-}4,2.5\%agar} = 5$). This decrease of osmotic pressure in *fer-4* cells reduces the difference of osmotic pressure with the medium $\Delta\Pi$ and could partially explain the lower growth rate observed in *fer-4* (see Results ◦ II.4.1). The rescue observed for the two parameters (*b* and *c*) could be either the effect of decreasing the tensile stress in the cell wall or the hydraulic properties, which are both linked.

To confirm the results, we used a different osmolyte. We repeated the same experiment with solutions of NaCl but, due to the effect of salt on the cell wall and on *fer-4* (Feng et al., 2018), those results are to be interpreted carefully (Supplementary figure 3). Successive plasmolyses of cotyledons with NaCl or sorbitol provided comparable results concerning the cell wall deformability (a lower shrinkage for *fer-4* grown on 0.7% agar, rescued on 2.5% agar; $p_{0.7\%agar} = 0.002$; $p_{2.5\%agar} = 0.3$; $n_{Col\text{-}0,0.7\%agar} = 8$; $n_{fer\text{-}4,0.7\%agar} = 9$; $n_{Col\text{-}0,2.5\%agar} = 9$; $n_{fer\text{-}4,2.5\%agar} = 9$). However, we were not able to identify significant difference in the osmotic

pressure at equilibrium between *fer-4* and the WT when using NaCl ($p_{0.7\%agar}$ = 0.2; $p_{2.5\%agar}$ = 0.3; $n_{Col\text{-}0,0.7\%agar}$ = 8; $n_{fer\text{-}4,0.7\%agar}$ = 9; $n_{Col\text{-}0,2.5\%agar}$ = 9; $n_{fer\text{-}4,2.5\%agar}$ = 9).

II.4.4◦ fer-4 high water potential and high water content indicate a water saturation

The lower growth rate in *fer-4* cells was not conclusively rescued by a lower tension in the cell wall (see Results ◦ II.4.1), suggesting a defect independent from cell wall tension explaining at least part of the *fer-4* phenotypes. So far, tests have suggested a role for FER in cell wall reinforcement, but the last experiment also highlighted defects in osmotic pressure regulation in *fer-4*. Interestingly, smaller cells has been associated with a higher turgor pressure in WT cotyledons (Long et al., 2020), which could eventually (but not certainly) lead to a higher tension in the cell wall in *fer-4*. To analyse the osmotic status of *fer-4*, we used an even more integrative approach and analysed *fer-4* phenotype *in terra* in a very controlled and automated setting using the phenotyping platform Phenopsis (Granier et al., 2006).

WT and *fer-4* plants were grown at various humidity levels for 45 days, upon which they were harvested for measurement (Figure 29A, Supplementary Figure 4). We established the relevance of these growth conditions by assessing the presence of burst cells in *fer-4* leaves for each humidity level (red arrowheads, Figure 29B). The technique used (leaves imprints) did not allow a fine enough analysis to quantify the number of burst cells and indicate whether certain growth conditions were more conducive to burst cells than others.

We used a Scholander bomb (see Introduction ◦ I.2) to measure the water potential in *fer-4* and WT rosettes grown at humidity levels of 0.6, 0.8, 1.1 and 1.4 (measured in g of water per gram of soil) (Scholander et al., 1964). For each humidity level, the measured water potential was significantly higher in *fer-4* than in the WT: 50% higher at a humidity level of 0.6, 42% higher at a humidity level of 0.8, 31% higher at a humidity level of 1.1, 49% higher at a humidity level of 1.4 ($p_{humidity0.6} < 10^{-3}$; $p_{humidity0.8} < 10^{-3}$; $p_{humidity1.1}$ = 0.006; $p_{humidity1.4} < 10^{-3}$; $n_{Col\text{-}0,humidity0.6}$ = 6; $n_{fer\text{-}4,humidity0.6}$ = 8; $n_{Col\text{-}0,humidity0.8}$ = 9; $n_{fer\text{-}4,humidity0.8}$ = 8; $n_{Col\text{-}0,humidity1.1}$ = 8; $n_{fer\text{-}4,humidity1.1}$ = 7; $n_{Col\text{-}0,humidity1.4}$ = 9; $n_{fer\text{-}4,humidity1.4}$ = 7; Figure 29C). Such a high water potential in *fer-4* reflects low water attractivity, as if plants were internally saturated with water. According to the water potential equation (equation 2), a high water potential can be caused

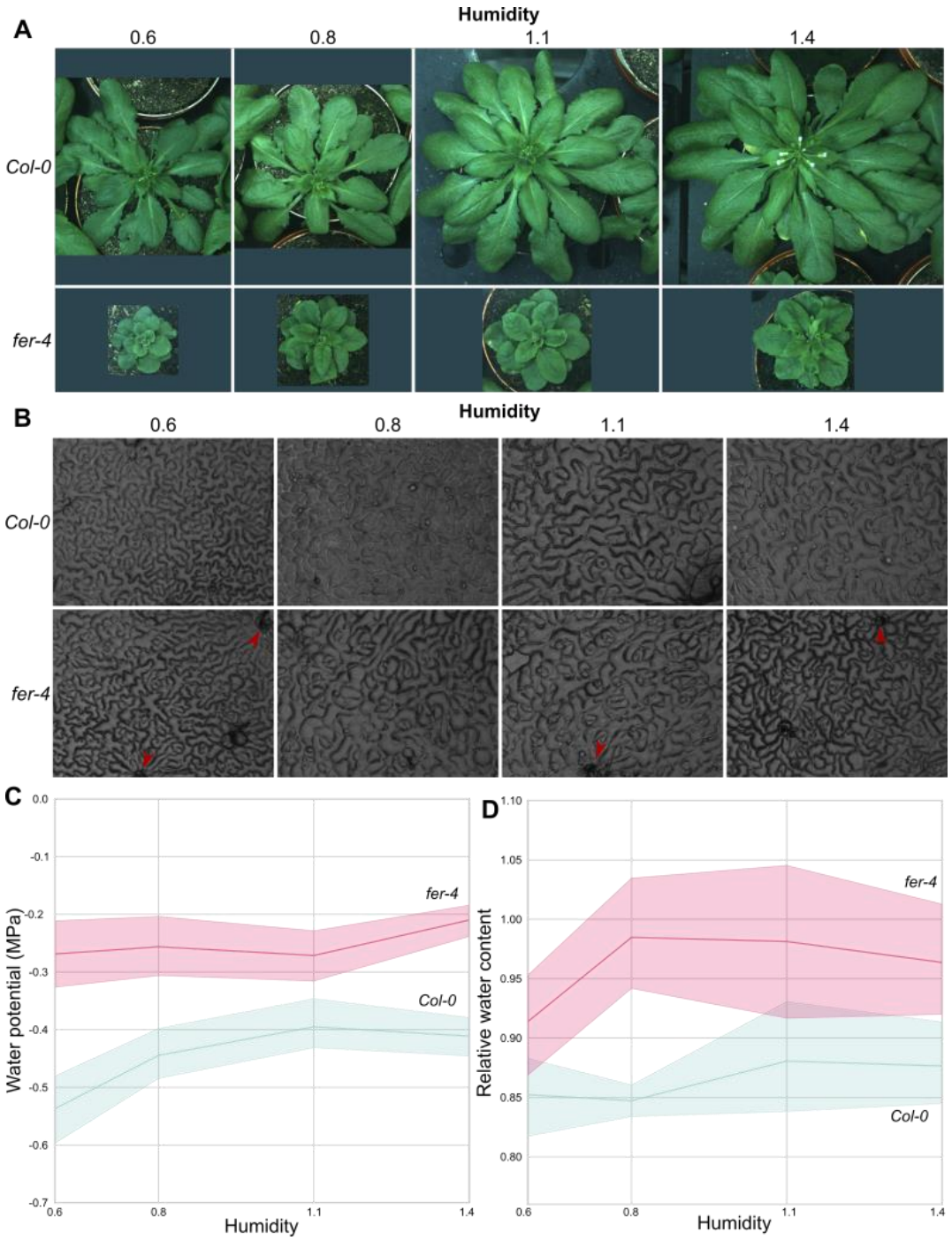

Figure 29: *fer-4* plants are saturated by water. **(A)** Representative images of *Col-0* and *fer-4* 42 DAG rosettes grown on soil with four different humidity level: 0.6, 0.8, 1.1 and 1.4 (g of water per g of soil). **(B)** Representative leaves imprints of *Col-0* and *fer-4* 43-45 DAG rosettes grown on soil with four different humidity level: 0.6, 0.8, 1.1 and 1.4 (g of water per g of soil). Red arrowheads point to burst cells. **(C)** Average water potential for *Col-0* and *fer-4* 43-45 DAG rosettes grown on soil with four different humidity level: 0.6, 0.8, 1.1 and 1.4 (g of water per g of soil). **(D)** Average relative water content *Col-0* and *fer-4* 43-45 DAG rosettes grown on soil with four different humidity level: 0.6, 0.8, 1.1 and 1.4 (g of water per g of soil).

by a high turgor pressure, or, as observed in the plasmolysis experiment (Results ◦ II.4.3), a low osmotic pressure. Looking at the evolution of the water potential with the humidity level of the medium, we also found that, if the WT water potential increased by 23% with humidity ($p_{Col\text{-}0,humidity0.6\text{-}1.4} = 0.007$; $n_{Col\text{-}0,humidity0.6} = 6$; $n_{Col\text{-}0,humidity1.4} = 9$), it did not significantly change in *fer-4* ($p_{fer\text{-}4,humidity0.6\text{-}1.4} = 0.2$; $n_{fer\text{-}4,humidity0.6} = 8$; $n_{fer\text{-}4,humidity1.4} = 7$).

The equation for the osmotic pressure (equation 1) shows that for cells at the same temperature (as is the case here), a lower osmotic pressure comes from a lower osmolarity. How could such lower osmolarity occur in *fer*? Defects in the regulation of glyceraldehyde-3-phosphate dehydrogenase (GAPDH) lead to an hyper-accumulation of starch in *fer-4*, which is generally hypersensitive to sucrose (Yang et al., 2015; Yeats et al., 2016). Such metabolic differences between *fer-4* and WT could trigger lower osmolarity through a lower number of solutes in *fer-4*. Another more direct evidence of low osmolarity is the presence of larger vacuoles in *fer-4*, when compared to the WT (Dünser et al., 2019), which usually correlate with a high water content in cells. We thus analysed the relative water content in *fer-4* and the WT by using the fresh weight, dry weight and rehydrated weight of mature leaves for each humidity level (see Results ◦ II.6.3). We found that *fer-4* displayed tendencies towards a higher relative water content than the WT for each humidity level except the lowest one: there was no significant difference at a humidity level of 0.6, and the relative water content was 16% higher at a humidity level of 0.8, 11% higher at a humidity level of 1.1 and 10% higher at a humidity level of 1.4 in *fer-4* ($p_{humidity0.6} = 0.07$; $p_{humidity0.8} < 10^{-3}$; $p_{humidity1.1} = 0.02$; $p_{humidity1.4} = 0.01$; $n_{Col\text{-}0,humidity0.6} = 9$; $n_{fer\text{-}4,humidity0.6} = 8$; $n_{Col\text{-}0,humidity0.8} = 8$; $n_{fer\text{-}4,humidity0.8} = 8$; $n_{Col\text{-}0,humidity1.1} = 9$; $n_{fer\text{-}4,humidity1.1} = 6$; $n_{Col\text{-}0,humidity1.4} = 9$; $n_{fer\text{-}4,humidity1.4} = 8$; Figure 29D).

In addition to explaining the low osmotic pressure, this higher water content in *fer-4* also allows us to ascribe the lower shrinkage observed after plasmolysis (see Results ◦ II.4.3) to a lower cell wall elasticity, and not to a lower turgor in cotyledons. As elasticity often correlates with elasticity when measured in living cells, *fer-4* cells would thus experience lower cell wall extensibility ϕ as well as higher water content. This would explain the decreased *fer-4* growth rate (see Results ◦ II.4.1), and this unique combination would make the cells more prone to burst.

II.5◦ Discussion

FER seems to play a role in cell mechanical properties through both the cell wall mechanics and the cell hydraulic properties. By comparison to the WT, *fer-4* cell walls are thinner and less deformable, which probably causes a lower cell wall extensibility ϕ. *fer-4* cells also display a higher water content leading to a lower difference in osmotic pressures between the cell and the medium $\Delta\Pi$. As we acquired these measures during growth, this could possibly be explained by a lower hydraulic conductance L and/or lower solute concentration inside the cell. Such a combination results in a lower cell growth, not necessarily because turgor is low, but instead, because cell walls are already stretched to the maximum. This is also consistent with frequent cell mechanical failure in the mutant. We did not look for a difference in the yield threshold Y because it is usually a very small value and rarely restricts growth (e.g. here the numerical mechanical parameter values for pollen tubes (Dumais, 2021)). From these results, we can go one step further and propose three refined, non-exclusive, hypotheses on why *fer-4* cells burst.

Hypothesis 1: The speed/quantity of cell wall expansion (synthesis and distribution) would be impaired in *fer-4*, leading cells to burst. This hypothesis would be compatible with the low growth rate, the thin cell wall and the less deformable cell wall observed in *fer-4*. As the cell wall takes up around half of the dry weight of a cell (Robbins and Moen, 1975), this hypothesis would also make the relative water content results appear in a new light: indicating a low proportion of dry matter rather than an over-uptake of water. Adding agar into the growth medium would lower the hydraulic pressure (maybe even create a hydraulically limited growth regime) and thus cells would better resist this lack of cell wall expansion. In addition to a possible lack in cell wall synthesis, the defects in cell wall expansion could be caused by a lower amount of demethylesterified pectins in *fer-4* (Duan et al., 2020), which seem essential for cell wall expansion in the frame of the expanding beam model (Haas et al., 2021). We can also wonder if the hydration of the cell wall would change its expansion, and if this hydration could be a parameter controlled by FER. Little is known for now on either cell wall mechanical properties in relation to hydration, or cell wall hydration control but these subjects could open a new understanding of cell mechanical properties.

Hypothesis 2: The cell wall material would be different in *fer-4* than in the WT and would be less deformable but more brittle, causing the cells to break instead of deforming after a water intake. This would lead to a low cell wall extensibility ϕ and would explain the low deformation of the cotyledon observed during the plasmolysis experiment, as well as the reduced growth rate in *fer-4*. A decrease in pectin demethylesterification, as observed in *fer-4* (Duan et al., 2020), could lead to differences in the cell wall mechanical properties and provide a mechanism for this hypothesis.

Hypothesis 3: The active regulation of water uptake could be defective in *fer-4*, i.e. letting too much water into the cell. This would cause pressure to build up in cells and lead to mechanical failure (in combination with wall defects). The high water content and low osmotic pressure observed would support this hypothesis, which would need to be confirmed by measuring the hydraulic conductance *L*. A possible molecular support for this scenario is provided by the binding of the kinase FER to plasma membrane aquaporins (Bellati et al., 2016), which can be regulated by phosphorylation. However, excessive water uptake alone would be contradictory with the low growth rate in *fer-4* and thus would need to be combined with at least one of the two others.

This project is still a work in progress. As we did not find a model for mechanical integrity yet, and used one for growth instead, there might be other parameters to consider in the cell mechanical response to stress (e.g. the many ways in which wall could break). Moreover, each measurement method suffers some biases, which requires us to add more measurements before drawing any definitive conclusion. On that note, we have already planned several other experiments to test further our results. First, we should increase the number of replicates in the plasmolysis experiment (Figure 28). We will also try to confirm our plasmolysis results at the cell scale in the hope of avoiding artefacts due to burst cells in *fer-4* (in particular, to make sure the protoplast does detach from the cell wall when cotyledon area reaches a plateau). By timing the relative cotyledon area change during the plasmolysis experiment, we should be able to deduce the hydraulic conductance *L* in *fer-4*. To gain insight into the role of water in the cell wall mechanical properties, we would also like to determine the hydrated cell wall thickness (the one determined by TEM is from dehydrated cell walls), by using the Airyscan module on a confocal microscope (which is resolutive enough to separate the fluorescent signal from plasma membranes from two contiguous cells).

Moreover, we are waiting for results from some collaborators. The team of Yuchen Long (National University of Singapore, Singapore) is performing indentation measurements with atomic force microscopy (AFM) to determine wall stiffness, wall tension, as well as turgor pressure in *fer-4* compared to the WT. Finally, Gregory Mouille (Institut Jean-Pierre Bourgin, Versailles) and his team will help us determine the biochemical composition of *fer-4* cell walls. Both datasets will be obtained from seedlings grown on 0.7% and 2.5% agar.

So far, our results are consistent with FER as a central mechanosensor, with dual roles in osmoregulation and wall reinforcement, which could explain the diversity of its roles. At this stage, we still cannot entirely exclude the possibility that FER performs its function only through one of these ways (i.e. the reinforcement of the cell wall or through a control of water intake). Yet, a dual function would be consistent with the apparent pleiotropy of FER. In the end, FER could be an environmental sensor through mechanosensing, detecting the tension in the cell wall (or another parameter) as a cue of water availability and adapting the plant development to many factors at once: soil humidity, heat, transpiration, etc. This process could be called mechano-eco-sensing and be one of the factors for developmental plasticity in plants.

II.6◦ Material and methods

II.6.1◦ Plant material and growth conditions

All plants were in the Columbia-0 (Col-0) ecotype. The two FERONIA null mutants used were *fer-4* (GABI 106_A06) (Duan et al., 2010) and *fer-2* (TAG insert) (Deslauriers and Larsen, 2010). For all experiments, except the *in terra* one (Figure 29), seeds were surface sterilized and individually sown on either: (Figure 27) Murashige and Skoog medium (MS medium, Duchefa, Haarlem, the Netherlands) or (Figure 26, Figure 28) *Arabidopsis* medium (custom-made Duchefa "*Arabidopsis*" medium (DU0742.0025, Duchefa Biochemie, The Netherlands)) with different agar concentrations (0.7%, 0.8% or 2.5%). Plants were placed to stratify 2 days in the dark at 4°C then transferred in a 20°C long day (16 hours of light) growth chamber for 4 days (4 DAG, Figure 26), 8 days (8DAG, Figure 27, Figure 28) or 12 days (12 DAG, Figure 26).

For the *in terra* experiment (Figure 29), plants were sown in soil in separate pots with a similar soil compaction and placed in the automated platform for phenotyping named

Phenopsis (Granier et al., 2006). The humidity of each pot of soil was controlled automatically by weighing the pots and watering them with the amount of water needed, to reach humidity levels of 0.6, 0.8, 1.1 and 1.4 (g of water per g of soil). Samples were placed randomly in the machine, and grown for 42-45 days at 21 ± 1°C in 12-hour light conditions and with a vapour-pressure deficit of 1.25 kPa.

II.6.2◦ Image acquisition

Confocal images (Figure 26) were re-used from a set of experiments published in (Malivert et al., 2021). Samples were imaged in a new medium plate after staining for 10 minutes with a 1/10 propidium iodide solution (Sigma; PI stains wall pectins and thus marks cell contours) and two rinsing steps. Cotyledons were manually flattened with forceps under a binocular stereoscopic microscope and imaged with a SP8 confocal microscope (Leica Microsystems, Germany) equipped with a 25× long-distance water objective (NA = 0.95).

For the transmission electron microscopy (TEM, Figure 27), cotyledons were fixed for 24 hours at 4°C with a solution of 2.5% glutaraldehyde buffered in 50mM phosphate at pH = 7. Samples were then rinsed three times for 15 minutes at room temperature in the 50mM phosphate buffer solution (pH = 7), post-fixated for 2 hours with a solution of 1% OsO_4 diluted in deionized water, rinsed in deionized water and dehydrated in a graded ethanol series. After dehydration, the samples were embedded in Epon resin. Ultrathin cross sections were cut in the middle of the cotyledon with diamond knife and mounted on copper grids (200 mesh) with a supporting film. Sections were doubly stained with uranyl acetate and lead citrate. They were inspected in Hitachi UHR FE-SEM SU8010 equipped with TE – detector.

For the plasmolysis experiment (Figure 28), cotyledons were dissected and placed in a water solution of sorbitol or NaCl between a well slide and a cover slip. Samples were incubated for 15 minutes in NaCl solutions and 18 minutes in sorbitol solutions, duration after which no change in cotyledon area was detectable anymore. Samples went successively through solutions of 0 M (ultrapure water), 0.1 M, 0.15 M, 0.175 M, 0.2 M, 0.225 M, 0.25 M, 0.3 M, 0.4 M and 0.5 M of sorbitol or NaCl diluted in ultrapure water, and were patted dry between each incubation. After each incubation, a picture was taken of the cotyledon in between in the well slide and the cover slip using a binocular stereomicroscope (either a Leica M212 or a Nikon SMZ18). The osmolarity of each solution was measured 3 times with a

cryoscopic osmometer (Osmomat 030, Gonotec) and the mean of these measurements was used for the analysis.

The leaves imprints (Figure 29) were taken by applying transparent nail polish on the surface of the 5th leave then using tape to reveal the imprint of cells. Imprints were then imaged with a Leica Dmrb 301-371.010 microscope

II..6.3◦ Hydraulic properties acquisition

To measure the hydraulic potential of the samples (Figure 29), the aerial part was cut and introduced into a Scholander bomb (SOILMOISTURE Equipment Corp.) with the base of the stem emerging. The pressure was increased inside the chamber (with N_2) until some liquid appeared at the base of the stem, which was equal to the bulk water potential in the plant aerial parts.

The relative water content (RWC) of the samples (Figure 29) were calculated using the fresh weight (FW), dry weight (DW) and rehydrated weight (RW) of a mature leaf:

$$RCW = \frac{FW-DW}{RW-DW} \qquad \text{(equation 8)}$$

with FW the weight of the leaf immediately after harvest, DW the weight of the leaf after 5 days at 60°C and RW the weight of the leaf after 24h in a cold room at 100% humidity.

II.6.4◦ Image analysis

Pavement cell areas (Figure 26) were obtained by first processing confocal images with the ImageJ (https://fiji.sc/) macro SurfCut (Erguvan et al., 2019) to obtain a projection of the flattened cell contours. Then the cell contour image was processed using PaCeQuant (Möller et al., 2017), an ImageJ plug-in quantifying up to 27 shape descriptors of pavement cells.

The cell wall thickness in TEM images (Figure 27), and the cotyledon areas in plasmolysis images (Figure 28) were analysed manually with ImageJ.

After image analyses, the brightness and contrast of all images presented in this study were enhanced to help visualization.

II.6.5◦ Statistical analysis

Statistical analyses were performed with R software (https://www.R-project.org) or Python software (https://www.python.org/). To extract pavement cell shape parameters (in particular pavement cell area (Figure 26), we used PaCeQuantAna, the R script that accompanies the PaCeQuant analysis (Möller et al., 2017). To compare the growth from different genotypes in different growth conditions (with a destructive sampling preventing us from imaging the same cotyledons at different time points), we calculated a mean and a standard deviation from t = 4 DAG for each condition, and used them to standardize the distribution of each condition at t = 12 DAG. The new distribution obtained was called growth rate index and used for the comparison (Supplementary figure 1).

To interpret the relative cotyledon area measured (Figure 28), a model of the decrease in cotyledon size was used, traced by this curve (Figure 28C):

$$y = c + \frac{1-c}{1+e^{a(x-b)}} \qquad \text{(equation 9)}$$

with y the relative area of the cotyledon and *a*, *b* and *c* parameters describing cotyledon properties. In this model, the cotyledon decreases in size when increasing the osmotic pressure of the medium and reaches a plateau at the inflexion point. The parameter *b* describes the osmotic pressure at which the inflexion point is reached (higher *b* for a higher osmotic pressure at equilibrium) and the parameter *c* describes the shrinkage of the cotyledon between the beginning and the reaching point of the plateau (lower c for a higher shrinkage). The model was automatically fitted to the relative area evolution of each cotyledon with the Python function scipy.optimize.curve_fit, which returned the parameters *a*, *b*, and *c* for this fit. We then compared the distribution of those parameters between the different conditions.

All quantitative measures were compared with a Wilcoxon–Mann–Whitney test on the different distributions. As a Wilcoxon–Mann–Whitney test can be directed or not, the *p*-value shown in all experiments with a Wilcoxon–Mann–Whitney test was that of a non-directed test for non-significant *p*-value (to ensure that neither distribution was higher than the other) and that of a directed test in the significant direction for a significant *p*-value. The data was visualised using either violin plots or curves representing the mean (coloured line) and the 95% confidence interval (coloured area) of the distribution.

For all experiments, differences with p-values that were under 1% were considered significant, and those between the commonly used thresholds of 5% and 1% were considered as tendencies. The sample size is indicated in the main text.

II.7◦ Supporting information

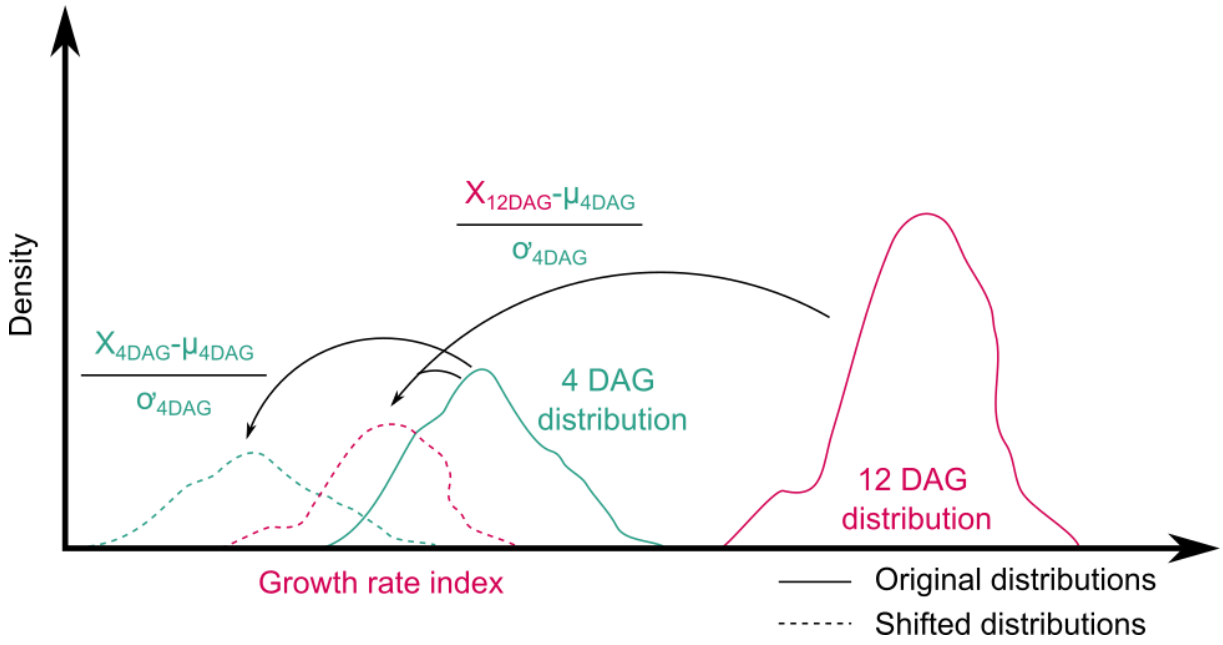

Supplementary figure 1: Growth rate index. The continuous green and pink lines represent the distribution of the actual measurement of pavement cell relative area at 4 DAG (green) and 12 DAG (pink). To compare growth between several conditions despite measuring different samples at 4 DAG and 12 DAG, we normalized the distribution of cell area at 12 DAG according to the one at 4 DAG, following the standard score method. To do so, the parameters of the 4 DAG distribution (mean: μ_{4DAG}, standard deviation: σ'_{4DAG}) were used to shift the 4 DAG distribution around 0 (dashed green line) and the same parameters were used again to shift the 12 DAG distribution to the same extent (dashed pink line). With this method, the 4 DAG samples for all conditions have a value around 0, which then allows to reveal the growth difference in several conditions by comparing the normalized distributions of the 12 DAG samples (the growth rate index).

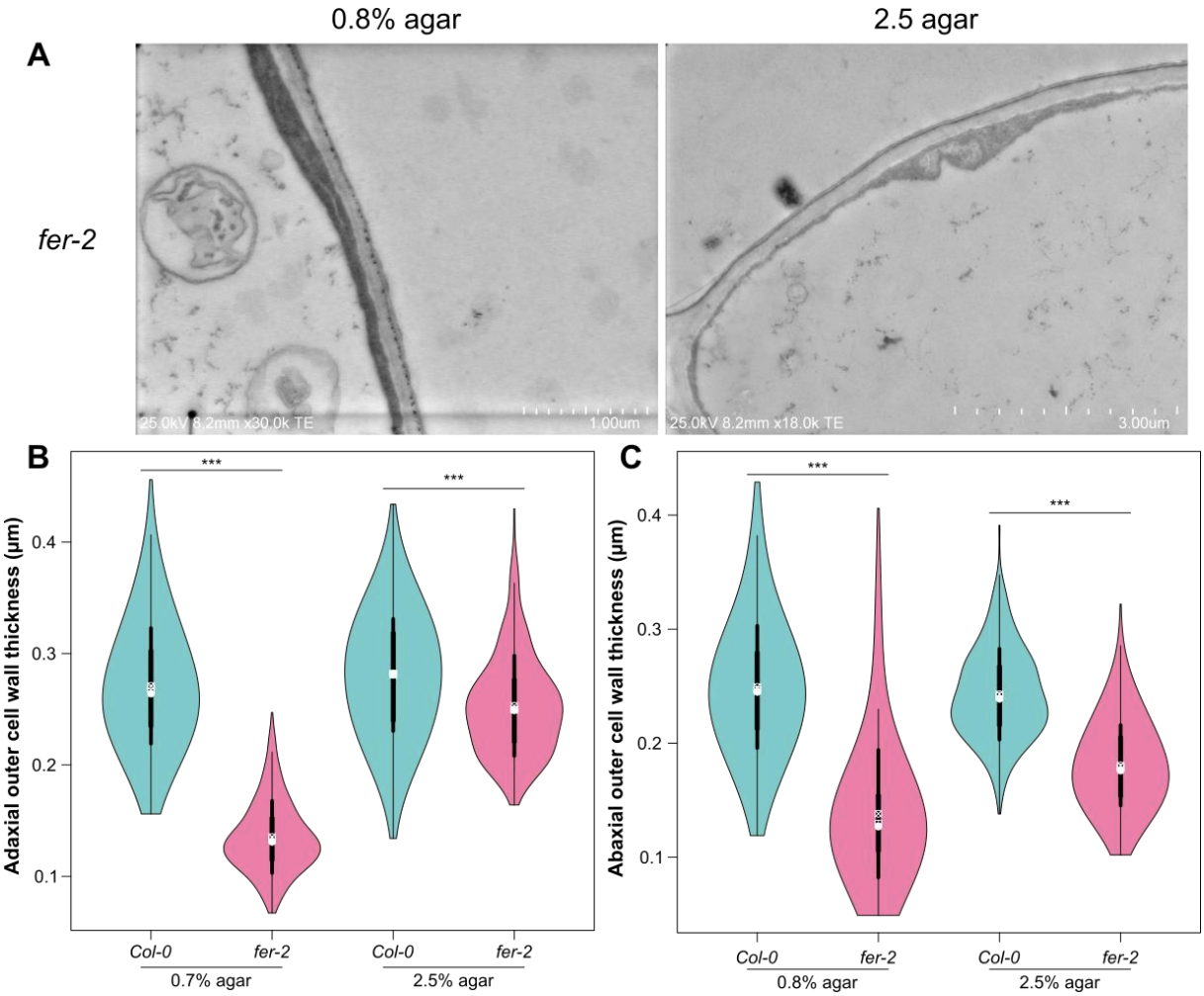

Supplementary figure 2: Cell wall thickness in *fer-2.* **(A)** Representative transmission electron microscopy images of *fer-2* pavement cells adaxial outer cell walls, from seedlings grown on a medium containing 0.8% or 2.5% agar at t = 8 DAG. **(B)** Adaxial cell wall thickness (violin plot) and *p*-values of Wilcoxon–Mann–Whitney tests in *Col-0* and *fer-2* pavement cells, from seedlings grown on a medium containing 0.8% or 2.5% agar at t = 8 DAG. **(C)** Abaxial cell wall thickness (violin plot) and *p*-values of Wilcoxon–Mann–Whitney tests in *Col-0* and *fer-2* pavement cells, from seedlings grown on a medium containing 0.8% or 2.5% agar at t = 8 DAG.

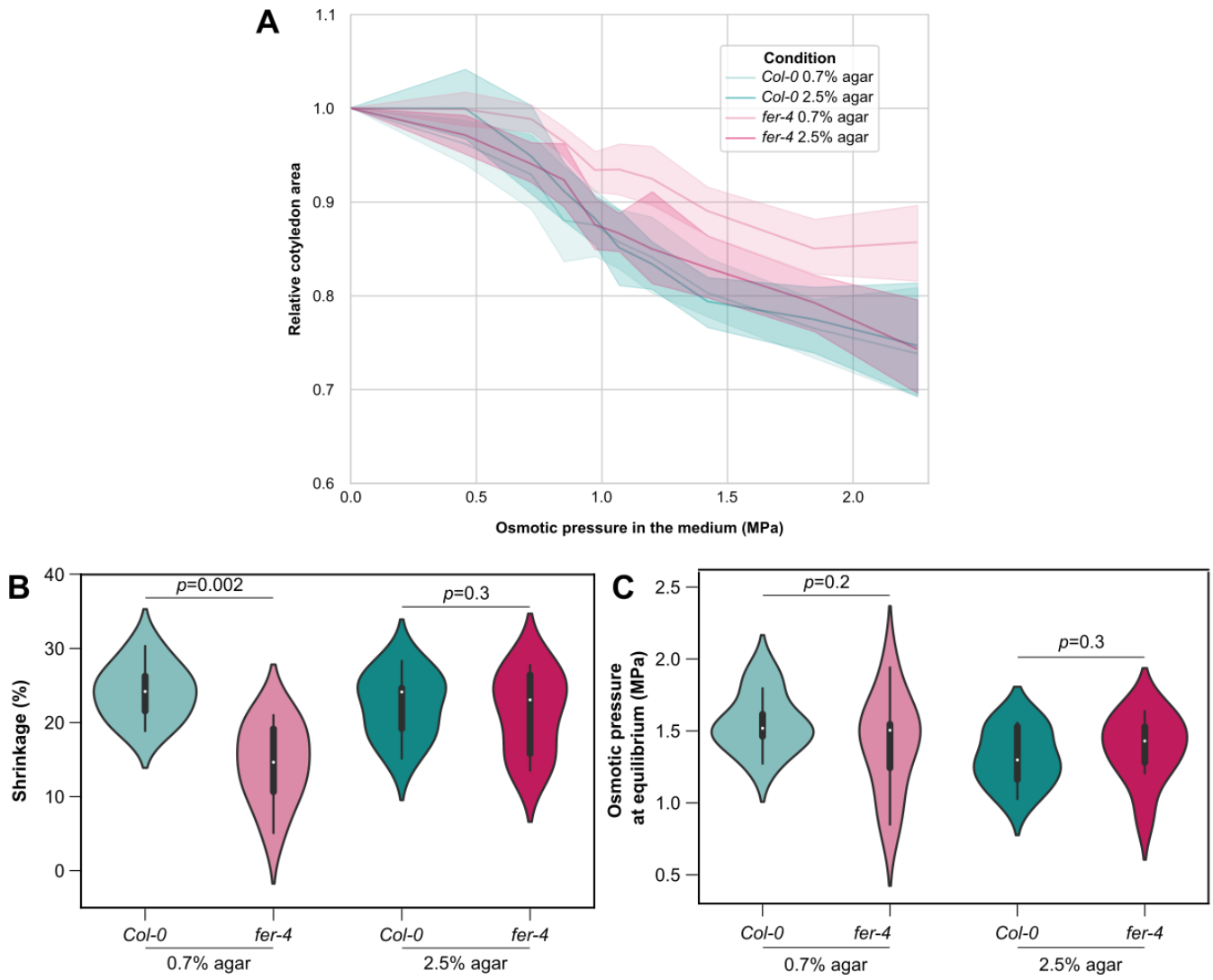

Supplementary figure 3: NaCl plasmolysis. **(A)** Average relative cotyledon area (compared to area in ultrapure water) for *Col-0* and *fer-4* seedlings grown on a medium containing 0.7% or 25% agar at t = 8 DAG in successive plasmolysis with NaCl solutions. **(B)** Parameter *c* representing the shrinkage of the cotyledon (violin plot) and *p*-values of Wilcoxon–Mann–Whitney tests in *Col-0* and *fer-4* pavement cells, from seedlings grown on a medium containing 0.7% or 2.5% agar at t = 8 DAG in successive plasmolysis with NaCl solutions. **(C)** Parameter b representing the osmotic pressure at equilibrium (violin plot) and *p*-values of Wilcoxon–Mann–Whitney tests in *Col-0* and *fer-4* pavement cells, from seedlings grown on a medium containing 0.7% or 2.5% agar at t = 8 DAG in successive plasmolysis with NaCl solutions.

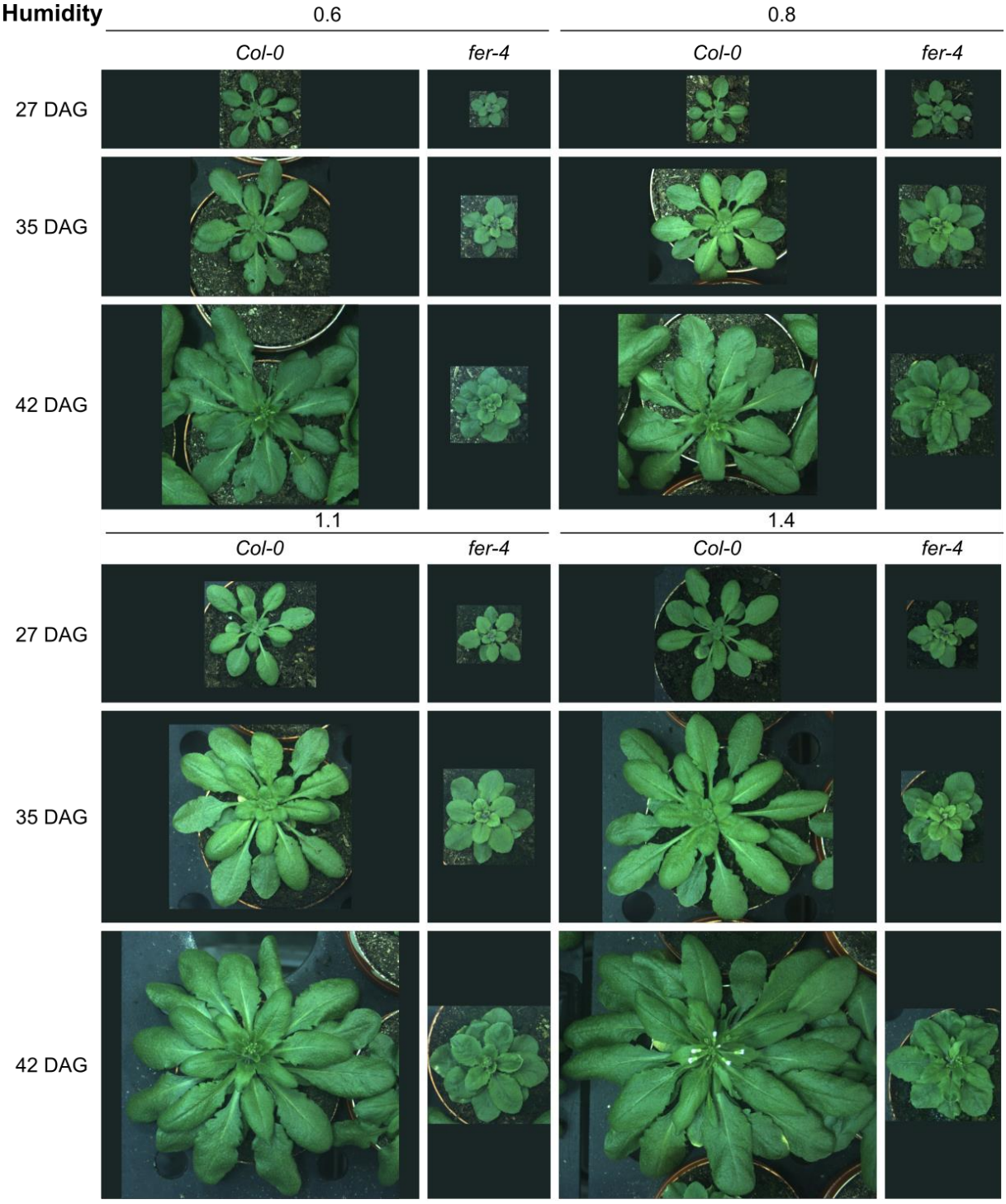

Supplementary figure 4: *Col-0* and *fer-4* growth kinetics (27 DAG, 35 DAG and 42 DAG) on soil with four different humidity level: 0.6, 0.8, 1.1 and 1.4 (g of water per g of soil). For ease of reading, the 42 DAG images are the same ones as in (Figure 29A).

General discussion

During my PhD I have investigated how cells detect mechanical cues induced by turgor pressure and integrate them to prevent mechanical failure. In the first part, I have screened several RLK mutants in search of sensors involved in the cellular response to shape- and growth-derived stress. These screens highlighted FER as an essential competent of the mechanical stress response pathway. Since cortical microtubules are prime components of the cellular response to mechanical stress with no known mechanosensor involved in the process, we looked at the link between the CMT pathway and the FER one. Surprisingly, we found that FER is not necessary for the microtubule response to stress. In the course of these experiments, we noticed an unusual phenotype in *fer* mutants: cells swelling and bursting causing growth defects in cotyledons and hypocotyls. As mutants with a compromised cellular mechanical integrity are extremely rare, we investigated this phenotype to better understand the cellular response to mechanical stress. We found that FER is involved in the thickness and mechanical reinforcement of the cell wall, as well as in cell hydraulic properties. FER thus appears as a "dual" mechanosensor, which may explain its unique role in maintaining the cellular mechanical integrity. This may also explain its pleiotropic role in development, and conversely help to integrate mechanosensing into developmental plasticity.

For example, response to drought could be associated with mechanotransduction in many ways. Drought reduces water uptake by the plant, and as such could be sensed by FER as a disruption in mechanical stress. FER has several links with the drought stress response. First, it is involved in the signaling of the drought stress messenger ABA signaling (Yu et al., 2012). Through JA signaling, it downregulates the drought-induced transcription factor *RESPONSIVE TO DESICCATION 26* (*RD26*) (Guo et al., 2018; Ye et al., 2017). Finally, FER triggers the alternative splicing of the drought-responsive *DROUGHT INDUCED LIKE9-7* (*DIL9-7*, also called *HYPERSENSITIVE TO RED AND BLUE 1 HRB1*) (Wang et al., 2020b). More generally, drought induces many responses that could be sensed through mechanosensing. For instance, the stiffening of the soil, as it becomes drier, has been shown to inhibit root growth (Whitmore and Whalley, 2009). Whether FER is involved in that process is unknown.

As another example, FER could play a role on immunity through its detection of mechanical stress, in a process called thigmoimmunity (Léger et al., 2021). Indeed, pathogen entry in plants causes a local stretch in the wall which disturbs the cell wall tension pattern and seems to trigger the reorientation of CMTs. The microtubule dynamics mutants *bot1* and *prefoldin6* (*pfd6-1*) display a lower resistance to the necrophytic pathogen *Sclerotinia sclerotiorum*, in association with defects in the upregulation of immunity genes after an infection (e.g. *BONZAI1* (*BON1*)). Interestingly, part of this response seems to be microtubule-independent and, following the results from this PhD, could thus involve FER. Indeed, the mutant background *pfd6-1* does not alter the infection-triggered downregulation of the immunity gene *MID1-COMPLEMENTING ACTIVITY 1* (*MCA1*), which upregulates JA signaling (Engelsdorf et al., 2018). To support this idea, there is also indirect evidence of a CrRLK protein in this pathway: *MCA1,* a mechanosensitive Ca^{2+} channel, is acting downstream of THE1 (Engelsdorf et al., 2018; Yamanaka et al., 2010), linking thigmommunity to CrRLKs in a microtubule-independent manner. We could then speculate that FER (or other CrRLKs) would be able to regulate several immunity genes through mechanosensing. Even further, FER may be able to interpret different signals as similar mechanical cues, and to integrate them into a broad mechanical response. This could explain how FER plays a role in so many different phenotypes and integrates so many different environmental cues.

Considering the pleiotropic role of FER in *A. thaliana*, we can wonder about the contribution that other RLKs (and in particular CrRLKs) play in wall sensing and in particular in mechanosensing. The *ERECTA* RLK for example shares with *FER* a dual role in immunity and development (Sánchez-Rodríguez et al., 2009). Some RLKs appear closer to *FER* than others: its closest homologs ANXUR1/2 (ANX1/2) are expressed in pollen and are also involved in fertility (Boisson-Dernier et al., 2009). Interestingly, one of the only tissues where *FER* is not expressed is pollen (Escobar-Restrepo et al., 2007). FER and ANX1/2 appear to play complementary roles in respectively female and male fertility as pollen tubes do not burst in *fer* pistils, whereas *anx1 anx2* pollen tubes burst before reaching the female gametophyte (Boisson-Dernier et al., 2009; Huck et al., 2003; Miyazaki et al., 2009; Rotman et al., 2003). This defect can also be related to that of another tip-growth cell type in *fer*: root hairs tend to burst, similarly to the pollen tube in *anx1 anx2* (Duan et al., 2010).

THE1 and *HERK1* also share similarities with *FER*. Indeed, those three CrRLKs are coexpressed (Ruprecht et al., 2014) and a double mutant line *herk1 the1* exhibits a similar transcriptome profile than a miRNA line reducing FER levels (Guo et al., 2009). *herk1 the1* plants also seem to display burst cells in their petiole (Guo et al., 2009), as well as defects in the salt stress response including high cotyledon bleaching and a low root growth recovery after a salt stress (Gigli-Bisceglia et al., 2021), similarly to *fer* mutants. Interestingly, *THE1* itself appears involved in the coordination of turgor and cell wall stiffness in root cells (Bacete et al., 2022) and in that presumably fills a very close function to FER.

One answer to these questions about function and redundancy can be found in the light of evolution. In *Marchantia polymorpha*, only one gene can be found in the CrRLK family, similar in sequence to *THE1* (Honkanen et al., 2016) and most often called *MpFER* (Westermann et al., 2019). It is expressed in most tissues, and the phenotypes found in *M. polymorpha* mutants of this gene are very similar to the ones in *A. thaliana* CrRLK mutants: defects in cell size and mechanical integrity leading to defects in thallus size, defects in tip-growing cells (rhizoids), in reproduction, etc (Mecchia et al., 2020; Westermann et al., 2019). The high number (17) of CrRLKs genes in A. thaliana is due to gene duplication, which could lead to functional redundancy and functional diversification: *AtTHE1* appears to have a role in resisting isoxaben treatments, which *MpFER* does not (Mecchia et al., 2020). These evolutive events led *AtFER* and *MpFER* to not fully complement each other interspecifically, in a process probably linked to subfunctionalization and neofunctionalization (Mecchia et al., 2020). More studies could help reveal the distribution of the specific functions of *MpFER* in CrRLKs.

Another question arising from my research is the role of apoplastic water on cell mechanical properties. Indeed, in addition to the high matrix potential that a network of carbohydrates is bound to create, the cell wall holds ions, sugars and proteins and as such must display a high osmotic pressure. The cell wall thus attracts water and in fact is composed of 75-80% of water (Cosgrove, 1997). Whether this amount of water is regulated by the cell is still an open question. In theory, this would be a very straightforward way for the cell to control its turgor pressure, simply because the apolastic compartment is smaller and is the interface at which hydrostatic pressure develops. We could expect this regulation to encompass ion displacement and cell wall material production. A higher water attractivity in the cell wall could eventually affect the mechanical properties of the cell and consequently

growth, first because of a decreased difference in water potential between the cell and the cell wall. In addition, water localization could have an impact on the mechanical properties of the cell wall. Most experiments on the cell wall are conducted in well hydrated mediums because of the high viscosity of in vitro cell walls and of the other roles of water in plant life. However, the incompressibility of water may play a role in the resistance of cell wall to mechanical forces. Moreover, since demethylesterified pectins are often under an anionic form, the conformation of pectins and its impact on cell growth *(Haas et al., 2020)* is most certainly linked to water presence in the cell wall. This calls for a deep analysis of water content (with related parameters, such as matrix potential or porosity) in cell walls. Emerging approaches with artificial cell walls may be a promising to address these question (see e.g. (Stimpson et al., 2020)).

In this context, cell wall porosity may be a prime subject of study. It describes the space in between cell wall elements and is strongly dependent on cell wall material deposition (Liu et al., 2019; Rondeau-Mouro et al., 2008). Cell wall porosity could be involved in the exchanges of water and solutes between cells and the cell wall, and between different cells through the apoplastic pathway. Its impact on the mechanical properties of the cell wall has not been examined yet, but as an indirect indication of crosslinks between cell wall elements, studying cell wall porosity could help better understand cell wall properties. Because the cell wall largely remains a black box, with many counterintuitive or contradictory findings, provocative models are emerging: for example, the hypothesized mechanical hotspots have been postulated to act as growth-liming sites in the cell wall (Park and Cosgrove, 2015). The contribution of turgor in cell wall deformation is even questioned (Haas et al., 2020). Finally, the role of cell edges as landmarks of polarity and of geometry for microtubule nucleation is starting to appear, with new questions about their role in mechanics (Kirchhelle et al., 2019).

This study was conducted in Arabidopsis, but other model organisms may help understand the functions of FER (or its homologs). In particular, FER homologs have been identified in several crops (strawberry, apple, tomato) for fruit ripening through its action on hormonal pathways (Jia et al., 2017a; Jia et al., 2017b). Homologs of FER have also been found in the rice crop, where it plays a role in morphogenesis, fertility and immunity (Li et al., 2016b). Interestingly, rice is a crop often grown in fresh water and as such has a strong mechanical response to hypo-osmotic shocks (Kurusu et al., 2012a; Kurusu et al., 2012b). Studying the

mechanical role of FER could thus provide new understandings of its function, in this species as well as in other species where water plays an important role: for example species with explosive seed dispersal (e.g. *Cardamine hirsute* (Galstyan and Hay, 2018)).

Conversely, new experimental and computational modelling approaches may be necessary to go beyond the current bottlenecks. If growth has been extensively investigated, cell mechanical integrity still remains unexplored. We also discussed here the contribution of water in cell walls as an emerging topic of study. This could be extended to the contribution of local heterogeneities in cell walls (in composition, texture, mechanical properties, dynamics, etc.) as well as its lack of order. Very much like computational models of microtubule arrays emerging from local interactions, and explaining many large-scale behaviors and structures, we are still missing a wall model which would account for such self-organized behavior.

Nomenclature

Abbreviations

A. thaliana	*Arabidopsis thaliana*
ABA	Abscisic acid
ABI2	ABA insensitive 2
ACR4	*Arabidopsis thaliana* homolog of crinkly 4
AGPs	Arabinogalactan proteins
ALE2	Abnormal leaf shape 2
ANX1	Anxur 1
ANX2	Anxur 2
ARFs	Auxin response factors
ATL6	Arabidopsis tóxicos en levadura 6
ATML1	*Arabidopsis thaliana* meristem L1
B^+	Boron ion
BAK1	BRI 1-associated kinase 1
BON1	Bonzai 1
BOT1	Botero1 (Katanin protein)
BRI1	BR insensitive 1
BRs	Brassinosteroids
C/N	Carbone/Nitrogen
Ca^{2+}	Calcium ion
CDKAs	A-type cyclin-dependent kinases

CEL12A	Cellulase family-12A
CESAs	Cellulose synthases
CMFs	Cellulose microfibrils
CMTs	Cortical microtubules
Col-0	*Columbia-0* (ecotype)
CrRLK/CrRLK1L	Catharanthus roseus RLK/Catharanthus roseus RLK 1-like
CSI1	CESA interactive protein 1
CUCs	Cup shaped cotyledon genes
CVY1	Curvy 1
CW	Cell wall
DAG	Days after germination
DEK1	Defective kernel 1
DIL9	Drought induced like 9
DMSO	Dimethyl sulfoxide
DNA	Deoxyribonucleic acid
DW	Dried weight
EBP1	ErbB3-binding protein 1
EFR	EF-Tu receptor
EF-Tu	Elongation factor thermo unstable
eIF4E1	Eukaryotic translation initiation factor 4E1
EXPs	Expansins
EXTs	Extensins
FER	Feronia

FLG22	Flagellin sensitive 2
FLS2	Flagellin-sensing 2
FW	Fresh weight
GFP	Green fluorescent protein
GPI-APs	Glycosylphosphatidylinositol-anchored proteins
GRP7	Glycine-rich RNA binding protein 7
GST	Glutathione S-transferase
GTP	Guanosine-5'-triphosphate
H^+	Hydrogen ion
HD-ZIP IV	Homodomain-leucine zipper IV
HERKs	Hercules receptor kinases
HGs	Homogalacturonans
HRB1	Hypersensitive to red and blue 1
JA	Jasmonic acid
K^+	Potassium ion
KTN	Katanin
LLGs	LRE-like GPI-APs
LRE	Lorelei
LRXs	Leucine rich repeat extensins
MBD	Microtubule binding domain (from MAP4)
MCA1	Mid1-complementing activity 1
mCit	mCitrine
MDIS1	Male discoverer 1

$MgCl_2$	Magnesium chloride
MIK2	Mdis 1-interacting receptor-like kinase 2
mRNA	Messenger ribonucleic acid
MSL10	Mechanosensitive channel of small conductance-like 10
Na^+	Sodium ion
NaCl	Sodium chloride
NEK6	NIMA Related Kinase 6
NIMA	Never in mitosis, gene A
NMR	Nuclear magnetic resonance
NPA	Naphtylphtalamic acid
PAMPs	Pathogen associated molecular patterns
PCA	Principal component analysis
PDF1	Protodermal factor 1
PDF2	Protodermal factor 2
PFD6	Prefoldin6
PGs	Polygalacturonases
PGA	Polygalacturonic acid
PI	Propidium iodide
PINs	Pin-formed proteins (auxin efflux carriers)
PIPs	Plasma membrane intrinsic protein
PMEs	Pectin methylesterases
PMEIs	PME inhibitors
PPB	Preprophase band

RALFs	Rapid alkalinization factors
RD26	Responsive to desiccation 26
RIPK	Resistance to Pseudomonas Syringae1-induced protein kinase
RLKs	Receptor-like kinases
RMA channel	Rapid mechanically activated channel
ROPs	Rho-like GTPases
ROP-GEFs	ROP guanine nucleotide exchange factors
ROS	Reactive oxygen species
RW	Rehydrated weight
RWC	Relative water content
SA	Salicylic acid
SAM	Shoot apical meristem
SHV3	Shaven 3
SPR2	Spiral 2
SRN	Siren
STM	Shoot meristemless
TCHs	Touch response genes
TEM	Transmission electron microscopy
TFR1	THE1/FER related 1
THE1	Theseus1
TM	Transmembrane
TUA	Tubulin alpha
TUB	Tubulin beta

UV	Ultraviolet
WAKs	Wall-associated kinases
WS-4	*Wassilewskija-4* (ecotype)
WT	Wild type
XTHs	Xyloglucan endotransglucosylases
XXTs	Xyloglucan xylosyltransferases

Symbols

A	Area
c_M	Molar concentration
d	Deformation
E	Apparent elastic modulus
F	Force
i	Van't Hoff index
J	Flux of water
k	Stiffness
L	Diffusion coefficient
l	Length
P	Turgor pressure
R	Molar gas constant
r	Volumetric expansion
S	Surface of diffusion
T	Temperature
Y	Yield pressure
ε	Strain
Π	Osmotic pressure
σ	Mechanical stress
Φ	Cell wall extensibility
Ψ	Water potential

Annexes

Annexe 1: Internship report from Mylan Ansel (L3 student). Shape, cell wall stiffness and turgor pressure of pavement cells.

Annexe 2: Internship report from Théophile Peyraud (L3 student). Perfectionnement du protocole de recherche permettant de mettre en évidence la réponse des microtubules du mutant *feronia* (*fer-4*) chez *Arabidopsis thaliana*.

Annexe 3: Internship report from Amaya Richer (L3 student). Changing mechanical integrity in *Arabidopsis thaliana* FERONIA mutant with growth conditions.

Shape, cell wall stiffness and turgor pressure of pavement cells

Mylan Ansel[1]

[1]Laboratoire Reproduction et Développement des Plantes, Ecole Normale Supérieure de Lyon, France

Introduction

Shape and functions of cells are related. In plants, cells display an important diversity of shape. For instance, leaf and cotyledon epidermal cells can have various shapes like trichomes, stomatal or pavement cells. Existing in many eudicot plants, pavement cells present a complex shape composed of necks and lobes making them look like jigsaw-puzzle pieces (1). Their formation requires a highly regulated cell growth (2–4).

Cell growth depends on two main parameters: turgor pressure and cell wall stiffness (5). The turgor pressure, caused by the water stored within cells, pushes the membrane against the cell wall, generating a pressure on it. Thus, it causes stress on the cell wall, that elastically or plastically deforms. The primary cell wall, that surrounds plant cells and resists turgor pressure, is notably composed of cellulose. Its disposition, which is guided by microtubules, mainly determines the resistance of the cell wall against the turgor pressure. Because microtubule organization responds to the stress, it creates a stress feedback loop which is essential for puzzle shape formation. In addition, independently of microtubules, other mechanisms control the cell wall stiffness (6).

Functions of puzzle shape are still unclear. It has been suggested that this shape could play a role in chemical signaling or tissue integrity (7–9) and, more recently, that it would allow cell size increase without increasing cell stress (10). In circular cells, the stress will increase with cell size and become, after reaching a threshold, high enough to break the cell wall. In puzzle shaped cells, the stress will increase more slowly with cell size, turning the threshold for rupture above non physiological stress values.

Nevertheless, some mutant plants display pavement cells without a puzzle shape (4). While these cells must be exposed to a higher stress, no cell wall rupture has been observed. Two hypotheses are conceivable: either the puzzle shape does not play a role in preventing cell bursting, or compensation mechanisms that prevent cell bursting are triggered in those cells. This compensation could be an increase of cell wall stiffness or a decrease of turgor pressure, both resulting in a stress decrease.

Here we investigated compensation upon loss of puzzle cell shape. For this purpose, we altered pavement cells shape of cotyledons of A*rabidopsis thaliana* by disrupting microtubule organization via oryzalin, and quantified cell wall stiffness as well as turgor pressure.

Results

Puzzle shape is lost when pavement cells grow exposed to oryzalin.

To change pavement cell shape, we made the plants grow in mediums with increasing concentration of oryzalin, a drug which depolymerizes microtubules (11). We used a fluorescent microtubules reporter (*pPDF1::mCitrine-MBD*) to confirm that they were disturbed (Supp data 1).

Then, to quantify the shape change, we took pavement cells images for each condition with confocal microscopy (Fig 1). We used a propidium iodide (PI) treatment to visualize cell walls. We found that cells became smaller when oryzalin concentration increased (Fig 1A,B). To quantify how lobed cells were, we calculated the solidity (1), defined as the cell area divided by the convex hull area (Fig 1C). The less a cell has lobes, so the further away from a puzzle shape it is, the closer to 1 its solidity is. The solidity increased with oryzalin concentration (from 0.75 without oryzalin to 0.95 from 5µM) meaning that pavement cells progressively lost their puzzle shape (Fig 1D). After 10µM, there were no significant differences of shape between conditions (Fig 1A,D) and some pavement cells started dying, as shown by the PI inside cells. In addition, we found some burst cells (some of them are indicated by red arrows), potential indicators of too high stress (Fig 1A). So, because these pavement cells lost their puzzle shape, were they exposed to a higher stress?

The Largest Empty Circle (LEC) (Fig 2A) is known to be a proxy of the stress (10). We observed that the LEC increases linearly with cell area (Fig 2B), meaning that the bigger the cell, the larger the LEC, and therefore the higher stress it was exposed to. However, the slope of the ratio LEC/area was steeper the higher the oryzalin concentration. This confirms that puzzle shape is a way to reduce the stress during cell growth. The LEC radius was higher for cells exposed to 0.5, 1 and 2µM of oryzalin than for untreated cells (Fig 2C). This can be explained by the fact that for these conditions, cells were more circular, but their area was still large.

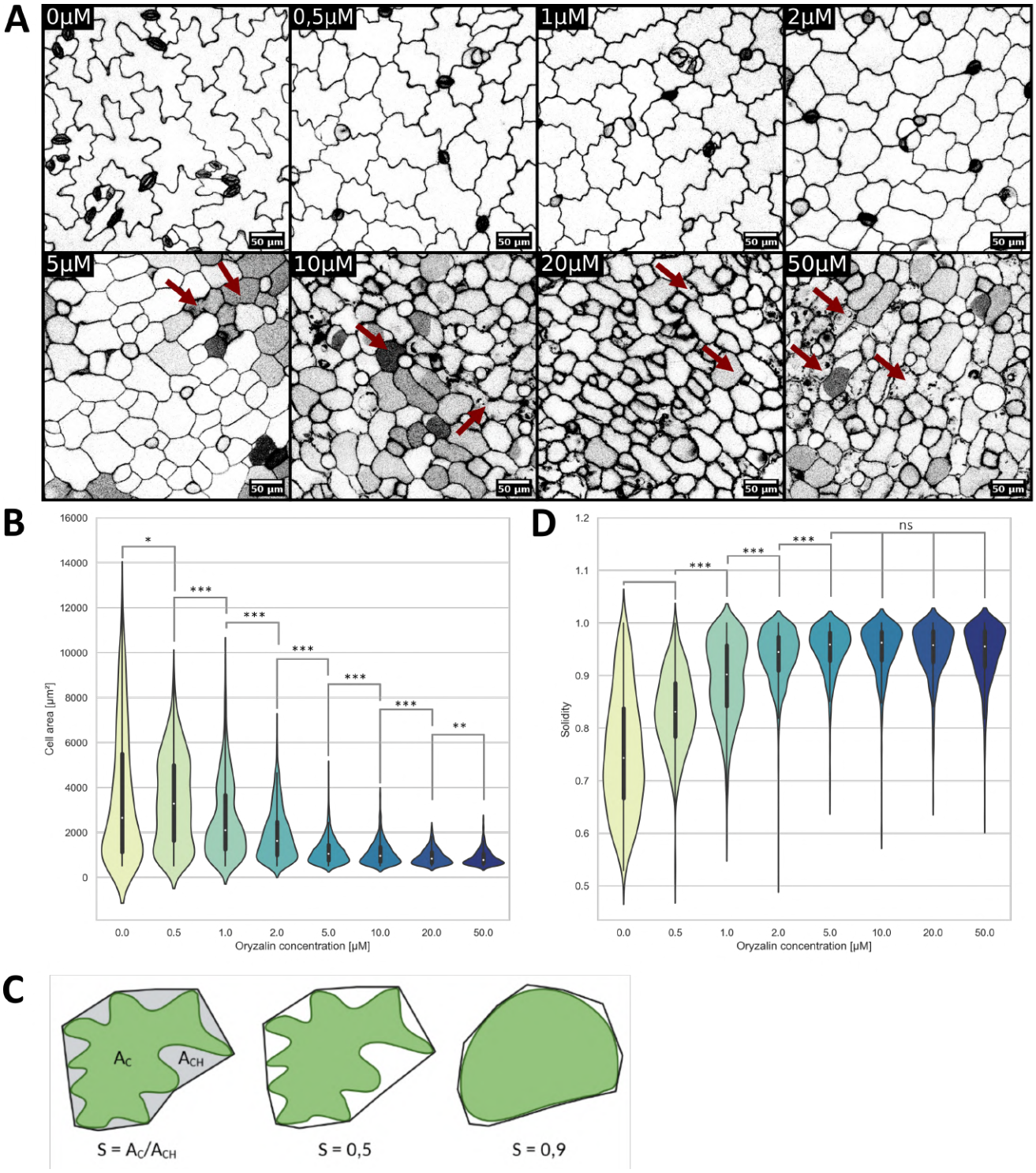

Fig. 1. Pavement cells lose their puzzle shape when plants grow exposed to oryzalin.
Shape analysis of pavement cells of *Col-0* cotyledons. **(A)** Representative confocal images for oryzalin concentrations after a PI treatment (45µM, 30min). Colors are inverted, red arrows indicate some burst cells. **(B)** Cell area for each condition. **(C)** Schematic representation of solidity (cell area divided by convex hull area). **(D)** Solidity for each condition. Statistical analysis on at least 518 cells and 4-6 cotyledons. Mann Whitney test, ns: p-value>0.5, *: p-value<0.05, **: p-value<0.01, ***: p-value<0.001. .

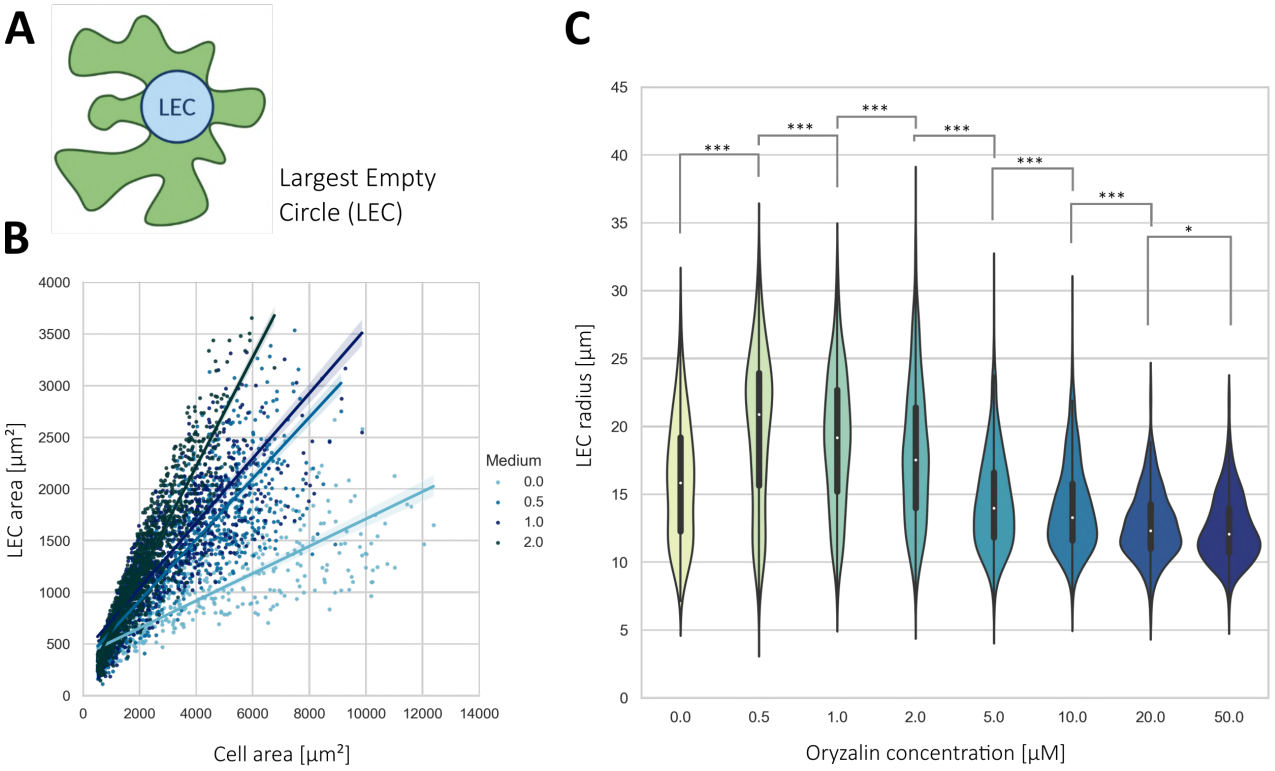

Fig. 2. Pavement cells are not exposed to the same stress in each condition.
Largest Empty Circle (LEC) analysis of pavement cells of *Col-0* cotyledons. **(A)** Schematic representation of the LEC. **(B)** LEC area in function of cell area for 4 oryzalin conditions, R^2 are respectively 0.67, 0.73, 0.74 and 0.87 for 0, 0.5, 1 and 2µM. **(C)** LEC radius for each condition. Statistical analysis at least 518 cells and 4-6 cotyledons. Mann Whitney test, *: p-value<0.05, ***: p-value<0.001.

Thus, if we make the hypothesis that turgor pressures were similar between these conditions, the stress is predicted to be more important. In contrast, after 5µM of oryzalin, the LEC became smaller than for untreated cells. Surprisingly, while cell area, and therefore LEC were smaller for these concentrations, it was also the only ones in which we observed cells burst.

No detectable compensation for puzzle shape loss by cell wall stiffening.

The stress was predicted to be more important for 0.5, 1 and 2µM of oryzalin. Thus, it is possible that cells compensated for it by stiffening their cell wall. To test it, we determined the relative cell wall stiffness. After a PI treatment, we measured cell area in water and after 50min in a sorbitol solution. This osmotic treatment plasmolyzed cells and thus the plasma membrane no longer pushed on the cell wall (Fig 3A). Therefore, upon relaxation the cell wall shrinks. The more the cell wall shrinks, the less it is stiff (12). We confirmed that plasmolysis occurred by visualizing the plasma membrane (*pATML1::mCitrine-RCI2A*) for all oryzalin concentrations (Fig 3A for 0µM, data not shown for other concentrations). In addition, we controlled that the cell area did not impact shrinkage measures (Fig 3B), nor the cell shape (Fig 3D). Surprisingly, we noticed a huge variability of measures between cotyledons of the same condition (Fig 3C). The shrinkage increased with oryzalin concentrations, from 10.4% at 0µM to 16.7% at 2µM (Fig 3E). Hence, cell walls became less stiff when cells were grown exposed to oryzalin meaning there is no compensation by cell wall stiffening. However, another possibility is compensation by a decrease of turgor pressure.

Pavement cells might compensate for puzzle shape loss by decreasing their turgor pressure.

To see if turgor pressure changes in response to puzzle shape loss, we measured the global turgor pressure of cotyledons. We successively measured cotyledon area after 15min in solutions with an increasing concentration of NaCl (Fig 4A). We determined the osmotic pressure of each NaCl solution (0, 0.538, 0.841, 0.968, 1.050, 1.139, 1.291, 1.537 and 1.939MPa). Thus, by dividing the cotyledon area in each solution by the one in the solution with no NaCl, we obtained the relative cotyledon area in function of the osmotic pressure of the solution (Fig 4B,C). First, we calculated the shrinkage of cotyledons (Fig 4D). This shrinkage, defined with the relative cotyledon area in the last NaCl solution, increased with increasing oryzalin concentrations (from 17.6% at 0µM to 23% at 2µM). This trend is consistent with our precedent measures (Fig 3E), nevertheless, the values are around 40%

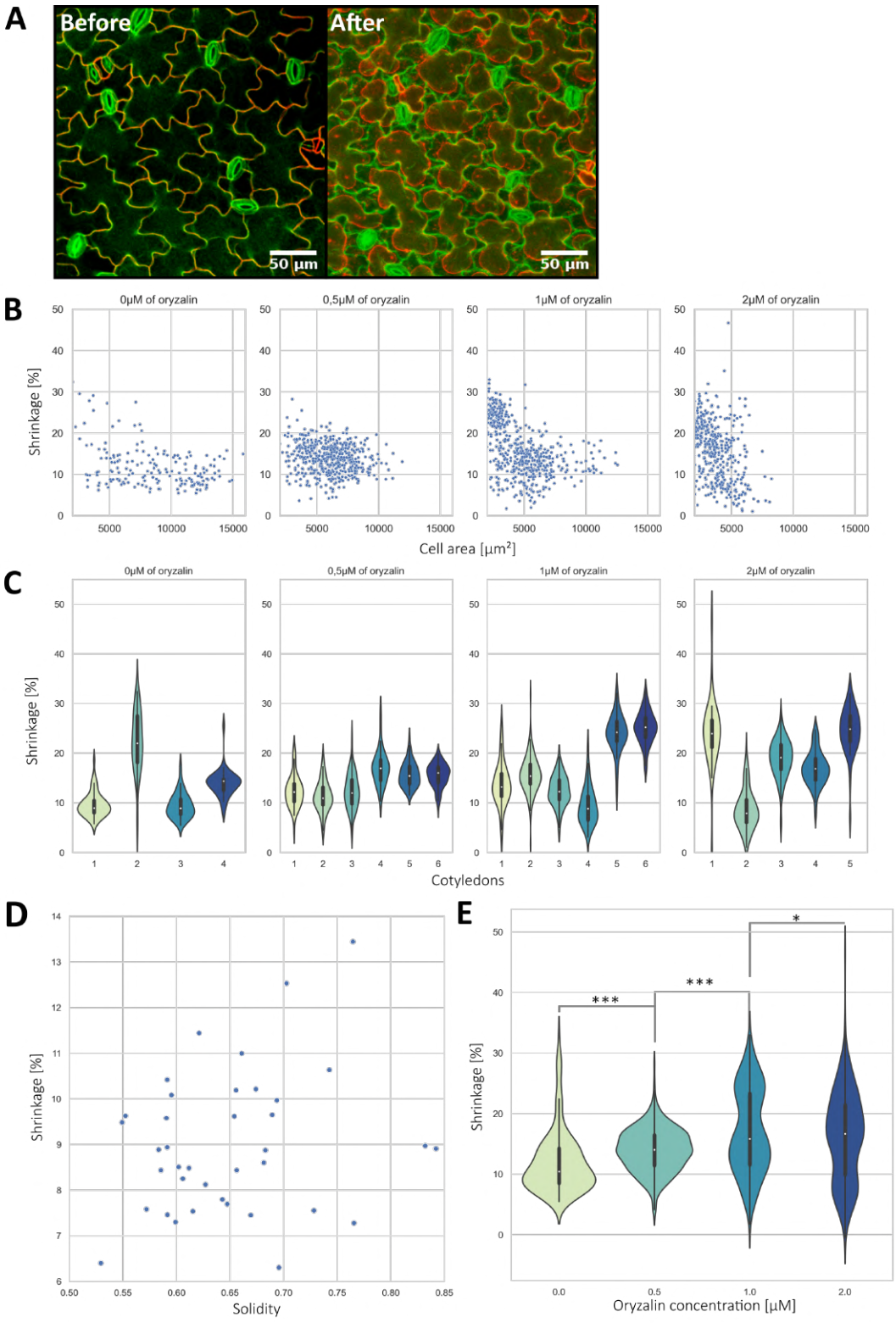

Fig. 3. Pavement cells do not compensate for puzzle shape loss by cell wall stiffening

Shrinkage measures of pavement cells of *Col-0* cotyledons for 4 oryzalin conditions after an osmotic treatment (50min in sorbitol 0.6M). **(A)** Representative image of a cotyledon not exposed to oryzalin, before and after the osmotic treatment. Cell walls are in green (PI) and plasma membrane in red (*pATML1::mCitrine-RCI2A*) **(B)** Shrinkage in function of cell area. **(C)** Shrinkage for each cotyledon. **(D)** Shrinkage in function of solidity for one cotyledon not exposed to oryzalin. **(E)** Shrinkage measures for each condition. Statistical analysis on at least 189 cells and 4-6 cotyledons. Mann Whitney test, *: p-value<0.05, ***: p-value<0.001.

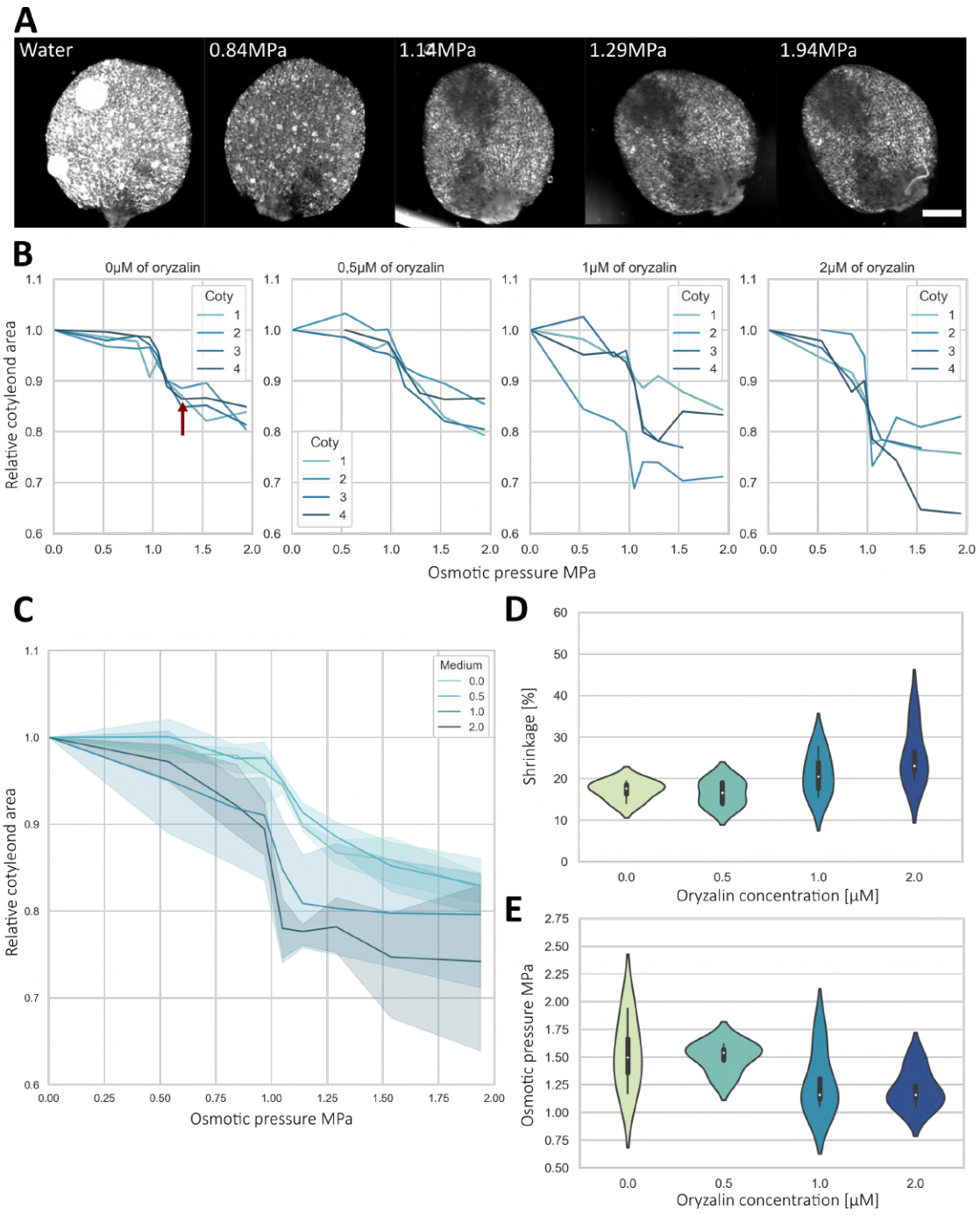

Fig. 4. Pavement cells might compensate for puzzle shape loss by decreasing their turgor pressure
Turgor pressure analysis for 4 oryzalin conditions **(A)** Representative images of a cotyledon not exposed to oryzalin after 15min successively in different NaCl solutions. Scale bar = 100µM **(B)** Relative cotyledon areas in function of the osmotic pressure of the NaCl solutions. The red arrow indicates one inflexion point **(C)** Average relative cotyledon areas for each oryzalin condition (mediums). **(D)** Shrinkage of cotyledons for each condition. **(E)** Osmotic pressure corresponding to the inflexion point of each curve in (B). No statistical analysis because too few repetitions (n=4).

higher. Secondly, we obtained relative indications of turgor pressure in cotyledons. Indeed, when the osmotic pressure in the medium increases, the turgor pressure decreases (13). At the inflexion point (one is indicating by a red arrow in Fig 4B), the turgor pressure is equal to zero. Thus, the lower the osmotic pressure corresponding to this point is, the lower the initial turgor pressure was. It seems that the inflexion point is reached for a lower osmotic pressure when oryzalin concentration increases, 1.49MPa at 0µM and 1.16MPa at 2µM of oryzalin (Fig 4E). This trend might indicate a compensation by a decrease of turgor pressure. However, because of time constraints, only four samples per condition were measured and no statistical conclusions can be drawn.

Discussion

We saw that pavement cells lose their puzzle shape when grown exposed to oryzalin. At higher concentration, they become smaller, and many cells burst and die. At lower concentration they keep practically their standard size. For these conditions, we measured no compensation via cell wall stiffening but our preliminary results seem to indicate a compensation by a decrease of turgor pressure.

We confirmed that oryzalin disturbed pavement cells shape (14), but it could impact more than just the shape. Likely it may affect cell number (15) or cause chemical stresses. To confirm that our results are a direct consequence of shape change, we could use mutants with circular pavement cells like katanin mutants (16). We could also count the number of pavement cells in each cotyledon to check our results are not due to improper cell numbers, however, it seems that pavement cell divisions are resistant to oryzalin treatments (14).

We saw that cell grown with 5µM of oryzalin have a LEC smaller than untreated cells (Fig 2C) in correlation with a 3 times smaller cell area (Fig 1B). If we expand the cell wall weakening trend we measured, it is also possible that the cell wall becomes so weak that cells cannot even resist the tensile stress applied. In this hypothesis, only small cells (which undergo a lower stress) would resist the tension (10). Small cell size could then be a direct consequence of cell bursting, even though we cannot rule out a controlled regulation by cells to prevent such bursting or growth limitations due to biotic stress. Quantification of cell bursting (Fig 1A) revealed to be quite difficult with our setup but would likely help answering those questions.

Shrinkage measures are based on two main hypotheses. The first one is that the cell wall must be in the same tensile state for the different conditions before the plasmolysis experiment. The second one is that cell walls must react independently of cell shape to plasmolysis and therefore for the different conditions. We found no correlation between shrinkage and cell area or solidity, suggesting independence of cell shape and plasmolysis (Fig 3B,D). Unfortunately, the first one may not be completely respected because it seems that turgor pressure is not the same in each condition (Fig 4E). However, it would mean that we overvalued the cell wall stiffness for conditions with oryzalin meaning that its reduction would be more important than what we measured. The variability of shrinkage between cotyledons of the same condition (Fig 3C) may indicate imprecisions of quantification or be caused by natural variability between individuals. Increasing the number of repetitions and performing measurements via other methods such as AFM would help answer these questions.

In opposition to our hypothesis, the cell wall stiffness decreases when pavement cells lose their shape (Fig 3E, 4D). It may be because cellulose disposition is less efficient when microtubules are disturbed (17). Other mechanisms which could reinforce the cell wall would not be sufficient to counterbalance this cellulose loss. A chemical analysis of the cell wall would both reveal how cellulose and other components are affected. The differences between our two measures of cell wall stiffness (Fig 3E, 4D) could be explained because on one side we measured cell contraction and tissue contraction on the other.

Direct measures of turgor pressure are complicated. With our protocol, osmotic pressures at the inflexion point are supposed to be equal to turgor pressures but their values clearly exceed other estimation (13). It is known that this protocol overestimates real values (13), but we can assume that relative differences are conserved. Thus, our preliminary results seem to indicate a turgor pressure regulation in response to the stress. It could implicate mecanosentive ion transporters, aquaporins and other mechanosensors (13).

In conclusion, we propose here a method which highlights compensation linked with cell wall defects. This method could be used to identify and verify the role of mechanosensors or other actors of this compensation.

Materials & Methods

Plant materials and growth condition.

Three genotypes have been used: *Col-0*, *pAR169* (*pATML1::mCitrine-RCI2A*) to see the plasma membrane, and *mCit-MBD* (*pPDF1::mCit-MBD*) which marks microtubules. We used MS medium (0.7% agar, no sugar and vitamins) with addition of oryzalin at different concentrations (0, 0.5, 1, 2, 5, 10, 20, 50µM) and with compensatory volumes of DMSO. Seed surface sterilized, individually sown and stratified in the cold room for one night. Seedlings were then placed to grow in long-day phytotrons (20°C, 16h light) and observed 6 days after germination.

Image acquisitions.

For shape and cell wall study, cotyledons were dissected and imaged using a Leica SP8 microscope with x25 water immersion objective. *Col-0* and *pAR169* cotyledons were treated with a propidium iodide solution (PI) (45µM, 30min) to visualize cell walls. Using a 514nm laser excitation, the fluorescence signal was collected from 605nm to 642nm for PI and from 521nm to 551nm for *mCit-MBD* and *pAR169*. Each cotyledon was imaged first in water and again after 50min in a sorbitol solution (0.6M).

For turgor pressure study, *Col-0* cotyledons were dissected and imaged using a Nikon SMZ18 stereomicroscope with x6 zoom. They were placed between a curved microscope slide and lamella with water or NaCl solution drops. Pictures were taken after 15min in NaCl solutions of increasing concentrations (0, 0.1, 0.15, 0.175, 0.2, 0.225, 0.25, 0.3, and 0.4M).

Image analysis.

For shape analysis, we projected cell contours of *Col-0* cotyledons with an ImageJ macro, SurfCut (18) and used an ImageJ plugin, PaCeQuant (19), to automatically quantify descriptors of pavement cell shape. For cell wall study, confocal images of *Col-0* cotyledons were analyzed using MorphoGraphX (20) to extract the shrinkage (Supp data 2). For turgor pressure study, cotyledon areas were determined using a manual segmentation in ImageJ. We determined the osmotic pressure after measuring the average osmotic concentration of each solution via a Gonotec osmomat 030 cryoscopic osmometer.

Bibliography

1. Vőfély RV, Gallagher J, Pisano GD, Bartlett M, Braybrook SA (2019) Of puzzles and pavements: a quantitative exploration of leaf epidermal cell shape. *The New Phytologist* 221(1):540–552.
2. Bidhendi AJ, Geitmann A (2019) Geometrical Details Matter for Mechanical Modeling of Cell Morphogenesis. *Developmental Cell* 50(1):117–125.e2.
3. Majda M, et al. (2017) Mechanochemical Polarization of Contiguous Cell Walls Shapes Plant Pavement Cells. *Developmental Cell* 43(3):290–304.e4.
4. Lin D, et al. (2013) Rho GTPase Signaling Activates Microtubule Severing to Promote Microtubule Ordering in Arabidopsis. *Current Biology* 23(4):290–297.
5. Hamant O, Traas J (2010) The mechanics behind plant development. *New Phytologist* 185(2):369–385.
6. Marowa P, Ding A, Kong Y (2016) Expansins: roles in plant growth and potential applications in crop improvement. *Plant Cell Reports* 35(5):949–965.
7. Galletti R, Ingram GC (2015) Communication is key: Reducing DEK1 activity reveals a link between cell-cell contacts and epidermal cell differentiation status. *Communicative & Integrative Biology* 8(5):e1059979.
8. Sotiriou P, Giannoutsou E, Panteris E, Galatis B, Apostolakos P (2018) Local differentiation of cell wall matrix polysaccharides in sinuous pavement cells: its possible involvement in the flexibility of cell shape. *Plant Biology* 20(2):223–237. _eprint: https://onlinelibrary.wiley.com/doi/pdf/10.1111/plb.12681.
9. Jacques E, et al. (2014) Review on shape formation in epidermal pavement cells of the Arabidopsis leaf. *Functional Plant Biology* 41(9):914–921. Publisher: CSIRO PUBLISHING.
10. Sapala A, et al. (2018) Why plants make puzzle cells, and how their shape emerges. *eLife* 7:e32794.
11. Strachan SD, Hess FD (1983) The biochemical mechanism of action of the dinitroaniline herbicide oryzalin. *Pesticide Biochemistry and Physiology* 20(2):141–150.
12. Sapala A, Smith RS (2020) Osmotic Treatment for Quantifying Cell Wall Elasticity in the Sepal of Arabidopsis thaliana in *Plant Stem Cells*, eds. Naseem M, Dandekar T. (Springer US, New York, NY) Vol. 2094, pp. 101–112. Series Title: Methods in Molecular Biology.
13. Beauzamy L, Nakayama N, Boudaoud A (2014) Flowers under pressure: ins and outs of turgor regulation in development. *Annals of Botany* 114(7):1517–1533.
14. Akita K, Higaki T, Kutsuna N, Hasezawa S (2015) Quantitative analysis of microtubule orientation in interdigitated leaf pavement cells. *Plant Signaling & Behavior* 10(5):e1024396. Publisher: Taylor & Francis _eprint: https://doi.org/10.1080/15592324.2015.1024396.
15. Corson F, et al. (2009) Turning a plant tissue into a living cell froth through isotropic growth. *Proceedings of the National Academy of Sciences* 106(21):8453–8458.
16. Eng RC, et al. (2021) KATANIN and CLASP function at different spatial scales to mediate microtubule response to mechanical stress in Arabidopsis cotyledons. *Current Biology*.
17. Burk DH, Liu B, Zhong R, Morrison WH, Ye ZH (2001) A Katanin-like Protein Regulates Normal Cell Wall Biosynthesis and Cell Elongation. *The Plant Cell* 13(4):807–828.
18. Erguvan Louveaux M, Hamant O, Verger S (2019) ImageJ SurfCut: a user-friendly pipeline for high-throughput extraction of cell contours from 3D image stacks. *BMC biology* 17(1):38.
19. Möller B, Poeschl Y, Plötner R, Bürstenbinder K (2017) PaCeQuant: A Tool for High-Throughput Quantification of Pavement Cell Shape Characteristics. *Plant Physiology* 175(3):998–1017.
20. Barbier de Reuille P, et al. (2015) MorphoGraphX: A platform for quantifying morphogenesis in 4D. *eLife* 4:e05864. Publisher: eLife Sciences Publications, Ltd.

Supplementary data

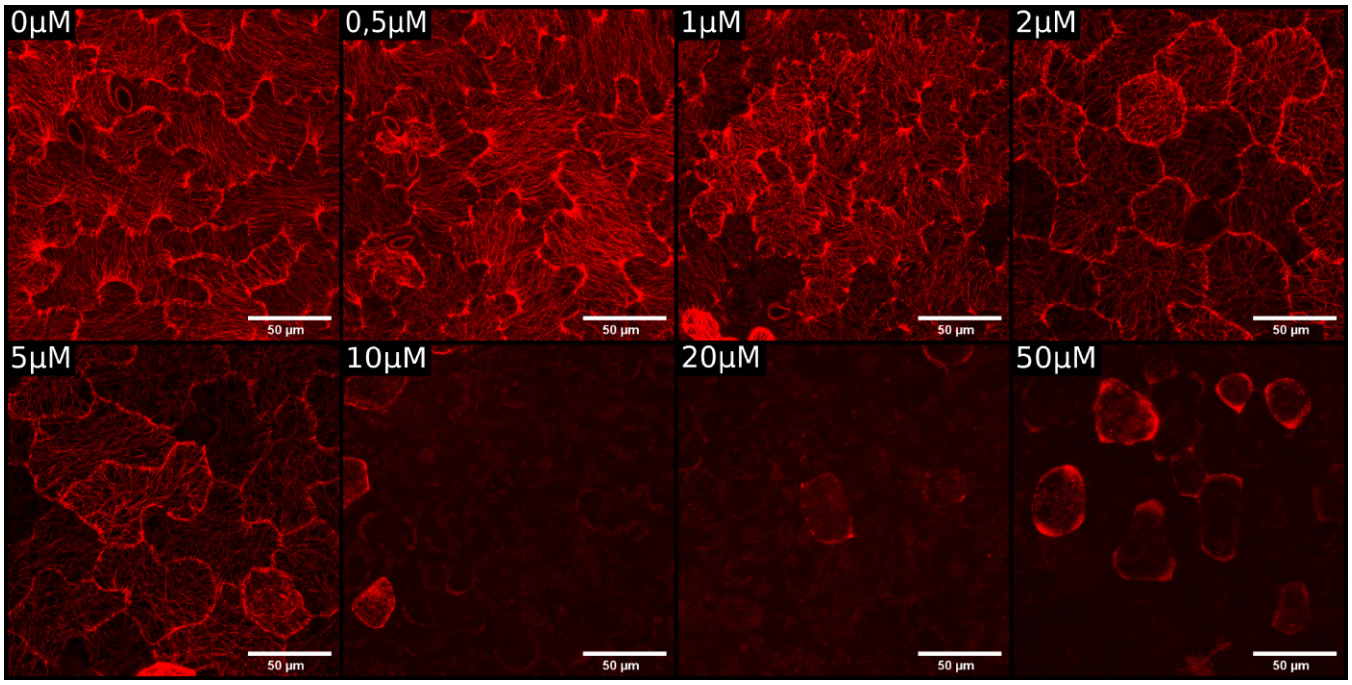

Fig. 5. Microtubules are gradually disturbed when plants grow exposed to oryzalin.
Representative confocal images of microtubules (*pPDF1::mCit-MBD*) of pavement cells for eight oryzalin concentrations. The higher oryzalin concentration is, the less microtubules are visible. Cells seemed to become more circular when oryzalin concentration increases. This confirms that microtubules are gradually disturbed when plants grow exposed to a gradual oryzalin concentration.

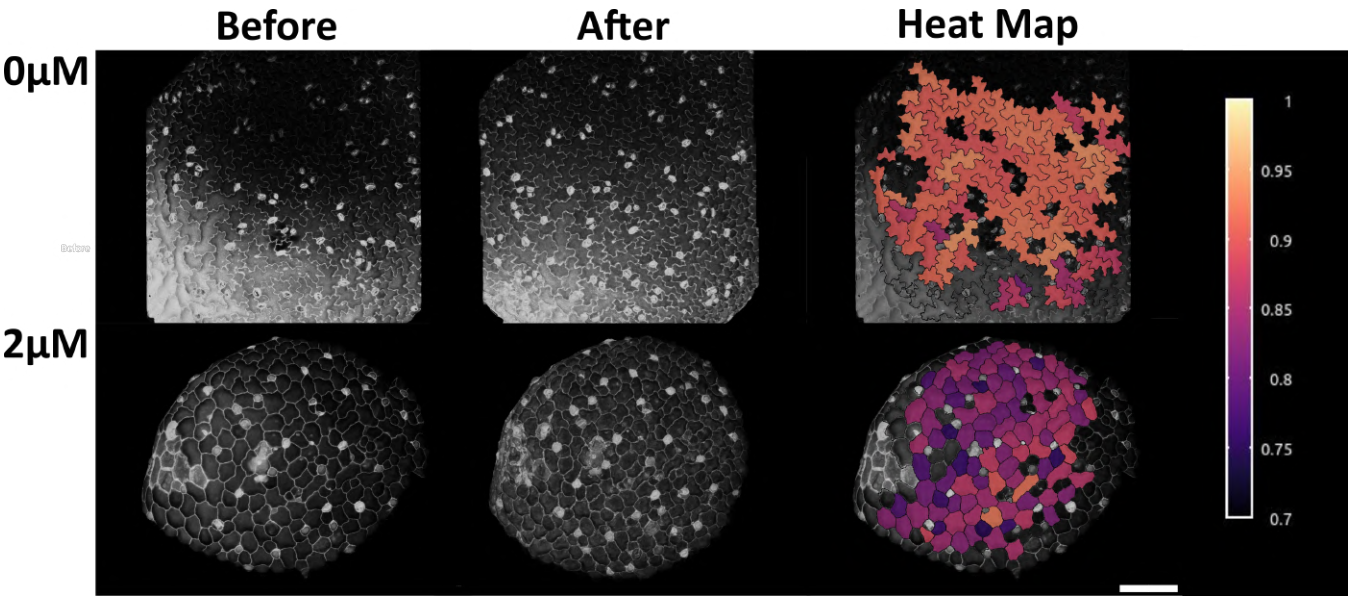

Fig. 6. Segmentation and shrinkage measures on MorphoGraphX.
Visualization of cotyledons from mediums with 0µM and 2µM of oryzalin, before and after the osmotic treatment (sorbitol 0.6M, 50min). Cell walls are visualized by a PI treatment. The comparison of cell area before and after the osmotic treatment defined the shrinkage represented on the Heat Map. The color gradient indicates shrinkage values. Scale bar = 200µm.

ESTBB
Licence Sciences de la Vie
Majeure Biologie Mineure Humanité

Faculté des Sciences
Université Catholique de Lyon
10 place des Archives
69002 LYON

Ecole Normale Supérieure de Lyon - ENS
Laboratoire de reproduction et développement des plantes – RDP

ENS de Lyon
46, allée d'Italie,
69364 LYON Cedex 07

Licence Science de la Vie – Majeure Biologie – Mineure Humanités

Rapport de Stage de 3ème année

PEYRAUD Théophile

Perfectionnement du protocole de recherche permettant de mettre en évidence la réponse des microtubules du mutant *feronia (fer-4)* chez *Arabidopsis thaliana*

Maître de stage : MALIVERT Alice & HAMANT Olivier

Stage de 3ème année, du 31 août 2020 au 16 octobre 2020

Remerciements

Je commence par remercier mon maitre de stage Alice MALIVERT, qui a su prendre le temps de m'expliquer avec passions ses projets, de me faire découvrir le monde de la recherche. Merci à toi de m'avoir encadré au cours des différentes expériences, de m'avoir fait confiance au cours de ce stage pour les manipulations, les traitements de données, et de m'avoir aidé à rédiger ce rapport. J'ai aimé travailler à tes côtés, échanger sur nos multiples sujets de conversations, et très hâte de découvrir l'issue de ce projet dont j'ai eu l'opportunité de travailler dessus durant ces 7 semaines.

Je remercie également Olivier HAMANT, pour sa réponse positive et rapide lors de ma candidature. Merci de m'avoir donné ma chance, de ta confiance pour cette période de stage et de ton aide précieuse pour la réalisation de notre interview pour ma vidéo de stage. J'ai beaucoup apprécié nos conversations, nos débats qui m'ont inspiré et qui m'aideront pour mon projet professionnel, afin de choisir un métier et un projet professionnel qui ait du sens et en accord avec mes valeurs.

Un grand merci à l'ensemble du RDP de m'avoir accueilli chaleureusement au sein du laboratoire pour ces 7 semaines de stage. Un remerciement en particulier pour l'équipe MéchanoDévo dont j'ai eu l'opportunité d'intégrer, de présenter mon projet de stage et à l'équipe Mosaic que j'ai pu rencontrer et échanger lors des pauses.

Je tiens également à remercier mon tuteur de stage, de l'ESTBB de l'Université Catholique de Lyon, Yohann BESSET-MANZONI, qui a su me guider pour l'écriture, et la relecture de ce rapport.

Table des matières

Liste des abréviations

Col-0 : *Arabidopsis thaliana*, lignée sauvage Columbia provenant de Californie.
fer-4 : *Arabidopsis thaliana,* lignée mutante du gène FERONIA (codant pour un receptor-like kinase)
mcit : Protéine fluorescente.
MTs : Microtubules.
Pi : Iodure de Propidium.
RDP : Laboratoire de Recherche et Développement des Plantes.
WT : Wild Type.

Glossaire

Apex (nom) / apical (adj) : Extrémité d'un organe (tige, racine, pousses…). Chez les végétaux, lieu où les cellules qui se sont divisées s'allongent.
Arabidopsis thaliana : Plante du genre herbacées de la famille des Brassicaceae, utilisée en biologie végétale et biologie fondamentale comme organisme modèle.
Cellules pavimenteuses : Cellules épidermiques des cotylédons et des feuilles ayant une forme particulière de puzzle, intéressantes pour étudier les différents patrons de contraintes.
Echelle subcellulaire : Niveau en dessous du niveau cellulaire.
Echelle tissulaire : Au niveau des tissus.
fer-4 : Lignée mutante dans l'écotype Columbia, très caractéristique du fait de ses cellules qui explosent naturellement, de son absence de poils racinaires et de sa couleur légèrement violette sur les nervures des feuilles.
FM4-64 : Colorant lipophile permettant de colorer sélectivement les membranes d'une fluorescence rouge.
Hypocotyle : Zone formant la tige de la plantule qui se situe entre la zone racinaire et la zone apicale sous les cotylédons.
mcit : Protéine émettant dans le vert (550 nm) lorsqu'on l'excite dans le vert (514 nm) issue d'Aequorea victoria (méduse bioluminescente).
Méristème : Tissu de cellules souches végétales (non-différenciées, pluripotente, à multiplication rapide).
Microtubules : Organites cylindriques composés de 13 protofilaments de tubuline α et β, faisant partie du cytosquelette, assurant entre autres un rôle de support structural chez les cellules végétales.
Morphogénèse : Ensemble des transformations permettant la création de formes, et de structure.
Oryzalin : Drogue utilisée pour dépolymériser les microtubules.
Pi : Colorant qui se fixe sur les charges négatives de la paroi végétale (pectines démethylestérifiées) et du noyau lorsqu'il rentre dans les cellules et renvoie une lumière fluorescente dans la rouge (650 nm) lorsqu'on l'excite dans le vert (514 nm).
Pression de turgescence : Pression exercée par l'eau lorsqu'elle s'infiltre dans les cellules végétales, créant un gonflement de la cellule en poussant la paroi pectocellulosique à son maximum.
Propriété isotrope / anisotrope : Propriété non dépendante de la direction (isotrope) ou dépendante d'une ou plusieurs directions (anisotrope). Utilisé pour qualifier un stress mécanique s'exerçant dans toutes les directions ou dans une direction principale.
Stress mécanique : Force mécanique exercée sur une surface, perpendiculaire à la déformation créée par la force.
Wild Type : caractérise un individu issue d'une lignée sauvage, sans mutation.

Introduction générale

J'ai récemment été accueilli au laboratoire de reproduction et développement des plantes (RDP) au sein de l'école normale supérieure de Lyon (ENS), afin d'effectuer mon stage de 3ème année de licence « Sciences de la vie & Humanité » à l'Ecole Supérieure de Biologie-Biochimie, Biotechnologie (ESTBB). Le RDP centre son travail sur la recherche fondamentale en développement végétatif et reproducteur végétal, à différentes échelles, du génome à l'organisme.

Ainsi, différentes équipes couvrent différentes spécialités dans lesquelles, on retrouve la biophysique du développement, l'évolution de la fleur, la modélisation informatique, le développement de la graine, ou encore la biologie cellulaire. Ces équipes collaborent autour de plusieurs projets de recherche en développement végétal.
Le RDP s'est forgé une renommée sur la scène internationale, grâce aux grands noms de la recherche comme Jan Traas, Teva Vernoux, Olivier Hamant, Yvon Jaillais, Arezki Boudahoud et des découvertes telles que le séquençage de la rose ont permis d'ouvrir les portes de journaux internationaux (Nature, Science…).

Au cours de ce stage, j'ai principalement travaillé sur l'amélioration et le perfectionnement d'un protocole permettant d'étudier la réaction d'un mutant d'*Arabidopsis thaliana* à la dépolymérisation de ses microtubules par un traitement à l'oryzalin. Dans ce rapport, nous suivrons le perfectionnement du protocole, grâce à l'évolution des concentrations d'oryzalin testées et des différentes colorations utilisées, afin d'optimiser le rendu des observations microscopiques.

Durant cette période, du 31 août au 16 octobre, j'ai travaillé au sein de l'équipe « Méchanotransduction et développement » où j'ai eu l'opportunité de découvrir et d'apprendre différentes techniques expérimentales au sein d'un laboratoire de recherche en développement végétal. J'ai travaillé sous la tutelle de mon maître de stage Alice MALIVERT qui prépare une thèse sur les signaux mécaniques et la robustesse de la morphogénèse. L'un des axes de cette étude, auquel j'ai contribué, est la réponse des microtubules aux stress mécaniques. Dans ce cadre, j'ai pu planifier et réaliser des expériences, analyser leurs résultats, présenter mes travaux en réunion d'équipe, participer aux réunions et séminaires du laboratoire.
Aux travers de mes différentes missions de stage, j'ai travaillé avec pour objectif, celui de découpler l'effet de la réponse de la paroi de la cellule végétale et celui de la réponse des microtubules à la suite d'un stress mécanique.

L'étude du stress mécanique est très importante, puisque que les contraintes mécaniques sont un problème qui peut nuire aux cultures agricoles. Par exemple, les vents violents ou même le gel peuvent détruire les plantations, en créant des déformations à différentes échelles. Dans le cas du gel, la tige casse, car les cellules explosent, et les tissus se déchirent ce qui diminue le rendement des récoltes. Ainsi, il est utile de comprendre comment les forces mécaniques agissent sur les plantes.
Au japon, le Mugifumi (« mugi » est le terme qui désigne le blé, l'orge et « fumi » signifie foulage), est une méthode qui consiste à fouler les jeunes plants de blé et d'orge traditionnellement avec les pieds, mais aussi avec des rouleaux. Dans cet exemple, les contraintes mécaniques permettent d'altérer bénéfiquement les cultures agricoles (Lida Hidetoshi,2014). Ainsi, les dégâts engendrés par le foulage sur les plants de blé facilitent l'évaporation de l'eau, augmente l'osmolalité des cellules, ce qui permet une meilleure résistance au froid et donc de former des plantations résistantes au gel (Ohtani, 1950).

La recherche en développement végétal porte une grande attention à la formation de structures et de formes chez les plantes. Cette thématique implique entre autres la notion physique de forces mécaniques. Celles-ci, exercent des contraintes qui modulent le développement de l'individu. Dans le monde végétal, du fait de leur vie fixée les plantes sont constamment exposées à des contraintes mécaniques dans leur environnement, comme le vent, le gel, et doivent s'adapter en conséquence pour augmenter leur chance de survie.
Les contraintes mécaniques sont présentes à tous les niveaux chez la plante, aussi bien à l'échelle cellulaire qu'à l'échelle tissulaire, au niveau de l'épiderme par exemple. En effet, au niveau cellulaire, les cellules végétales sont entourées d'une paroi pectocellulosique rigide permettant de conserver la forme et résistant à la pression de turgescence (pression hydrostatique d'origine osmotique). Ce phénomène se produit aussi à l'échelle tissulaire, où

l'épiderme ayant une croissance plus lente que les tissus internes se retrouve sous tension et exerce une pression sur les cellules internes. L'élément supposé procure sa rigidité à la paroi végétale et donc le responsable de la résistance aux stress mécaniques est la cellulose, un polysaccharide polymérisé par la cellulose synthase. Dans la paroi, les microfibrilles de cellulose sont déposées en suivant les microtubules (MTs) corticaux (au niveau de la membrane) à l'intérieur des cellules. Ce réseau de MTs corticaux peut s'orienter et se réorienter. Des expériences *in vivo* et *in silico* associées ont permis de visualiser la direction du stress mécanique en condition normale et lors de stress mécaniques (l'ablation d'une cellule) et de la comparer à l'orientation des MTs (Hamant et al., 2008). Il ressort de ces expériences que les MTs corticaux se réorientent dans la direction du stress mécanique maximal.

Ainsi, en se réorientant, ils impactent l'orientation du dépôt de la cellulose par les celluloses synthases. La cellulose renforce la paroi, ce qui par la suite permet à la cellule et aux tissus de grandir dans la direction perpendiculaire au dépôt de cellulose, et amplifie la forme. La nouvelle forme intensifiée de la cellule, amplifie le stress mécanique dans la direction de départ, ce qui forme une boucle de rétroaction positive, (Figure 1 - A), (Sampathkumar et al, 2014).

Il semblerait qu'une deuxième réponse au stress mécanique vienne s'ajouter à celle des microtubules. Lors d'un crible visant à étudier la détection du stress mécanique par les microtubules, l'équipe MechanoDevo a trouvé un mutant dont les cellules subissent des dégâts mécaniques alors que la boucle de rétroaction impliquant les microtubules ne semblait pas touchée (Malivert et al, in prep.). Ce mutant est celui d'une protéine nommée FERONIA (FER), un récepteur transmembranaire soupçonné d'établir des interactions avec un autre composant de la paroi : les pectines. Lors de stress mécaniques hydriques, les cellules du mutant *fer-4* explosent, ce qui n'est pas le cas lorsqu'on baisse le potentiel hydrique des cellules en augmentant la concentration d'agar dans le milieu de culture. Puisque les microtubules de ce mutant se réorientent normalement à la suite de contraintes mécaniques, la réponse des cellules aux contraintes mécaniques passe également par une étape indépendante des microtubules et impliquant FER, (Figure 1 - B).

Ma problématique de stage était la suivante : Comment découpler l'effet de la réponse de la paroi de la cellule végétale et celui de la réponse des microtubules à la suite d'un stress mécanique ?

Durant ce stage, j'ai principalement contribué à développer un protocole permettant de visualiser séparément ces deux mécanismes. Pour cela, j'ai utilisé le mutant *fer-4* ayant poussé sur des milieux contant 0.7% ou 2.5% d'agar et dépolymérisé ses MTs à l'aide d'oryzalin, afin de suivre l'évolution du nombre de cellules explosées. La mise au point du protocole a consisté à tester une gamme de concentrations d'oryzalin, différentes méthodes d'imagerie et de coloration pour obtenir une réponse de *fer-4* sur plusieurs jours. J'ai également analysé des images de *fer-4* prises avant mon arrivée à différents temps de sa croissance et dans différentes concentrations d'agar, pour étudier l'évolution du phénotype de cellules explosées au cours du temps.

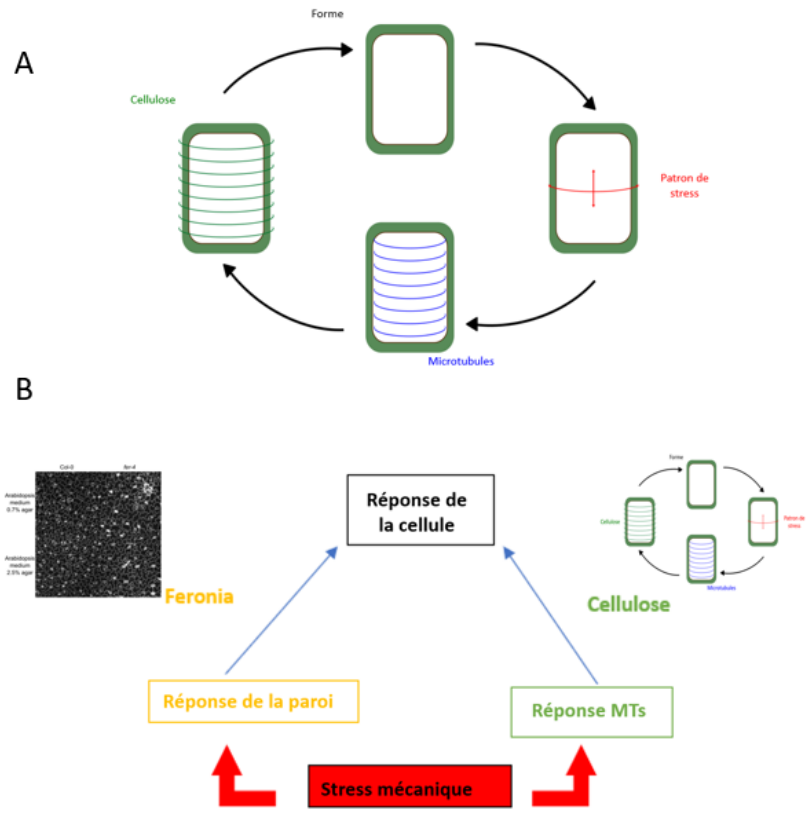

Figure 1 - Représentation des différentes réponses au stress mécanique chez Arabidopsis thaliana
(A) Modèle de la boucle de rétroaction mécanique. (B) Représentation des deux voies de réponse au stress mécanique : réponse de la paroi et réponse des MTs

Matériels et méthodes

Lors de nos expériences afin de perfectionner notre protocole, nous avons testé une première méthode de semis, culture, et dépolymérisation des plantes (1.a), pour les tests de 1 à 4, permettant d'utiliser une dose variable d'oryzalin ($C_{Oryzalin}$ = 1 µM à 20 µM) sur une courte durée (3h). Et une seconde méthode (1.b), pour le test 5, cumulant une culture des plantes dans un milieu contenant de l'oryzalin, mais avec une faible dose ($C_{Oryzalin} = 5$ µM) sur un temps de traitement plus long (4 jours). Ensuite, tous les tests ont suivi le même protocole.

- **Pour les tests 1 à 4**

1.a. Semis in vitro et culture des plantes, n=4, (tous les tests sauf le 5)

Les plantes ont été choisis dans l'écotype Col-0, et les croisements ont été réalisés par le RDP.
Au barichlore les graines mcit-MBD et *fer-4* mcit-MBD étaient récoltées et stérilisées.
Puis, elles ont été déposées individuellement sur milieu *Arabidopsis* (pH=5.8) contenant 0.7% ou 2.5% d'agar. Les boites de cultures ont été stratifiées 2 jours à 4°C dans le noir. Puis, elles ont été cultivées verticalement à 20°C en jours longs (16h lumière) pendant 5 jours.

1.a. Dépolymérisation à l'oryzalin des MTs, n=4, (tous les tests sauf le 5)

Les plantules ont été placées sur des lames d'observation préalablement recouvertes de milieu arabidopsis (pH=5.8) contenant 0.7 % ou 2.5% d'agar, puis ont été traitées avec une solution d'oryzalin (Gamme de concentration : $C_{Oryzalin}$ = 1 µM / 10 µM / 20 µM) pendant 3 h à 100% d'humidité. Les lames ont été rincées à l'eau distillée après les 3h de traitement à l'oryzalin.

- **Pour le test 5**

1.b. Semis, et culture en milieu contenant de l'oryzalin, n=1, (seulement pour le test 5)

Les milieux 0.7% et 2.5 % agar ont été préparés pour un volume final de 500ml chacun. Ces milieux ont été divisés en deux, afin d'obtenir un milieu témoin contenant du DMSO ($V_{Témoin\ DMSO} = 19\ \mu L, pour\ V_{Total} = 250\ mL$) et un milieu contenant de l'oryzalin ($C_{Oryzalin} = 5$ µM, $V_{Oryzalin} = 19$ µL, pour $V_{Total} = 250\ mL$) pour chacune des concentrations d'agar (soit 4 milieux différents pour une manipulation).
Les graines mcit-MBD et *fer-4* mcit-MBD ont été déposées individuellement sur les 4 milieux (2 témoins 0.7%, 2.5% et 2 à l'oryzalin avec 0.7%, 2.5% agar), de pH = 5.8. Les boites de cultures ont été stratifiées 2 jours à 4°C dans le noir. Puis, elles ont été cultivées verticalement à 20°C en jours longs (16h lumière) pendant 5 jours.

Manipulations techniques communes à tous les tests

- **Coloration des plantules d'*Arabidopsis* à l'Iodure de Propidium (Pi), n=4**

Les lames ont été immergées d'une solution de PI (C_{PI} = 10 µg/mL), pendant 10 minutes, et été rincées à l'eau distillées avant d'être montées avec une goutte d'eau et lamelle.

- **Coloration des plantules d'*Arabidopsis* au FM4-64, n=4**

Les lames ont été immergées d'une solution de FM4-64 (C_{FM4-64} = 1 µM) pendant 30 minutes, avant d'être montées avec une goutte d'eau et lamelle.

- **Observations des plantules d'*Arabidopsis* (Col-0/*fer-4*) au microscope confocal LEICA SP8**

Les hypocotyles des plantules sur lames ont été imagés à trois points de temps toutes les 24 heures avec un microscope confocal SP8 (Leica), par un objectif à eau 25X.
L 'acquisition s'est faite grâce à une excitation par les laser à 488 nm, 514 nm, 552 nm (mcit ; PI ; FM4-64) et une récupération sur plusieurs canaux (mcit = 520 - 538 nm ; PI = 594 – 627 nm, FM4-64 = 576 – 666 nm) en simultané ou en séquentiel. Chaque tranche optique (déplacement de l'objectif dans l'axe z) a été moyennée sur 10 images.

- **Analyse d'images**

Les images ont été traitées avec une macro nommée SurfCut développée par le RDP pour le logiciel ImageJ.
SurfCut permet de détecter la surface d'un tissu (ici l'hypocotyle ou le cotylédon) et de faire une projection en 2D sur une certaine épaisseur par rapport à cette surface, afin d'aplanir des tissus courbés et de visualiser les contours des cellules.

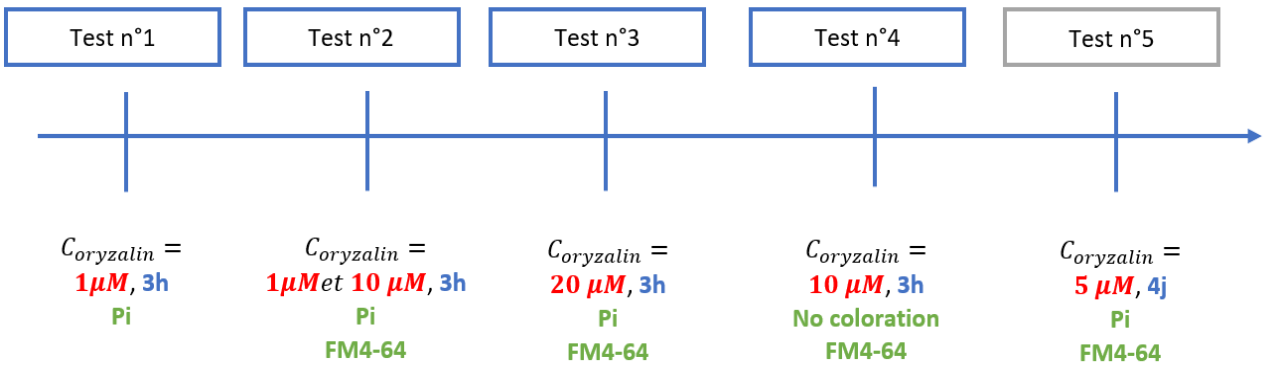

***Figure 2** – Chronologie des tests réalisés au cours du stage, utilisant des conditions variables d'un test à un autre.*

Cette figure permet de comprendre que nous n'effectuons pas un réplica identique 5 fois, mais bien notre expérience dans 5 conditions différentes pour trouver les variables optimales, afin de perfectionner notre protocole. Pour les tests 1 à 4 (carrés bleus) les méthodes de semis, cultures des plantes et traitement à l'oryzalin sont similaires, suivant la méthode 1.a décrit dans le protocole, tandis que le test 5 utilise la méthode 1.b.(carré gris). Chaque résultat de test a permis de choisir les facteurs à faire varier (la concentration d'oryzalin, le temps d'exposition à l'oryzalin, et la technique de coloration) pour le test suivant.

Résultats

Pour répondre à un stress mécanique, il semblerait que les cellules végétales passent par deux voies de signalisation, l'une impliquant les microtubules et l'autre non (Malivert *et al.*,in prep). En combinant un traitement à l'oryzalin dépolymérisant les microtubules et le mutant *fer-4* dont la voie de réponse au stress indépendante des microtubules est affectée, on peut inhiber l'une, l'autre, ou les deux voies de réponse de la cellule au stress mécanique. Pour caractériser, l'état de notre hypocotyle en fonction de la surface et du nombre de cellules explosées à la fin de notre expérience nous utilisons 3 termes : actif, semi-passif, et passif, permettant de définir si l'hypocotyle met en place les deux voies de réponses, une seule, ou bien aucunes.

Ainsi nous pouvons partir d'un système actif, dont les cellules répondent parfaitement aux contraintes mécaniques, à un système passif, dont les deux voies de signalisation sont affaiblies, en passant par un ensemble de systèmes semi-passifs, (Figure 3). En plus, de fournir un protocole optimal, nous cherchons à partir de l'interprétation de nos observations microscopiques, de classer les différentes conditions testées en fonction de l'état du matériau (actif, semi-passif, passif) afin de construire une échelle croissante de l'intensité du stress mécanique simulée par l'utilisation de *fer-4* ou de l'oryzalin, en étudiant le nombre de cellules détruites au cours du temps, (Figure 8).

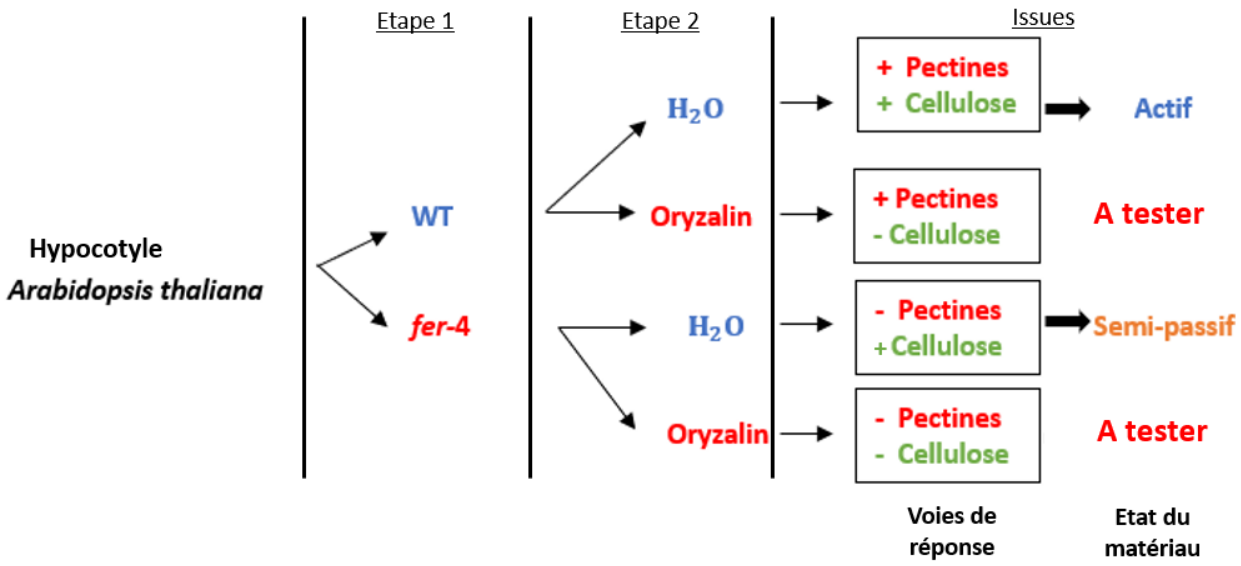

Figure 3 - *Arbre de prédiction de l'état final du WT ou de fer-4 selon les différentes conditions utilisées au cours de l'expérience. Cet arbre permet de caractériser l'état du matériau (hypocotyle d'Arabidopsis thaliana) à la fin de notre expérience, en fonction des traitements utilisés (H2O, oryzalin).*

La racine de l'arbre met en évidence, le matériau à tester : hypocotyle d'Arabidopsis thaliana. L'étape 1, est le choix entre le Wild Type (WT) d'Arabidopsis thaliana ou bien son mutant (fer-4). L'étape 2, représente les deux traitements des cellules de l'hypocotyle de la plante soit à l'eau (H2O), ou bien à l'oryzalin (dépolymérisation des MTs). Enfin, les issues caractérisent l'état du matériau à la fin de l'expérience : le terme actif est utilisé si les deux voies fonctionnent (+ pectines / + cellulose) et semi-passif, si l'une des deux voies est inhibée ou inactivée (- pectines / + cellulose). Pour rappel, le mutant fer-4, ne possède pas la voie de la pectine (due au génotype), et l'utilisation de l'oryzalin inhibe la voie de la cellulose. Dans nos expériences, nous allons tester le traitement à l'oryzalin sur le sauvage et le mutant. Dans notre perfectionnement de protocole, les conditions importantes à tester sont celles de WT et fer-4 avec un traitement à l'oryzalin.

Durant ma période de stage, j'ai réalisé l'expérience cinq fois en faisant varier trois facteurs différents : la coloration des lames, avec le Pi, le FM4-64 ou sans coloration, la concentration en oryzalin de 1 µM à 20 µM, le temps d'immersion des plantes dans l'oryzalin de 3h à 4 jours (Figure 2). Cette partie résultats se compose en sous-parties, permettant de valider les variables optimales de notre protocole. Nous retrouvons la validation de la technique de coloration, la vérification des bons résultats de nos témoins positifs, la validation de la concentration d'oryzalin optimale, ainsi que du mode de culture des plantes.

- **<u>Validation d'une technique de coloration optimale</u>**

La technique de coloration, est la première variable à définir au sein de notre protocole, car elle nous permet d'optimiser nos résultats, lorsque que nous voulons quantifier le nombre de cellules détruites, et leurs surfaces, afin de créer des graphiques représentant l'intensité du stress mécanique, pour la suite de l'expérience, une fois le protocole validé.

Dans un premiers temps, nous avons utilisé le PI. Celui-ci se fixe sur les charges négatives de la paroi (pectines démethylestérifiées), et rentre dans les cellules explosées, ce qui les marque de façon très visible, mais nous avons remarqué qu'il est toxique à forte dose et empêche la croissance des cellules. Ainsi, nous avons pensé que la coloration au PI était peut-être trop toxique pour que les cellules grandissent.

C'est pourquoi, nous avons testé une autre technique de coloration, le FM4-64. Le FM4-64 colore les membranes des cellules et est beaucoup moins toxique pour la plante ; il est absorbé par les cellules au cours du temps et nécessite donc d'être appliqué sur les hypocotyles à chaque séance d'imagerie. A partir du test 5, nous avons réussi à obtenir les bons paramètres de microscopie afin d'obtenir un rendu optimal. Cependant, nous nous sommes aperçus que la croissance des cellules était très faible durant l'expérience, même pour le WT (Figure 4).

Nous avons également réalisé un test sans coloration afin de vérifier l'impact de la coloration sur la croissance des cellules. Nous avons donc imagé uniquement la protéine fluorescente mcitrine marquant les microtubules sur des hypocotyles dans les mêmes conditions. Cette expérience nous a permis de vérifier que la coloration au FM4-64 n'affectait pas la croissance des cellules, mais elle n'a pas permis de voir les contours des cellules de façon suffisamment détaillée. Dans nos critères, nous cherchons un colorant suffisamment efficace, pour observer instantanément l'effet de l'utilisation de l'oryzalin sur l'explosion de nos cellules (Figure 4).

Ainsi, même si l'utilisation du PI est toxique, elle reste la technique de coloration optimale pour notre protocole.

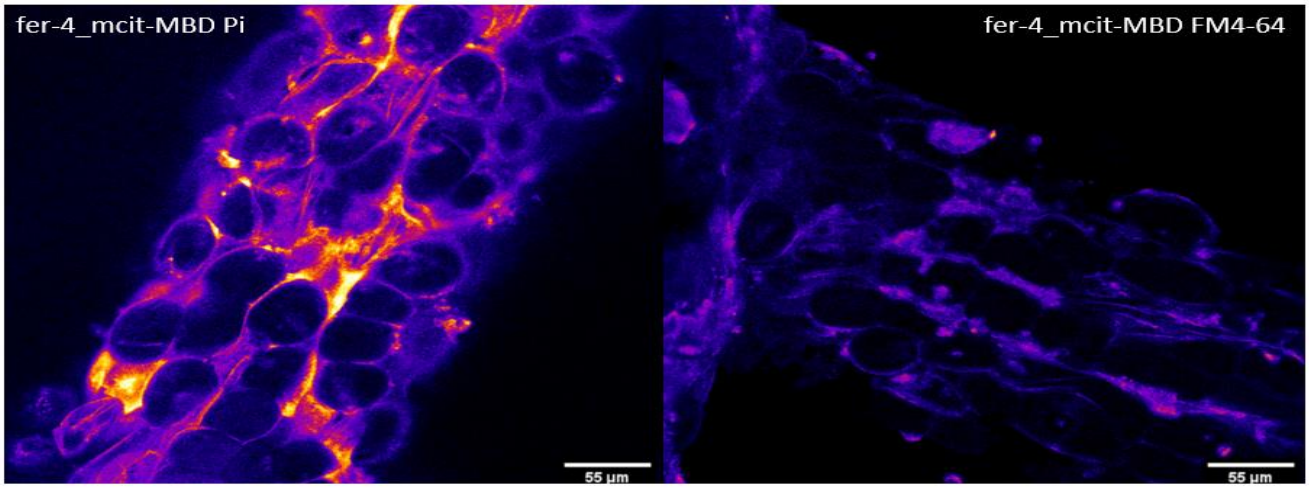

Figure 4 *- Observations des hypocotyles fer-4 mcit-MBD à 24h après avoir été cultivé sur un milieu contenant de l'oryzalin ($C_{Oryzalin}$ = 5 µM) et 0.7 % d'agar pendant 4jours.*
Deux techniques de colorations différentes sont utilisées avec à gauche, coloration au Pi (10 µg/mL) pendant 10 minutes, puis rinçage et à droite au FM4-64 (10 µg/mL) pendant 30 minutes sans rinçage. Nous remarquons, que la coloration au PI à gauche, permet de mieux visualiser le stress mécanique (zones colorées), avec la déformation de la structure des cellules (rondes, plus volumineuse), qu'avec le FM4-64, à droite.

- **<u>Validation de nos témoins *fer-4* et WT, traitement H2O</u>**

Dans un second temps, pour chaque test, il était nécessaire de vérifier nos témoins avant d'observer nos résultats, dans cette situation, nous vérifions que le stress mécanique est bien présent pour le mutant *fer-4*, contrairement au sauvage, le tout sans l'utilisation de l'oryzalin. En effet, nous avons remarqué que *fer-4* possédait des cellules rondes et plus volumineuse, que le sauvage. Celui-ci ne possède pas la réponse de la paroi, puisque que la mutation de la protéine FERONIA, empêche les récepteurs transmembranaires impliqués à mettre en place une réponse adaptée face aux tensions exercées par la faible concentration en agar du milieu (0.7%). Nos témoins ont été validé pour tous nos tests (Figure 5).

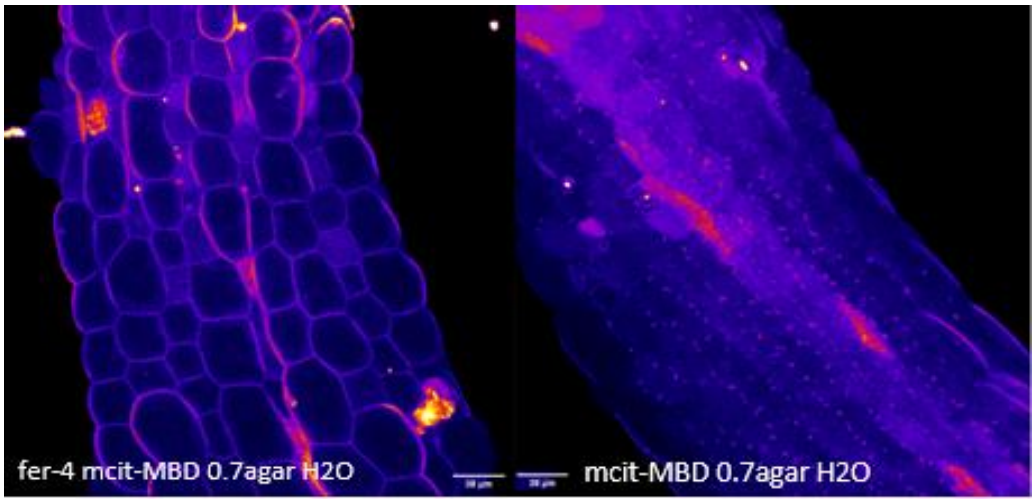

***Figure 5** - Observations des hypocotyles, à gauche de fer-4 mcit-MBD à T0h après un traitement à l'H2O sur 0.7 % d'agar, à droite de mcit-MBD à T0h après un traitement à l'H2O sur 0.7 %. Les hypocotyles sont colorés au Pi (10 µg/mL) pendant 10 minutes.*
Dans ce témoin, nous remarquons la différence entre fer-4 et le WT. En effet, nous observons sur le mutant (à gauche) les déformations des cellules de l'hypocotyle (rondes, volume plus important) dû aux tensions exercées par la faible concentration en agar du milieu (augmentation du potentiel hydrique des cellules). Contrairement, au sauvage (à droite), nous remarquons les tensions au niveau des zones colorées, mais les cellules ne se déforment, car celui-ci ne possède pas de mutation de la protéine FERONIA, *ainsi l'hypocotyle peut donc ressentir le stress mécanique, et mettre en place une réponse adaptée au niveau de la paroi afin de résister aux contraintes mécaniques.*

- **<u>Recherche de la concentration d'oryzalin optimale</u>**

De plus, nous avons remarqué qu'en augmentant la concentration d'oryzalin nous obtenions plus de cellules de *fer-4* explosées. Cependant, la difficulté est de trouver la bonne concentration, celle qui nous permet de visualiser un nombre important de cellules explosées mais une concentration qui ne doit pas être trop toxique et qui empêcherait la plante de se développer. L'efficacité de la concentration en oryzalin, sur les observations microscopiques se manifeste par une zone de couleur allant du violet au jaune, gradient d'intensité du stress mécanique (plus la couleur est chaud, plus l'état de la cellule est critique, Figure 6).

Nous avons observé qu'à 1 uM d'oryzalin la concentration n'est pas assez forte pour mettre en évidence les cellules explosées (très peu de cellules mortes), alors qu'à 10 uM il y a suffisamment de cellules explosées pour pouvoir les observer, les quantifier et gardant l'hypocotyle encore viable.
Tandis qu'à 20 uM nous avons remarqué que l'hypocotyle ne réagissait plus car il n'est plus viable dû à la concentration d'oryzalin trop intense (Figure 6).

Nous en avons déduit donc que la concentration d'oryzalin optimale à utiliser pour cette expérience est de 10 uM, ce qui concorde avec les expériences de ce type réalisées dans la littérature (Paredez *et al.*, 2006).

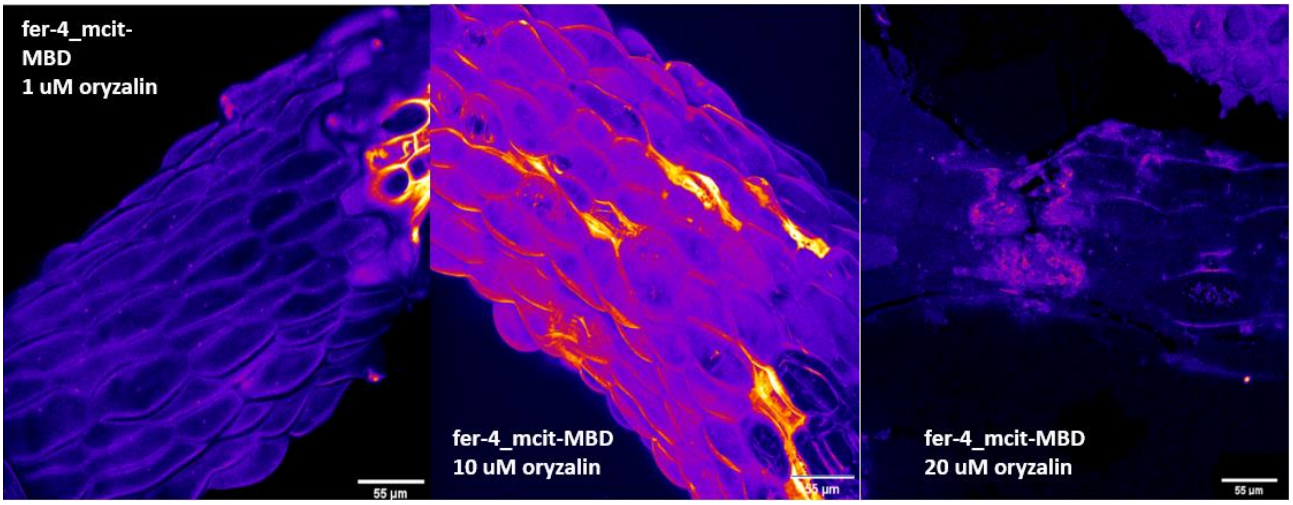

Figure 6 *- Observations des hypocotyles fer-4 mcit-MBD à 48h après un traitement à l'oryzalin sur 2.5 % d'agar, avec 3 concentrations d'oryzalin différentes (de gauche à droite : $C_{Oryzalin}$ = 1 µM, 10 µM, 20 µM).*

Les hypocotyles sont traités à l'oryzalin pendant 3h, avant rinçage, et colorés au Pi (10 µg/mL) pendant 10 minutes. En faisant varier la concentration de 1 µM à 20 µM, nous constatons que la concentration à 10 µM est la plus efficace. En effet, puisqu'avec 1 µM, il y a très peu de cellules mortes (petite zone colorée en haut à droite), et à 20 µM trop important (plus de zone colorée, destruction de l'hypocotyle).

- **<u>Recherche du mode de culture adéquat</u>**

Le dernier paramètre que nous avons fait varier est le temps d'exposition des plantes à la solution d'oryzalin.
En effet, pour les quatre premiers tests nous avions réalisé un traitement court (trois heures) avec une forte concentration d'oryzalin. Pour le dernier test, les semis ont été réalisés dans des milieux Arabidopsis (0.7% et 2.5% agar) contenant une faible concentration d'oryzalin (5 µM). Les plantes ont ainsi reçu un traitement long (quatre jours) avec une faible concentration d'oryzalin.
Les cellules ayant reçu un traitement long et de faible concentration à l'oryzalin ont grandi de façon plus homogène que celles traitées moins longtemps avec une forte concentration, elles ont mieux survécu et montrent de fortes différences de phénotype dès le premier temps d'imagerie, (Figure 7).

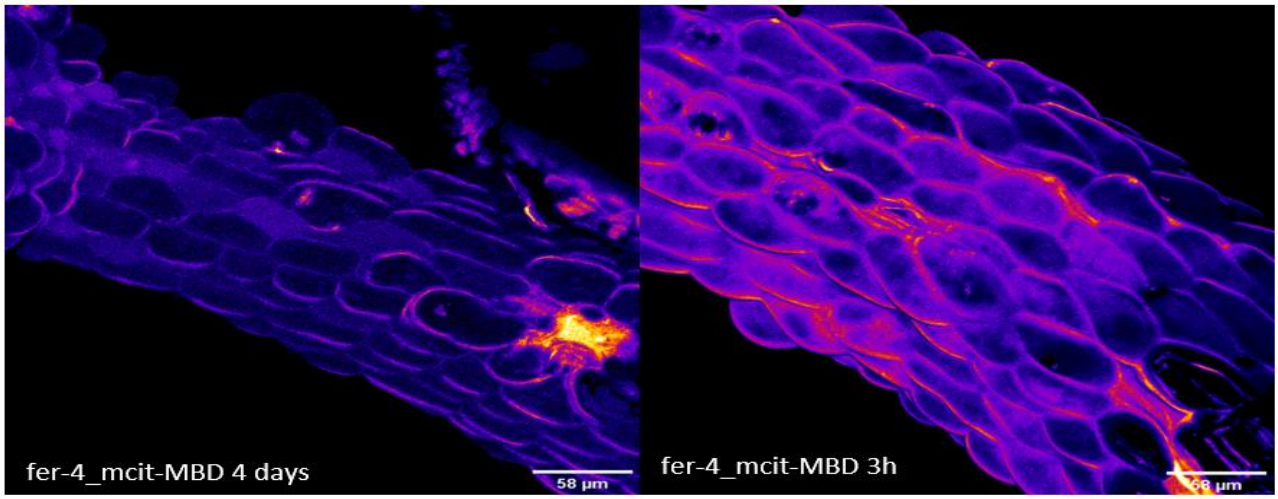

Figure 7 *- Observations des hypocotyles fer-4 mcit-MBD à T0h après avoir été cultivé sur un milieu contenant de l'oryzalin ($C_{Oryzalin}$ = 5 µM) pendant 4 jours sur 2.5% d'agar (à gauche) et à la suite d'un traitement à l'oryzalin ($C_{Oryzalin}$ = 10 µM) pendant 3 heures, avant rinçage, et colorés au Pi (10 µg/mL) pendant 10 minutes. Cette figure, attire notre attention sur le phénotype de ces deux hypocotyles. Nous remarquons, à gauche que la structure des cellules est davantage homogène, et que celles-ci ont mieux survécu, car les contraintes mécaniques sont moins importantes à gauche qu'à droite.*

Discussion

Nous avons réussi à faire évoluer le protocole de recherche jusqu'à obtenir des résultats satisfaisants pour l'analyse. La coloration au FM4-64, peut-être une solution alternative au Pi, puisqu'elle colore les membranes, tout en étant bien moins toxique. Néanmoins, le PI reste tout de même la solution la plus efficace pour visualiser les cellules explosées dû au stress mécanique exercé sur les cellules de l'hypocotyle. La concentration d'oryzalin adéquate pour un traitement court se situe à 10µM, puisqu'à 1µM l'effet n'est pas assez visible et beaucoup trop important à 20µM. Mais la solution optimale pour l'observation se trouve être un traitement plus long et moins concentré, qui permet à toutes les cellules de grandir assez pour exploser.

Au début de notre étude, nous avons cherché également à caractériser l'état du matériau (hypocotyle d'*Arabidopsis thaliana*), lorsqu'il est traité à l'oryzalin. Pour le WT, nous avons remarqué que la voie de la réponse de la paroi avec Feronia était toujours présente, tandis que la réponse de la cellulose avec les MTs n'était plus fonctionnelle. Ainsi, l'état du WT traité à l'oryzalin peut-être caractérisé de « semi-passif ».
De plus, pour le mutant les deux voies de réponses sont inhibées. En effet, *fer-4* ne possède pas la protéine FERONIA et ne peut mettre en place une réponse par la voie de la paroi, et la voie des MTs avec la cellulose, est inhibé du fait de l'utilisation de l'oryzalin, nous avons dans ces conditions, un hypocotyle « passif ».

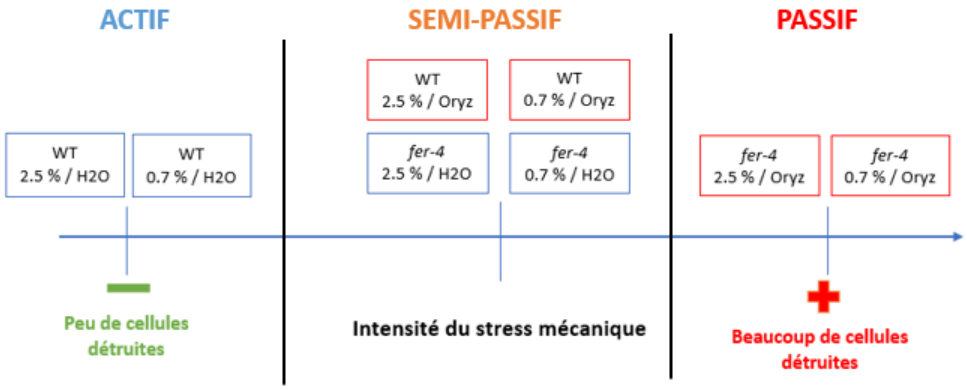

***Figure 8** - Echelle classant les 3 états de l'hypocotyle d'Arabidopsis thaliana en fonction de l'évolution de l'intensité du stress mécanique simulé.*

L'intensité du stress mécanique est simulée par l'utilisation du mutant Arabidopsis thaliana (fer-4) et avec le traitement à l'oryzalin. Cette intensité augmente de gauche à droite, de l'état actif à l'état passif, celle-ci a déjà été étudiée pour le WT et fer-4, avec les deux concentrations d'agar et le traitement avec H_2O (carrés en bleu). Or, dans cette expérience nous avons cherché à replacer les quatre mêmes conditions mais avec l'oryzalin sur l'échelle d'intensité. Au niveau de l'intensité du stress mécanique, le milieu 0.7 % agar, exerce une plus grande tension sur les cellules que le milieu 2.5% d'agar. De plus, l'utilisation de l'oryzalin, et le mutant fer-4 sont 2 autres facteurs qui augmentent le stress mécanique en inhibant les réponses de la paroi ou des MTs. Pour rappel, la mutation fer-4, ne possède pas la réponse de la paroi (due au génotype), et l'utilisation de l'oryzalin inhibe la voie de la cellulose.

Enfin, nous pouvons dire que notre expérience est limitée. De ce fait, le gène FER est impliqué dans beaucoup de processus biologiques, autrement dit nous ne savons pas vraiment dans quelle mesure ce gène a été modifié, puisque les cellules évoluent vers un état délétère, sans compter la toxicité de nos colorants (Pi, FM4-64), de l'oryzalin, ce qui nous empêche d'interpréter correctement nos résultats d'un point de vue biologique. De plus, le protocole commence à être efficace pour nos recherches, et le nombre d'échantillon doit-être augmenté (nombre de n) et la quantification des cellules explosées n'a pas encore été réalisé au cours de ces sept semaines de stages. Néanmoins, cette étape est prévue pour la suite de cette étude, et nécessaire afin de créer des graphiques et tableaux statistiques permettant de quantifier l'intensité du stress mécanique prenant compte le nombre de cellules explosées, et la surface de ces cellules.

La compréhension de l'impact du stress mécanique sur le développement végétal est essentielle, pour le domaine scientifique, et peut être adaptée dans le domaine agronomique. Les forces mécaniques, perçues comme des contraintes négatives peuvent être utilisées à bon escient pour obtenir des résultats encourageants, et quasiment similaires à l'utilisation de certains engrais ou produits chimiques dans les cultures agricoles. De même, pour la fabrication de matériaux, ces études permettent également de créer de nouvelles infrastructures en bois dont la forme se modifie (se rétracte ou se dilate) selon l'hygrométrie et, où le mouvement du bois peut être transformé en électricité, afin d'alimenter une partie du bâtiment.

Bibliographie

Comment les plantes acquièrent-elles leur forme ? Une contribution des signaux mécaniques *Planet-Vie*.

Coutand, C. Contribution à l'étude du contrôle des dimensions et de la forme des axes aériens par des signaux mécaniques et lumineux chez les ligneux. 108.

Erguvan, Ö., Louveaux, M., Hamant, O. and Verger, S. (2019). ImageJ SurfCut: a user-friendly pipeline for high-throughput extraction of cell contours from 3D image stacks. *BMC Biol.* **17**, 38.

Gendreau, E., Traas, J., Desnos, T., Grandjean, O., Caboche, M. and Hofte, H. (1997). Cellular Basis of Hypocotyl Growth in Arabidopsis thaliana. *Plant Physiol.* **114**, 295–305.

Grandazzi, G. (2006). The Flip Side of Technoscientific Companies. *Ecol. Polit.* **No 32**, 61–73.

Hamant, O., Heisler, M. G., Jönsson, H., Krupinski, P., Uyttewaal, M., Bokov, P., Corson, F., Sahlin, P., Boudaoud, A., Meyerowitz, E. M., et al. (2008). Developmental Patterning by Mechanical Signals in Arabidopsis. *Science* **322**, 1650–1655.

Iida, H. (2014). Mugifumi, a beneficial farm work of adding mechanical stress by treading to wheat and barley seedlings. *Front. Plant Sci.* **5**,.

La recherche fondamentale *Inserm - Sci. Pour Santé*.

Lambert, T. mCitrine at FPbase. *FPbase*.

Lambert, T. mCherry at FPbase. *FPbase*.

microtubules.pdf.

Morel, P., Crespel, L., Galopin, G. and Moulia, B. (2012). Effect of mechanical stimulation on the growth and branching of garden rose. *Sci. Hortic.* **135**, 59–64.

Sampathkumar, A., Krupinski, P., Wightman, R., Milani, P., Berquand, A., Boudaoud, A., Hamant, O., Jönsson, H. and Meyerowitz, E. M. (2014). Subcellular and supracellular mechanical stress prescribes cytoskeleton behavior in Arabidopsis cotyledon pavement cells. *eLife* **3**, e01967.

Résumé

Dans le domaine du développement végétal, les forces mécaniques internes et externes qui interviennent dans le processus de développement de la plante, constituent un sujet au cœur des débats dans le domaine de la recherche fondamentale. Ce rapport a pour but de mettre en évidence le travail et l'évolution d'un protocole de recherche au cours des expériences, afin de devenir celui qui correspondra le mieux pour découpler l'effet de la réponse de la paroi de la cellule végétale et celui de la réponse des microtubules à la suite d'un stress mécanique. C'est pourquoi, la concentration d'oryzalin et la technique de coloration sont les deux facteurs que feront varier les expérimentateurs. La concentration d'oryzalin à 1 µM et 10 µM ne permettra pas de montrer distinctement les cellules explosées chez Feronia (*fer-4*), tandis que la concentration à 20 µM sera la plus optimale. De même, pour la coloration à l'Iodure de Propidium qui en se fixant sur les charges négatives autour des MTs, permets de mieux de distinguer les cellules mortes, contrairement à la coloration au FM4-64 qui colore sélectivement les membranes. Ce travail a permis de faire évoluer le protocole, néanmoins celui-ci nécessite d'autres répétitions d'expériences, et la quantification des cellules explosées avant d'être opérationnel.

Abstract

In the domain of plant development, the internal and external mechanical forces involved in the plant development process are in the center of the debates in the field of fundamental research. This report aims to highlight the work and development of a research protocol during experiments, in order to become the most appropriate one to decouple the effect of the response of the plant cell wall and the response of microtubules following mechanical stress. Therefore, the concentration of oryzalin and the technique of coloring are the two factors that will vary the experimenters. The concentration of oryzalin at 1 µM and 10 µM will not allow to show clearly the exploded cells in Feronia (*fer-4*), while the concentration at 20 µM will be the most optimal. Similarly, for the coloring with the iodide of Propidium which by fixing on the negative charges around the Mts, allow to better distinguish the dead cells, contrary to the coloring with FM4-64 which selectively colors the membranes. This work made it possible to evolve the protocol, however it requires further repetitions of experiments, and the quantification of burst cells before being operational.

Mots clés

stress mécanique / forces mécanique / microtubules / méchanosenseur / cytosquelette / *Arabidopsis thaliana* / *fer-4* / oryzalin

Changing mechanical integrity in Arabidopsis thaliana FERONIA mutant with growth conditions

2021 L3 Internship report
Amaya Richer

RDP Laboratory, ENS de Lyon

Introduction

Amongst the different signals that plants receive during their development, mechanical forces give important information to the growing plants in order to adapt themselves to their environment. At a cellular scale, the inner pressure can go up to 1 MPa in plant cells [1], exerting a high tension to which the cell has to resist. Cells are able to face important mechanical stress thanks to their resistant cell wall. The cell wall is mostly made of water, but the cellulose microfibrils, pectin and bounding hemicellulose that compose the cell wall enable mechanical resistance [2]. Furthermore, not only can the cell wall resist tension, it can respond to mechanical stress by modulating its structure and dynamic [3]. An example of this plasticity is cellulose reinforcement on pavement cells, puzzle-shaped cells in leaves: the cellulose reinforcement at some particular spots in the cell wall creates the remarkable lobed shape of these cells, allowing resistance to osmotic stress [4,5].

In order to respond to mechanical cues, cells first have to sense these forces. A few mechanosensors have already been studied in plants, such as some members of the *Arabidopsis thaliana* family of receptor-like kinases RLKs. Most proteins belonging to this family are important for growth and reproduction (for example THESEUS1 or ANXUR1,2) [6]. In this study, we focused on the FERONIA receptor-like kinase, a transmembrane protein which has extracellular motifs similar to malectin, an animal protein, potentially able to bind to cell wall carbohydrates in plants [6]. FERONIA is a receptor for RALF1, a peptide which fixation leads to the phosphorylation of a FERONIA cytoplasmic domain [6]. FERONIA is involved in many different functions, such as flowering, nutrition metabolism, stomatal movement, female fertility, cell elongation, response to hormones and pathogens, root-hair development (bursting cells have been observed in several *fer* mutants), and mechanosensing [6–8]. Previous studies showed that FERONIA is a putative mechanosensor in the root: growth behavior of *fer* mutant on a stiff surface, as well as calcium, pH and TOUCH genes response after mechanical stimulus are different arguments to mechanosensing [9,10]. FERONIA is involved in the cell response to a mechanical stress, as bursting pavement cells in the loss of function *fer-4* mutant suggest [13]. This bursting phenomenon is due to a passive response to tension in the mutant, whereas there is an active cell wall or pressure response in the wild-type. Furthermore, increasing the osmolarity, therefor decreasing the water potential of the gels on which plants were grown can partially rescue the phenotype, as it limits cell bursting. The phenotype rescue is also visible at an organ scale: cotyledon area is lower in *fer-4* than in Col-0 wild-type on 0.7% agar gels (lower osmolarity) but is partially restored as of 8 days after germination on 2.5% agar gels (higher osmolarity) [13]. Here, we studied how modifying growth conditions could impact mechanical integrity in *fer-4.* The different growth conditions tested were the following: changing the gel composition by using PEG gels instead of agar gels to modify the osmolarity; modifying the light conditions by placing the plants in short days and continuous days

(respectively 8 hours and 24 hours of light exposure in 24 hours) instead of long days conditions (16 hours of light exposure in 24 hours); and finally stressing the plants with a cold period. To evaluate the mechanical integrity of plants at both cellular and organ scales, cell bursting and cell area were measured on pavement cells whereas cotyledon area and cotyledon circularity were quantified. Result for agar and PEG gels were similar, as the phenotype was partially rescued in *fer-4* in both growth condition. In short and continuous days condition, there were more burst cells in *fer-4* than there were in long days conditions. Short days and long days cotyledons had respectively lower and higher area than long days ones. Moreover, the rescue in continuous days conditions was less important than in long days condition, probably due to rapid growth, preventing the mutant from adapting to stress. Finally, results on plants which were exposed to stress from a cold shock period showed a less important rescue, similarly to continuous days conditions, most likely due to a growth burst following the end of the cold period. Overall, in every condition, a phenotype rescue was observed on a higher osmolarity gel, proving the robustness of this rescue.

Results

Phenotype rescue of *fer-4* with higher osmolarity agar gels in long days growth conditions

In order to understand the impact of growth condition modifications on the mechanical integrity of *fer-4*, it was important to first do the experiments with a ‘control’ growth condition, which had already been studied previously. Therefor, *fer-4* response to mechanics was observed in long days and on agar gels growth conditions [13]. Two different agar concentrations were used: 0.7% and 2.5% agar gels. Increasing the agar concentration in the gels allowed to higher the osmolarity, therefor decreasing the hydric potential of the gels. This reduced the water flow entering in the cells and led to lower cellular tension in higher concentrated gels [13]. To study the response to mechanics in both Col-0 control and *fer-4* mutant, different quantitative parameters were used at cellular and organ scale. At a cellular scale, as a cell bursting phenomenon occurred, pavement cells bursting index was measured in cotyledons SP8 images. Cell area was also quantified in pavement cells. At an organ scale, cotyledon area and circularity were measured. Results showed that on 0.7% agar gels, *fer-4* cells were already bursting as of 4 days after germination, and up to 12 days after germination. This did not occur in Col-0 cotyledons (Fig. 1, A.1, A.2). Cell bursting in the mutant is due to a passive response to tension in *fer*-4, whereas the Col-0 cells respond actively to mechanical stress by hypothetically modifying their cell wall. Moreover, cell area was lower in *fer-4* than in Col-0 (S1.A). On 2.5% agar gels, the phenotype was partially rescued as there was less or even no bursting (Fig. 1, A.1, A.2). This rescue was also visible at organ scale: *fer-4* cotyledons globally had a smaller area (Fig. 1, A.3, A.4) and were less circular (S2.A) than Col-0 cotyledons on 0.7% agar gels. However, the circularity was rescued on 2.5% gels (S2.A, see 8 days after germination). These results show that in long days conditions, higher osmolarity gels partially rescues the phenotype in *fer-4*. Indeed, on 0.7% agar gels, cells are under mechanical stress, and *fer-4* cells respond passively to tension by bursting, leading to smaller and less circular cotyledons; however, on 2.5% agar gels, the tension is less important explaining the phenotype rescue. This proves that FERONIA is a mechanosensor in the cotyledons.

Changing the gel composition does not affect the phenotype rescue

Increasing the agar concentration allows to higher the osmolarity of the gels, but it also increases their rigidity. To verify that modifying the rigidity does not impact the response to mechanics, a different gel composition was used: polyethylene glycol (PEG) gels at 0 g/L and 100 g/L were used in comparison to 0.7% and 2.5% agar gels. PEG has the particularity of increasing the osmolarity without increasing the rigidity of the gels. The osmolarity of the PEG gels was measured with an osmometer: the 0 g/L and 100 g/L gels were at 67,7 mOsm and 189,7 mOsm respectively, which corresponds to a pressure of 0,165 MPa and 0.462 MPa. With

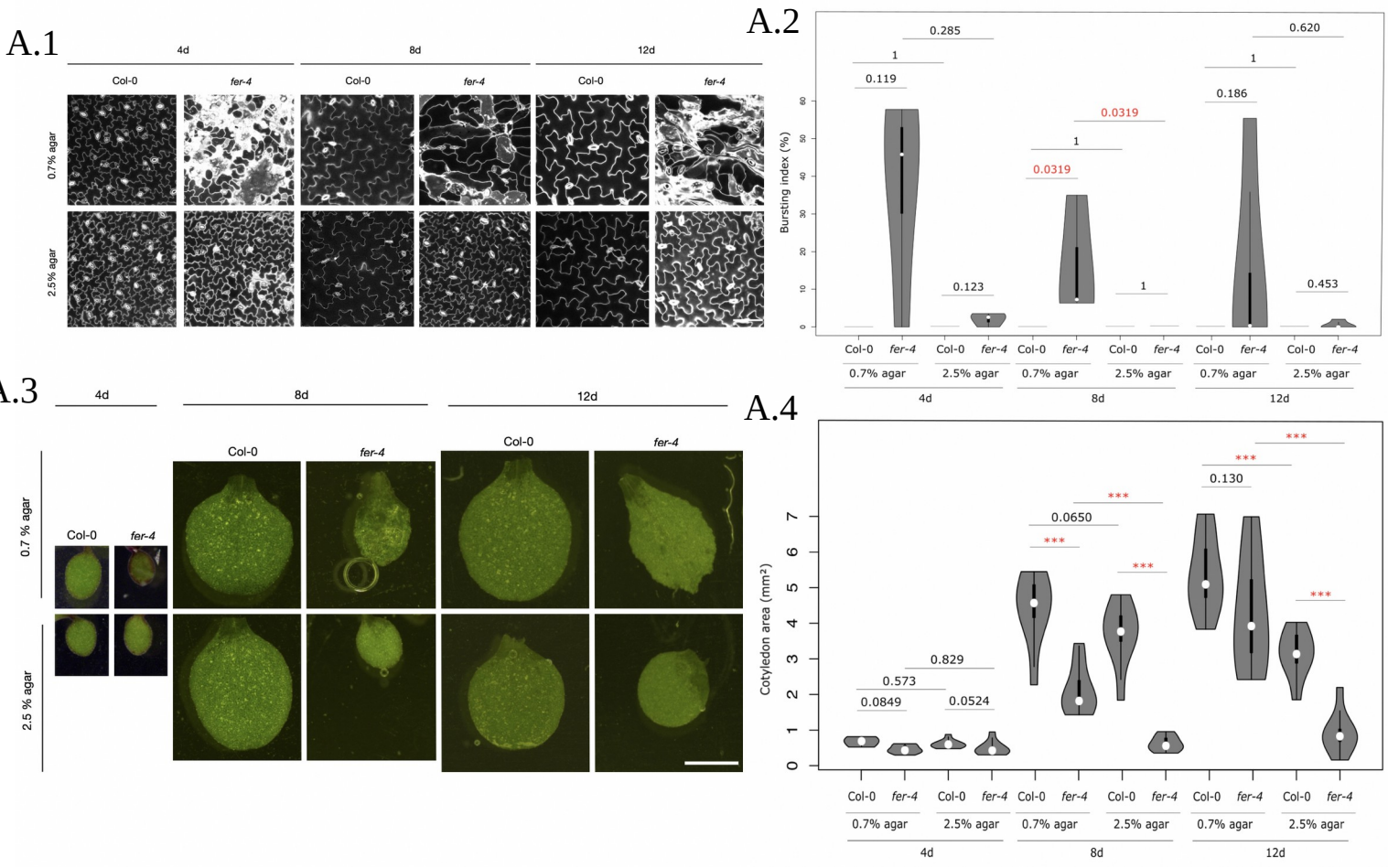
A.1
4d
8d
12d
Col-0
fer-4
0.7% agar
2.5% agar
A.2
Bursting index (%)
0.285
1
0.119
0.123
0.0319
1
0.0319
1
0.620
1
0.186
0.453
Col-0
fer-4
0.7% agar
2.5% agar
4d
8d
12d

A.3
4d
8d
12d
Col-0
fer-4
0.7 % agar
2.5 % agar
A.4
Cotyledon area (mm²)
0.829
0.573
0.0849
0.0524
0.0650
0.130
***
0.7% agar
2.5% agar
4d
8d
12d

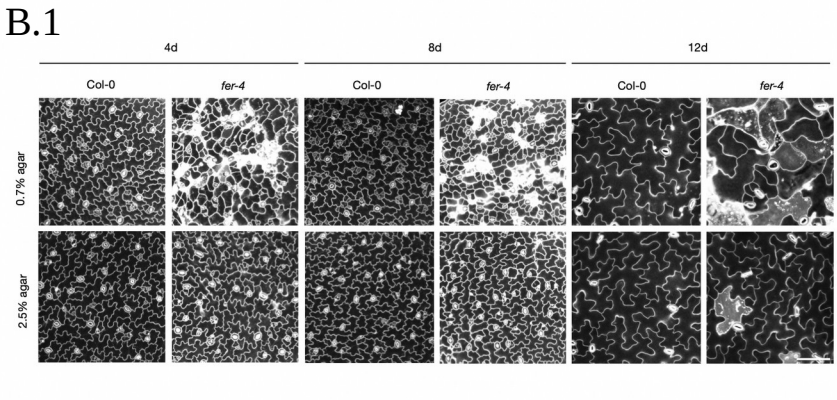
B.1
4d
8d
12d
Col-0
fer-4
0.7% agar
2.5% agar

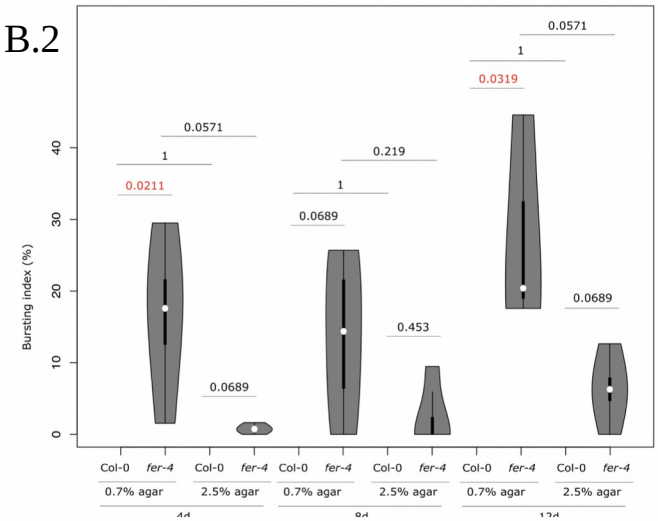
B.2
Bursting index (%)
0.0571
1
0.0211
0.0689
0.219
1
0.0689
0.453
0.0571
1
0.0319
0.0689
0.7% agar
2.5% agar
4d
8d
12d

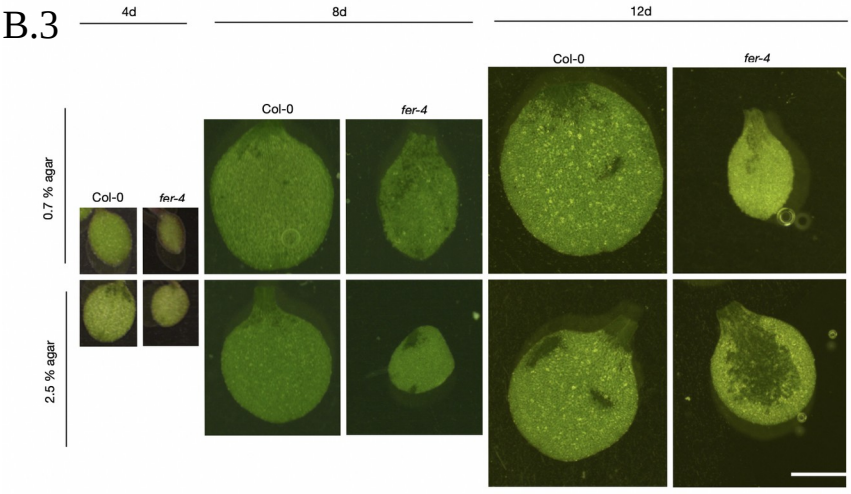
B.3
4d
8d
12d
Col-0
fer-4
0.7 % agar
2.5 % agar

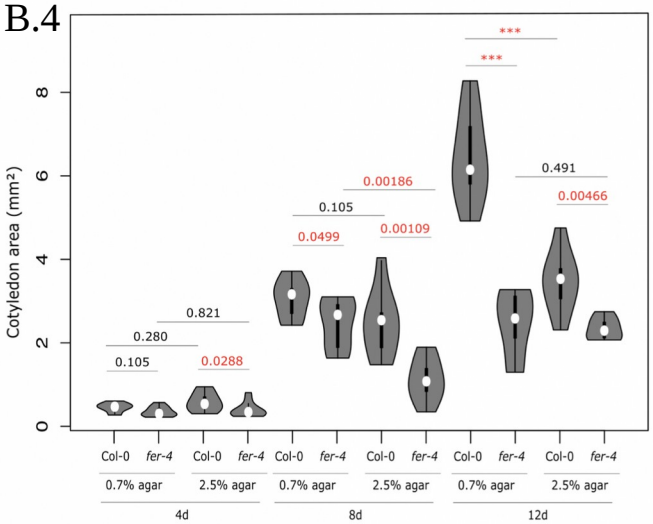
B.4
Cotyledon area (mm²)
0.821
0.280
0.105
0.0288
0.105
0.0499
0.00186
0.00109
0.491
0.00466
***
0.7% agar
2.5% agar
4d
8d
12d

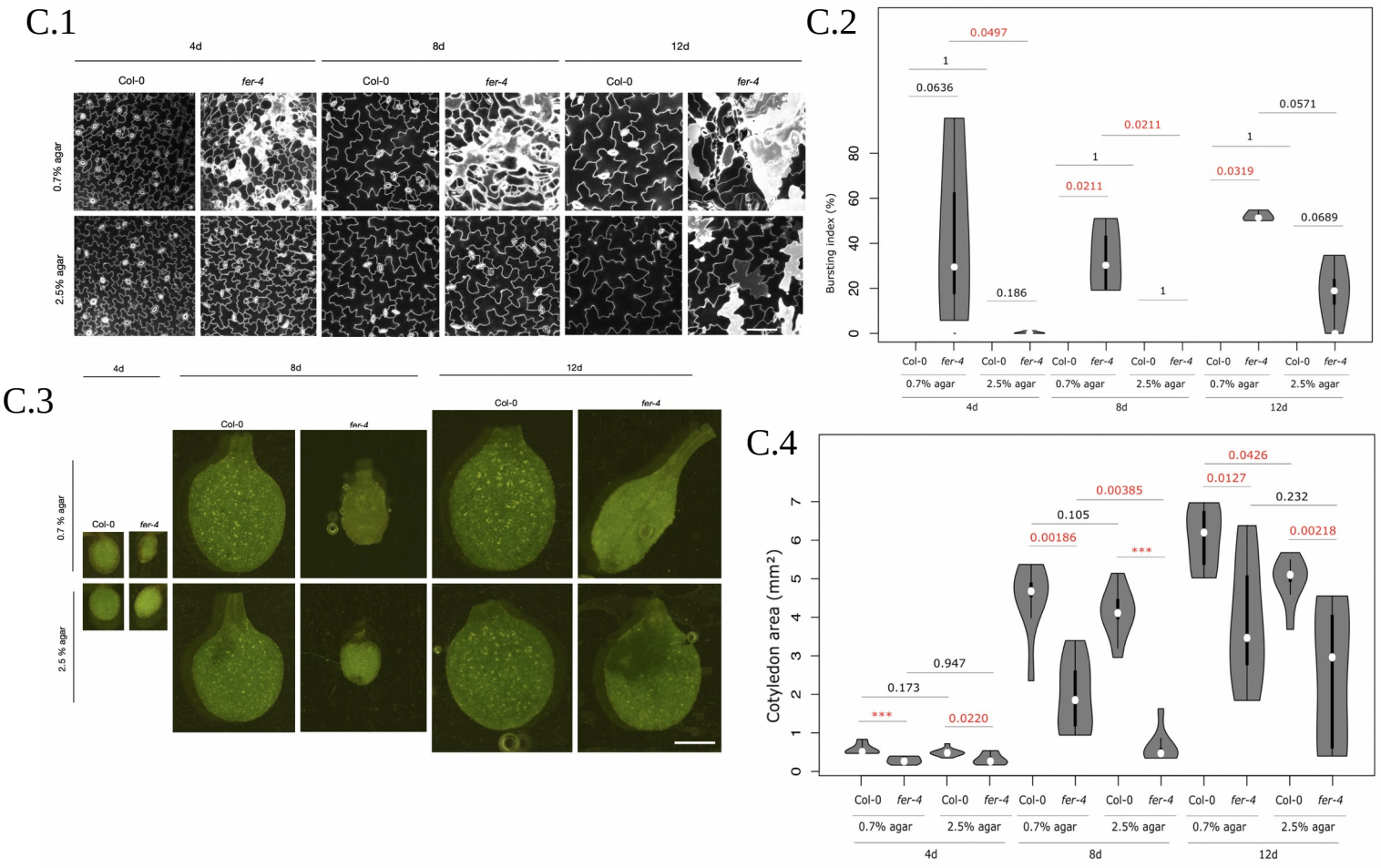

Figure 1. Effect of photoperiod on FERONIA's response to mechanics: testing long, short and continuous days conditions

A.1-A.4*: Long days conditions (16 hours of light in 24 hours);* ***B.1-B.4****: Short days conditions (8 hours of light in 24 hours);* ***C.1-C.4****: Continuous days conditions (24 hours of light in 24 hours);* ***A.1, B.1, C.1****: Confocal images of Col-0 and* fer-4 *pavement cells of seedlings grown on 0.7% or 2.5% agar gels, 4, 8 and 12 days after germination (PI staining). Scale: 100µm;* ***A.2, B.2, C.2****: Bursting index in Col-0 and* fer-4 *pavement cells of seedlings grown on 0.7% or 2.5% agar gels, 4, 8 and 12 days after germination.* p*-values from Wilcoxon-Mann-Whitney are indicated in red if considered significative (*p*<0.05), and by *** if* p*<0.01. The liability of these* p*-values is low, as n=4 .* ***A.3, B.3, C.3****: Images of Col-0 and* fer-4 *cotyledons of seedlings grown on 0.7% or 2.5% agar gels, 4, 8 and 12 days after germination. Scale: 1mm;* ***A.4, B.4,C.4****: Cotyledon area in Col-0 and* fer-4 *pavement cells of seedlings grown on 0.7% or 2.5% agar gels, 4, 8 and 12 days after germination.* p*-values from Wilcoxon-Mann-Whitney are indicated in red if considered significative (*p*<0.05), and by *** if* p*<0.01 (n=10).*

same long days conditions, similar results were found between PEG and agar gels: cell bursting was observed increasingly from 2 days to 12 days after germination in *fer-4* on 0 g/L but not on 100 g/L PEG gels (Fig.2, A, B). As on agar gels, cell area was lower in *fer-4* than in Col-0 (S1.B, see 12 days after germination). Cotyledon area was rescued as of 12 days after germination on 100 g/L gels (Fig.2, B, C), and cotyledon circularity was rescued at 8 days after germination (S2.B). A notable difference between agar gels and PEG gels conditions was that the tissues were more damaged on PEG gels: the bursting index was globally higher and the cotyledons were smaller and vitrified on PEG gels. This could be explained by PEG gel making protocol: gels were soaked for two days long in a PEG solution for the PEG to infiltrate in the gels. This soaking period could have led to a PEG gel containing more water than agar gels, which did not have to soak. In any case, the phenotype rescue worked as well on PEG than on agar gels, proving that the FERONIA response to tension is not rigidity-dependent.

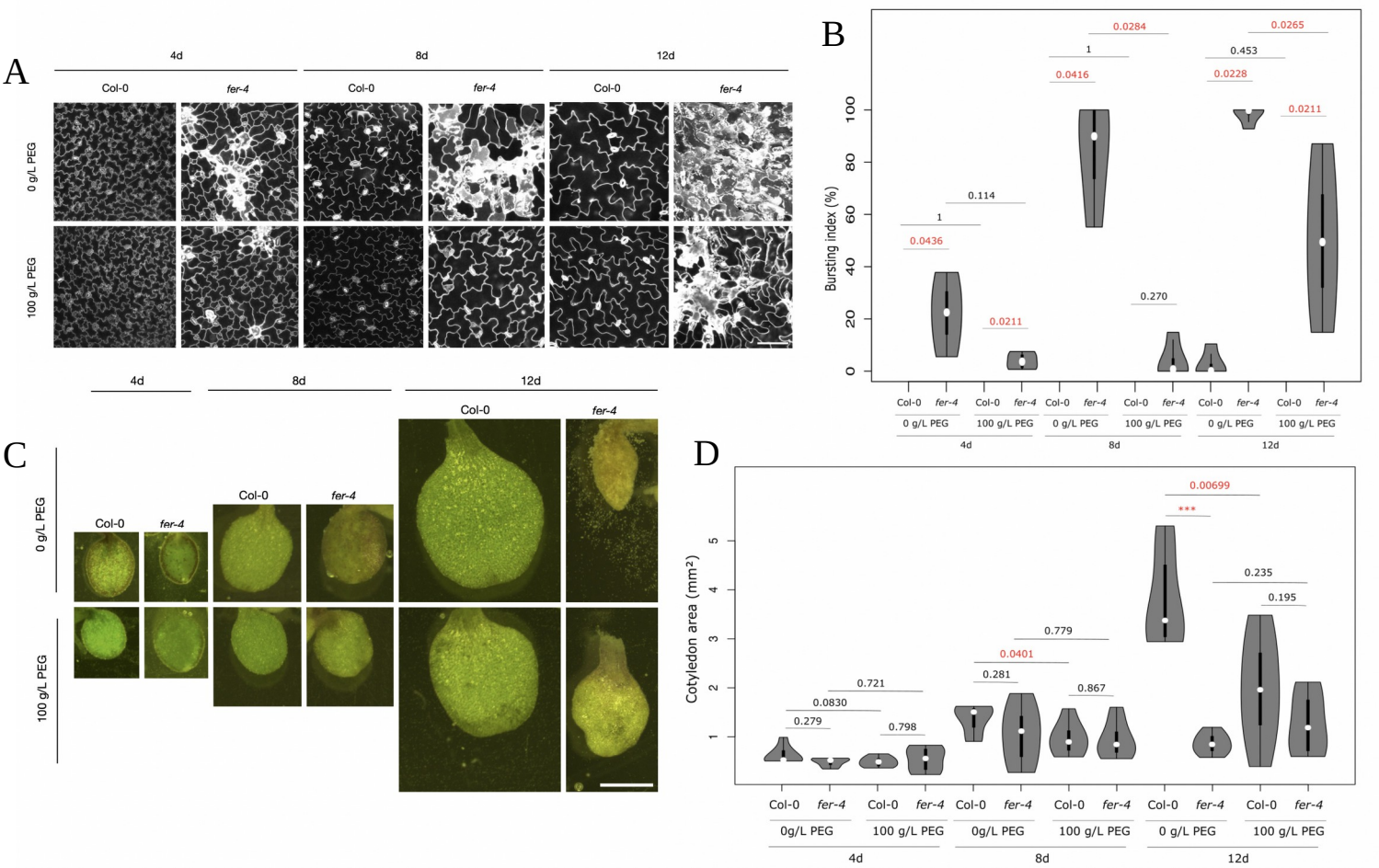

Figure 2. Changing the gel composition from agar to PEG does not prevent a phenotype rescue of* fer-4 *on higher osmolarity gels

A*: Confocal images of Col-0 and* fer-4 *pavement cells of seedlings grown on 0 g/L or 100 g/L PEG gels, 4, 8 and 12 days after germination (PI staining). Scale: 100µm;* ***B****: Bursting index in Col-0 and* fer-4 *pavement cells of seedlings grown on 0 g/L or 100 g/L PEG gels, 4, 8 and 12 days after germination.* p*-values from Wilcoxon-Mann-Whitney are indicated in red if considered significative (*p*<0.05), and by *** if* p*<0.01. The liability of these* p*-values is low, as n=4 .* ***C****: Images of Col-0 and* fer-4 *cotyledons of seedlings grown on 0 g/L or 100 g/L PEG gels, 4, 8 and 12 days after germination. Scale: 1mm;* ***D****: Cotyledon area in Col-0 and* fer-4 *pavement cells of seedlings grown on 0 g/L or 100 g/L PEG gels, 4, 8 and 12 days after germination.* p*-values from Wilcoxon-Mann-Whitney are indicated in red if considered significative (*p*<0.05), and by *** if* p*<0.01 (n=10).*

Impact of photoperiod on mechanical integrity

After the gel composition, the growth condition that was changed was light exposure. Plant were grown in short days or continuous days conditions, instead of long days. To compare the effect of the different photoperiods on the FERONIA response to mechanics, plants were grown on 0.7% and 2.5% agar gels in each of the light conditions. Modifying the light exposure was a way of controlling the growth rate: hypothetically, plants grown in short days conditions should have a slower growth rate than plants grown in long days conditions, whereas continuous days should allow faster growth than long days.

Short days correspond to 8 hours of light in 24

A.1

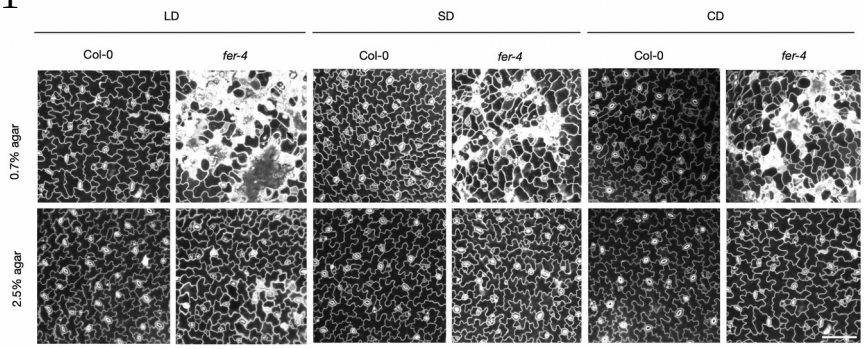

A.2

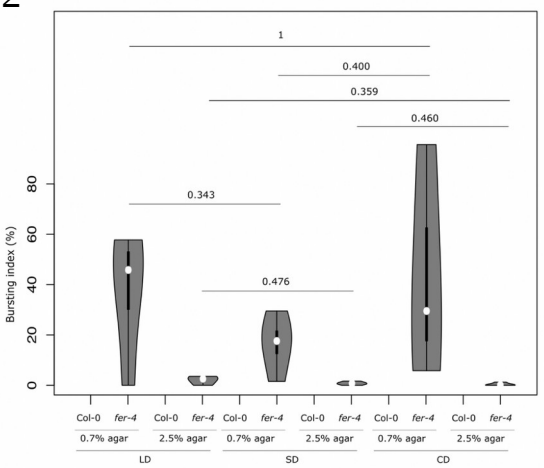

A.3

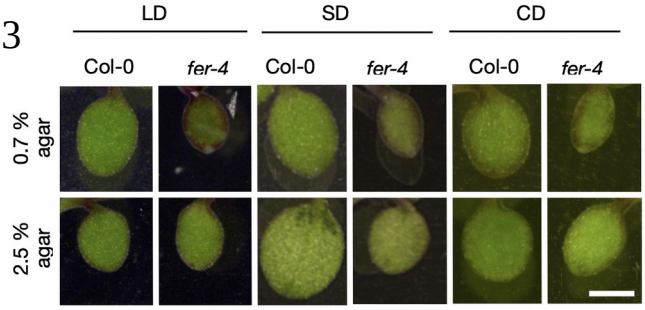

A.4

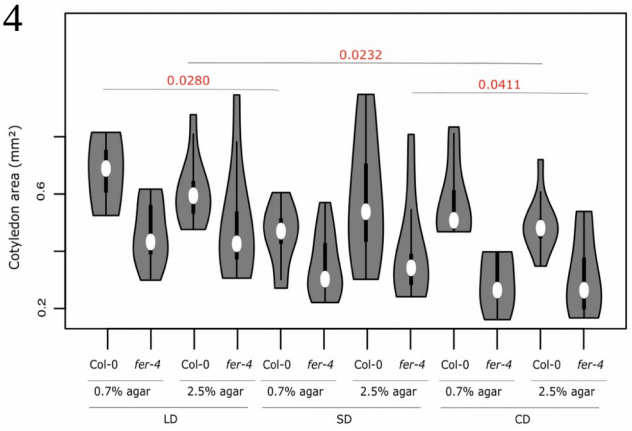

B.1

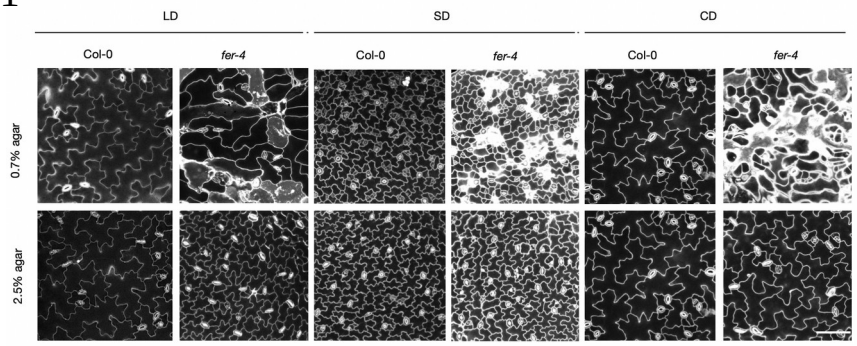

B.2

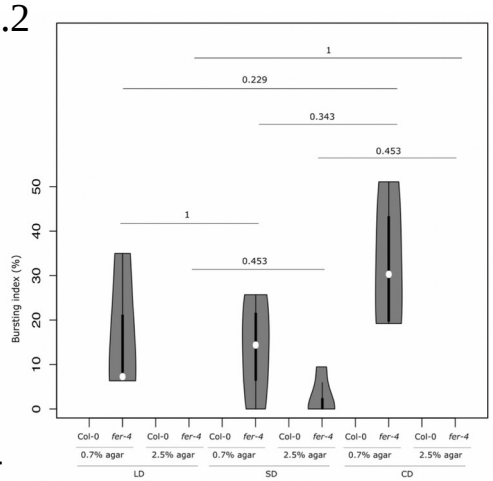

B.3

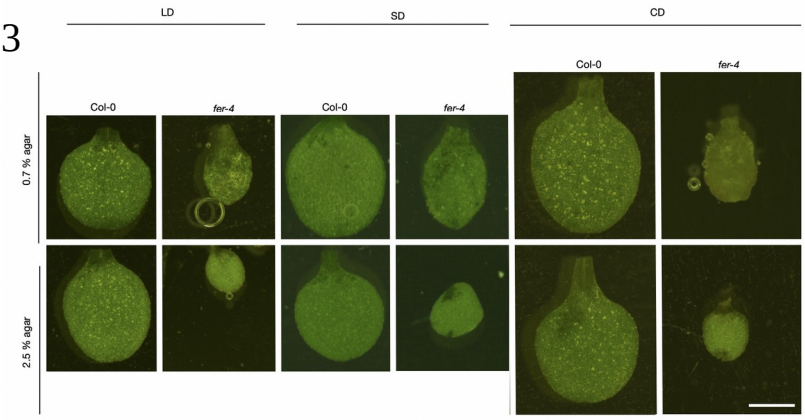

B.4

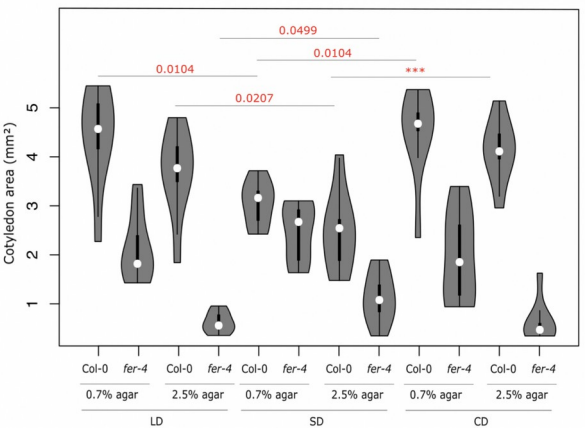

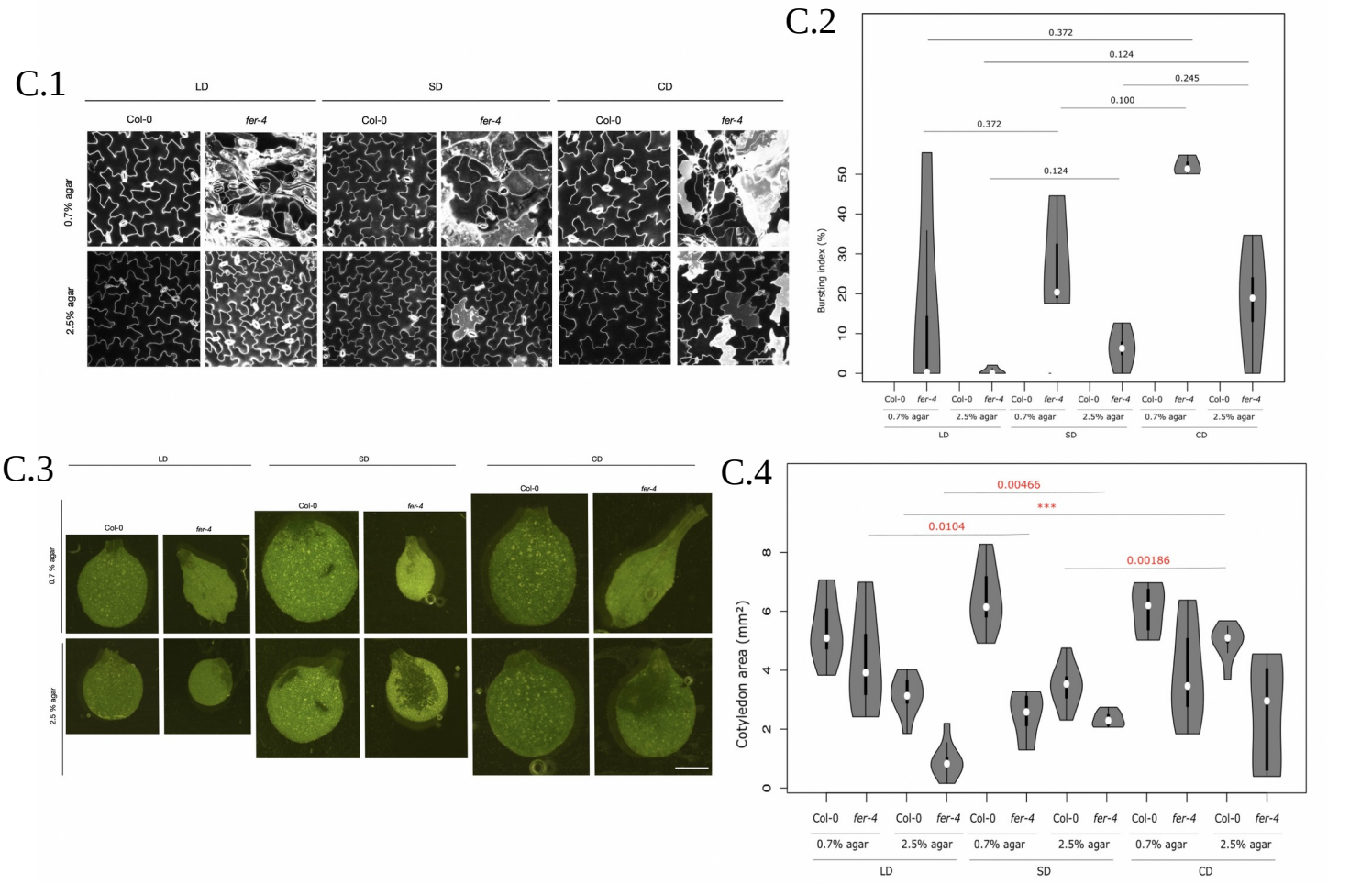

Figure 3. Comparing the FERONIA response of seedling grown in long, short and continuous days, at 4, 8 and 12 days after germination

A.1-A.4*: seedlings 4 days after germination grown in long days (LD), short days (SD) and continuous days (CD) conditions;* ***B.1-B.4****: seedlings 8 days after germination grown in long, short and continuous days conditions;* ***C.1-C.4****: seedlings 12 days after germination grown in long, short and continuous days conditions;* ***A.1, B.1, C.1****: Confocal images of Col-0 and* fer-4 *pavement cells of seedlings grown on 0.7% or 2.5% agar gels, in long, short or continuous days (PI staining). Scale: 100µm;* ***A.2, B.2, C.2****: Bursting index in Col-0 and* fer-4 *pavement cells of seedlings grown on 0.7% or 2.5% agar gels, in long, short or continuous days.* p*-values from Wilcoxon-Mann-Whitney are indicated in red if considered significative (*p*<0.05), and by *** if* p*<0.01. The liability of these* p*-values is low, as n=4 .* ***A.3, B.3, C.3****: Images of Col-0 and* fer-4 *cotyledons of seedlings grown on 0.7% or 2.5% agar gels, in long, short or continuous days. Scale: 0.5mm for* ***A.3****, 1mm for* ***B.3*** *and* ***C.3*** *;* ***A.4, B.4,C.4****: Cotyledon area in Col-0 and* fer-4 *pavement cells of seedlings grown on 0.7% or 2.5% agar gels, in long, short or continuous days.* p*-values from Wilcoxon-Mann-Whitney are indicated in red if considered significative (*p*<0.05), and by *** if* p*<0.01 (n=10).*

hours, and continuous days correspond to 24 hours of light in 24 hours (compared to a 16 hours light period in 24 hours for the long days condition). The first interesting result was that in short and continuous days conditions, the response was globally similar to long days conditions: cell bursting occurred increasingly in *fer-4* from 4 to 8 to 12 days on 0.7% agar gels, and cell bursting was almost absent on 2.5% agar gels. The differences between the bursting index in Col-0 and in *fer-4* were significant on 0.7% agar but not in 2.5% agar gels (see *p*-values in Fig. 1, B.2, C.2), showing a phenotype rescue in short and continuous days conditions as well as in long days. The pavement cells area was globally lower in *fer-4* than in Col-0, in all three conditions (long, short and continuous days). At an organ scale, some long days results were also found in short or continuous days conditions: cotyledons were smaller on 2.5% agar gels than on 0.7% agar gels, and *fer-4* cotyledons were smaller than

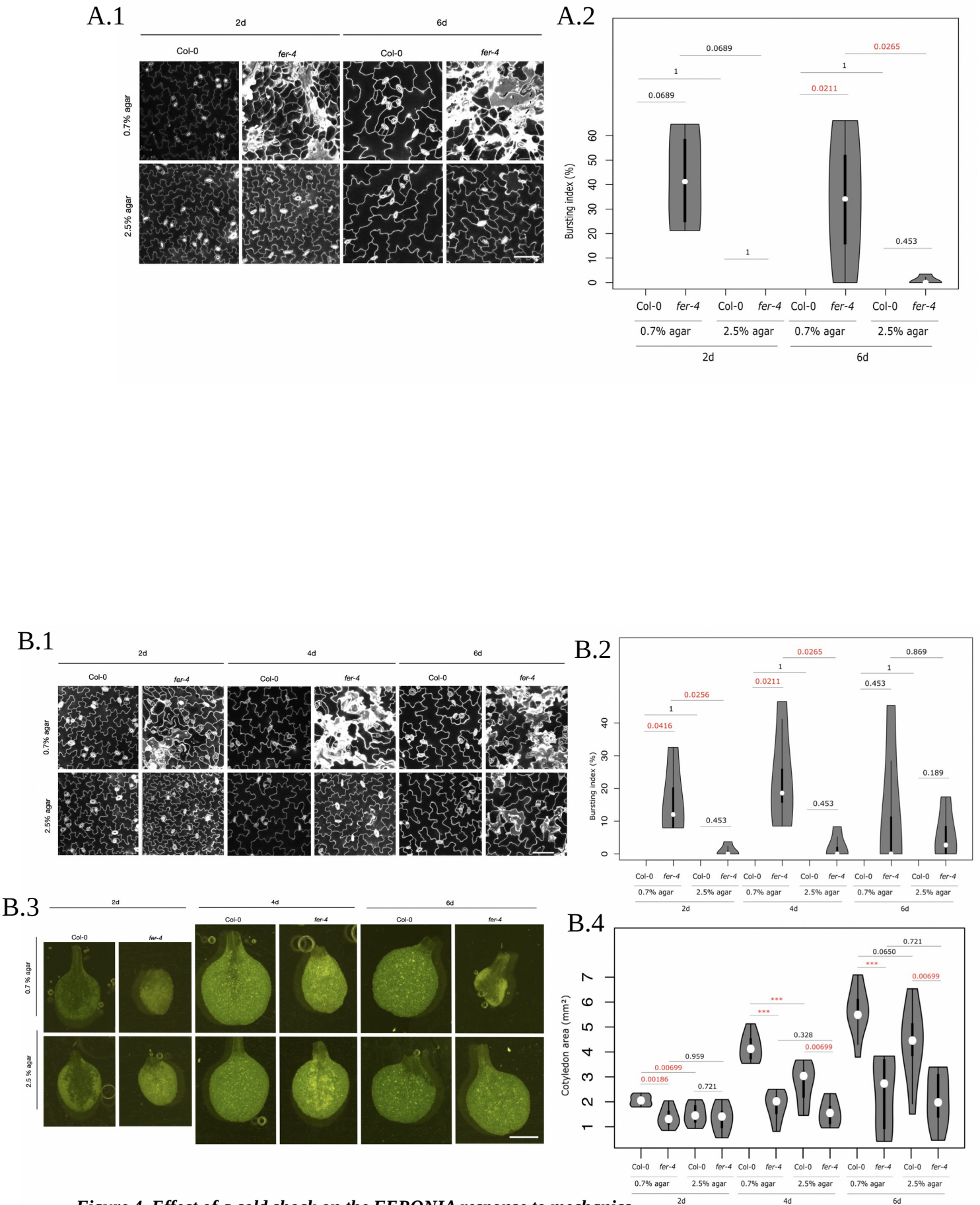

Figure 4. Effect of a cold shock on the FERONIA response to mechanics

A.1-A.2*: seedlings 2 and 6 days after a 2 days long shock period;* ***B.1-B.4****: seedlings 2, 4 and 6 days after a 7 days long shock period;* ***A.1,B.1****: Confocal images of Col-0 and* fer-4 *pavement cells of seedlings grown on 0.7% or 2.5% agar gels, 2, 4 and 6 days after shock period (PI staining). Scale: 100µm;* ***A.2,B.2****: Bursting index in Col-0 and* fer-4 *pavement cells of seedlings grown on 0.7% or 2.5% agar gels, 2, 4 and 6 days after shock period.* p*-values from Wilcoxon-Mann-Whitney are indicated in red if considered significative (*p*<0.05), and by *** if* p*<0.01. The liability of these* p*-values is low, as n=4 .* ***B.3****: Images of Col-0 and* fer-4 *cotyledons of seedlings grown on 0.7% or 2.5% agar gels, 2, 4 and 6 days after shock period. Scale: 1mm;* ***B.4****: Cotyledon area in Col-0 and* fer-4 *pavement cells of seedlings grown on 0.7% or 2.5% agar gels, 2, 4 and 6 days after shock period.* p*-values from Wilcoxon-Mann-Whitney are indicated in red if considered significative (*p*<0.05), and by *** if* p*<0.01 (n=10).*

Col-0 cotyledons (Fig. 1, B.3, B.4, C.3, C.4), which is coherent with smaller cells in *fer-4* compared to Col-0. Circularity of the cotyledons was rescued on 2.5% agar gels at 12 days after germination in short days conditions (S2.C). These results show the robustness of the phenotype rescue, as it does not depend on photoperiod, working in long, short and continuous days conditions.
However, there were some differences in the response to mechanics from a condition to another. Indeed, in short and continuous days conditions, there were more burst cells in *fer-4* than in long days conditions, at 8 and 12 days after germination (Fig. 3, B.1, B.2, C.1, C.2). Short days cotyledons were smaller than in long days (Fig. 3, B.3, B.4), while continuous days cotyledons were bigger than in long days (Fig. 3, C.3, C.4). These differences could be explained by a slower and faster growth in respectively short and continuous days conditions. Moreover, although the phenotype was partially rescued on 2.5% agar gels in long, short and continuous days, the rescue was less important in continuous days conditions, probably because rapid growth doesn't allow time for the plant to respond and adapt to mechanical stress as well. This would explain the high bursting index in *fer-4* cells on 2.5% agar, 12 days after germination (Fig. 3, C.1, C.2).

Effect of a cold shock on the FERONIA response to mechanics

Modifying the photoperiod was a way of controlling the growth rate. However, light controls many other biologic phenomena than growth. Therefor, to verify the effect of growth on the response to mechanics in *fer-4*, a cold shock was applied to plants growing in long days and agar gels conditions. A period of cold supposedly inhibits a germinated plant's growth. Two conditions were tested: a 2 days and a 7 days cold period, which both started 2 days after germination.
Results showed that 2 days of cold were not enough to have a noticeable effect (Fig. 4, A), but in plants that went through a 7 days cold period, the rescue was less important than the long days without a cold shock control (see at 6 days in Fig. 4, B). This could be explained in a similar way as for continuous days conditions: there could be a growth burst as soon as the plants are placed out of cold temperatures, at the end of the cold period, which would induce rapid growth, similarly to continuous days conditions. All in all, in both cold shock conditions, the presence of a phenotype rescue showed once again the robustness of such a rescue on higher osmolarity gels.

Discussion

This study shows the robustness of the phenotype rescue result found on higher osmolarity gels: it is not dependent of agar gels stiffness, as PEG gels results suggest; we also tested the variability response due to growth conditions with different light exposure conditions; finally, dynamics was experimented through cold shock response. All in all, changes in the plant's mechanical environment can rescue the *fer*-4 mutant, showing its mechanosensing role, in many growth conditions.
The main difficulty encountered when modifying growth conditions is trying not to modify other parameters than growth. Indeed, changing light exposure or stressing the plants with a cold shock both impact growth, as well as may other biological functions: metabolism or hormone signaling for instance. This is why it was important to combine different methods of growth control, by testing several growth conditions. Another limit to this study was the poor statistical weight, due to little samples in SP8 Imaging (n=4). Repeating the experiments on pavement cells is necessary in order to obtain significative statistics.
A question that was not tackled in this study is whether the cell bursting phenomenon in *fer-4* is due to a thinner cell wall or with a poor composition, or whether it is linked to higher pressure in the cells. More importantly, our results on FERONIA's morphological response to tension could be completed with the molecular processes at stake. Some studies have already focused on this question: in root cells, FERONIA induces cell-specific calcium transients that maintain cell-wall integrity [11]; FERONIA could also regulate the H+-ATPase when phosphorylated [6].

A plant's ability to sense its mechanical environment and to respond to it during development is a key process to mechanoecosensing, e.g. cellular sensing of the mechanical cues of the cell's microenvironment (for instance, substrate rigidity, topology or adhesiveness) [12].

Material and Methods

Plant material and growth conditions

Both wild-type and *fer-4* mutant were in the Columbia-0 (Col-0) ecotype. The *fer-4* mutation was the GK-106A06-012499 T-DNA mutation.
The in-line sowings of Col-0 or *fer-4* sterilized seeds were done either on Arabidopsis medium 0.7% and 2.5% agar concentration gels, or on PEG 0 g/L and 100 g/L concentration gels for the PEG condition. All sown seeds were placed in cold chamber (4°C and no light) for two days in order to synchronize germination, after which the plants were transferred in a growth chamber (long days chamber: 20°C, 16 hours of light in 24 hours; short days chamber : 22°C days, 18°C night, 8 hours of light in 24 hours; continuous days chamber: 20°C, 24 hours of light in 24 hours). For cold period conditions, plants were placed in cold chamber for 2 or 7 days of cold, 4 days after germination, and then replaced in growth chamber.

Image acquisition

For all growth conditions except the cold period condition, plants were image with a SP8 Leica confocal microscope, at 4, 8 and 12 days after germination. For the cold period condition, SP8 imaging was done at 2 and 6 days after the end of cold exposure for the 2 days of cold condition, and at 2, 4 and 6 days after the end of cold exposure for the 7 days of cold condition. A 25x long-distance water objective (NA=0.95) was used for imaging. Cell contours and bursting cells were visualized by pectin coloration with a 1/10 dil. propidium iodide (PI) solution (10 minutes staining before imaging). In confocal microscopy images, the Z-Step size was 0.5 µm and the zoom factor was 1,25. For every condition, 4 replicates were done. A same central zone in the cotyledons was chosen for each image.

For cotyledon binocular images, the zoom factor was set at 1. For every condition, 8 to 10 replicates were done.

Image analysis

SP8 Z-stacks were analyzed with SurfCut (REF Erguvan et al., 2019) in order to obtain projections of the flattened cell contours. The SurfCut projections were manually analyzed with ImageJ for cell burst area (bursting index corresponds to the ratio of bursted area on total area), and processed with PaCeQuant (REF Möller et al., 2017) for pavement cell area.
Cotyledon area and circularity was measured manually with ImageJ.

Statistical analysis

R studio was used to obtain violin plots with *p*-values of the Wilcoxon-Mann-Whitney test. *p*-values under 0.001 were indicated by ***, *p*-values under 0.05 were written in red and considered as significant differences.

References

1. Beauzamy L, Nakayama N, Boudaoud A: **Flowers under pressure: ins and outs of turgor regulation in development**. *Ann. Bot.* 2014, **114**:1517–1533. [doi: 10.1093/aob/mcu187] [PMID: 25288632] [PMCID: PMC4204789]

2. Wolfenson H, Yang B, Sheetz MP: **Steps in Mechanotransduction Pathways that Control Cell Morphology**. *Annu. Rev. Physiol.* 2019, **81**:585–605. [doi: 10.1146/annurev-physiol-021317-121245] [PMID: 30403543] [PMCID: PMC7476682]

3. Bacete L, Hamann T: **The Role of Mechanoperception in Plant Cell Wall Integrity Maintenance**. *Plants Basel Switz.* 2020, **9**. [doi: 10.3390/plants9050574] [PMID: 32369932] [PMCID: PMC7285163]

4. Altartouri B, Bidhendi AJ, Tani T, Suzuki J, Conrad C, Chebli Y, Liu N, Karunakaran C, Scarcelli G, Geitmann A: **Pectin Chemistry and Cellulose Crystallinity Govern Pavement Cell Morphogenesis in a Multi-Step Mechanism**. *Plant Physiol.* 2019, **181**:127–141. [doi: 10.1104/pp.19.00303] [PMID: 31363005] [PMCID: PMC6716242]

5. Cosgrove DJ, Anderson CT: **Plant Cell Growth: Do Pectins Drive Lobe Formation in Arabidopsis Pavement Cells?** *Curr. Biol. CB* 2020, **30**:R660–R662. [doi: 10.1016/j.cub.2020.04.007] [PMID: 32516619]

6. Li C, Wu H-M, Cheung AY: **FERONIA and Her Pals: Functions and Mechanisms**. *Plant Physiol.* 2016, **171**:2379–2392. [doi: 10.1104/pp.16.00667] [PMID: 27342308] [PMCID: PMC4972288]

7. Huck N, Moore JM, Federer M, Grossniklaus U: **The Arabidopsis mutant feronia disrupts the female gametophytic control of pollen tube reception**. *Dev. Camb. Engl.* 2003, **130**:2149–2159. [doi: 10.1242/dev.00458] [PMID: 12668629]

8. Ji D, Chen T, Zhang Z, Li B, Tian S: **Versatile Roles of the Receptor-Like Kinase Feronia in Plant Growth, Development and Host-Pathogen Interaction**. *Int. J. Mol. Sci.* 2020, **21**:E7881. [doi: 10.3390/ijms21217881] [PMID: 33114219] [PMCID: PMC7660594]

9. Shih H-W, Miller ND, Dai C, Spalding EP, Monshausen GB: **The receptor-like kinase FERONIA is required for mechanical signal transduction in Arabidopsis seedlings**. *Curr. Biol. CB* 2014, **24**:1887–1892. [doi: 10.1016/j.cub.2014.06.064] [PMID: 25127214]

10. Duan Q, Kita D, Li C, Cheung AY, Wu H-M: **FERONIA receptor-like kinase regulates RHO GTPase signaling of root hair development**. *Proc. Natl. Acad. Sci. U. S. A.* 2010, **107**:17821–17826. [doi: 10.1073/pnas.1005366107] [PMID: 20876100] [PMCID: PMC2955125]

11. Feng W, Kita D, Peaucelle A, Cartwright HN, Doan V, Duan Q, Liu M-C, Maman J, Steinhorst L, Schmitz-Thom I, et al.: **The FERONIA Receptor Kinase Maintains Cell-Wall Integrity during Salt Stress through Ca2+ Signaling**. *Curr. Biol. CB* 2018, **28**:666-675.e5. [doi: 10.1016/j.cub.2018.01.023] [PMID: 29456142] [PMCID: PMC5894116]

12. Chen Y, Ju L, Rushdi M, Ge C, Zhu C: **Receptor-mediated cell mechanosensing**. *Mol. Biol. Cell* 2017, **28**:3134–3155. [doi: 10.1091/mbc.E17-04-0228] [PMID: 28954860] [PMCID: PMC5687017]

13. Malivert A, Erguvan Ö, Chevallier A, Dehem A, Friaud R, Liu M, Martin M, Peyraud T, Hamant O, Verger S: **Turning plants from passive to active material: FERONIA and microtubules independently contribute to mechanical feedback**. BioRxiv. 2021. [bioRxiv preprint doi: https://doi.org/10.1101/2021.03.24.436809]

Supplementary Data

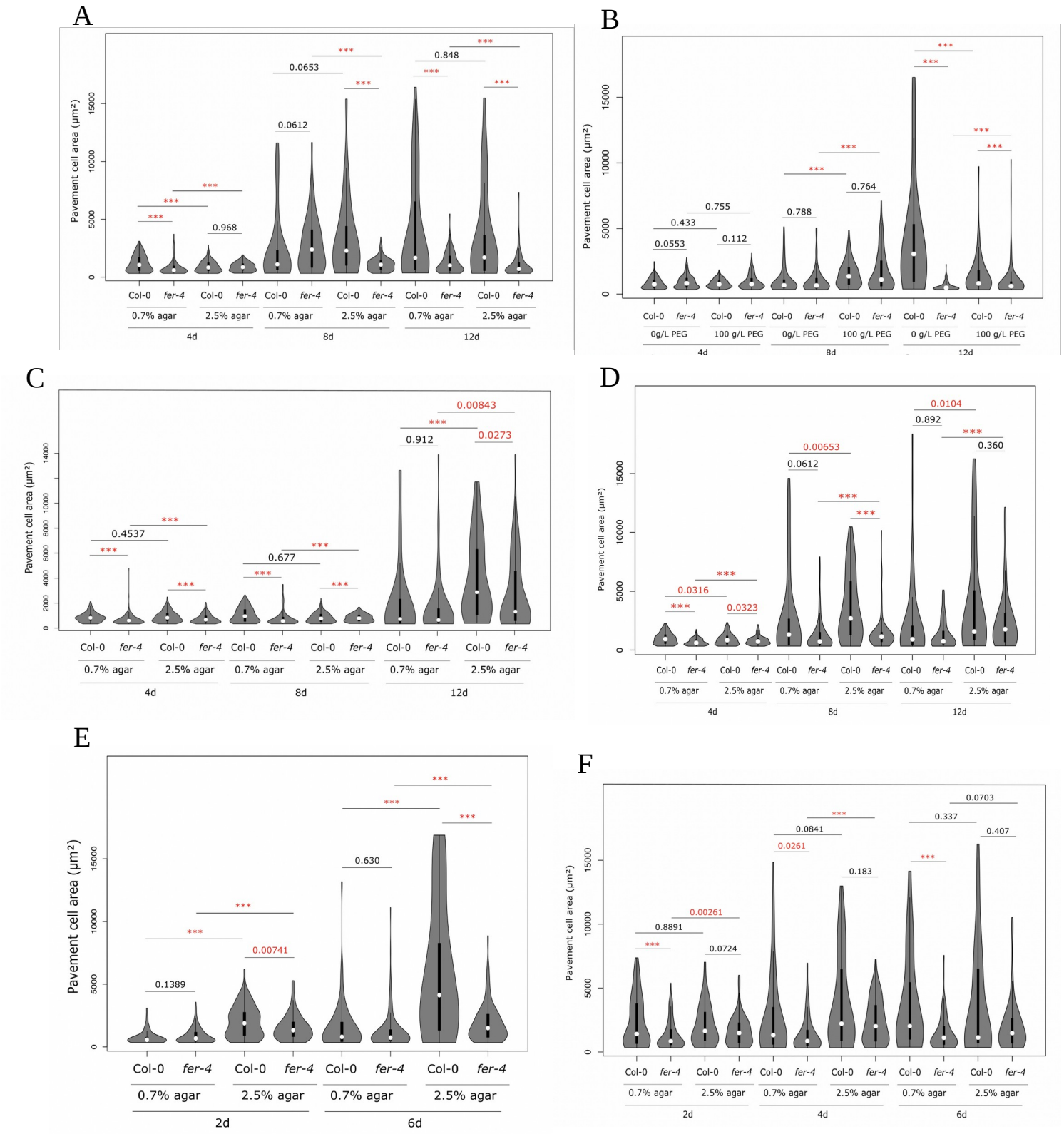

S1. Pavement cell area of different growth conditions

***A**: Long days conditions, agar gels; **B**: Long days conditions, PEG gels; **C**: Short days conditions, agar gels; **D**: Continuous days conditions, agar gels; **E**: 2 days long cold shock conditions; **F**: 7 days long cold shock conditions.* p-*values from Wilcoxon-Mann-Whitney are indicated in red if considered significative (*p<*0.05), and by *** if* p<*0.01.*

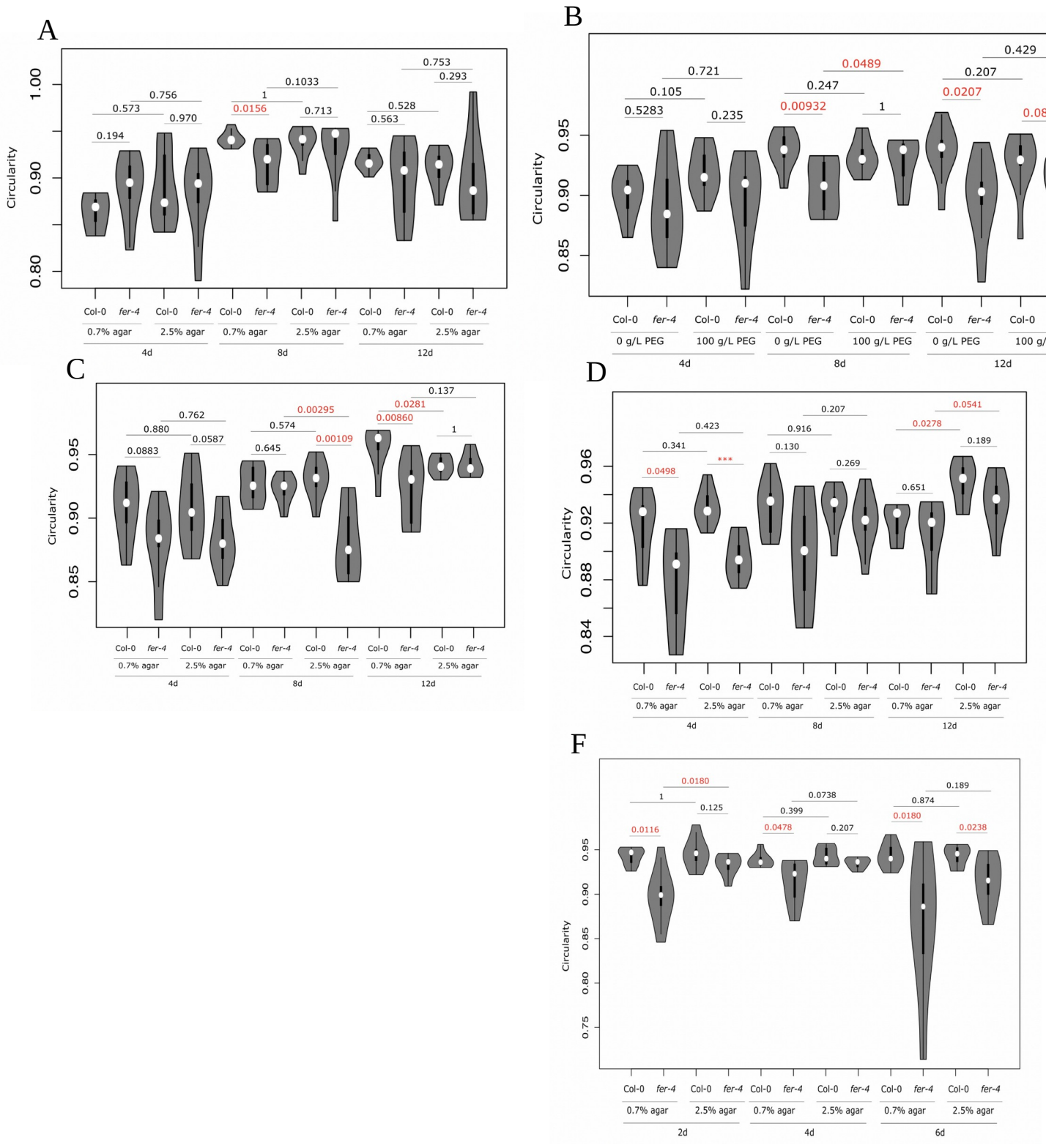

S2. Cotyledon circularity of different growth conditions

***A**: Long days conditions, agar gels; **B**: Long days conditions, PEG gels; **C**: Short days conditions, agar gels; **D**: Continuous days conditions, agar gels; **E**: 2 days long cold shock conditions; **F**: 7 days long cold shock conditions.* p-*values from Wilcoxon-Mann-Whitney are indicated in red if considered significative (*p<*0.05), and by *** if* p<*0.01. (n=10).*

References

Abe, M., Katsumata, H., Komeda, Y. and Takahashi, T. (2003). Regulation of shoot epidermal cell differentiation by a pair of homeodomain proteins in Arabidopsis. *Dev. Camb. Engl.* **130**, 635–643.

Ackermann, F. and Stanislas, T. (2020). The Plasma Membrane—An Integrating Compartment for Mechano-Signaling. *Plants* **9**, 505.

Alberts, B. (2015). *Molecular biology of the cell*.

Alonso-Serra, J., Shi, X., Peaucelle, A., Rastas, P., Bourdon, M., Immanen, J., Takahashi, J., Koivula, H., Eswaran, G. and Muranen, S. (2020). ELIMÄKI locus is required for vertical proprioceptive response in birch trees. *Curr. Biol.* **30**, 589–599.

Al-Qsous, S., Carpentier, E., Klein-Eude, D., Burel, C., Mareck, A., Dauchel, H., Gomord, V. and Balangé, A. P. (2004). Identification and isolation of a pectin methylesterase isoform that could be involved in flax cell wall stiffening. *Planta* **219**, 369–378.

Amanda, D., Doblin, M. S., Galletti, R., Bacic, A., Ingram, G. C. and Johnson, K. L. (2016). DEFECTIVE KERNEL1 (DEK1) Regulates Cell Walls in the Leaf Epidermis. *Plant Physiol.* **172**, 2204–2218.

Amanda, D., Doblin, M. S., Galletti, R., Bacic, A., Ingram, G. C. and Johnson, K. L. (2017). Regulation of cell wall genes in response to DEFECTIVE KERNEL1 (DEK1)-induced cell wall changes. *Plant Signal. Behav.* **12**, e1345405.

Ambrose, C., Allard, J. F., Cytrynbaum, E. N. and Wasteneys, G. O. (2011). A CLASP-modulated cell edge barrier mechanism drives cell-wide cortical microtubule organization in Arabidopsis. *Nat. Commun.* **2**, 430.

Amsbury, S., Kirk, P. and Benitez-Alfonso, Y. (2018). Emerging models on the regulation of intercellular transport by plasmodesmata-associated callose. *J. Exp. Bot.* **69**, 105–115.

Anderson, C. T. and Kieber, J. J. (2020). Dynamic Construction, Perception, and Remodeling of Plant Cell Walls. *Annu. Rev. Plant Biol.* **71**, 39–69.

Anisimov, A. V. and Egorov, A. G. (2002). Plasmodesmata as a Modulator of Osmotic Water Fluxes in Plants. *Russ. J. Plant Physiol.* **49**, 677–684.

Antonacci, G., Beck, T., Bilenca, A., Czarske, J., Elsayad, K., Guck, J., Kim, K., Krug, B., Palombo, F., Prevedel, R., et al. (2020). Recent progress and current opinions in Brillouin microscopy for life science applications. *Biophys. Rev.* **12**, 615–624.

Asaoka, M., Ooe, M., Gunji, S., Milani, P., Runel, G., Horiguchi, G., Hamant, O., Sawa, S., Tsukaya, H. and Ferjani, A. (2021). Stem integrity in Arabidopsis thaliana requires a load-bearing epidermis. *Dev. Camb. Engl.* **148**, dev198028.

Bacete, L. and Hamann, T. (2020). The Role of Mechanoperception in Plant Cell Wall Integrity Maintenance. *Plants* **9**, 574.

Bacete, L., Schulz, J., Engelsdorf, T., Bartosova, Z., Vaahtera, L., Yan, G., Gerhold, J. M., Tichá, T., Øvstebø, C., Gigli-Bisceglia, N., et al. (2022). THESEUS1 modulates cell wall stiffness and abscisic acid production in Arabidopsis thaliana. *Proc. Natl. Acad. Sci.* **119**,.

Bagriantsev, S. N., Gracheva, E. O. and Gallagher, P. G. (2014). Piezo proteins: regulators of mechanosensation and other cellular processes. *J. Biol. Chem.* **289**, 31673–31681.

Baral, A., Morris, E., Aryal, B., Jonsson, K., Verger, S., Xu, T., Bennett, M., Hamant, O. and Bhalerao, R. P. (2020). *External mechanical cues reveal core molecular pathway behind tissue bending in plants*. Plant Biology.

Barbez, E., Dünser, K., Gaidora, A., Lendl, T. and Busch, W. (2017). Auxin steers root cell expansion via apoplastic pH regulation in Arabidopsis thaliana. *Proc. Natl. Acad. Sci.* **114**, E4884–E4893.

Barbier de Reuille, P., Routier-Kierzkowska, A.-L., Kierzkowski, D., Bassel, G. W., Schüpbach, T., Tauriello, G., Bajpai, N., Strauss, S., Weber, A., Kiss, A., et al. (2015). MorphoGraphX: A platform for quantifying morphogenesis in 4D. *eLife* **4**, 05864.

Baskin, T. I. (2001). On the alignment of cellulose microfibrils by cortical microtubules: a review and a model. *Protoplasma* **215**, 150–171.

Baskin, T. I. (2005). Anisotropic expansion of the plant cell wall. *Annu. Rev. Cell Dev. Biol.* **21**, 203–222.

Bassel, G. W., Stamm, P., Mosca, G., Barbier de Reuille, P., Gibbs, D. J., Winter, R., Janka, A., Holdsworth, M. J. and Smith, R. S. (2014). Mechanical constraints imposed by 3D cellular geometry and arrangement modulate growth patterns in the Arabidopsis embryo. *Proc. Natl. Acad. Sci.* **111**, 8685–8690.

Bastien, R., Legland, D., Martin, M., Fregosi, L., Peaucelle, A., Douady, S., Moulia, B. and Höfte, H. (2016). KymoRod: a method for automated kinematic analysis of rod-shaped plant organs. *Plant J. Cell Mol. Biol.* **88**, 468–475.

Basu, D. and Haswell, E. S. (2017). Plant mechanosensitive ion channels: an ocean of possibilities. *Curr. Opin. Plant Biol.* **40**, 43–48.

Batchelder, E. L., Hollopeter, G., Campillo, C., Mezanges, X., Jorgensen, E. M., Nassoy, P., Sens, P. and Plastino, J. (2011). Membrane tension regulates motility by controlling lamellipodium organization. *Proc. Natl. Acad. Sci.* **108**, 11429–11434.

Bauer, S. (2012). Mass Spectrometry for Characterizing Plant Cell Wall Polysaccharides. *Front. Plant Sci.* **3**,.

Beauzamy, L., Nakayama, N. and Boudaoud, A. (2014). Flowers under pressure: ins and outs of turgor regulation in development. *Ann. Bot.* **114**, 1517–1533.

Beauzamy, L., Louveaux, M., Hamant, O. and Boudaoud, A. (2015a). Mechanically, the Shoot Apical Meristem of Arabidopsis Behaves like a Shell Inflated by a Pressure of About 1 MPa. *Front. Plant Sci.* **6**, 1038.

Beauzamy, L., Derr, J. and Boudaoud, A. (2015b). Quantifying hydrostatic pressure in plant cells by using indentation with an atomic force microscope. *Biophys. J.* **108**, 2448–2456.

Becraft, P. W., Li, K., Dey, N. and Asuncion-Crabb, Y. (2002). The maize dek1 gene functions in embryonic pattern formation and cell fate specification. *Dev. Camb. Engl.* **129**, 5217–5225.

Bellati, J., Champeyroux, C., Hem, S., Rofidal, V., Krouk, G., Maurel, C. and Santoni, V. (2016). Novel Aquaporin Regulatory Mechanisms Revealed by Interactomics *. *Mol. Cell. Proteomics* **15**, 3473–3487.

Belteton, S. A., Sawchuk, M. G., Donohoe, B. S., Scarpella, E. and Szymanski, D. B. (2018). Reassessing the Roles of PIN Proteins and Anticlinal Microtubules during Pavement Cell Morphogenesis. *Plant Physiol.* **176**, 432–449.

Belteton, S. A., Li, W., Yanagisawa, M., Hatam, F. A., Quinn, M. I., Szymanski, M. K., Marley, M. W., Turner, J. A. and Szymanski, D. B. (2021). Real-time conversion of tissue-scale mechanical forces into an interdigitated growth pattern. *Nat. Plants* 1–16.

Benkert, R., Obermeyer, G. and Bentrup, F.-W. (1997). The turgor pressure of growing lily pollen tubes. *Protoplasma* **198**, 1–8.

Bergonci, T., Ribeiro, B., Ceciliato, P. H. O., Guerrero-Abad, J. C., Silva-Filho, M. C. and Moura, D. S. (2014). Arabidopsis thaliana RALF1 opposes brassinosteroid effects on root cell elongation and lateral root formation. *J. Exp. Bot.* **65**, 2219–2230.

Besson, S. and Dumais, J. (2011). Universal rule for the symmetric division of plant cells. *Proc. Natl. Acad. Sci.* **108**, 6294–6299.

Bidhendi, A. J., Altartouri, B., Gosselin, F. P. and Geitmann, A. (2019). Mechanical Stress Initiates and Sustains the Morphogenesis of Wavy Leaf Epidermal Cells. *Cell Rep.* **28**, 1237-1250.e6.

Bidhendi, A. j., Chebli, Y. and Geitmann, A. (2020). Fluorescence visualization of cellulose and pectin in the primary plant cell wall. *J. Microsc.* **278**, 164–181.

Blackburn, M. R., Haruta, M. and Moura, D. S. (2020). Twenty Years of Progress in Physiological and Biochemical Investigation of RALF Peptides1 [OPEN]. *Plant Physiol.* **182**, 1657–1666.

Boersma, A. J., Zuhorn, I. S. and Poolman, B. (2015). A sensor for quantification of macromolecular crowding in living cells. *Nat. Methods* **12**, 227–229.

Boisson-Dernier, A., Roy, S., Kritsas, K., Grobei, M. A., Jaciubek, M., Schroeder, J. I. and Grossniklaus, U. (2009). Disruption of the pollen-expressed FERONIA homologs ANXUR1 and ANXUR2 triggers pollen tube discharge. *Dev. Camb. Engl.* **136**, 3279–3288.

Borowska-Wykręt, D. and Kwiatkowska, D. (2018). Folding, Wrinkling, and Buckling in Plant Cell Walls. In *Plant Biomechanics: From Structure to Function at Multiple Scales* (ed. Geitmann, A.) and Gril, J.), pp. 209–233. Cham: Springer International Publishing.

Borowska-Wykręt, D., Elsner, J., De Veylder, L. and Kwiatkowska, D. (2013). Defects in leaf epidermis of Arabidopsis thaliana plants with CDKA;1 activity reduced in the shoot apical meristem. *Protoplasma* **250**, 955–961.

Bou Daher, F., Chen, Y., Bozorg, B., Clough, J., Jönsson, H. and Braybrook, S. A. (2018). Anisotropic growth is achieved through the additive mechanical effect of material anisotropy and elastic asymmetry. *eLife* **7**, e38161.

Boudaoud, A. (2010). An introduction to the mechanics of morphogenesis for plant biologists. *Trends Plant Sci.* **15**, 353–360.

Boudaoud, A., Burian, A., Borowska-Wykręt, D., Uyttewaal, M., Wrzalik, R., Kwiatkowska, D. and Hamant, O. (2014). FibrilTool, an ImageJ plug-in to quantify fibrillar structures in raw microscopy images. *Nat. Protoc.* **9**, 457–463.

Boudon, F., Chopard, J., Ali, O., Gilles, B., Hamant, O., Boudaoud, A., Traas, J. and Godin, C. (2015). A Computational Framework for 3D Mechanical Modeling of Plant Morphogenesis with Cellular Resolution. *PLOS Comput. Biol.* **11**, e1003950.

Bouton, S., Leboeuf, E., Mouille, G., Leydecker, M.-T., Talbotec, J., Granier, F., Lahaye, M., Höfte, H. and Truong, H.-N. (2002). QUASIMODO1 encodes a putative membrane-bound glycosyltransferase required for normal pectin synthesis and cell adhesion in Arabidopsis. *Plant Cell* **14**, 2577–2590.

Bovio, S., Long, Y. and Monéger, F. (2019). Use of Atomic Force Microscopy to Measure Mechanical Properties and Turgor Pressure of Plant Cells and Plant Tissues. *J. Vis. Exp. JoVE*.

Boyer, J. S. (1988). Cell enlargement and growth-induced water potentials. *Physiol. Plant.* **73**, 311–316.

Braam, J. (2005). In touch: plant responses to mechanical stimuli. *New Phytol.* **165**, 373–389.

Braam, J. and Davis, R. W. (1990). Rain-, wind-, and touch-induced expression of calmodulin and calmodulin-related genes in Arabidopsis. *Cell* **60**, 357–364.

Brown, D. (2003). The ins and outs of aquaporin-2 trafficking. *Am. J. Physiol. Renal Physiol.* **284**, F893-901.

Bruck, D. K. and Walker, D. B. (1985). Cell Determination during Embryogenesis in Citrus jambhiri. II. Epidermal Differentiation as a One-Time Event. *Am. J. Bot.* **72**, 1602–1609.

Brutus, A., Sicilia, F., Macone, A., Cervone, F. and Lorenzo, G. D. (2010). A domain swap approach reveals a role of the plant wall-associated kinase 1 (WAK1) as a receptor of oligogalacturonides. *Proc. Natl. Acad. Sci.* **107**, 9452–9457.

Burian, A., Ludynia, M., Uyttewaal, M., Traas, J., Boudaoud, A., Hamant, O. and Kwiatkowska, D. (2013). A correlative microscopy approach relates microtubule behaviour, local organ geometry, and cell growth at the Arabidopsis shoot apical meristem. *J. Exp. Bot.* **64**, 5753–5767.

Caon, M. (2014). Osmoles, osmolality and osmotic pressure: Clarifying the puzzle of solution concentration. *Contemp. Nurse*.

Capron, A., Gourgues, M., Neiva, L. S., Faure, J.-E., Berger, F., Pagnussat, G., Krishnan, A., Alvarez-Mejia, C., Vielle-Calzada, J.-P., Lee, Y.-R., et al. (2008). Maternal Control of Male-Gamete Delivery in Arabidopsis Involves a Putative GPI-Anchored Protein Encoded by the LORELEI Gene. *Plant Cell* **20**, 3038–3049.

Carter, R., Woolfenden, H., Baillie, A., Amsbury, S., Carroll, S., Healicon, E., Sovatzoglou, S., Braybrook, S., Gray, J. E., Hobbs, J., et al. (2017). Stomatal Opening Involves Polar, Not Radial, Stiffening Of Guard Cells. *Curr. Biol.* **27**, 2974-2983.e2.

Castilleux, R., Plancot, B., Vicré, M., Nguema-Ona, E. and Driouich, A. (2021). Extensin, an underestimated key component of cell wall defence? *Ann. Bot.* **127**, 709–713.

Cavalier, D. M., Lerouxel, O., Neumetzler, L., Yamauchi, K., Reinecke, A., Freshour, G., Zabotina, O. A., Hahn, M. G., Burgert, I., Pauly, M., et al. (2008). Disrupting two Arabidopsis thaliana xylosyltransferase genes results in plants deficient in xyloglucan, a major primary cell wall component. *Plant Cell* **20**, 1519–1537.

Chakrabortty, B., Willemsen, V., de Zeeuw, T., Liao, C.-Y., Weijers, D., Mulder, B. and Scheres, B. (2018). A Plausible Microtubule-Based Mechanism for Cell Division Orientation in Plant Embryogenesis. *Curr. Biol.* **28**, 3031-3043.e2.

Chakraborty, J., Luo, J. and Dyson, R. J. (2021). Lockhart with a twist: Modelling cellulose microfibril deposition and reorientation reveals twisting plant cell growth mechanisms. *J. Theor. Biol.* **525**, 110736.

Chan, J. and Coen, E. (2020). Interaction between Autonomous and Microtubule Guidance Systems Controls Cellulose Synthase Trajectories. *Curr. Biol.* S0960982219316999.

Chaumont, F., Moshelion, M. and Daniels, M. J. (2005). Regulation of plant aquaporin activity. *Biol. Cell* **97**, 749–764.

Chebli, Y. and Geitmann, A. (2017). Cellular growth in plants requires regulation of cell wall biochemistry. *Curr. Opin. Cell Biol.* **44**, 28–35.

Chebli, Y., Kaneda, M., Zerzour, R. and Geitmann, A. (2012). The Cell Wall of the Arabidopsis Pollen Tube—Spatial Distribution, Recycling, and Network Formation of Polysaccharides. *Plant Physiol.* **160**, 1940–1955.

Cheddadi, I., Génard, M., Bertin, N. and Godin, C. (2019). Coupling water fluxes with cell wall mechanics in a multicellular model of plant development. *PLOS Comput. Biol.* **15**, e1007121.

Chehab, E. W., Eich, E. and Braam, J. (2009). Thigmomorphogenesis: a complex plant response to mechano-stimulation. *J. Exp. Bot.* **60**, 43–56.

Chen, J., Yu, F., Liu, Y., Du, C., Li, X., Zhu, S., Wang, X., Lan, W., Rodriguez, P. L., Liu, X., et al. (2016). FERONIA interacts with ABI2-type phosphatases to facilitate signaling cross-talk between abscisic acid and RALF peptide in Arabidopsis. *Proc. Natl. Acad. Sci. U. S. A.* **113**, E5519-5527.

Chen, Y., Ju, L., Rushdi, M., Ge, C. and Zhu, C. (2017). Receptor-mediated cell mechanosensing. *Mol. Biol. Cell* **28**, 3134–3155.

Cheung, A. Y. and Wu, H.-M. (2011). THESEUS 1, FERONIA and relatives: a family of cell wall-sensing receptor kinases? *Curr. Opin. Plant Biol.* **14**, 632–641.

Choquet, D., Felsenfeld, D. P. and Sheetz, M. P. (1997). Extracellular matrix rigidity causes strengthening of integrin-cytoskeleton linkages. *Cell* **88**, 39–48.

Codjoe, J. M., Miller, K. and Haswell, E. S. (2022). Plant cell mechanobiology: Greater than the sum of its parts. *Plant Cell* **34**, 129–145.

Colin, L., Chevallier, A., Tsugawa, S., Gacon, F., Godin, C., Viasnoff, V., Saunders, T. E. and Hamant, O. (2020). Cortical tension overrides geometrical cues to orient microtubules in confined protoplasts. *Proc. Natl. Acad. Sci.* **117**, 32731–32738.

Colin, L., Martin-Arevalillo, R., Bovio, S., Bauer, A., Vernoux, T., Caillaud, M.-C., Landrein, B. and Jaillais, Y. (2022). Imaging the living plant cell: From probes to quantification. *Plant Cell* **34**, 247–272.

Colom, A., Derivery, E., Soleimanpour, S., Tomba, C., Molin, M. D., Sakai, N., González-Gaitán, M., Matile, S. and Roux, A. (2018). A fluorescent membrane tension probe. *Nat. Chem.* **10**, 1118.

Colombani, M. and Forterre, Y. (2011). Biomechanics of rapid movements in plants: poroelastic measurements at the cell scale. *Comput. Methods Biomech. Biomed. Engin.* **14**, 115–117.

Corson, F., Hamant, O., Bohn, S., Traas, J., Boudaoud, A. and Couder, Y. (2009). Turning a plant tissue into a living cell froth through isotropic growth. *Proc. Natl. Acad. Sci.* **106**, 8453–8458.

Cosentino Lagomarsino, M., Tanase, C., Vos, J. W., Emons, A. M. C., Mulder, B. M. and Dogterom, M. (2007). Microtubule organization in three-dimensional confined geometries: evaluating the role of elasticity through a combined in vitro and modeling approach. *Biophys. J.* **92**, 1046–1057.

Cosgrove, D. J. (1993). Water Uptake by Growing Cells: An Assessment of the Controlling Roles of Wall Relaxation, Solute Uptake, and Hydraulic Conductance. *Int. J. Plant Sci.* **154**, 10–21.

Cosgrove, D. J. (1997). Assembly and enlargement of the primary cell wall in plants. *Annu. Rev. Cell Dev. Biol.* **13**, 171–201.

Cosgrove, D. J. (2000). Loosening of plant cell walls by expansins. *Nature* **407**, 321–326.

Cosgrove, D. J. (2005). Growth of the plant cell wall. *Nat. Rev. Mol. Cell Biol.* **6**, 850–861.

Cosgrove, D. J. (2014). Re-constructing our models of cellulose and primary cell wall assembly. *Curr. Opin. Plant Biol.* **22**, 122–131.

Cosgrove, D. J. (2016a). Plant cell wall extensibility: connecting plant cell growth with cell wall structure, mechanics, and the action of wall-modifying enzymes. *J. Exp. Bot.* **67**, 463–476.

Cosgrove, D. J. (2016b). Catalysts of plant cell wall loosening.

Cosgrove, D. J. (2022). Building an Extensible Cell Wall. *Plant Physiol.* kiac184.

Crowe, J. D., Hao, P., Pattathil, S., Pan, H., Ding, S.-Y., Hodge, D. B. and Jensen, J. K. (2021). Xylan Is Critical for Proper Bundling and Alignment of Cellulose Microfibrils in Plant Secondary Cell Walls. *Front. Plant Sci.* **12**, 737690.

Cuevas-Velazquez, C. L., Vellosillo, T., Guadalupe, K., Schmidt, H. B., Yu, F., Moses, D., Brophy, J. A. N., Cosio-Acosta, D., Das, A., Wang, L., et al. (2021). Intrinsically disordered protein biosensor tracks the physical-chemical effects of osmotic stress on cells. *Nat. Commun.* **12**, 5438.

Dardelle, F., Lehner, A., Ramdani, Y., Bardor, M., Lerouge, P., Driouich, A. and Mollet, J.-C. (2010). Biochemical and immunocytological characterizations of Arabidopsis pollen tube cell wall. *Plant Physiol.* **153**, 1563–1576.

De Storme, N. and Geelen, D. (2014). Callose homeostasis at plasmodesmata: molecular regulators and developmental relevance. *Front. Plant Sci.* **5**,.

Delauney, A. J. and Verma, D. P. S. (1993). Proline biosynthesis and osmoregulation in plants. *Plant J.* **4**, 215–223.

Demko, V., Perroud, P.-F., Johansen, W., Delwiche, C. F., Cooper, E. D., Remme, P., Ako, A. E., Kugler, K. G., Mayer, K. F. X., Quatrano, R., et al. (2014). Genetic analysis of DEFECTIVE KERNEL1 loop function in three-dimensional body patterning in Physcomitrella patens. *Plant Physiol.* **166**, 903–919.

Deslauriers, S. D. and Larsen, P. B. (2010). FERONIA Is a Key Modulator of Brassinosteroid and Ethylene Responsiveness in Arabidopsis Hypocotyls. *Mol. Plant* **3**, 626–640.

Dievart, A., Gottin, C., Périn, C., Ranwez, V. and Chantret, N. (2020). Origin and Diversity of Plant Receptor-Like Kinases. *Annu. Rev. Plant Biol.* **71**, 131–156.

Doineau, E., Coqueugniot, G., Pucci, M. F., Caro, A.-S., Cathala, B., Bénézet, J.-C., Bras, J. and Le Moigne, N. (2021). Hierarchical thermoplastic biocomposites reinforced with flax fibres modified by xyloglucan and cellulose nanocrystals. *Carbohydr. Polym.* **254**, 117403.

Donaldson, L. A. and Singh, A. P. (2016). Chapter 6 - Reaction Wood. In *Secondary Xylem Biology* (ed. Kim, Y. S.), Funada, R.), and Singh, A. P.), pp. 93–110. Boston: Academic Press.

Dong, Q., Zhang, Z., Liu, Y., Tao, L.-Z. and Liu, H. (2019). FERONIA regulates auxin-mediated lateral root development and primary root gravitropism. *FEBS Lett.* **593**, 97–106.

Dresselhaus, T., Sprunck, S. and Wessel, G. M. (2016). Fertilization Mechanisms in Flowering Plants. *Curr. Biol. CB* **26**, R125-139.

Du, C., Li, X., Chen, J., Chen, W., Li, B., Li, C., Wang, L., Li, J., Zhao, X., Lin, J., et al. (2016). Receptor kinase complex transmits RALF peptide signal to inhibit root growth in Arabidopsis. *Proc. Natl. Acad. Sci.* **113**, E8326–E8334.

Du, S., Qu, L.-J. and Xiao, J. (2018). Crystal structures of the extracellular domains of the CrRLK1L receptor-like kinases ANXUR1 and ANXUR2. *Protein Sci.* **27**, 886–892.

Duan, Q., Kita, D., Li, C., Cheung, A. Y. and Wu, H.-M. (2010). FERONIA receptor-like kinase regulates RHO GTPase signaling of root hair development. *Proc. Natl. Acad. Sci. U. S. A.* **107**, 17821–17826.

Duan, Q., Kita, D., Johnson, E. A., Aggarwal, M., Gates, L., Wu, H.-M. and Cheung, A. Y. (2014). Reactive oxygen species mediate pollen tube rupture to release sperm for fertilization in Arabidopsis. *Nat. Commun.* **5**, 3129.

Duan, Q., Liu, M.-C. J., Kita, D., Jordan, S. S., Yeh, F.-L. J., Yvon, R., Carpenter, H., Federico, A. N., Garcia-Valencia, L. E., Eyles, S. J., et al. (2020). FERONIA controls pectin- and nitric oxide-mediated male–female interaction. *Nature* 1–6.

Dumais, J. (2021). Mechanics and hydraulics of pollen tube growth. *New Phytol.* **232**, 1549–1565.

Dumais, J. and Steele, C. R. (2000). New Evidence for the Role of Mechanical Forces in the Shoot Apical Meristem. *J. Plant Growth Regul.* **19**, 7–18.

Dünser, K., Gupta, S., Herger, A., Feraru, M. I., Ringli, C. and Kleine-Vehn, J. (2019). Extracellular matrix sensing by FERONIA and Leucine-Rich Repeat Extensins controls vacuolar expansion during cellular elongation in Arabidopsis thaliana. *EMBO J.* **38**, e100353.

Durand-Smet, P., Chastrette, N., Guiroy, A., Richert, A., Berne-Dedieu, A., Szecsi, J., Boudaoud, A., Frachisse, J.-M., Bendahmane, M., Bendhamane, M., et al. (2014). A comparative mechanical analysis of plant and animal cells reveals convergence across kingdoms. *Biophys. J.* **107**, 2237–2244.

Durand-Smet, P., Spelman, T. A., Meyerowitz, E. M. and Jönsson, H. (2020). Cytoskeletal organization in isolated plant cells under geometry control. *Proc. Natl. Acad. Sci.* **117**, 17399–17408.

Elsayad, K., Werner, S., Gallemí, M., Kong, J., Sánchez Guajardo, E. R., Zhang, L., Jaillais, Y., Greb, T. and Belkhadir, Y. (2016). Mapping the subcellular mechanical properties of live cells in tissues with fluorescence emission–Brillouin imaging. *Sci. Signal.* **9**, rs5–rs5.

Emons, A. M. C. and van Maaren, N. (1987). Helicoidal cell-wall texture in root hairs. *Planta* **170**, 145–151.

Engelsdorf, T., Gigli-Bisceglia, N., Veerabagu, M., McKenna, J. F., Vaahtera, L., Augstein, F., Van der Does, D., Zipfel, C. and Hamann, T. (2018). The plant cell wall integrity maintenance and immune signaling systems cooperate to control stress responses in *Arabidopsis thaliana*. *Sci. Signal.* **11**, eaao3070.

Engelsdorf, T., Kjaer, L., Gigli-Bisceglia, N., Vaahtera, L., Bauer, S., Miedes, E., Wormit, A., James, L., Chairam, I., Molina, A., et al. (2019). Functional characterization of genes mediating cell wall metabolism and responses to plant cell wall integrity impairment. *BMC Plant Biol.* **19**, 320.

Engineer, C. B., Ghassemian, M., Anderson, J. C., Peck, S. C., Hu, H. and Schroeder, J. I. (2014). Carbonic anhydrases, EPF2 and a novel protease mediate CO2 control of stomatal development. *Nature* **513**, 246–250.

Erguvan, Ö., Louveaux, M., Hamant, O. and Verger, S. (2019). ImageJ SurfCut: a user-friendly pipeline for high-throughput extraction of cell contours from 3D image stacks. *BMC Biol.* **17**, 38.

Errera, L. (1886). Sur une condition fondamentale d'équilibre des cellules vivantes. *Ann. Société Belge Microsc. 1876* **13**, 12–16.

Escobar-Restrepo, J.-M., Huck, N., Kessler, S., Gagliardini, V., Gheyselinck, J., Yang, W.-C. and Grossniklaus, U. (2007). The FERONIA Receptor-like Kinase Mediates Male-Female Interactions During Pollen Tube Reception. *Science*.

Evans, M. J., Fanucchi, M. V., Miller, L. A., Carlson, M. A., Nishio, S. J. and Hyde, D. M. (2010). Reduction of collagen VII anchoring fibrils in the airway basement membrane zone of infant rhesus monkeys exposed to house dust mite. *Am. J. Physiol.-Lung Cell. Mol. Physiol.* **298**, L543–L547.

Fàbregas, N., Li, N., Boeren, S., Nash, T. E., Goshe, M. B., Clouse, S. D., de Vries, S. and Caño-Delgado, A. I. (2013). The BRASSINOSTEROID INSENSITIVE1–LIKE3 Signalosome Complex Regulates Arabidopsis Root Development[C][W][OPEN]. *Plant Cell* **25**, 3377–3388.

Fal, K., Asnacios, A., Chabouté, M.-E. and Hamant, O. (2017). Nuclear envelope: a new frontier in plant mechanosensing? *Biophys. Rev.* **9**, 389–403.

Fal, K., Korsbo, N., Alonso-Serra, J., Teles, J., Liu, M., Refahi, Y., Chabouté, M.-E., Jönsson, H. and Hamant, O. (2021). Tissue folding at the organ–meristem boundary results in nuclear compression and chromatin compaction. *Proc. Natl. Acad. Sci.* **118**, e2017859118.

Fan, Y., Burkart, G. M. and Dixit, R. (2018). The Arabidopsis SPIRAL2 Protein Targets and Stabilizes Microtubule Minus Ends. *Curr. Biol. CB* **28**, 987-994.e3.

Feng, W., Kita, D., Peaucelle, A., Cartwright, H. N., Doan, V., Duan, Q., Liu, M.-C., Maman, J., Steinhorst, L., Schmitz-Thom, I., et al. (2018). The FERONIA Receptor Kinase Maintains Cell-Wall Integrity during Salt Stress through Ca2+ Signaling. *Curr. Biol. CB* **28**, 666-675.e5.

Fleming, A. J., McQueen-Mason, S., Mandel, T. and Kuhlemeier, C. (1997). Induction of Leaf Primordia by the Cell Wall Protein Expansin. *Science* **276**, 1415–1418.

Forterre, Y., Marmottant, P., Quilliet, C. and Noblin, X. (2016). Physics of rapid movements in plants. *Europhys. News* **47**, 27–30.

Franck, A. D., Powers, A. F., Gestaut, D. R., Gonen, T., Davis, T. N. and Asbury, C. L. (2007). Tension applied through the Dam1 complex promotes microtubule elongation providing a direct mechanism for length control in mitosis. *Nat. Cell Biol.* **9**, 832–837.

Fricke, W., Jarvis, M. and Brett, C. (2000). Turgor pressure, membrane tension and the control of exocytosis in higher plants.

Fu, Y., Gu, Y., Zheng, Z., Wasteneys, G. and Yang, Z. (2005). Arabidopsis interdigitating cell growth requires two antagonistic pathways with opposing action on cell morphogenesis. *Cell* **120**, 687–700.

Galletti, R. and Ingram, G. C. (2015). Communication is key: Reducing DEK1 activity reveals a link between cell-cell contacts and epidermal cell differentiation status. *Commun. Integr. Biol.* **8**, e1059979.

Galletti, R., Johnson, K. L., Scofield, S., San-Bento, R., Watt, A. M., Murray, J. A. H. and Ingram, G. C. (2015). DEFECTIVE KERNEL 1 promotes and maintains plant epidermal differentiation. *Dev. Camb. Engl.* **142**, 1978–1983.

Galletti, R., Verger, S., Hamant, O. and Ingram, G. C. (2016). Developing a “thick skin”: a paradoxical role for mechanical tension in maintaining epidermal integrity? *Dev. Camb. Engl.* **143**, 3249–3258.

Galstyan, A. and Hay, A. (2018). Snap, crack and pop of explosive fruit. *Curr. Opin. Genet. Dev.* **51**, 31–36.

Geitmann, A. (2006). Experimental approaches used to quantify physical parameters at cellular and subcellular levels. *Am. J. Bot.* **93**, 1380–1390.

Gifford, M. L., Dean, S. and Ingram, G. C. (2003). The Arabidopsis ACR4 gene plays a role in cell layer organisation during ovule integument and sepal margin development. *Dev. Camb. Engl.* **130**, 4249–4258.

Gigli-Bisceglia, N., Zelm, E. van, Huo, W., Lamers, J. and Testerink, C. (2021). Arabidopsis root responses to salinity depend on pectin modification and cell wall sensing. 2020.12.18.423458.

Gonneau, M., Desprez, T., Martin, M., Doblas, V. G., Bacete, L., Miart, F., Sormani, R., Hématy, K., Renou, J., Landrein, B., et al. (2018). Receptor Kinase THESEUS1 Is a Rapid Alkalinization Factor 34 Receptor in Arabidopsis. *Curr. Biol. CB* **28**, 2452-2458.e4.

González-Fontes, A., Rexach, J., Navarro-Gochicoa, M. T., Herrera-Rodríguez, M. B., Beato, V. M., Maldonado, J. M. and Camacho-Cristóbal, J. J. (2008). Is boron involved solely in structural roles in vascular plants? *Plant Signal. Behav.* **3**, 24–26.

Goodbody, K. C. and Lloyd, C. W. (1990). Actin filaments line up acrossTradescantia epidermal cells, anticipating wound-induced divison planes. *Protoplasma* **157**, 92–101.

Goswami, R., Asnacios, A., Milani, P., Graindorge, S., Houlné, G., Mutterer, J., Hamant, O. and Chabouté, M.-E. (2020). Mechanical Shielding in Plant Nuclei. *Curr. Biol.* **30**, 2013-2025.e3.

Granier, C., Aguirrezabal, L., Chenu, K., Cookson, S. J., Dauzat, M., Hamard, P., Thioux, J.-J., Rolland, G., Bouchier-Combaud, S., Lebaudy, A., et al. (2006). PHENOPSIS, an automated platform for reproducible phenotyping of plant responses to soil water deficit in Arabidopsis thaliana permitted the identification of an accession with low sensitivity to soil water deficit. *New Phytol.* **169**, 623–635.

Green, P. B. (1962). Mechanism for Plant Cellular Morphogenesis. *Science* **138**, 1404–1405.

Green, P. B. (1968). Growth Physics in Nitella: a Method for Continuous in Vivo Analysis of Extensibility Based on a Micro-manometer Technique for Turgor Pressure 1. *Plant Physiol.* **43**, 1169–1184.

Green, P. B. and Cummins, W. R. (1974). Growth rate and turgor pressure: auxin effect studies with an automated apparatus for single coleoptiles. *Plant Physiol.* **54**, 863–869.

Green, P. B. and King, A. (1966). A mechanism for the origin of specifically oriented textures in development with special reference to Nitella wall texture. *Aust J Biol Sci* **19**, 421–437.

Gregor, T. (2017). Beyond D'Arcy Thompson: Future challenges for quantitative biology. *Mech. Dev.* **145**, 10–12.

Gronnier, J., Franck, C. M., Stegmann, M., DeFalco, T. A., Abarca, A., von Arx, M., Dünser, K., Lin, W., Yang, Z., Kleine-Vehn, J., et al. (2022). Regulation of immune receptor kinase plasma membrane nanoscale organization by a plant peptide hormone and its receptors. *eLife* **11**, e74162.

Gruel, J., Landrein, B., Tarr, P., Schuster, C., Refahi, Y., Sampathkumar, A., Hamant, O., Meyerowitz, E. M. and Jönsson, H. (2016). An epidermis-driven mechanism positions and scales stem cell niches in plants. *Sci. Adv.* **2**, e1500989.

Gu, Y., Kaplinsky, N., Bringmann, M., Cobb, A., Carroll, A., Sampathkumar, A., Baskin, T. I., Persson, S. and Somerville, C. R. (2010). Identification of a cellulose synthase-associated protein required for cellulose biosynthesis. *Proc. Natl. Acad. Sci.* **107**, 12866–12871.

Gudipaty, S. A., Lindblom, J., Loftus, P. D., Redd, M. J., Edes, K., Davey, C. F., Krishnegowda, V. and Rosenblatt, J. (2017). Mechanical stretch triggers rapid epithelial cell division through Piezo1. *Nature* **543**, 118–121.

Guerringue, Y., Thomine, S. and Frachisse, J.-M. (2018). Sensing and transducing forces in plants with MSL10 and DEK1 mechanosensors. *FEBS Lett.* **592**, 1968–1979.

Guo, H., Li, L., Ye, H., Yu, X., Algreen, A. and Yin, Y. (2009). Three related receptor-like kinases are required for optimal cell elongation in Arabidopsis thaliana. *Proc. Natl. Acad. Sci. U. S. A.* **106**, 7648–7653.

Guo, H., Nolan, T. M., Song, G., Liu, S., Xie, Z., Chen, J., Schnable, P. S., Walley, J. W. and Yin, Y. (2018). FERONIA Receptor Kinase Contributes to Plant Immunity by Suppressing Jasmonic Acid Signaling in Arabidopsis thaliana. *Curr. Biol. CB* **28**, 3316-3324.e6.

Haas, K. T. and Peaucelle, A. (2021). From monocots to dicots: the multifold aspect of cell wall expansion. *J. Exp. Bot.* **72**, 1511–1513.

Haas, K. T., Wightman, R., Meyerowitz, E. M. and Peaucelle, A. (2020). Pectin homogalacturonan nanofilament expansion drives morphogenesis in plant epidermal cells. *Science* **367**, 1003–1007.

Haas, K. T., Wightman, R., Peaucelle, A. and Höfte, H. (2021). The role of pectin phase separation in plant cell wall assembly and growth. *Cell Surf.* **7**, 100054.

Hamant, O. and Haswell, E. S. (2017). Life behind the wall: sensing mechanical cues in plants. *BMC Biol.* **15**, 59.

Hamant, O. and Saunders, T. E. (2020). Shaping Organs: Shared Structural Principles Across Kingdoms. *Annu. Rev. Cell Dev. Biol.* **36**, 385–410.

Hamant, O., Heisler, M. G., Jönsson, H., Krupinski, P., Uyttewaal, M., Bokov, P., Corson, F., Sahlin, P., Boudaoud, A., Meyerowitz, E. M., et al. (2008). Developmental Patterning by Mechanical Signals in Arabidopsis. *Science* **322**, 1650–1655.

Hamant, O., Inoue, D., Bouchez, D., Dumais, J. and Mjolsness, E. (2019a). Are microtubules tension sensors? *Nat. Commun.* **10**, 2360.

Hamant, O., Inoue, D., Bouchez, D., Dumais, J. and Mjolsness, E. (2019b). Are microtubules tension sensors? *Nat. Commun.* **10**, 2360.

Hamilton, E. S., Schlegel, A. M. and Haswell, E. S. (2015a). United in diversity: mechanosensitive ion channels in plants. *Annu. Rev. Plant Biol.* **66**, 113–137.

Hamilton, E. S., Jensen, G. S., Maksaev, G., Katims, A., Sherp, A. M. and Haswell, E. S. (2015b). Mechanosensitive channel MSL8 regulates osmotic forces during pollen hydration and germination. *Science* **350**, 438–441.

Hampoelz, B. and Lecuit, T. (2011). Nuclear mechanics in differentiation and development. *Curr. Opin. Cell Biol.* **23**, 668–675.

Haruta, M., Sabat, G., Stecker, K., Minkoff, B. B. and Sussman, M. R. (2014). A peptide hormone and its receptor protein kinase regulate plant cell expansion. *Science* **343**, 408–411.

Haswell, E. S., Phillips, R. and Rees, D. C. (2011). Mechanosensitive channels: what can they do and how do they do it? *Struct. Lond. Engl. 1993* **19**, 1356–1369.

Hatte, G., Prigent, C. and Tassan, J.-P. (2017). Tight junctions negatively regulate mechanical forces applied to adherens junctions in vertebrate epithelial tissue. *J Cell Sci* jcs.208736.

Hayashi, S., Ishii, T., Matsunaga, T., Tominaga, R., Kuromori, T., Wada, T., Shinozaki, K. and Hirayama, T. (2008). The Glycerophosphoryl Diester Phosphodiesterase-Like Proteins SHV3 and its Homologs Play Important Roles in Cell Wall Organization. *Plant Cell Physiol.* **49**, 1522–1535.

Hayat, S., Hayat, Q., Alyemeni, M. N., Wani, A. S., Pichtel, J. and Ahmad, A. (2012). Role of proline under changing environments. *Plant Signal. Behav.* **7**, 1456–1466.

Heath, J. P. and Dunn, G. A. (1978). Cell to substratum contacts of chick fibroblasts and their relation to the microfilament system. A correlated interference-reflexion and high-voltage electron-microscope study. *J. Cell Sci.* **29**, 197–212.

Heisler, M. G., Ohno, C., Das, P., Sieber, P., Reddy, G. V., Long, J. A. and Meyerowitz, E. M. (2005). Patterns of auxin transport and gene expression during primordium development revealed by live imaging of the Arabidopsis inflorescence meristem. *Curr. Biol. CB* **15**, 1899–1911.

Heisler, M. G., Hamant, O., Krupinski, P., Uyttewaal, M., Ohno, C., Jönsson, H., Traas, J. and Meyerowitz, E. M. (2010). Alignment between PIN1 Polarity and Microtubule Orientation in the Shoot Apical Meristem Reveals a Tight Coupling between Morphogenesis and Auxin Transport. *PLoS Biol.* **8**,.

Hejnowicz, Z. (2011). Plants as Mechano-Osmotic Transducers. In *Mechanical Integration of Plant Cells and Plants* (ed. Wojtaszek, P.), pp. 241–267. Berlin, Heidelberg: Springer.

Hejnowicz, Z., Rusin, A. and Rusin, T. (2000). Tensile Tissue Stress Affects the Orientation of Cortical Microtubules in the Epidermis of Sunflower Hypocotyl. *J. Plant Growth Regul.* **19**, 31–44.

Hématy, K. and Höfte, H. (2008). Novel receptor kinases involved in growth regulation. *Curr. Opin. Plant Biol.* **11**, 321–328.

Hématy, K., Sado, P.-E., Van Tuinen, A., Rochange, S., Desnos, T., Balzergue, S., Pelletier, S., Renou, J.-P. and Höfte, H. (2007). A receptor-like kinase mediates the response of Arabidopsis cells to the inhibition of cellulose synthesis. *Curr. Biol. CB* **17**, 922–931.

Herger, A., Dünser, K., Kleine-Vehn, J. and Ringli, C. (2019). Leucine-Rich Repeat Extensin Proteins and Their Role in Cell Wall Sensing. *Curr. Biol.* **29**, R851–R858.

Hernandez, L. and Green, P. (1993). Transductions for the Expression of Structural Pattern: Analysis in Sunflower. *Plant Cell* **5**, 1725–1738.

Hernández-Hernández, V., Benítez, M. and Boudaoud, A. (2020). Interplay between turgor pressure and plasmodesmata during plant development. *J. Exp. Bot.* **71**, 768–777.

Hervieux, N., Dumond, M., Sapala, A., Routier-Kierzkowska, A.-L., Kierzkowski, D., Roeder, A. H. K., Smith, R. S., Boudaoud, A. and Hamant, O. (2016). A Mechanical Feedback Restricts Sepal Growth and Shape in Arabidopsis. *Curr. Biol. CB*.

Hervieux, N., Tsugawa, S., Fruleux, A., Dumond, M., Routier-Kierzkowska, A.-L., Komatsuzaki, T., Boudaoud, A., Larkin, J. C., Smith, R. S., Li, C.-B., et al. (2017). Mechanical Shielding of Rapidly Growing Cells Buffers Growth Heterogeneity and Contributes to Organ Shape Reproducibility. *Curr. Biol.* **27**, 3468-3479.e4.

Hill, A. E. and Shachar-Hill, Y. (2015). Are Aquaporins the Missing Transmembrane Osmosensors? *J. Membr. Biol.* **248**, 753–765.

Hill, A. E., Shachar-Hill, B. and Shachar-Hill, Y. (2004). What are aquaporins for? *J. Membr. Biol.* **197**, 1–32.

Himmelspach, R., Williamson, R. E. and Wasteneys, G. O. (2003). Cellulose microfibril alignment recovers from DCB-induced disruption despite microtubule disorganization. *Plant J.* **36**, 565–575.

Höfte, H. (2015). The Yin and Yang of Cell Wall Integrity Control: Brassinosteroid and FERONIA Signaling. *Plant Cell Physiol.* **56**, 224–231.

Holdaway-Clarke, T. L., Walker, N. A., Hepler, P. K. and Overall, R. L. (2000). Physiological elevations in cytoplasmic free calcium by cold or ion injection result in transient closure of higher plant plasmodesmata. *Planta* **210**, 329–335.

Hong, L., Dumond, M., Tsugawa, S., Sapala, A., Routier-Kierzkowska, A.-L., Zhou, Y., Chen, C., Kiss, A., Zhu, M., Hamant, O., et al. (2016). Variable Cell Growth Yields Reproducible Organ Development through Spatiotemporal Averaging. *Dev. Cell* **38**, 15–32.

Honkanen, S., Jones, V. A. S., Morieri, G., Champion, C., Hetherington, A. J., Kelly, S., Proust, H., Saint-Marcoux, D., Prescott, H. and Dolan, L. (2016). The Mechanism Forming the Cell Surface of Tip-Growing Rooting Cells Is Conserved among Land Plants. *Curr. Biol.* **26**, 3238–3244.

Huck, N., Moore, J. M., Federer, M. and Grossniklaus, U. (2003). The Arabidopsis mutant feronia disrupts the female gametophytic control of pollen tube reception. *Development* **130**, 2149–2159.

Hyman, A. J., Tumova, S. and Beech, D. J. (2017). Chapter Two - Piezo1 Channels in Vascular Development and the Sensing of Shear Stress. In *Current Topics in Membranes* (ed. Gottlieb, P. A.), pp. 37–57. Academic Press.

Inoue, D., Mahmot, B., Kabir, A. M. R., Farhana, T. I., Tokuraku, K., Sada, K., Konagaya, A. and Kakugo, A. (2015). Depletion force induced collective motion of microtubules driven by kinesin. *Nanoscale* **7**, 18054–18061.

Inoue, D., Nitta, T., Kabir, A. M. R., Sada, K., Gong, J. P., Konagaya, A. and Kakugo, A. (2016). Sensing surface mechanical deformation using active probes driven by motor proteins. *Nat. Commun.* **7**, 12557.

Ishida, T., Kaneko, Y., Iwano, M. and Hashimoto, T. (2007). Helical microtubule arrays in a collection of twisting tubulin mutants of Arabidopsis thaliana. *Proc. Natl. Acad. Sci.* **104**, 8544–8549.

Jaffe, M. J. (1973). Thigmomorphogenesis: The response of plant growth and development to mechanical stimulation. *Planta* **114**, 143–157.

Javot, H., Lauvergeat, V., Santoni, V., Martin-Laurent, F., Güçlü, J., Vinh, J., Heyes, J., Franck, K. I., Schäffner, A. R., Bouchez, D., et al. (2003). Role of a Single Aquaporin Isoform in Root Water Uptake. *Plant Cell* **15**, 509–522.

Jia, M., Ding, N., Zhang, Q., Xing, S., Wei, L., Zhao, Y., Du, P., Mao, W., Li, J., Li, B., et al. (2017a). A FERONIA-Like Receptor Kinase Regulates Strawberry (Fragaria × ananassa) Fruit Ripening and Quality Formation. *Front. Plant Sci.* **8**, 1099.

Jia, M., Du, P., Ding, N., Zhang, Q., Xing, S., Wei, L., Zhao, Y., Mao, W., Li, J., Li, B., et al. (2017b). Two FERONIA-Like Receptor Kinases Regulate Apple Fruit Ripening by Modulating Ethylene Production. *Front. Plant Sci.* **8**, 1406.

Johnson, K. L., Degnan, K. A., Ross Walker, J. and Ingram, G. C. (2005). AtDEK1 is essential for specification of embryonic epidermal cell fate. *Plant J. Cell Mol. Biol.* **44**, 114–127.

Johnson, K. L., Faulkner, C., Jeffree, C. E. and Ingram, G. C. (2008). The phytocalpain defective kernel 1 is a novel Arabidopsis growth regulator whose activity is regulated by proteolytic processing. *Plant Cell* **20**, 2619–2630.

Kahn, J., Shwartz, Y., Blitz, E., Krief, S., Sharir, A., Breitel, D. A., Rattenbach, R., Relaix, F., Maire, P., Rountree, R. B., et al. (2009). Muscle contraction is necessary to maintain joint progenitor cell fate. *Dev. Cell* **16**, 734–743.

Kapilan, R., Vaziri, M. and Zwiazek, J. J. (2018). Regulation of aquaporins in plants under stress. *Biol. Res.* **51**, 4.

Kärkönen, A. and Kuchitsu, K. (2015). Reactive oxygen species in cell wall metabolism and development in plants. *Phytochemistry* **112**, 22–32.

Keinath, N. F., Kierszniowska, S., Lorek, J., Bourdais, G., Kessler, S. A., Shimosato-Asano, H., Grossniklaus, U., Schulze, W. X., Robatzek, S. and Panstruga, R. (2010). PAMP (pathogen-associated molecular pattern)-induced changes in plasma membrane compartmentalization reveal novel components of plant immunity. *J. Biol. Chem.* **285**, 39140–39149.

Kessler, S. A., Shimosato-Asano, H., Keinath, N. F., Wuest, S. E., Ingram, G., Panstruga, R. and Grossniklaus, U. (2010). Conserved Molecular Components for Pollen Tube Reception and Fungal Invasion. *Science* **330**, 968–971.

Kierzkowski, D., Nakayama, N., Routier-Kierzkowska, A.-L., Weber, A., Bayer, E., Schorderet, M., Reinhardt, D., Kuhlemeier, C. and Smith, R. S. (2012). Elastic Domains Regulate Growth and Organogenesis in the Plant Shoot Apical Meristem. *Science* **335**, 1096–1099.

Kim, S.-J., Chandrasekar, B., Rea, A. C., Danhof, L., Zemelis-Durfee, S., Thrower, N., Shepard, Z. S., Pauly, M., Brandizzi, F. and Keegstra, K. (2020). The synthesis of xyloglucan, an abundant plant cell wall polysaccharide, requires CSLC function. *Proc. Natl. Acad. Sci.* **117**, 20316–20324.

Kim, D., Yang, J., Gu, F., Park, S., Combs, J., Adams, A., Mayes, H. B., Jeon, S. J., Bahk, J. D. and Nielsen, E. (2021). A temperature-sensitive FERONIA mutant allele that alters root hair growth. *Plant Physiol.* **185**, 405–423.

Kirchhelle, C., Garcia-Gonzalez, D., Irani, N. G., Jérusalem, A. and Moore, I. (2019). Two mechanisms regulate directional cell growth in Arabidopsis lateral roots. *eLife* **8**,.

Krouk, G., Lacombe, B., Bielach, A., Perrine-Walker, F., Malinska, K., Mounier, E., Hoyerova, K., Tillard, P., Leon, S., Ljung, K., et al. (2010). Nitrate-regulated auxin transport by NRT1.1 defines a mechanism for nutrient sensing in plants. *Dev. Cell* **18**, 927–937.

Kulasinski, K., Keten, S., Churakov, S. V., Derome, D. and Carmeliet, J. (2014). A comparative molecular dynamics study of crystalline, paracrystalline and amorphous states of cellulose. *Cellulose* **21**, 1103–1116.

Kumar, S. B., Venkateswaran, K. and Kundu, S. (2013). Alternative Conformational Model of a Seed Protein DeK1 for Better Understanding of Structure-Function Relationship. *J. Proteins Proteomics* **1**,.

Kurusu, T., Nishikawa, D., Yamazaki, Y., Gotoh, M., Nakano, M., Hamada, H., Yamanaka, T., Iida, K., Nakagawa, Y., Saji, H., et al. (2012a). Plasma membrane protein OsMCA1 is involved in regulation of hypo-osmotic shock-induced Ca2+influx and modulates generation of reactive oxygen species in cultured rice cells. *BMC Plant Biol.* **12**, 11.

Kurusu, T., Iida, H. and Kuchitsu, K. (2012b). Roles of a putative mechanosensitive plasma membrane Ca2+-permeable channel OsMCA1 in generation of reactive oxygen species and hypo-osmotic signaling in rice. *Plant Signal. Behav.* **7**, 796–798.

Kutschera, U. (1991). Determination of the Longitudinal Tissue Stresses in the Growing and Non-Growing Regions of Sunflower Hypocotyls. *J. Plant Physiol.* **138**, 460–465.

Kutschera, U. and Niklas, K. J. (2007). The epidermal-growth-control theory of stem elongation: an old and a new perspective. *J. Plant Physiol.* **164**, 1395–1409.

Kwiatkowska, D. and Dumais, J. (2003). Growth and morphogenesis at the vegetative shoot apex of Anagallis arvensis L. *J. Exp. Bot.* **54**, 1585–1595.

Landrein, B., Lathe, R., Bringmann, M., Vouillot, C., Ivakov, A., Boudaoud, A., Persson, S. and Hamant, O. (2013). Impaired cellulose synthase guidance leads to stem torsion and twists phyllotactic patterns in Arabidopsis. *Curr. Biol. CB* **23**, 895–900.

Landrein, B., Kiss, A., Sassi, M., Chauvet, A., Das, P., Cortizo, M., Laufs, P., Takeda, S., Aida, M., Traas, J., et al. (2015). Mechanical stress contributes to the expression of the STM homeobox gene in Arabidopsis shoot meristems. *eLife* **4**, e07811.

Landrein, B., Formosa-Jordan, P., Malivert, A., Schuster, C., Melnyk, C. W., Yang, W., Turnbull, C., Meyerowitz, E. M., Locke, J. C. W. and Jönsson, H. (2018). Nitrate modulates stem cell dynamics in Arabidopsis shoot meristems through cytokinins. *Proc. Natl. Acad. Sci. U. S. A.* **115**, 1382–1387.

Lê, S., Josse, J. and Husson, F. (2008). FactoMineR: An R Package for Multivariate Analysis. *J. Stat. Softw.* **25**, 1–18.

Le Gall, H., Philippe, F., Domon, J.-M., Gillet, F., Pelloux, J. and Rayon, C. (2015). Cell Wall Metabolism in Response to Abiotic Stress. *Plants* **4**, 112–166.

Lee, D., Lal, N. K., Lin, Z.-J. D., Ma, S., Liu, J., Castro, B., Toruño, T., Dinesh-Kumar, S. P. and Coaker, G. (2020). Regulation of reactive oxygen species during plant immunity through phosphorylation and ubiquitination of RBOHD. *Nat. Commun.* **11**, 1838.

Léger, O., Garcia, F., Khafif, M., Leblanc-Fournier, N., Duclos, A., Tournat, V., Badel, E., Didelon, M., Ru, A. L., Raffaele, S., et al. (2021). Pathogen-derived mechanical cues regulate the spatio-temporal implementation of plant defense. 2021.10.18.464859.

Li, J., Hou, B., Tumova, S., Muraki, K., Bruns, A., Ludlow, M. J., Sedo, A., Hyman, A. J., McKeown, L., Young, R. S., et al. (2014). Piezo1 integration of vascular architecture with physiological force. *Nature* **515**, 279–282.

Li, J., Hou, B. and Beech, D. J. (2015a). Endothelial Piezo1: Life depends on it. *Channels* **9**, 1–2.

Li, C., Yeh, F.-L., Cheung, A. Y., Duan, Q., Kita, D., Liu, M.-C., Maman, J., Luu, E. J., Wu, B. W., Gates, L., et al. (2015b). Glycosylphosphatidylinositol-anchored proteins as chaperones and co-receptors for FERONIA receptor kinase signaling in Arabidopsis. *eLife* **4**, e06587.

Li, C., Wu, H.-M. and Cheung, A. Y. (2016a). FERONIA and Her Pals: Functions and Mechanisms. *Plant Physiol.* **171**, 2379–2392.

Li, C., Wang, L., Cui, Y., He, L., Qi, Y., Zhang, J., Lin, J., Liao, H., Lin, Q., Yang, T., et al. (2016b). Two FERONIA-like receptor (FLR) genes are required to maintain architecture, fertility, and seed yield in rice. *Mol. Breed.* **36**, 151.

Li, L., Wang, F., Yan, P., Jing, W., Zhang, C., Kudla, J. and Zhang, W. (2017). A phosphoinositide-specific phospholipase C pathway elicits stress-induced Ca2+ signals and confers salt tolerance to rice. *New Phytol.* **214**, 1172–1187.

Li, C., Liu, X., Qiang, X., Li, X., Li, X., Zhu, S., Wang, L., Wang, Y., Liao, H., Luan, S., et al. (2018). EBP1 nuclear accumulation negatively feeds back on FERONIA-mediated RALF1 signaling. *PLoS Biol.* **16**, e2006340.

Li, T., Yan, A., Bhatia, N., Altinok, A., Afik, E., Durand-Smet, P., Tarr, P. T., Schroeder, J. I., Heisler, M. G. and Meyerowitz, E. M. (2019). Calcium signals are necessary to establish auxin transporter polarity in a plant stem cell niche. *Nat. Commun.* **10**, 726.

Li, Z. P., Paterlini, A., Glavier, M. and Bayer, E. M. (2020). Intercellular trafficking via plasmodesmata: molecular layers of complexity. *Cell. Mol. Life Sci.*

Liang, Z., Brown, R. C., Fletcher, J. C. and Opsahl-Sorteberg, H.-G. (2015). Calpain-Mediated Positional Information Directs Cell Wall Orientation to Sustain Plant Stem Cell Activity, Growth and Development. *Plant Cell Physiol.* **56**, 1855–1866.

Liao, H., Tang, R., Zhang, X., Luan, S. and Yu, F. (2017). FERONIA Receptor Kinase at the Crossroads of Hormone Signaling and Stress Responses. *Plant Cell Physiol.* **58**, 1143–1150.

Lid, S. E., Gruis, D., Jung, R., Lorentzen, J. A., Ananiev, E., Chamberlin, M., Niu, X., Meeley, R., Nichols, S. and Olsen, O.-A. (2002). The defective kernel 1 (dek1) gene required for aleurone

cell development in the endosperm of maize grains encodes a membrane protein of the calpain gene superfamily. *Proc. Natl. Acad. Sci.* **99**, 5460–5465.

Lin, W., Tang, W., Anderson, C. T. and Yang, Z. (2018). *FERONIA's sensing of cell wall pectin activates ROP GTPase signaling in* Arabidopsis. Plant Biology.

Lin, W., Tang, W., Pan, X., Huang, A., Gao, X., Anderson, C. T. and Yang, Z. (2021). Arabidopsis pavement cell morphogenesis requires FERONIA binding to pectin for activation of ROP GTPase signaling. *Curr. Biol.*

Liscum, E., Askinosie, S. K., Leuchtman, D. L., Morrow, J., Willenburg, K. T. and Coats, D. R. (2014). Phototropism: growing towards an understanding of plant movement. *Plant Cell* **26**, 38–55.

Liu, X., Li, J., Zhao, H., Liu, B., Günther-Pomorski, T., Chen, S. and Liesche, J. (2019). Novel tool to quantify cell wall porosity relates wall structure to cell growth and drug uptake. *J Cell Biol* jcb.201810121.

Livanos, P., Galatis, B. and Apostolakos, P. (2014). The interplay between ROS and tubulin cytoskeleton in plants. *Plant Signal. Behav.* **9**,.

Lockhart, J. A. (1965). An analysis of irreversible plant cell elongation. *J. Theor. Biol.* **8**, 264–275.

Long, Y., Cheddadi, I., Mosca, G., Mirabet, V., Dumond, M., Kiss, A., Traas, J., Godin, C. and Boudaoud, A. (2020). Cellular Heterogeneity in Pressure and Growth Emerges from Tissue Topology and Geometry. *Curr. Biol. CB* **30**, 1504-1516.e8.

Louveaux, M., Julien, J.-D., Mirabet, V., Boudaoud, A. and Hamant, O. (2016). Cell division plane orientation based on tensile stress in Arabidopsis thaliana. *Proc. Natl. Acad. Sci. U. S. A.* **113**, E4294-4303.

Lu, P., Porat, R., Nadeau, J. A. and O'Neill, S. D. (1996). Identification of a Meristem L1 Layer-Specific Gene in Arabidopsis That Is Expressed during Embryonic Pattern Formation and Defines a New Class of Homeobox Genes. *Plant Cell* **8**, 2155–2168.

Majda, M., Grones, P., Sintorn, I.-M., Vain, T., Milani, P., Krupinski, P., Zagórska-Marek, B., Viotti, C., Jönsson, H., Mellerowicz, E. J., et al. (2017). Mechanochemical Polarization of Contiguous Cell Walls Shapes Plant Pavement Cells. *Dev. Cell* **43**, 290-304.e4.

Majda, M., Trozzi, N., Mosca, G. and Smith, R. S. (2022). How Cell Geometry and Cellular Patterning Influence Tissue Stiffness. *Int. J. Mol. Sci.* **23**, 5651.

Malivert, A., Hamant, O. and Ingram, G. (2018). The contribution of mechanosensing to epidermal cell fate specification. *Curr. Opin. Genet. Dev.* **51**, 52–58.

Malivert, A., Erguvan, Ö., Chevallier, A., Dehem, A., Friaud, R., Liu, M., Martin, M., Peyraud, T., Hamant, O. and Verger, S. (2021). FERONIA and microtubules independently contribute to mechanical integrity in the Arabidopsis shoot. *PLOS Biol.* **19**, e3001454.

Manfield, I. W., Orfila, C., McCartney, L., Harholt, J., Bernal, A. J., Scheller, H. V., Gilmartin, P. M., Mikkelsen, J. D., Knox, J. P. and Willats, W. G. T. (2004). Novel cell wall architecture of isoxaben-habituated Arabidopsis suspension-cultured cells: Global transcript profiling and cellular analysis. *Plant J.* **40**, 260–275.

Mao, D., Yu, F., Li, J., Van de Poel, B., Tan, D., Li, J., Liu, Y., Li, X., Dong, M., Chen, L., et al. (2015). FERONIA receptor kinase interacts with S-adenosylmethionine synthetase and suppresses S-adenosylmethionine production and ethylene biosynthesis in Arabidopsis. *Plant Cell Environ.* **38**, 2566–2574.

Martinez, E., Cancela, J. J., Cuesta, T. and Neira, X. (2011). Review. Use of psychrometers in field measurements of plant material: accuracy and handling difficulties. *Span. J. Agric. Res.* **9**, 313–328.

Martinière, A., Fiche, J. B., Smokvarska, M., Mari, S., Alcon, C., Dumont, X., Hematy, K., Jaillais, Y., Nollmann, M. and Maurel, C. (2019). Osmotic Stress Activates Two Reactive Oxygen Species Pathways with Distinct Effects on Protein Nanodomains and Diffusion. *Plant Physiol.* **179**, 1581–1593.

Marzol, E., Borassi, C., Bringas, M., Sede, A., Rodríguez Garcia, D. R., Capece, L. and Estevez, J. M. (2018). Filling the Gaps to Solve the Extensin Puzzle. *Mol. Plant* **11**, 645–658.

Masachis, S., Segorbe, D., Turrà, D., Leon-Ruiz, M., Fürst, U., El Ghalid, M., Leonard, G., López-Berges, M. S., Richards, T. A., Felix, G., et al. (2016). A fungal pathogen secretes plant alkalinizing peptides to increase infection. *Nat. Microbiol.* **1**, 16043.

Mateu, B. P., Bock, P. and Gierlinger, N. (2020). Raman Imaging of Plant Cell Walls. In *The Plant Cell Wall: Methods and Protocols* (ed. Popper, Z. A.), pp. 251–295. New York, NY: Springer.

Matsumoto, S., Kumasaki, S., Soga, K., Wakabayashi, K., Hashimoto, T. and Hoson, T. (2010). Gravity-induced modifications to development in hypocotyls of Arabidopsis tubulin mutants. *Plant Physiol.* **152**, 918–926.

Maurel, C., Reizer, J., Schroeder, J. I. and Chrispeels, M. J. (1993). The vacuolar membrane protein gamma-TIP creates water specific channels in Xenopus oocytes. *EMBO J.* **12**, 2241–2247.

Maurel, C., Boursiac, Y., Luu, D.-T., Santoni, V., Shahzad, Z. and Verdoucq, L. (2015). Aquaporins in Plants. *Physiol. Rev.* **95**, 1321–1358.

Mecchia, M. A., Rövekamp, M., Giraldo-Fonseca, A., Meier, D., Gadient, P., Bowman, J. L. and Grossniklaus, U. (2020). Characterization of the single FERONIA homolog in Marchantia polymorpha reveals an ancestral role of CrRLK1L receptor kinases in regulating cell expansion and morphological integrity. 2020.12.23.424085.

Mersmann, S., Bourdais, G., Rietz, S. and Robatzek, S. (2010). Ethylene signaling regulates accumulation of the FLS2 receptor and is required for the oxidative burst contributing to plant immunity. *Plant Physiol.* **154**, 391–400.

Micheli, F. (2001). Pectin methylesterases: cell wall enzymes with important roles in plant physiology. *Trends Plant Sci.* **6**, 414–419.

Michels, L., Gorelova, V., Harnvanichvech, Y., Borst, J. W., Albada, B., Weijers, D. and Sprakel, J. (2020). Complete microviscosity maps of living plant cells and tissues with a toolbox of targeting mechanoprobes. *Proc. Natl. Acad. Sci.* **117**, 18110–18118.

Mielke, S., Zimmer, M., Meena, M. K., Dreos, R., Stellmach, H., Hause, B., Voiniciuc, C. and Gasperini, D. (2021). Jasmonate biosynthesis arising from altered cell walls is prompted by turgor-driven mechanical compression. *Sci. Adv.* **7**, eabf0356.

Mirabet, V., Das, P., Boudaoud, A. and Hamant, O. (2011). The role of mechanical forces in plant morphogenesis. *Annu. Rev. Plant Biol.* **62**, 365–385.

Miyazaki, S., Murata, T., Sakurai-Ozato, N., Kubo, M., Demura, T., Fukuda, H. and Hasebe, M. (2009). ANXUR1 and 2, sister genes to FERONIA/SIRENE, are male factors for coordinated fertilization. *Curr. Biol. CB* **19**, 1327–1331.

Möller, B., Poeschl, Y., Plötner, R. and Bürstenbinder, K. (2017). PaCeQuant: A Tool for High-Throughput Quantification of Pavement Cell Shape Characteristics. *Plant Physiol.* **175**, 998–1017.

Morris, E. R. and Walker, J. C. (2003). Receptor-like protein kinases: the keys to response. *Curr. Opin. Plant Biol.* **6**, 339–342.

Moussu, S., San-Bento, R., Galletti, R., Creff, A., Farcot, E. and Ingram, G. (2013). Embryonic cuticle establishment. *Plant Signal. Behav.* **8**, e27491.

Moussu, S., Augustin, S., Roman, A. O., Broyart, C. and Santiago, J. (2018). Crystal structures of two tandem malectin-like receptor kinases involved in plant reproduction. *Acta Crystallogr. Sect. Struct. Biol.* **74**, 671–680.

Moustacas, A. M., Nari, J., Borel, M., Noat, G. and Ricard, J. (1991). Pectin methylesterase, metal ions and plant cell-wall extension. The role of metal ions in plant cell-wall extension. *Biochem. J.* **279 (Pt 2)**, 351–354.

Muncie, J. M. and Weaver, V. M. (2018). Chapter One - The Physical and Biochemical Properties of the Extracellular Matrix Regulate Cell Fate. In *Current Topics in Developmental Biology* (ed. Litscher, E. S.) and Wassarman, P. M.), pp. 1–37. Academic Press.

Nakamura, M., Lindeboom, J. J., Saltini, M., Mulder, B. M. and Ehrhardt, D. W. (2018). SPR2 protects minus ends to promote severing and reorientation of plant cortical microtubule arrays. *J. Cell Biol.* **217**, 915–927.

Nakayama, N., Smith, R. S., Mandel, T., Robinson, S., Kimura, S., Boudaoud, A. and Kuhlemeier, C. (2012). Mechanical regulation of auxin-mediated growth. *Curr. Biol. CB* **22**, 1468–1476.

Naseer, S., Lee, Y., Lapierre, C., Franke, R., Nawrath, C. and Geldner, N. (2012). Casparian strip diffusion barrier in Arabidopsis is made of a lignin polymer without suberin. *Proc. Natl. Acad. Sci.* **109**, 10101–10106.

Ndoye, M. S., Burridge, J., Bhosale, R., Grondin, A. and Laplaze, L. (2022). Root traits for low input agroecosystems in Africa: Lessons from three case studies. *Plant Cell Environ.* **45**, 637–649.

Nezhad, A. S., Naghavi, M., Packirisamy, M., Bhat, R. and Geitmann, A. (2013). Quantification of the Young's modulus of the primary plant cell wall using Bending-Lab-On-Chip (BLOC). *Lab. Chip* **13**, 2599–2608.

Ngo, Q. A., Vogler, H., Lituiev, D. S., Nestorova, A. and Grossniklaus, U. (2014). A Calcium Dialog Mediated by the FERONIA Signal Transduction Pathway Controls Plant Sperm Delivery. *Dev. Cell* **29**, 491–500.

Nishiyama, Y. (2018). Molecular interactions in nanocellulose assembly. *Philos. Trans. R. Soc. Math. Phys. Eng. Sci.* **376**, 20170047.

Nongpiur, R. C., Singla-Pareek, S. L. and Pareek, A. (2020). The quest for osmosensors in plants. *J. Exp. Bot.* **71**, 595–607.

Okamoto, H., Miwa, C., Masuda, T., Nakahori, K. and Katou, K. (1990). Effects of Auxin and Anoxia on the Cell Wall Yield Threshold Determined by Negative Pressure Jumps in Segments of Cowpea Hypocotyl. *Plant Cell Physiol.* **31**, 783–788.

Olesen, S.-P., Claphamt, D. and Davies, P. (1988). Haemodynamic shear stress activates a K+ current in vascular endothelial cells. *Nature* **331**, 168–170.

Oparka, K. j. and Prior, D. a. m. (1992). Direct evidence for pressure-generated closure of plasmodesmata. *Plant J.* **2**, 741–750.

Ortega, J. K. E. (1985). Augmented Growth Equation for Cell Wall Expansion 1. *Plant Physiol.* **79**, 318–320.

Ortiz-Morea, F. A., Liu, J., Shan, L. and He, P. (2022). Malectin-like receptor kinases as protector deities in plant immunity. *Nat. Plants* **8**, 27–37.

Osmotic burst of blood cells (2012).

Ozturk, M., Turkyilmaz Unal, B., García-Caparrós, P., Khursheed, A., Gul, A. and Hasanuzzaman, M. (2021). Osmoregulation and its actions during the drought stress in plants. *Physiol. Plant.* **172**, 1321–1335.

Paredez, A. R., Somerville, C. R. and Ehrhardt, D. W. (2006). Visualization of cellulose synthase demonstrates functional association with microtubules. *Science* **312**, 1491–1495.

Park, Y. B. and Cosgrove, D. J. (2012a). Changes in Cell Wall Biomechanical Properties in the Xyloglucan-Deficient xxt1/xxt2 Mutant of Arabidopsis. *Plant Physiol.* **158**, 465–475.

Park, Y. B. and Cosgrove, D. J. (2012b). A Revised Architecture of Primary Cell Walls Based on Biomechanical Changes Induced by Substrate-Specific Endoglucanases. *Plant Physiol.* **158**, 1933–1943.

Park, Y. B. and Cosgrove, D. J. (2015). Xyloglucan and its Interactions with Other Components of the Growing Cell Wall. *Plant Cell Physiol.* **56**, 180–194.

Park, K., Knoblauch, J., Oparka, K. and Jensen, K. H. (2019). Controlling intercellular flow through mechanosensitive plasmodesmata nanopores. *Nat. Commun.* **10**, 3564.

Pascut, F. C., Couvreur, V., Dietrich, D., Leftley, N., Reyt, G., Boursiac, Y., Calvo-Polanco, M., Casimiro, I., Maurel, C., Salt, D. E., et al. (2021). Non-invasive hydrodynamic imaging in plant roots at cellular resolution. *Nat. Commun.* **12**, 4682.

Peaucelle, A., Braybrook, S. A., Le Guillou, L., Bron, E., Kuhlemeier, C. and Höfte, H. (2011). Pectin-induced changes in cell wall mechanics underlie organ initiation in Arabidopsis. *Curr. Biol. CB* **21**, 1720–1726.

Peaucelle, A., Braybrook, S. and Höfte, H. (2012). Cell wall mechanics and growth control in plants: the role of pectins revisited. *Front. Plant Sci.* **3**, 121.

Peaucelle, A., Wightman, R. and Höfte, H. (2015). The Control of Growth Symmetry Breaking in the Arabidopsis Hypocotyl. *Curr. Biol. CB* **25**, 1746–1752.

Pérez García, M., Zhang, Y., Hayes, J., Salazar, A., Zabotina, O. A. and Hong, M. (2011). Structure and interactions of plant cell-wall polysaccharides by two- and three-dimensional magic-angle-spinning solid-state NMR. *Biochemistry* **50**, 989–1000.

Peyronnet, R., Tran, D., Girault, T. and Frachisse, J.-M. (2014). Mechanosensitive channels: feeling tension in a world under pressure. *Front. Plant Sci.* **5**,.

Phyo, P., Gu, Y. and Hong, M. (2019). Impact of acidic pH on plant cell wall polysaccharide structure and dynamics: insights into the mechanism of acid growth in plants from solid-state NMR. *Cellulose* **26**, 291–304.

Pietruszka, M. and Lewicka, S. (2007). Anisotropic plant growth due to phototropism. *J. Math. Biol.* **54**, 45–55.

Poolman, B., Blount, P., Folgering, J. H. A., Friesen, R. H. E., Moe, P. C. and van der Heide, T. (2002). How do membrane proteins sense water stress? *Mol. Microbiol.* **44**, 889–902.

Popko, J., Hänsch, R., Mendel, R.-R., Polle, A. and Teichmann, T. (2010). The role of abscisic acid and auxin in the response of poplar to abiotic stress. *Plant Biol.* **12**, 242–258.

Postaire, O., Tournaire-Roux, C., Grondin, A., Boursiac, Y., Morillon, R., Schäffner, A. R. and Maurel, C. (2010). A PIP1 Aquaporin Contributes to Hydrostatic Pressure-Induced Water Transport in Both the Root and Rosette of Arabidopsis1[C][W]. *Plant Physiol.* **152**, 1418–1430.

Prado, K., Cotelle, V., Li, G., Bellati, J., Tang, N., Tournaire-Roux, C., Martinière, A., Santoni, V. and Maurel, C. (2019). Oscillating Aquaporin Phosphorylation and 14-3-3 Proteins Mediate the Circadian Regulation of Leaf Hydraulics. *Plant Cell* **31**, 417–429.

Proseus, T. E. and Boyer, J. S. (2007). Tension required for pectate chemistry to control growth in Chara corallina. *J. Exp. Bot.* **58**, 4283–4292.

Proseus, T. E. and Boyer, J. S. (2008). Calcium pectate chemistry causes growth to be stored in Chara corallina: a test of the pectate cycle. *Plant Cell Environ.* **31**, 1147–1155.

Qiu, D., Xu, S., Wang, Y., Zhou, M. and Hong, L. (2021). Primary Cell Wall Modifying Proteins Regulate Wall Mechanics to Steer Plant Morphogenesis. *Front. Plant Sci.* **12**,.

Ramahaleo, T., Morillon, R., Alexandre, J. and Lassalles, J.-P. (1999). Osmotic Water Permeability of Isolated Protoplasts. Modifications during Development. *Plant Physiol.* **119**, 885–896.

Ranade, S. S., Qiu, Z., Woo, S.-H., Hur, S. S., Murthy, S. E., Cahalan, S. M., Xu, J., Mathur, J., Bandell, M., Coste, B., et al. (2014). Piezo1, a mechanically activated ion channel, is required for vascular development in mice. *Proc. Natl. Acad. Sci.* **111**, 10347–10352.

Reinhardt, D., Frenz, M., Mandel, T. and Kuhlemeier, C. (2003a). Microsurgical and laser ablation analysis of interactions between the zones and layers of the tomato shoot apical meristem. *Development* **130**, 4073–4083.

Reinhardt, D., Pesce, E.-R., Stieger, P., Mandel, T., Baltensperger, K., Bennett, M., Traas, J., Friml, J. and Kuhlemeier, C. (2003b). Regulation of phyllotaxis by polar auxin transport. *Nature* **426**, 255–260.

Renuart, E. and Viney, C. (2000). Chapter 8 - Biological Fibrous Materials: Self-Assembled Structures and Optimised Properties. In *Pergamon Materials Series* (ed. Elices, M.), pp. 223–267. Pergamon.

Richter, J., Ploderer, M., Mongelard, G., Gutierrez, L. and Hauser, M.-T. (2017). Role of CrRLK1L Cell Wall Sensors HERCULES1 and 2, THESEUS1, and FERONIA in Growth Adaptation Triggered by Heavy Metals and Trace Elements. *Front. Plant Sci.* **8**, 1554.

Ringli, C. (2010). Monitoring the Outside: Cell Wall-Sensing Mechanisms. *Plant Physiol.* **153**, 1445–1452.

Ringli, C., Bigler, L., Kuhn, B. M., Leiber, R.-M., Diet, A., Santelia, D., Frey, B., Pollmann, S. and Klein, M. (2008). The Modified Flavonol Glycosylation Profile in the Arabidopsis rol1 Mutants Results in Alterations in Plant Growth and Cell Shape Formation. *Plant Cell* **20**, 1470–1481.

Risca, V. I., Wang, E. B., Chaudhuri, O., Chia, J. J., Geissler, P. L. and Fletcher, D. A. (2012). Actin filament curvature biases branching direction. *Proc. Natl. Acad. Sci. U. S. A.* **109**, 2913–2918.

Riveline, D., Zamir, E., Balaban, N. Q., Schwarz, U. S., Ishizaki, T., Narumiya, S., Kam, Z., Geiger, B. and Bershadsky, A. D. (2001). Focal Contacts as Mechanosensors: Externally Applied Local Mechanical Force Induces Growth of Focal Contacts by an Mdia1-Dependent and Rock-Independent Mechanism. *J. Cell Biol.* **153**, 1175–1186.

Robbins, C. T. and Moen, A. N. (1975). Composition and Digestibility of Several Deciduous Browses in the Northeast. *J. Wildl. Manag.* **39**, 337–341.

Robinson, S. (2021). Mechanobiology of cell division in plant growth. *New Phytol.* **231**, 559–564.

Roca-Cusachs, P., Iskratsch, T. and Sheetz, M. P. (2012). Finding the weakest link-exploring integrin-mediated mechanical molecular pathways. *J. Cell Sci.* **125**, 3025–3038.

Rodrigues, O., Reshetnyak, G., Grondin, A., Saijo, Y., Leonhardt, N., Maurel, C. and Verdoucq, L. (2017). Aquaporins facilitate hydrogen peroxide entry into guard cells to mediate ABA- and pathogen-triggered stomatal closure. *Proc. Natl. Acad. Sci. U. S. A.* **114**, 9200–9205.

Roeder, A. H. K., Otegui, M. S., Dixit, R., Anderson, C. T., Faulkner, C., Zhang, Y., Harrison, M. J., Kirchhelle, C., Goshima, G., Coate, J. E., et al. (2021). Fifteen compelling open questions in plant cell biology. *Plant Cell*.

Rojas, E. R., Hotton, S. and Dumais, J. (2011). Chemically Mediated Mechanical Expansion of the Pollen Tube Cell Wall. *Biophys. J.* **101**, 1844–1853.

Rondeau-Mouro, C., Defer, D., Leboeuf, E. and Lahaye, M. (2008). Assessment of cell wall porosity in Arabidopsis thaliana by NMR spectroscopy. *Int. J. Biol. Macromol.* **42**, 83–92.

Rotman, N., Rozier, F., Boavida, L., Dumas, C., Berger, F. and Faure, J.-E. (2003). Female Control of Male Gamete Delivery during Fertilization in Arabidopsis thaliana. *Curr. Biol.* **13**, 432–436.

Ruan, Y.-L., Llewellyn, D. J. and Furbank, R. T. (2001). The Control of Single-Celled Cotton Fiber Elongation by Developmentally Reversible Gating of Plasmodesmata and Coordinated Expression of Sucrose and K+ Transporters and Expansin. *Plant Cell* **13**, 47–60.

Ruprecht, C., Carroll, A. and Persson, S. (2014). T-DNA-induced chromosomal translocations in feronia and anxur2 mutants reveal implications for the mechanism of collapsed pollen due to chromosomal rearrangements. *Mol. Plant* **7**, 1591–1594.

Rydahl, M. G., Hansen, A. R., Kračun, S. K. and Mravec, J. (2018). Report on the Current Inventory of the Toolbox for Plant Cell Wall Analysis: Proteinaceous and Small Molecular Probes. *Front. Plant Sci.* **9**,.

Rygol, J., Pritchard, J., Zhu, J. J., Tomos, A. D. and Zimmermann, U. (1993). Transpiration Induces Radial Turgor Pressure Gradients in Wheat and Maize Roots. *Plant Physiol.* **103**, 493–500.

Sagar, S. and Singh, A. (2021). Emerging role of phospholipase C mediated lipid signaling in abiotic stress tolerance and development in plants. *Plant Cell Rep.* **40**, 2123–2133.

Sampathkumar, A., Krupinski, P., Wightman, R., Milani, P., Berquand, A., Boudaoud, A., Hamant, O., Jönsson, H. and Meyerowitz, E. M. (2014). Subcellular and supracellular mechanical stress prescribes cytoskeleton behavior in Arabidopsis cotyledon pavement cells. *eLife* **3**, e01967.

Sampathkumar, A., Peaucelle, A., Fujita, M., Schuster, C., Persson, S., Wasteneys, G. O. and Meyerowitz, E. M. (2019). Primary wall cellulose synthase regulates shoot apical meristem mechanics and growth. *Development* dev.179036.

San-Bento, R., Farcot, E., Galletti, R., Creff, A. and Ingram, G. (2014). Epidermal identity is maintained by cell-cell communication via a universally active feedback loop in Arabidopsis thaliana. *Plant J. Cell Mol. Biol.* **77**, 46–58.

Sánchez-Rodríguez, C., Estévez, J. M., Llorente, F., Hernández-Blanco, C., Jordá, L., Pagán, I., Berrocal, M., Marco, Y., Somerville, S. and Molina, A. (2009). The ERECTA Receptor-Like Kinase Regulates Cell Wall–Mediated Resistance to Pathogens in Arabidopsis thaliana. *Mol. Plant-Microbe Interactions®* **22**, 953–963.

Sapala, A. and Smith, R. S. (2020). Osmotic Treatment for Quantifying Cell Wall Elasticity in the Sepal of Arabidopsis thaliana. In *Plant Stem Cells: Methods and Protocols* (ed. Naseem, M.) and Dandekar, T.), pp. 101–112. New York, NY: Springer US.

Sapala, A., Runions, A., Routier-Kierzkowska, A.-L., Das Gupta, M., Hong, L., Hofhuis, H., Verger, S., Mosca, G., Li, C.-B., Hay, A., et al. (2018). Why plants make puzzle cells, and how their shape emerges. *eLife* **7**,.

Sassi, M., Ali, O., Boudon, F., Cloarec, G., Abad, U., Cellier, C., Chen, X., Gilles, B., Milani, P., Friml, J., et al. (2014). An auxin-mediated shift toward growth isotropy promotes organ formation at the shoot meristem in Arabidopsis. *Curr. Biol. CB* **24**, 2335–2342.

Sato, Y. and Kudoh, H. (2017). Herbivore-Mediated Interaction Promotes the Maintenance of Trichome Dimorphism through Negative Frequency-Dependent Selection. *Am. Nat.* **190**, E67–E77.

Savaldi-Goldstein, S., Peto, C. and Chory, J. (2007). The epidermis both drives and restricts plant shoot growth. *Nature* **446**, 199–202.

Sawada, D., Kalluri, U. C., O'Neill, H., Urban, V., Langan, P., Davison, B. and Pingali, S. V. (2018). Tension wood structure and morphology conducive for better enzymatic digestion. *Biotechnol. Biofuels* **11**, 44.

Scarcelli, G., Polacheck, W. J., Nia, H. T., Patel, K., Grodzinsky, A. J., Kamm, R. D. and Yun, S. H. (2015). Noncontact three-dimensional mapping of intracellular hydromechanical properties by Brillouin microscopy. *Nat. Methods* **12**, 1132–1134.

Schallus, T., Jaeckh, C., Fehér, K., Palma, A. S., Liu, Y., Simpson, J. C., Mackeen, M., Stier, G., Gibson, T. J., Feizi, T., et al. (2008). Malectin: a novel carbohydrate-binding protein of the endoplasmic reticulum and a candidate player in the early steps of protein N-glycosylation. *Mol. Biol. Cell* **19**, 3404–3414.

Scheible, W. R., Eshed, R., Richmond, T., Delmer, D. and Somerville, C. (2001). Modifications of cellulose synthase confer resistance to isoxaben and thiazolidinone herbicides in Arabidopsis Ixr1 mutants. *Proc. Natl. Acad. Sci. U. S. A.* **98**, 10079–10084.

Scheller, H. V. and Ulvskov, P. (2010). Hemicelluloses. *Annu. Rev. Plant Biol.* **61**, 263–289.

Scholander, P. F., Hammel, H. T., Hemmingsen, E. A. and Bradstreet, E. D. (1964). HYDROSTATIC PRESSURE AND OSMOTIC POTENTIAL IN LEAVES OF MANGROVES AND SOME OTHER PLANTS*. *Proc. Natl. Acad. Sci. U. S. A.* **52**, 119–125.

Schopfer, P. (2006). Biomechanics of plant growth. *Am. J. Bot.* **93**, 1415–1425.

Schultink, A., Liu, L., Zhu, L. and Pauly, M. (2014). Structural Diversity and Function of Xyloglucan Sidechain Substituents. *Plants* **3**, 526–542.

Sénéchal, F., L'Enfant, M., Domon, J.-M., Rosiau, E., Crépeau, M.-J., Surcouf, O., Esquivel-Rodriguez, J., Marcelo, P., Mareck, A., Guérineau, F., et al. (2015). Tuning of Pectin Methylesterification: PECTIN METHYLESTERASE INHIBITOR 7 MODULATES THE PROCESSIVE ACTIVITY OF CO-EXPRESSED PECTIN METHYLESTERASE 3 IN A pH-DEPENDENT MANNER *. *J. Biol. Chem.* **290**, 23320–23335.

Serrano, M., Coluccia, F., Torres, M., L'Haridon, F. and Métraux, J.-P. (2014). The cuticle and plant defense to pathogens. *Front. Plant Sci.* **5**, 274.

Shedletzky, E., Shmuel, M., Delmer, D. P. and Lamport, D. T. A. (1990). Adaptation and Growth of Tomato Cells on the Herbicide 2,6-Dichlorobenzonitrile Leads to Production of Unique Cell Walls Virtually Lacking a Cellulose-Xyloglucan Network 1. *Plant Physiol.* **94**, 980–987.

Shen, Q., Bourdais, G., Pan, H., Robatzek, S. and Tang, D. (2017). Arabidopsis glycosylphosphatidylinositol-anchored protein LLG1 associates with and modulates FLS2 to regulate innate immunity. *Proc. Natl. Acad. Sci. U. S. A.* **114**, 5749–5754.

Shih, H.-W., Miller, N. D., Dai, C., Spalding, E. P. and Monshausen, G. B. (2014). The receptor-like kinase FERONIA is required for mechanical signal transduction in Arabidopsis seedlings. *Curr. Biol. CB* **24**, 1887–1892.

Shiu, S. H. and Bleecker, A. B. (2003). Expansion of the receptor-like kinase/Pelle gene family and receptor-like proteins in Arabidopsis. *Plant Physiol.* **132**, 530–543.

Shivashankar, G. V. (2019). Mechanical regulation of genome architecture and cell-fate decisions. *Curr. Opin. Cell Biol.* **56**, 115–121.

Sieber, P., Schorderet, M., Ryser, U., Buchala, A., Kolattukudy, P., Métraux, J.-P. and Nawrath, C. (2000). Transgenic Arabidopsis Plants Expressing a Fungal Cutinase Show Alterations in the Structure and Properties of the Cuticle and Postgenital Organ Fusions. *Plant Cell* **12**, 721–737.

Sieriebriennikov, B. and Sommer, R. J. (2018). Developmental Plasticity and Robustness of a Nematode Mouth-Form Polyphenism. *Front. Genet.* **9**,.

Solis-Miranda, J. and Quinto, C. (2021). The CrRLK1L subfamily: One of the keys to versatility in plants. *Plant Physiol. Biochem.* **166**, 88–102.

Sowinski, E. E., Westman, B. M., Redmond, C. R., Kong, Y., Olek, A. T., Olek, J., McCann, M. C. and Carpita, N. C. (2022). Lack of xyloglucan in the cell walls of the Arabidopsis xxt1/xxt2 mutant results in specific increases in homogalacturonan and glucomannan. *Plant J. Cell Mol. Biol.* **110**, 212–227.

Stanislas, T., Platre, M., Liu, M., Rambaud-Lavigne, L. E. S., Jaillais, Y. and Hamant, O. (2018). A phosphoinositide map at the shoot apical meristem in Arabidopsis thaliana. *BMC Biol.* **16**, 20.

Stegmann, M., Monaghan, J., Smakowska-Luzan, E., Rovenich, H., Lehner, A., Holton, N., Belkhadir, Y. and Zipfel, C. (2017). The receptor kinase FER is a RALF-regulated scaffold controlling plant immune signaling. *Science* **355**, 287–289.

Stimpson, T. C., Cathala, B., Moreau, C., Moran-Mirabal, J. M. and Cranston, E. D. (2020). Xyloglucan Structure Impacts the Mechanical Properties of Xyloglucan–Cellulose Nanocrystal Layered Films—A Buckling-Based Study. *Biomacromolecules* **21**, 3898–3908.

Szabados, L. and Savouré, A. (2010). Proline: a multifunctional amino acid. *Trends Plant Sci.* **15**, 89–97.

Takada, S. and Jürgens, G. (2007). Transcriptional regulation of epidermal cell fate in the Arabidopsis embryo. *Development* **134**, 1141–1150.

Takada, S., Takada, N. and Yoshida, A. (2013). ATML1 promotes epidermal cell differentiation in Arabidopsis shoots. *Dev. Camb. Engl.* **140**, 1919–1923.

Takatani, S., Verger, S., Okamoto, T., Takahashi, T., Hamant, O. and Motose, H. (2020). Microtubule Response to Tensile Stress Is Curbed by NEK6 to Buffer Growth Variation in the Arabidopsis Hypocotyl. *Curr. Biol.* S0960982220301974.

Tan, L., Eberhard, S., Pattathil, S., Warder, C., Glushka, J., Yuan, C., Hao, Z., Zhu, X., Avci, U., Miller, J. S., et al. (2013). An Arabidopsis Cell Wall Proteoglycan Consists of Pectin and Arabinoxylan Covalently Linked to an Arabinogalactan Protein[W]. *Plant Cell* **25**, 270–287.

Tanaka, H., Onouchi, H., Kondo, M., Hara-Nishimura, I., Nishimura, M., Machida, C. and Machida, Y. (2001). A subtilisin-like serine protease is required for epidermal surface formation in Arabidopsis embryos and juvenile plants. *Development* **128**, 4681–4689.

Tanaka, T., Tanaka, H., Machida, C., Watanabe, M. and Machida, Y. (2004). A new method for rapid visualization of defects in leaf cuticle reveals five intrinsic patterns of surface defects in Arabidopsis. *Plant J.* **37**, 139–146.

Tanaka, H., Watanabe, M., Sasabe, M., Hiroe, T., Tanaka, T., Tsukaya, H., Ikezaki, M., Machida, C. and Machida, Y. (2007). Novel receptor-like kinase ALE2 controls shoot development by specifying epidermis in Arabidopsis. *Development* **134**, 1643–1652.

Tang, W., Lin, W., Zhou, X., Guo, J., Dang, X., Li, B., Lin, D. and Yang, Z. (2021). Mechano-transduction via the pectin-FERONIA complex activates ROP6 GTPase signaling in Arabidopsis pavement cell morphogenesis. *Curr. Biol.*

Tang, J., Wu, D., Li, X., Wang, L., Xu, L., Zhang, Y., Xu, F., Liu, H., Xie, Q., Dai, S., et al. (2022). Plant immunity suppression via PHR1-RALF-FERONIA shapes the root microbiome to alleviate phosphate starvation. *EMBO J.* **41**, e109102.

Tenhaken, R. (2015). Cell wall remodeling under abiotic stress. *Front. Plant Sci.* **5**,.

Thompson, D. W. (1942). *On growth and form,*. Cambridge [England: The University Press.

Thompson, D. W. (1992). *On Growth and Form*. (ed. Bonner, J. T.) Cambridge: Cambridge University Press.

Toriyama, H. and Jaffe, M. J. (1972). Migration of Calcium and Its Role in the Regulation of Seismonasty in the Motor Cell of Mimosa pudica L. 1. *Plant Physiol.* **49**, 72–81.

Touzard, M. (2019). Matériaux biomimétiques de la paroi cellulaire végétale et modifications enzymatiques.

Toyooka, K., Goto, Y., Asatsuma, S., Koizumi, M., Mitsui, T. and Matsuoka, K. (2009). A Mobile Secretory Vesicle Cluster Involved in Mass Transport from the Golgi to the Plant Cell Exterior. *Plant Cell* **21**, 1212–1229.

Tran, L.-S. P., Urao, T., Qin, F., Maruyama, K., Kakimoto, T., Shinozaki, K. and Yamaguchi-Shinozaki, K. (2007). Functional analysis of AHK1/ATHK1 and cytokinin receptor histidine kinases in response to abscisic acid, drought, and salt stress in Arabidopsis. *Proc. Natl. Acad. Sci.* **104**, 20623–20628.

Tran, D., Galletti, R., Neumann, E. D., Dubois, A., Sharif-Naeini, R., Geitmann, A., Frachisse, J.-M., Hamant, O. and Ingram, G. C. (2017). A mechanosensitive Ca(2+) channel activity is dependent on the developmental regulator DEK1. *Nat. Commun.* **8**, 1009.

Trinh, D.-C., Alonso-Serra, J., Asaoka, M., Colin, L., Cortes, M., Malivert, A., Takatani, S., Zhao, F., Traas, J., Trehin, C., et al. (2021). How Mechanical Forces Shape Plant Organs. *Curr. Biol.* **31**, R143–R159.

Trushko, A., Schäffer, E. and Howard, J. (2013). The growth speed of microtubules with XMAP215-coated beads coupled to their ends is increased by tensile force. *Proc. Natl. Acad. Sci. U. S. A.* **110**, 14670–14675.

Uhler, C. and Shivashankar, G. V. (2017). Regulation of genome organization and gene expression by nuclear mechanotransduction. *Nat. Rev. Mol. Cell Biol.* **18**, 717–727.

Urao, T., Yakubov, B., Satoh, R., Yamaguchi-Shinozaki, K., Seki, M., Hirayama, T. and Shinozaki, K. (1999). A transmembrane hybrid-type histidine kinase in Arabidopsis functions as an osmosensor. *Plant Cell* **11**, 1743–1754.

Usov, I., Nyström, G., Adamcik, J., Handschin, S., Schütz, C., Fall, A., Bergström, L. and Mezzenga, R. (2015). Understanding nanocellulose chirality and structure–properties relationship at the single fibril level. *Nat. Commun.* **6**, 7564.

Uyttewaal, M., Burian, A., Alim, K., Landrein, B., Borowska-Wykręt, D., Dedieu, A., Peaucelle, A., Ludynia, M., Traas, J., Boudaoud, A., et al. (2012). Mechanical stress acts via katanin to amplify differences in growth rate between adjacent cells in Arabidopsis. *Cell* **149**, 439–451.

Vaahtera, L., Schulz, J. and Hamann, T. (2019). Cell wall integrity maintenance during plant development and interaction with the environment. *Nat. Plants* **5**, 924–932.

Vaseva, I. I., Qudeimat, E., Potuschak, T., Du, Y., Genschik, P., Vandenbussche, F. and Van Der Straeten, D. (2018). The plant hormone ethylene restricts Arabidopsis growth via the epidermis. *Proc. Natl. Acad. Sci. U. S. A.* **115**, E4130–E4139.

Veley, K. M., Marshburn, S., Clure, C. E. and Haswell, E. S. (2012). Mechanosensitive channels protect plastids from hypoosmotic stress during normal plant growth. *Curr. Biol. CB* **22**, 408–413.

Verger, S., Chabout, S., Gineau, E. and Mouille, G. (2016). Cell adhesion in plants is under the control of putative O-fucosyltransferases. *Dev. Camb.* **143**, 2536–2540.

Verger, S., Long, Y., Boudaoud, A. and Hamant, O. (2018). A tension-adhesion feedback loop in plant epidermis. *eLife* **7**,.

Veytsman, B. A. and Cosgrove, D. J. (1998). A model of cell wall expansion based on thermodynamics of polymer networks. *Biophys. J.* **75**, 2240–2250.

Vidal, E. A., Araus, V., Lu, C., Parry, G., Green, P. J., Coruzzi, G. M. and Gutiérrez, R. A. (2010). Nitrate-responsive miR393/AFB3 regulatory module controls root system architecture in Arabidopsis thaliana. *Proc. Natl. Acad. Sci.* **107**, 4477–4482.

Vőfély, R. V., Gallagher, J., Pisano, G. D., Bartlett, M. and Braybrook, S. A. (2019). Of puzzles and pavements: a quantitative exploration of leaf epidermal cell shape. *New Phytol.* **221**, 540–552.

Vogler, H., Felekis, D., Nelson, B. J. and Grossniklaus, U. (2015). Measuring the Mechanical Properties of Plant Cell Walls. *Plants* **4**, 167–182.

Wan, X., Steudle, E. and Hartung, W. (2004). Gating of water channels (aquaporins) in cortical cells of young corn roots by mechanical stimuli (pressure pulses): effects of ABA and of HgCl2. *J. Exp. Bot.* **55**, 411–422.

Wang, N., Butler, J. P. and Ingber, D. E. (1993). Mechanotransduction Across the Cell Surface and Through the Cytoskeleton. *Science* **260**, 1124–1127.

Wang, C., Barry, J. K., Min, Z., Tordsen, G., Rao, A. G. and Olsen, O.-A. (2003a). The calpain domain of the maize DEK1 protein contains the conserved catalytic triad and functions as a cysteine proteinase. *J. Biol. Chem.* **278**, 34467–34474.

Wang, W., Vinocur, B. and Altman, A. (2003b). Plant responses to drought, salinity and extreme temperatures: towards genetic engineering for stress tolerance. *Planta* **218**, 1–14.

Wang, Z.-Y., Xiong, L., Li, W., Zhu, J.-K. and Zhu, J. (2011). The Plant Cuticle Is Required for Osmotic Stress Regulation of Abscisic Acid Biosynthesis and Osmotic Stress Tolerance in Arabidopsis. *Plant Cell* **23**, 1971–1984.

Wang, L., Yang, T., Lin, Q., Wang, B., Li, X., Luan, S. and Yu, F. (2020a). Receptor kinase FERONIA regulates flowering time in Arabidopsis. *BMC Plant Biol.* **20**, 26.

Wang, L., Yang, T., Wang, B., Lin, Q., Zhu, S., Li, C., Ma, Y., Tang, J., Xing, J., Li, X., et al. (2020b). RALF1-FERONIA complex affects splicing dynamics to modulate stress responses and growth in plants. *Sci. Adv.* **6**, eaaz1622.

Wang, X., Wilson, L. and Cosgrove, D. J. (2020c). Pectin methylesterase selectively softens the onion epidermal wall yet reduces acid-induced creep. *J. Exp. Bot.* **71**, 2629–2640.

Wang, L., Yang, T., Wang, B., Lin, Q., Zhu, S., Li, C., Ma, Y., Tang, J., Xing, J., Li, X., et al. RALF1-FERONIA complex affects splicing dynamics to modulate stress responses and growth in plants. *Sci. Adv.* **6**, eaaz1622.

Wei, C., Lintilhac, L. S. and Lintilhac, P. M. (2006). Loss of stability, pH, and the anisotropic extensibility of Chara cell walls. *Planta* **223**, 1058–1067.

Westermann, J., Streubel, S., Franck, C. M., Lentz, R., Dolan, L. and Boisson-Dernier, A. (2019). An Evolutionarily Conserved Receptor-like Kinases Signaling Module Controls Cell Wall Integrity During Tip Growth. *Curr. Biol.* **29**, 3899-3908.e3.

Whitmore, A. P. and Whalley, W. R. (2009). Physical effects of soil drying on roots and crop growth. *J. Exp. Bot.* **60**, 2845–2857.

Wightman, R., Chomicki, G., Kumar, M., Carr, P. and Turner, S. R. (2013). SPIRAL2 determines plant microtubule organization by modulating microtubule severing. *Curr. Biol. CB* **23**, 1902–1907.

Williams, M. A. K. (2020). Pectin Gelation and Its Assembly into Functional Materials. In *Pectin: Technological and Physiological Properties* (ed. Kontogiorgos, V.), pp. 125–148. Cham: Springer International Publishing.

Williamson, R. (1990). Alignment of cortical microtubules by anisotropic wall stresses. *Aust J Plant Physiol* 601–613.

Wolf, S. (2017). Plant cell wall signalling and receptor-like kinases. *Biochem. J.* **474**, 471–492.

Wolf, S. (2022). Cell Wall Signaling in Plant Development and Defense. *Annu. Rev. Plant Biol.*

Wolfenson, H., Yang, B. and Sheetz, M. P. (2019). Steps in Mechanotransduction Pathways that Control Cell Morphology. *Annu. Rev. Physiol.* **81**, 585–605.

Wormit, A. and Usadel, B. (2018). The Multifaceted Role of Pectin Methylesterase Inhibitors (PMEIs). *Int. J. Mol. Sci.* **19**, 2878.

Xiao, C., Zhang, T., Zheng, Y., Cosgrove, D. J. and Anderson, C. T. (2016). Xyloglucan Deficiency Disrupts Microtubule Stability and Cellulose Biosynthesis in Arabidopsis, Altering Cell Growth and Morphogenesis. *Plant Physiol.* **170**, 234–249.

Xiao, Y., Stegmann, M., Han, Z., DeFalco, T. A., Parys, K., Xu, L., Belkhadir, Y., Zipfel, C. and Chai, J. (2019). Mechanisms of RALF peptide perception by a heterotypic receptor complex. *Nature* **572**, 270–274.

Xie, Y., Sun, P., Li, Z., Zhang, F., You, C. and Zhang, Z. (2022). FERONIA Receptor Kinase Integrates with Hormone Signaling to Regulate Plant Growth, Development, and Responses to Environmental Stimuli. *Int. J. Mol. Sci.* **23**, 3730.

Xu, T., Wen, M., Nagawa, S., Fu, Y., Chen, J.-G., Wu, M.-J., Perrot-Rechenmann, C., Friml, J., Jones, A. M. and Yang, Z. (2010). Cell surface- and rho GTPase-based auxin signaling controls cellular interdigitation in Arabidopsis. *Cell* **143**, 99–110.

Xu, G., Chen, W., Song, L., Chen, Q., Zhang, H., Liao, H., Zhao, G., Lin, F., Zhou, H. and Yu, F. (2019). FERONIA phosphorylates E3 ubiquitin ligase ATL6 to modulate the stability of 14-3-3 proteins in response to the carbon/nitrogen ratio. *J. Exp. Bot.* **70**, 6375–6388.

Yamanaka, T., Nakagawa, Y., Mori, K., Nakano, M., Imamura, T., Kataoka, H., Terashima, A., Iida, K., Kojima, I., Katagiri, T., et al. (2010). MCA1 and MCA2 That Mediate Ca2+ Uptake Have Distinct and Overlapping Roles in Arabidopsis. *Plant Physiol.* **152**, 1284–1296.

Yang, T., Wang, L., Li, C., Liu, Y., Zhu, S., Qi, Y., Liu, X., Lin, Q., Luan, S. and Yu, F. (2015). Receptor protein kinase FERONIA controls leaf starch accumulation by interacting with glyceraldehyde-3-phosphate dehydrogenase. *Biochem. Biophys. Res. Commun.* **465**, 77–82.

Ye, Q., Wiera, B. and Steudle, E. (2004). A cohesion/tension mechanism explains the gating of water channels (aquaporins) in Chara internodes by high concentration. *J. Exp. Bot.* **55**, 449–461.

Ye, H., Liu, S., Tang, B., Chen, J., Xie, Z., Nolan, T. M., Jiang, H., Guo, H., Lin, H.-Y., Li, L., et al. (2017). RD26 mediates crosstalk between drought and brassinosteroid signalling pathways. *Nat. Commun.* **8**, 14573.

Yeats, T. H. and Rose, J. K. C. (2013). The Formation and Function of Plant Cuticles. *Plant Physiol.* **163**, 5–20.

Yeats, T. H., Sorek, H., Wemmer, D. E. and Somerville, C. R. (2016). Cellulose Deficiency Is Enhanced on Hyper Accumulation of Sucrose by a H+-Coupled Sucrose Symporter. *Plant Physiol.* **171**, 110–124.

Yu, Y. and Assmann, S. M. (2018). Inter-relationships between the heterotrimeric Gβ subunit AGB1, the receptor-like kinase FERONIA, and RALF1 in salinity response. *Plant Cell Environ.* **41**, 2475–2489.

Yu, F., Qian, L., Nibau, C., Duan, Q., Kita, D., Levasseur, K., Li, X., Lu, C., Li, H., Hou, C., et al. (2012). FERONIA receptor kinase pathway suppresses abscisic acid signaling in Arabidopsis by activating ABI2 phosphatase. *Proc. Natl. Acad. Sci. U. S. A.* **109**, 14693–14698.

Yu, F., Li, J., Huang, Y., Liu, L., Li, D., Chen, L. and Luan, S. (2014). FERONIA receptor kinase controls seed size in Arabidopsis thaliana. *Mol. Plant* **7**, 920–922.

Yu, M., Yuan, X., Lu, C., Le, S., Kawamura, R., Efremov, A. K., Zhao, Z., Kozlov, M. M., Sheetz, M., Bershadsky, A., et al. (2017). mDia1 senses both force and torque during F-actin filament polymerization. *Nat. Commun.* **8**, 1–9.

Yu, Y., Chakravorty, D. and Assmann, S. M. (2018). The G Protein β-Subunit, AGB1, Interacts with FERONIA in RALF1-Regulated Stomatal Movement. *Plant Physiol.* **176**, 2426–2440.

Žádníková, P., Smet, D., Zhu, Q., Straeten, D. V. D. and Benková, E. (2015). Strategies of seedlings to overcome their sessile nature: auxin in mobility control. *Front. Plant Sci.* **6**, 218.

Zambryski, P. and Crawford, K. (2000). Plasmodesmata: gatekeepers for cell-to-cell transport of developmental signals in plants. *Annu. Rev. Cell Dev. Biol.* **16**, 393–421.

Zeiger, E., Farquhar, G. D. and Cowan, I. R. (1987). *Stomatal Function*. Stanford University Press.

Zerzour, R., Kroeger, J. and Geitmann, A. (2009). Polar growth in pollen tubes is associated with spatially confined dynamic changes in cell mechanical properties. *Dev. Biol.* **334**, 437–446.

Zhang, C., Halsey, L. E. and Szymanski, D. B. (2011). The development and geometry of shape change in Arabidopsis thalianacotyledon pavement cells. *BMC Plant Biol.* **11**, 27.

Zhang, T., Vavylonis, D., Durachko, D. M. and Cosgrove, D. J. (2017). Nanoscale movements of cellulose microfibrils in primary cell walls. *Nat. Plants* **3**,.

Zhang, T., Tang, H., Vavylonis, D. and Cosgrove, D. J. (2019). Disentangling loosening from softening: insights into primary cell wall structure. *Plant J.* **100**, 1101–1117.

Zhang, X., Yang, Z., Wu, D. and Yu, F. (2020a). RALF–FERONIA Signaling: Linking Plant Immune Response with Cell Growth. *Plant Commun.* **1**, 100084.

Zhang, X., Peng, H., Zhu, S., Xing, J., Li, X., Zhu, Z., Zheng, J., Wang, L., Wang, B., Chen, J., et al. (2020b). Nematode-Encoded RALF Peptide Mimics Facilitate Parasitism of Plants through the FERONIA Receptor Kinase. *Mol. Plant* **13**, 1434–1454.

Zhang, Y., Yu, J., Wang, X., Durachko, D. M., Zhang, S. and Cosgrove, D. J. (2021a). Molecular insights into the complex mechanics of plant epidermal cell walls. *Science* **372**, 706–711.

Zhang, L., Huang, J., Su, S., Wei, X., Yang, L., Zhao, H., Yu, J., Wang, J., Hui, J., Hao, S., et al. (2021b). FERONIA receptor kinase-regulated reactive oxygen species mediate self-incompatibility in Brassica rapa. *Curr. Biol.*

Zhao, C., Zayed, O., Yu, Z., Jiang, W., Zhu, P., Hsu, C.-C., Zhang, L., Tao, W. A., Lozano-Durán, R. and Zhu, J.-K. (2018). Leucine-rich repeat extensin proteins regulate plant salt tolerance in Arabidopsis. *Proc. Natl. Acad. Sci. U. S. A.* **115**, 13123–13128.

Zhao, C., Jiang, W., Zayed, O., Liu, X., Tang, K., Nie, W., Li, Y., Xie, S., Li, Y., Long, T., et al. (2021). The LRXs-RALFs-FER module controls plant growth and salt stress responses by modulating multiple plant hormones. *Natl. Sci. Rev.* **8**, nwaa149.

Zheng, Y., Wang, X., Chen, Y., Wagner, E. and Cosgrove, D. J. (2018). Xyloglucan in the primary cell wall: assessment by FESEM, selective enzyme digestions and nanogold affinity tags. *Plant J.* **93**, 211–226.

Zhu, S., Martínez Pacheco, J., Estevez, J. M. and Yu, F. (2020a). Autocrine regulation of root hair size by the RALF-FERONIA-RSL4 signaling pathway. *New Phytol.* **227**, 45–49.

Zhu, S., Estévez, J. M., Liao, H., Zhu, Y., Yang, T., Li, C., Wang, Y., Li, L., Liu, X., Pacheco, J. M., et al. (2020b). The RALF1-FERONIA Complex Phosphorylates eIF4E1 to Promote Protein Synthesis and Polar Root Hair Growth. *Mol. Plant* **13**, 698–716.

Zonia, L. and Munnik, T. (2007). Life under pressure: hydrostatic pressure in cell growth and function. *Trends Plant Sci.* **12**, 90–97.

Zsivanovits, G., MacDougall, A. J., Smith, A. C. and Ring, S. G. (2004). Material properties of concentrated pectin networks. *Carbohydr. Res.* **339**, 1317–1322.